

ИЗВЕСТИЯ ВЫСШИХ УЧЕБНЫХ ЗАВЕДЕНИЙ ЧЕРНАЯ МЕТАЛЛУРГИЯ

IZVESTIYA. FERROUS METALLURGY

fermet.misis.ru

2024 Том 67 № 2
Vol. No.

МЕТАЛЛУРГИЧЕСКИЕ ТЕХНОЛОГИИ

Оценка гомогенности рафинировочного шлака АКП
расчетным и экспериментальным методами

Исследование изменения температуры прессового инструмента
при обработке лазером

МАТЕРИАЛОВЕДЕНИЕ

Эволюция дислокационной структуры и фазового состава в процессе
нагрева деформированного высокоэнтропийного сплава $Al_{0.3}CoCrFeNi$

ИННОВАЦИИ В МЕТАЛЛУРГИЧЕСКОМ ПРОМЫШЛЕННОМ И ЛАБОРАТОРНОМ ОБОРУДОВАНИИ, ТЕХНОЛОГИЯХ И МАТЕРИАЛАХ

Напряженно-деформированное состояние керамической оболочковой
формы при формировании в ней стальной шарообразной отливки

ИЗВЕСТИЯ ВЫСШИХ УЧЕБНЫХ ЗАВЕДЕНИЙ ЧЕРНАЯ МЕТАЛЛУРГИЯ

Научно-технический журнал

Издается с января 1958 г. Выпускается 6 раз в год

2024 Том 67 № 2
Vol. No.

IZVESTIYA FERROUS METALLURGY

Scientific and Technical Journal

Published since January 1958. Issued 6 times a year

IZVESTIYA FERROUS METALLURGY

www.fermet.misis.ru

ISSN 0368-0797 (Print) ISSN 2410-2091 (Online)

Alternative title:

Izvestiya vuzov. Chernaya metallurgiya

Founders:



Editor-in-Chief:

Leopol'd I. Leont'ev, Academician, Adviser of the Russian Academy of Sciences; Dr. Sci. (Eng.), Prof., NUST "MISIS"; Chief Researcher, Institute of Metallurgy UB RAS, Moscow
4 Leninskii Ave., Moscow 119049, Russian Federation
National University of Science and Technology "MISIS"

Deputy Editor-in-Chief:

Evgenii V. Protopopov, Dr. Sci. (Eng.), Prof., Siberian State Industrial University, Novokuznetsk

Publisher:

National University of Science and Technology "MISIS"

Editorial Office Address:

in Moscow

4 Leninskii Ave., Moscow 119049, Russian Federation
National University of Science and Technology "MISIS"
Tel.: +7 (495) 638-44-11
E-mail: fermet.misis@mail.ru, ferrous@sisis.ru

in Novokuznetsk

42 Kirova Str., Novokuznetsk, Kemerovo Region – Kuzbass
654007, Russian Federation
Siberian State Industrial University
Tel.: +7 (3843) 74-86-28 E-mail: redjizvz@sibsiu.ru

Editorial Board:

Sailaubai O. Baisanov, Dr. Sci. (Eng.), Prof., Abishev Chemical-Metallurgical Institute, Karaganda, Republic of Kazakhstan
Vladimir D. Belov, Dr. Sci. (Eng.), Prof., NUST MISIS, Moscow
Anatolii A. Brodov, Cand. Sci. (Econ.), Bardin Central Research Institute for Ferrous Metallurgy, Moscow
Il'ya V. Chumanov, Dr. Sci. (Eng.), Prof., South Ural State Research University, Chelyabinsk
Andrei N. Dmitriev, Dr. Sci. (Eng.), Prof., Academician, RANS, A.M. Prokhorov Academy of Engineering Sciences, Institute of Metallurgy, Ural Branch of RAS, Ural Federal University, Yekaterinburg
Aleksei V. Dub, Dr. Sci. (Eng.), Prof., JSC "Science and Innovations", Moscow
Mikhail R. Filonov, Dr. Sci. (Eng.), Prof., NUST MISIS, Moscow
Sergei M. Gorbatyuk, Dr. Sci. (Eng.), Prof., NUST MISIS, Moscow
Konstantin V. Grigorovich, Academician of RAS, Dr. Sci. (Eng.), Baikov Institute of Metallurgy and Materials Science of RAS, Moscow
Victor E. Gromov, Dr. Sci. (Eng.), Prof., Siberian State Industrial University, Novokuznetsk
Aleksei G. Kolmakov, Dr. Sci. (Eng.), Corresponding Member of RAS, Baikov Institute of Metallurgy and Materials Science of RAS, Moscow
Valerii M. Kolokol'tsev, Dr. Sci. (Eng.), Prof., Magnitogorsk State Technical University, Magnitogorsk
Mariya V. Kostina, Dr. Sci. (Eng.), Baikov Institute of Metallurgy and Materials Science of RAS, Moscow
Konstantin L. Kosyrev, Dr. Sci. (Eng.), Academician of RANS, Electrosteel Heavy Engineering Works JSC, Moscow
Yuliya A. Kurganova, Dr. Sci. (Eng.), Prof., Bauman Moscow State Technical University, Moscow
Linn Horst, Linn High Therm GmbH, Hirschbach, Germany
Vladimir I. Lysak, Academician of RAS, Dr. Sci. (Eng.), Prof., Rector, Volgograd State Technical University, Volgograd
Valerii P. Meshalkin, Dr. Sci. (Eng.), Academician of RAS, Prof., D.I. Mendeleyev Russian Chemical-Technological University, Moscow
Radik R. Mulyukov, Dr. Sci. (Phys.-Chem.), Prof., Corresponding Member of RAS, Institute of Metals Superplasticity Problems of RAS, Ufa

Sergei A. Nikulin, Dr. Sci. (Eng.), Prof., Corresponding Member of RANS, NUST MISIS, Moscow
Asylbek Kh. Nurumgaliev, Dr. Sci. (Eng.), Prof., Karaganda State Industrial University, Karaganda, Republic of Kazakhstan
Oleg I. Ostrovski, Dr. Sci. (Eng.), Prof., University of New South Wales, Sydney, Australia
Loris Pietrelli, Dr., Scientist, Italian National Agency for New Technologies, Energy and Sustainable Economic Development, Rome, Italy
Igor' Yu. Pyshmintsev, Dr. Sci. (Eng.), Russian Research Institute of the Pipe Industry, Chelyabinsk
Andrei I. Rudskoi, Academician of RAS, Dr. Sci. (Eng.), Prof., Rector, Peter the Great Saint-Petersburg Polytechnic University, Saint-Petersburg
Oleg Yu. Sheshukov, Dr. Sci. (Eng.), Prof., Ural Federal University, Yekaterinburg
Laura M. Simonyan, Dr. Sci. (Eng.), Prof., NUST MISIS, Moscow
Robert F. Singer, Dr. Sci. (Eng.), Prof., Friedrich-Alexander University, Germany
Boris A. Sivak, Cand. Sci. (Eng.), Prof., VNIIMETMASH Holding Company, Moscow
Leonid A. Smirnov, Dr. Sci. (Eng.), Prof., Academician of RAS, OJSC "Ural Institute of Metals", Yekaterinburg
Sergei V. Solodov, Cand. Sci. (Eng.), NUST MISIS, Moscow
Speidel Marcus, Dr. Natur. Sci., Prof., Swiss Academy of Materials, Switzerland
Nikolai A. Spirin, Dr. Sci. (Eng.), Prof., Ural Federal University, Yekaterinburg
Tang Guoi, Institute of Advanced Materials of Tsinghua University, Shenzhen, China
Mikhail V. Temlyantsev, Dr. Sci. (Eng.), Prof., Siberian State Industrial University, Novokuznetsk
Ekaterina P. Volynkina, Dr. Sci. (Eng.), Advisor, ALE "Kuzbass Association of Waste Processors", Novokuznetsk
Aleksei B. Yur'ev, Dr. Sci. (Eng.), Rector, Siberian State Industrial University, Novokuznetsk
Vladimir S. Yusupov, Dr. Sci. (Eng.), Prof., Baikov Institute of Metallurgy and Materials Science of RAS, Moscow
Vladimir I. Zhuchkov, Dr. Sci. (Eng.), Prof., Institute of Metallurgy, Ural Branch of RAS, Ural Federal University, Yekaterinburg
Michael Zinigrad, Dr. Sci. (Physical Chemistry), Prof., Rector, Ariel University, Israel
Vladimir I. Zolotukhin, Dr. Sci. (Eng.), Prof., Tula State University, Tula

In accordance with paragraph 5 of the Rules for the formation of the Higher Attestation Commission list journal "Izvestiya. Ferrous metallurgy" is included in the list of leading peer-reviewed scientific journals, publication in which is taken into account in the defense of candidate and doctoral dissertations, as indexed in international data bases.

Indexed: Scopus, Russian Science Citation Index (RSCI), Research Bible, Chemical Abstracts, OCLC and Google Scholar
Registered in Federal Service for Supervision in the Sphere of Mass Communications **PI number FS77-35456.**



Articles are available under Creative Commons Attribution 4.0 License.

ИЗВЕСТИЯ ВЫСШИХ УЧЕБНЫХ ЗАВЕДЕНИЙ ЧЕРНАЯ МЕТАЛЛУРГИЯ

www.fermet.misis.ru

ISSN 0368-0797 (Print) ISSN 2410-2091 (Online)

Варианты названия:

Известия вузов. Черная металлургия

Izvestiya. Ferrous Metallurgy

Учредители:



Редакционная коллегия:

С. О. Байсанов, д.т.н., профессор, ХМИ им. Ж.Абишева, г. Караганда, Республика Казахстан

В. Д. Белов, д.т.н., профессор, НИТУ МИСИС, г. Москва

А. А. Бродов, к.экон.н., ФГУП «ЦНИИчермет им. И.П. Бардина», г. Москва

Е. П. Волынкина, д.т.н., советник, ОЮЛ «Кузбасская Ассоциация переработчиков отходов», г. Новокузнецк

С. М. Горбатько, д.т.н., профессор, НИТУ МИСИС, г. Москва

К. В. Григорович, академик РАН, д.т.н., ИМЕТ им. А.А. Байкова РАН, г. Москва

В. Е. Громов, д.ф.-м.н., профессор, СибГИУ, г. Новокузнецк

А. Н. Дмитриев, д.т.н., профессор, академик РАЕН, академик АИН РФ, г. Екатеринбург

А. В. Дуб, д.т.н., профессор, ЗАО «Наука и инновации», г. Москва

В. И. Жучков, д.т.н., профессор, ИМЕТ УрО РАН, г. Екатеринбург

Р. Ф. Зингер, д.т.н., профессор, Институт Фридриха-Александра, Германия

М. Зиниград, д.т.н., профессор, Институт Ариэля, Израиль

В. И. Золотухин, д.т.н., профессор, ТулГУ, г. Тула

А. Г. Колмаков, д.т.н., чл.-корр. РАН, ИМЕТ им. А.А. Байкова РАН, г. Москва

В. М. Колокольцев, д.т.н., профессор, МГТУ им. Г.И. Носова, г. Магнитогорск

М. В. Костина, д.т.н., ИМЕТ им. А.А. Байкова РАН, г. Москва

К. Л. Косырев, д.т.н., академик РАЕН, ОАО «Электростальский завод тяжелого машиностроения», г. Москва

Ю. А. Курганова, д.т.н., профессор, МГТУ им. Н.Э. Баумана, г. Москва

Х. Линн, ООО «Линн Хай Терм», Германия

В. И. Лысак, академик РАН, д.т.н., профессор, ВолгГТУ, г. Волгоград

В. П. Мешалкин, академик РАН, д.т.н., профессор, РХТУ им. Д.И. Менделеева, г. Москва

В соответствии п. 5 Правил формирования перечня ВАК журнал «Известия вузов. Черная металлургия» входит в перечень ведущих рецензируемых научных журналов и изданий, публикация в которых учитывается при защитах кандидатских и докторских диссертаций как индексируемый в МБД.

Главный редактор:

Леопольд Игоревич Леонтьев, академик РАН, советник, Президиум РАН; д.т.н., профессор, НИТУ «МИСИС»; главный научный сотрудник, Институт металлургии УрО РАН
Россия, 119049, Москва, Ленинский просп., д. 4, стр. 1, Национальный исследовательский технологический университет «МИСИС»

Заместитель главного редактора:

Евгений Валентинович Протопопов, д.т.н., профессор, Сибирский государственный индустриальный университет г. Новокузнецк

Издатель:

Национальный исследовательский технологический университет «МИСИС»

Адреса подразделений редакций:

в Москве

Россия, 119049, Москва, Ленинский просп., д. 4, стр. 1
Национальный исследовательский технологический университет «МИСИС»
Тел.: +7 (495) 638-44-11 E-mail: ferrous@sisis.ru

в Новокузнецке

Россия, 654007, Новокузнецк,
Кемеровская обл. – Кузбасс, ул. Кирова, зд. 42
Сибирский государственный индустриальный университет
Тел.: +7 (3843) 74-86-28 E-mail: redjizvz@sibsiu.ru

Р. Р. Мулюков, д.ф.м.-н., профессор, чл.-корр. ФГБУН ИПСМ РАН, г. Уфа
С. А. Никулин, д.т.н., профессор, чл.-корр. РАЕН, НИТУ МИСИС, г. Москва
А. Х. Нурумгалиев, д.т.н., профессор, КГИУ, г. Караганда, Республика Казахстан
О. И. Островский, д.т.н., профессор, Университет Нового Южного Уэльса, Сидней, Австралия
Л. Пиетрелли, д.т.н., Итальянское национальное агентство по новым технологиям, энергетике и устойчивому экономическому развитию, Рим, Италия
И. Ю. Пышминцев, д.т.н., РосНИТИ, г. Челябинск
А. И. Рудской, академик РАН, д.т.н., профессор, СПбПУ Петра Великого, г. Санкт-Петербург
Б. А. Сивак, к.т.н., профессор, АО АХК «ВНИИМЕТМАШ», г. Москва
Л. М. Симонян, д.т.н., профессор, НИТУ МИСИС, г. Москва
Л. А. Смирнов, академик РАН, д.т.н., профессор, ОАО «Уральский институт металлов», г. Екатеринбург
С. В. Солодов, к.т.н., НИТУ МИСИС, г. Москва
Н. А. Спирин, д.т.н., профессор, УрФУ, г. Екатеринбург
Г. Танг, Институт перспективных материалов университета Циньхуа, г. Шеньжень, Китай
М. В. Темлянецев, д.т.н., профессор, СибГИУ, г. Новокузнецк
М. Р. Филонов, д.т.н., профессор, НИТУ МИСИС, г. Москва
И. В. Чуманов, д.т.н., профессор, ЮУрГУ, г. Челябинск
О. Ю. Шешуков, д.т.н., профессор УрФУ, г. Екатеринбург
М. О. Шпайдель, д.ест.н., профессор, Швейцарская академия материаловедения, Швейцария
А. Б. Юрьев, д.т.н., ректор, СибГИУ, г. Новокузнецк
В. С. Юсупов, д.т.н., профессор, ИМЕТ им. А.А. Байкова РАН, г. Москва

Индексирование: Scopus, Russian Science Citation Index (RSCI), Research Bible, Chemical Abstracts, OCLC и Google Scholar

Зарегистрирован Федеральной службой по надзору в сфере связи и массовых коммуникаций ПИ № ФС77-35456.



Статьи доступны под лицензией Creative Commons Attribution 4.0 License.

CONTENTS

СОДЕРЖАНИЕ

METALLURGICAL TECHNOLOGIES

- Murysev V.A., Sheshukov O.Yu., Safonov V.M., Somov S.A., Metelkin A.A., Egiazar'yan D.K. Assessment of homogeneity of ladle-furnace refining slag by calculation and experimental methods 140
- Stuk T.S., Pototskii E.P. Estimation of accident rate of blast furnace tuyeres 148
- Chichenev N.A., Gorbatyuk S.M., Solomonov K.N., Snitko S.A., Chicheneva O.N. Investigation of changes in temperature of pressing tool during laser processing 155

RESOURCE SAVING
IN FERROUS METALLURGY

- Akuov A.M., Kelamanov B.S., Zayakin O.V., Samuratov E.K., Yessengaliyev D.A. Influence of additives on properties of high-carbon ferrochrome slag 161

MATERIALS SCIENCE

- Popova N.A., Nikonenko E.L., Porfir'ev M.A., Kryukov R.E. Internal stresses and their sources in steels with BCC lattice 167
- Ivanov I.V., Akkuzin S.A., Safarova D.E., Litovchenko I.Yu., Bataev I.A. Evolution of dislocation structure and phase composition of deformed $Al_{0.3}CoCrFeNi$ high-entropy alloy during heating 176
- Nevskii S.A., Bashchenko L.P., Gromov V.E., Peregudov O.A., Gostevskaya A.N., Volodin T.V. Formation of the gradient of structural-phase states of high-speed steel during surfacing. Part 2. The role of the Mullins-Sekerka instability in formation of crystallization structures 185
- Gordienko A.I., Abdulmenova E.V., Kozlova T.V., Gomorova Yu.F., Vlasov I.V., Fotin I.A., Kayurov K.N., Buyakova S.P. Effect of heat treatment modes on structure and properties of 08Kh18N6AG10S steel 195

PHYSICO-CHEMICAL BASICS
OF METALLURGICAL PROCESSES

- Upolovnikova A.G., Shartdinov R.R., Smetannikov A.N. Effect of basicity on physical properties of ladle slags of $CaO - SiO_2 - Ce_2O_3 - Al_2O_3 - MgO$ system 205

МЕТАЛЛУРГИЧЕСКИЕ ТЕХНОЛОГИИ

- Мурысёв В.А., Шешуков О.Ю., Сафонов В.М., Сомов С.А., Метелкин А.А., Егиазарьян Д.К. Оценка гомогенности рафинировочного шлака АКП расчетным и экспериментальными методами 140
- Стук Т.С., Потоцкий Е.П. Оценка аварийности доменных фурм 148
- Чиченев Н.А., Горбатюк С.М., Соломонов К.Н., Снитко С.А., Чиченева О.Н. Исследование изменения температуры прессового инструмента при обработке лазером 155

РЕСУРСОСБЕРЕЖЕНИЕ
В ЧЕРНОЙ МЕТАЛЛУРГИИ

- Акуов А.М., Келаманов Б.С., Заякин О.В., Самуратов Е.К., Есенгалиев Д.А. Изучение влияния флюсующих добавок на свойства шлака высокоуглеродистого феррохрома 161

МАТЕРИАЛОВЕДЕНИЕ

- Попова Н.А., Никоненко Е.Л., Порфирьев М.А., Крюков Р.Е. Внутренние напряжения и их источники в сталях с ОЦК кристаллической решеткой 167
- Иванов И.В., Аккузин С.А., Сафарова Д.Э., Литовченко И.Ю., Батаев И.А. Эволюция дислокационной структуры и фазового состава в процессе нагрева деформированного высокоэнтропийного сплава $Al_{0.3}CoCrFeNi$ 176
- Невский С.А., Башченко Л.П., Громов В.Е., Перегудов О.А., Гостевская А.Н., Володин Т.В. Формирование градиента структурно-фазовых состояний быстрорежущей стали при наплавке. Часть 2. Роль неустойчивости Маллинза-Секерки в образовании структур кристаллизации 185
- Гордиенко А.И., Абдульменова Е.В., Козлова Т.В., Гоморова Ю.Ф., Власов И.В., Фотин И.А., Каюров К.Н., Буякова С.П. Влияние режимов термической обработки на структуру и свойства стали 08X18N6AG10C 195

ФИЗИКО-ХИМИЧЕСКИЕ ОСНОВЫ
МЕТАЛЛУРГИЧЕСКИХ ПРОЦЕССОВ

- Уполовникова А.Г., Шартдинов Р.Р., Сметанников А.Н. Влияние основности на физические свойства ковшевых шлаков системы $CaO - SiO_2 - Ce_2O_3 - Al_2O_3 - MgO$ 205

CONTENTS (CONTINUATION)

СОДЕРЖАНИЕ (ПРОДОЛЖЕНИЕ)

INNOVATIONS IN METALLURGICAL
INDUSTRIAL AND LABORATORY
EQUIPMENT, TECHNOLOGIES
AND MATERIALS

Odinokov V.I., Evstigneev A.I., Dmitriev E.A., Namok-
nov A.N., Evstigneeva A.A., Chernyshova D.V. Stress-
strain state of ceramic shell mold during formation of
spherical steel casting in it. Part 1 211

BASED ON THE MATERIALS
OF THE INTERNATIONAL CONFERENCE
“SCIENTIFIC AND PRACTICAL SCHOOL FOR
YOUNG METALLURGISTS”

Karasev V.S., Kodzhaspirov G.E., Fedorov A.S, Al'khi-
menko A.A., Zhitenev A.I. Increasing the corrosion
properties of duplex steel with REM modification 219

Rovbo A.S., Golubev I.A., Shaposhnikov N.O., Peni-
gin A.V., Fedorov A.S. Approaches to the selection of
material design of infrastructure facilities for transport
and injection of CO₂ 229

ECOLOGY AND RATIONAL USE
OF NATURAL RESOURCES

Rybenko I.A., Rozhikhina I.D., Nokhrina O.I., Golo-
dova M.A. Rational application of high quality manga-
nese concentrate 237

INFORMATION TECHNOLOGIES
AND AUTOMATIC CONTROL
IN FERROUS METALLURGY

Spirin N.A., Gurin I.A., Lavrov V.V., Zainullin L.A. In-
formation modeling system for movement of charge
layers and melt accumulation in a blast furnace well 245

ИННОВАЦИИ В МЕТАЛЛУРГИЧЕСКОМ
ПРОМЫШЛЕННОМ И ЛАБОРАТОРНОМ
ОБОРУДОВАНИИ, ТЕХНОЛОГИЯХ
И МАТЕРИАЛАХ

Одиноков В.И., Евстигнеев А.И., Дмитриев Э.А., На-
моконов А.Н., Евстигнеева А.А., Чернышова Д.В.
Напряженно-деформированное состояние кера-
мической оболочковой формы при формировании
в ней стальной шарообразной отливки. Часть 1 211

ПО МАТЕРИАЛАМ
МЕЖДУНАРОДНОЙ КОНФЕРЕНЦИИ
«НАУЧНО-ПРАКТИЧЕСКАЯ ШКОЛА
ДЛЯ МОЛОДЫХ МЕТАЛЛУРГОВ»

Карасев В.С., Коджаспиров Г.Е., Федоров А.С, Аль-
хименко А.А., Житенев А.И. Повышение корро-
зионных свойств дуплексной стали с помощью мо-
дифицирования РЗМ 219

Ровбо А.С., Голубев И.А., Шапошников Н.О., Пени-
гин А.В., Федоров А.С. Подходы к выбору мате-
риального исполнения инфраструктурных объек-
тов транспорта и закачки CO₂ 229

ЭКОЛОГИЯ И РАЦИОНАЛЬНОЕ
ПРИРОДОПОЛЬЗОВАНИЕ

Рыбенко И.А., Рожихина И.Д., Нохрина О.И., Голо-
дова М.А. Рациональные варианты применения
высококачественного марганцевого концентрата 237

ИНФОРМАЦИОННЫЕ ТЕХНОЛОГИИ
И АВТОМАТИЗАЦИЯ
В ЧЕРНОЙ МЕТАЛЛУРГИИ

Спирин Н.А., Гурин И.А., Лавров В.В., Зайнул-
лин Л.А. Информационно-моделирующая система
движения слоев шихты и накопления расплава
в горне доменной печи 245



UDC 669.046.58

DOI 10.17073/0368-0797-2024-2-140-147



Original article

Оригинальная статья

ASSESSMENT OF HOMOGENEITY OF LADLE-FURNACE REFINING SLAG BY CALCULATION AND EXPERIMENTAL METHODS

V. A. Murysev¹ , O. Yu. Sheshukov^{2, 3}, V. M. Safonov⁴,
S. A. Somov¹, A. A. Metelkin², D. K. Egiazar'yan^{2, 3}

¹ JSC “Vyksa Metallurgical Plant” (45 Br. Batashevskiy Str., Vyksa, Nizhny Novgorod Region 607060, Russian Federation)

² Ural Federal University named after the first President of Russia B.N. Yeltsin (19 Mira Str., Yekaterinburg 620002, Russian Federation)

³ Institute of Metallurgy, Ural Branch of the Russian Academy of Sciences (101 Amundsena Str., Yekaterinburg 620016, Russian Federation)

⁴ Vyksa Branch of the National University of Science and Technology “MISIS” (206 Kalinina Str., Shimorskoye, Vyksa District, Nizhny Novgorod Region 607036, Russian Federation)

murysev_va@vsw.ru

Abstract. The paper considers the issues of determining undissolved CaO and MgO particles in slags formed in a ladle-furnace unit. The assessment of slags by the presence and quantity of undissolved oxides CaO and MgO, depending on chemical composition, was carried out using a polymer model developed at UrFU and improved at IMeT UrB RAS. To determine the saturation of a multicomponent melt by CaO and MgO oxides, it is necessary to compare two parameters: thermodynamic activity of oxide in the melt, which depends on chemical composition, and saturation activity, which depends on temperature. The authors propose a method for estimating the content of undissolved particles in the slags formed at the steel ladle treatment at JSC VMZ. Most slags contain undissolved lime in an amount less than 10 %, which is sufficient for successful steel desulfurization. Theoretical calculations for determination of undissolved particles were confirmed in laboratory conditions during studies of industrial slags with a Stengelmeyer viscometer. Laboratory experiments showed the accuracy of the calculated method for determining the solid phase in the slags formed in ladle-furnace unit by comparing the viscosity changes with a decrease in the slags temperature. Solidification temperature of heterogeneous slag is 200 °C higher than that of homogeneous one. When temperature of heterogeneous slag decreased, enlarged agglomerates of solid oxides were formed, which fell under the measuring device, respectively, it showed an increased viscosity of the oxide system in the temperature range of 1570 – 590 °C. Laboratory experiments confirm the methodology for determining the solid phase in the slag.

Keywords: slag, ladle-furnace unit, undissolved particles, homogeneous slag, heterogeneous slag, viscometer, lime dissolution

Acknowledgements: The work was performed within the framework of the state task No. FEUZ-2023-0015.

For citation: Murysev V.A., Sheshukov O.Yu., Safonov V.M., Somov S.A., Metelkin A.A., Egiazar'yan D.K. Assessment of homogeneity of ladle-furnace refining slag by calculation and experimental methods. *Izvestiya. Ferrous Metallurgy*. 2024;67(2):140–147.

<https://doi.org/10.17073/0368-0797-2024-2-140-147>

ОЦЕНКА ГОМОГЕННОСТИ РАФИНИРОВОЧНОГО ШЛАКА АКП РАСЧЕТНЫМ И ЭКСПЕРИМЕНТАЛЬНЫМ МЕТОДАМИ

В. А. Мурысёв¹, О. Ю. Шешуков^{2,3}, В. М. Сафонов⁴,
С. А. Сомов¹, А. А. Метелкин², Д. К. Егизарьян^{2,3}

¹ АО «Выксунский металлургический завод» (Россия, 607060, Нижегородская обл., Выкса, ул. Братьев Баташевых, 45)

² Уральский федеральный университет имени первого Президента России Б.Н. Ельцина (620002, Екатеринбург, ул. Мира, 19)

³ Институт металлургии Уральского отделения РАН (Россия, 620016, Екатеринбург, ул. Амундсена, 101)

⁴ Выксунский филиал НИТУ «МИСИС» (Россия, 607036, Нижегородская обл., Выкса, п.г.т. Шиморское, ул. Калинина, 206)

✉ murysev_va@vsw.ru

Аннотация. В работе рассмотрены вопросы по определению нерастворенных частиц CaO и MgO в шлаках, формируемых в агрегате ковш–печь. Оценку шлаков по наличию и количеству нерастворенных оксидов CaO и MgO в зависимости от химического состава проводили с помощью полимерной модели, разработанной в УрФУ и усовершенствованной в ИМЕТ УрО РАН. Для определения насыщения многокомпонентного расплава по оксидам CaO и MgO необходимо сравнить два параметра: термодинамическую активность оксида в расплаве, которая зависит от химического состава, и активность насыщения, которая зависит от температуры. Предлагается методика оценки содержания нерастворенных частиц в шлаках, формируемых на участке ковшевой обработки стали АО «ВМЗ». Большинство шлаков содержит нерастворенную известь в количестве не более 10 %, что достаточно для успешной десульфурации стали. Теоретические расчеты по определению нерастворенных частиц были подтверждены в лабораторных условиях при исследованиях производственных шлаков на установке вискозиметра конструкции Штенгельмейера. Лабораторные опыты показали точность расчетного метода определения твердой фазы в шлаках, формируемых в агрегате ковш–печь, путем сравнения изменения вязкости при снижении температуры шлаков. Температура застывания гетерогенного шлака на 200 °С выше, чем гомогенного. При снижении температуры гетерогенного шлака образовывались укрупненные агломераты твердых оксидов, которые контактировали с измерительным зондом, повышая регистрируемую вязкость оксидной системы в интервале температур 1570 – 1590 °С. Результаты лабораторных опытов подтверждают методику определения твердой фазы в шлаке.

Ключевые слова: шлаки, агрегат ковш–печь, нерастворенные частицы, гомогенный шлак, гетерогенный шлак, вискозиметр, растворение извести

Благодарности: Статья выполнена в рамках государственной работы № FEUZ-2023-0015.

Для цитирования: Мурысёв В.А., Шешуков О.Ю., Сафонов В.М., Сомов С.А., Метелкин А.А., Егизарьян Д.К. Оценка гомогенности рафинировочного шлака АКП расчетным и экспериментальными методами. *Известия вузов. Черная металлургия*. 2024;67(2):140–147.

<https://doi.org/10.17073/0368-0797-2024-2-140-147>

INTRODUCTION

Ladle metallurgy represents a crucial stage in metal processing prior to pouring into a Continuous Casting Plant (CCP). Its primary objective is to refine the liquid metal to attain the specified and uniform chemical composition, the required temperature, and a high degree of purity from non-metallic inclusions and harmful impurities [1 – 3].

Within the ladle-furnace (LF) unit of the electric furnace shop of JSC Vyksa Metallurgical Plant (JSC VMZ), highly basic and liquid-active slags are formed. The primary purpose is to remove sulfur from the metal, which can compromise the steel's service properties. Additionally, the slag serves to protect the metal from secondary oxidation, reduce heat losses from the melt's surface, and absorb non-metallic inclusions [1].

A key objective in the ladle treatment of steel (LTS) is to form highly basic slag to ensure maximum desulfurizing properties. This is achieved through the pre-

sence of “free” oxygen anions, originating mainly from the oxides CaO and MgO [1; 8 – 11].

Based on experience gained from refining metal at the LTS site, it is understood that successful sulfur removal requires the formation of slags saturated with CaO with a slight degree of supersaturation, not exceeding 10 %. If lime completely dissolves, there will be a deficit of CaO oxide, adversely affecting the slag's refining properties. Conversely, if the amount of undissolved lime exceeds 10 %, it will diminish refining properties and increase consumption of slag-forming materials [1; 12].

To dissolve CaO, additives are necessary to lower its melting temperature and accelerate dissolution. Examples include fluorite (CaF₂), silica-containing additives, or aluminum-containing materials.

Although fluorite (fluorspar) is widely used in steel-making production as an efficient slag thinner, its use presents several significant drawbacks [13]:

– calcium fluoride promotes the erosion of refractory linings in steel ladles;

– at high temperatures, partial evaporation of CaF_2 occurs, contributing to environmental degradation.

At modern enterprises, there is a concerted effort to replace calcium fluoride with alternative fluxing additives.

To dissolve CaO in slag, materials based on silica and alumina can be utilized. These materials form low-melting eutectics with calcium oxide, effectively reducing its melting temperature. However, the use of SiO_2 -based materials for refining processes is not advisable. This is due to the importance of minimizing the SiO_2 content in the slag to achieve a high sulfur distribution coefficient during refining. Therefore, it is recommended to employ fluxing materials based on Al_2O_3 [15 – 17].

Furthermore, an evaluation of slags based on their saturation of CaO and MgO , depending on their chemical composition under the conditions of JSC VMZ, is deemed necessary.

EXPERIMENTAL

The evaluation of slags based on the presence and quantity of undissolved CaO and MgO oxides, depending on their chemical composition, was conducted using a polymer model (PM) developed at the Ural Federal University (UrFU) and further improved in [19].

The principle of determining the saturation of a multi-component melt with CaO and MgO involves comparing two parameters: the thermodynamic activity of the CaO oxide in the melt ($a_{\text{CaO}}^{\text{td}}$), which depends on the chemical composition, and the saturation activity of CaO ($a_{\text{CaO}}^{\text{sat}}$), which is temperature-dependent.

The method for determining the saturation of a melt with CaO and MgO is as follows (Fig. 1). At point 1, corresponding to temperature T_1 , the inequality $a_{\text{CaO}}^{\text{td}} < a_{\text{CaO}}^{\text{sat}}$ is valid, indicating that the melt is not saturated with CaO oxide.

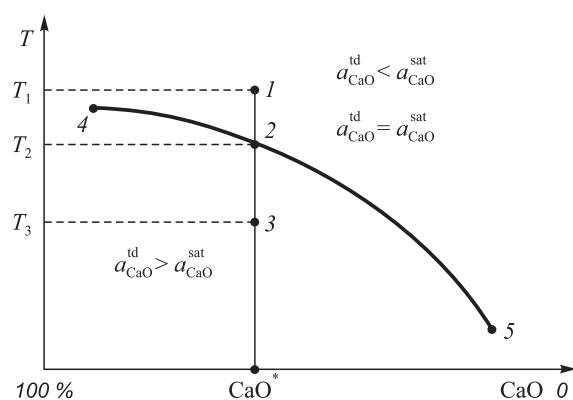


Fig. 1. Method for calculating the amount of solid CaO particles in heterogeneous slag

Рис. 1. Методика расчета количества твердых частиц оксида CaO в гетерогенном шлаке

From point 1 to point 2 (excluding point 2 itself) $a_{\text{CaO}}^{\text{sat}}$ decreases. At point 2, determined by temperature T_2 , the melt becomes saturated with CaO oxide, reaching the thermodynamic activity of this oxide in the melt, i.e., the equality $a_{\text{CaO}}^{\text{td}} = a_{\text{CaO}}^{\text{sat}}$ is valid. This condition corresponds to a certain value of CaO^* in the melt. With further decrease in temperature to T_3 and a constant slag composition, excess CaO oxide will be present in the form of a solid phase, as $a_{\text{CaO}}^{\text{td}} > a_{\text{CaO}}^{\text{sat}}$. Accordingly, the composition of the slag and the temperature at which the solid CaO phase begins to precipitate can be determined: this is line 4 – 2 – 5 (Fig. 1).

Thus, the method for determining the quantity of undissolved CaO and MgO particles and the complete composition of the liquid phase of a heterogeneous slag consists of the following steps:

- 1) determination of the minimum temperature at which the thermodynamic activities of CaO and MgO oxides do not exceed the saturation activities;
- 2) if necessary, reduction of the calculated amount of CaO and MgO oxides in the slag to satisfy the condition $a_{\text{CaO}}^{\text{td}} = a_{\text{CaO}}^{\text{sat}}$;
- 3) determination of the mass fraction of undissolved CaO and MgO particles based on the component balance of the initial slag composition at a given temperature.

To validate this method, slags formed in the steel casting ladle were selected from the LTS site at JSC VMZ with known chemical compositions (Table 1).

Using the proposed method and the polymer model (PM), the composition of the homogeneous phase of each slag and the quantity of the solid phase of CaO and MgO oxides were calculated (Table 2).

Slag 4 is homogeneous as it does not contain solid phases of CaO and MgO ; slag 5 is heterogeneous and contains solid phases of CaO and MgO ; slags 1 – 3, 6 are heterogeneous and only contain undissolved CaO oxide, the quantity of which does not exceed 10 %.

To determine the type of slags, their physical properties such as viscosity and melting temperature were compared using a laboratory unit.

Table 1. Chemical composition of the studied slags

Таблица 1. Химический состав исследуемых шлаков

Slag	Content, wt. %				
	CaO	SiO_2	Al_2O_3	MgO	FeO + MnO
1	52.7	9.8	27.0	6.1	<1.5
2	50.7	9.9	28.8	6.7	
3	52.7	8.4	29.6	5.2	
4	47.3	9.6	31.1	6.9	
5	50.9	9.3	26.2	9.2	
6	52.5	8.9	26.6	6.6	

Table 2. Chemical composition of homogeneous phase and presence of solid phase in the studied slags

Таблица 2. Химический состав гомогенной фазы и наличие твердой фазы в исследуемых шлаках

Slag	Content, wt. %, in liquid phase					Amount of heterogeneous slag deposited from the initial oxide mixture, wt. %	
	CaO	SiO ₂	Al ₂ O ₃	MgO	FeO + MnO	MgO	CaO
1	52.52	10.66	29.36	6.63	<1.5	0	4.56
2	52.00	10.26	29.84	6.94		0	0.52
3	52.75	9.03	31.80	5.59		0	3.73
4	49.33	10.01	32.43	7.20		0	0
5	49.87	10.39	29.26	9.50		0.72	6.47
6	51.56	10.07	30.10	7.47		0	7.28

In this study, viscosity was measured using a vibrational method. The vibrational viscometer operates in resonance mode, allowing for viscosity measurements of melts within the range of 0.1 – 15 Pa·s. Its high sensitivity is attributed to operating on resonance oscillations, where the viscosity of the slag disrupts the resonance conditions. Achieving resonance requires the frequency of the current supplying the vibrator coil to match the natural frequency of the mechanical oscillations of the viscometer's movable system. When resonance occurs, the amplitude of the movable system's oscillations reaches maximum, inducing the maximum electromotive force in the measuring coil. The design of the vibrational viscometer used in this study was developed by Stengel-meyer [20] (refer to Fig. 2).

The principle of operation is that when the probe is immersed in the slag melt, resonance oscillation is disrupted: the higher the viscosity of the slag, the smaller the amplitude of the movable system's oscillations becomes, resulting in a smaller electromotive force in the measuring coil. Tuning the viscometer to resonance is achieved using an autogenerator. Since the measuring coil is located in the magnetic field of a ring magnet, a current is induced in it, with a frequency equal to the frequency of the oscillations of the viscometer's movable system, i.e., a current of resonance frequency appears in it. The power of these current oscillations is increased using an amplification circuit powered by a direct current source. The amplified oscillations are then reapplied to the vibrator coil, thus automatically maintaining the resonance oscillations of the viscometer.

To prevent the transmission of vibration energy from the viscometer to the support of the micropipette manipulator, the viscometer was placed on damping springs, consisting of four pairs of spiral springs. Additionally, to ensure the stability of operation of the electrodynamic sensors, the viscometer was shielded from thermal radiation.

When measuring the viscosity of melts, a 300 mm long probe made of tungsten wire with a diameter of 1.5 mm

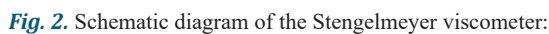
was utilized. The probe was immersed into the flux melt to a depth of 10 mm. Immersion of the probe into the studied melt was facilitated using a micrometer screw lift, upon which the viscometer was mounted. The depth of immersion was measured using the scale of the micrometer screw lift, with the starting point (contact with the melt by the probe) being fixed using the TRM-200 meter. This was achieved by detecting the signal drop relative to the movement of the probe in the air. A digital multimeter, connected in parallel to the measuring coil, was employed for viscosity measurement, with its readings being proportional to the amplitude and frequency of the vibrations of the measuring coil. Temperature signals and the output signal of the multimeter were automatically recorded using the two-channel TRM-200 meter. The output signal of the meter, which has an RS-485 interface, was transmitted to a computer via an OVEN AC-4 automatic converter with USB/RS-485 interface and recorded in Excel spreadsheets. Signals were continuously recorded throughout the experiment with a 1 s interval.

The calibration of the viscometer was conducted on slag containing 40 wt. % CaO, 40 wt. % SiO₂, and 20 wt. % Al₂O₃, where the viscosity of this slag at various temperatures is known [7]. This facilitated a “hot” calibration to be performed on slags with pre-known viscosity. The results of several calibrations were aggregated and overlaid on a single graph illustrating the dependence of viscosity on the signal obtained from the viscometer. Subsequently, an equation that most accurately described the obtained results was selected:

$$\eta = 2 \left(-6.263 + \frac{43.088}{\ln E} \right),$$

where η is the dynamic viscosity, Pa·s; E is the EMF recorded by the meter, mV.

The coefficients of the equation were determined by analyzing more than 20 points obtained during the calibration of the viscometer. Each point was derived



- 1 – Al₂O₃ case; 2 – resistance furnace; 3 – vibrating rod, the lower part of which is a probe; 4 – digital multimeter; 5 – shock-absorbing springs; 6 – viscometer housing; 7 – flat springs; 8 – vibrator core; 9 – annular magnet; 10 – measuring coil; 11 – digital TRM-200 meter; 12 – auto generator; 13 – armature winding; 14 – vibrator anchor; 15 – water-cooled lid; 16 – W – WRe thermo-steam; 17 – crucible with melt

1 – чехол из Al_2O_3 ; 2 – печь сопротивления; 3 – вибрирующий стержень, нижняя часть которого является зондом; 4 – мультиметр цифровой; 5 – амортизирующие пружины; 6 – корпус вискозиметра; 7 – плоские пружины; 8 – сердечник вибратора; 9 – кольцевой магнит; 10 – измерительная катушка; 11 – измеритель цифровой TPM-200; 12 – автогенератор; 13 – обмотка якоря; 14 – якорь вибратора; 15 – водоохлаждаемая крышка; 16 – W – WRe термопара; 17 – тигель с расплавом

The viscosity of homogeneous and heterogeneous slags 4 and 5 was measured (Table 2). Viscosity measurements are depicted in Figs. 3 and 4.

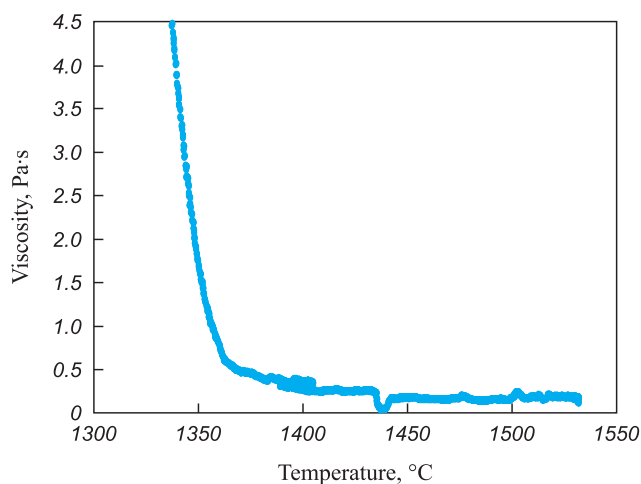


Fig. 3. Dependence of viscosity of homogeneous slag on temperature

Рис. 3. Зависимость вязкости гомогенного шлака от температуры

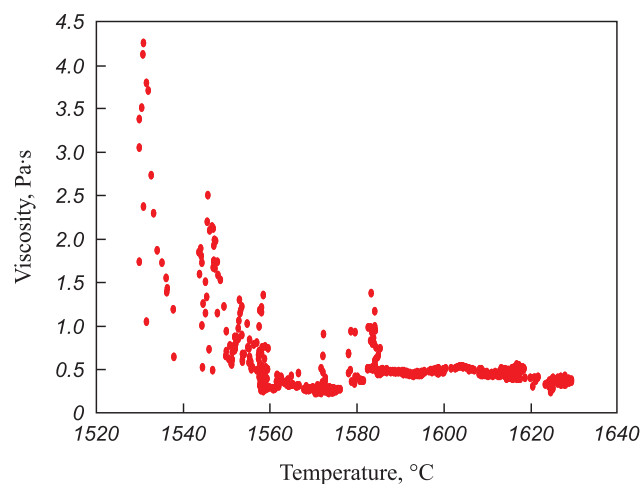


Fig. 4. Dependence of viscosity of heterogeneous slag on temperature

Рис. 4. Зависимость вязкости гетерогенного шлака от температуры

The presented data reveal the following:

- direct viscosity measurement of heterogeneous slags presents a challenge, as significant interference is introduced into the recorded signal due to the interaction between the viscometer probe and the solid slag particles;

- heterogeneous slag exhibits increased viscosity due to the presence of solid particles in its volume, even with relatively similar chemical composition parameters;

- heterogeneous slag has an elevated crystallization temperature because the undissolved particles can act as substrates during the liquid slag crystallization process. This is manifested in a shorter crystallization interval from the onset of noticeable viscosity growth to solidification (around 20 – 30 °C for heterogeneous slag compared to 60 °C for homogeneous slag).

Slag saturated with MgO and CaO oxides exhibits increased viscosity, with its solidification temperature being 200 °C higher than that of homogeneous slag. For refining processes, it is imperative to utilize high-basicity homogeneous slag.

From the comparison of the data presented in Figs. 3 and 4, it can be deduced that heterogeneous slag possesses an elevated melting temperature. The solidification temperature of homogeneous slag falls within the range of 1350 – 1370 °C, consistent with theoretical data. In contrast, the melting temperature of the presented heterogeneous slag ranges from 1560 – 1590 °C. Additionally, it is noteworthy that as the temperature of the heterogeneous slag decreases, agglomerates of solid oxides form, contacting the measuring probe and resulting in increased viscosity of the oxide system (within the temperature range of 1570 – 1590 °C).

ANALYSIS AND DISCUSSION

At the LTS site of JSC VMZ six slag samples were selected, and the content of the solid phase of CaO and MgO oxides at a temperature of 1600 °C was determined by calculation method based on the methodology presented in Fig. 1. The following results were obtained:

- slag 4 was found to be completely homogeneous, with no solid phase present;

- slag 5 contained solid phases of CaO and MgO oxides;

- slags 1–3 and 6 contained a solid phase of CaO oxide, with the amount not exceeding 10 %.

Laboratory experiments validated the adequacy of the calculation method for determining the presence of a solid phase in slags formed in the electric arc furnace. This was achieved by comparing the viscosity changes as the temperature of slags 4 and 5 decreased. It was observed that the solidifying temperature of the heterogeneous slag was 200 °C higher, despite a relatively similar composition of the slag. Additionally, it was noted that as the temperature of the heterogeneous slag decreased, coarser agglomerates of solid oxides formed, which came into contact with the measuring probe. This resulted in an increase in the registered viscosity of the oxide system within the temperature range of 1570 – 1590 °C.

CONCLUSIONS

Recently, there has been a complete abandonment of using fluorite in steel production, aimed at enhancing efficiency and environmental safety. The addition of fluorite traditionally facilitated the quick dissolution of lime and the formation of a liquid refining slag. Consequently,

ensuring optimal properties of the slag formed in the ladle furnace has become a highly relevant task. The developed method for determining the solubility limit of calcium oxide in the refining slag enables monitoring and adjustment of both the current ladle refining technology and the design of new variants.

The methodology for determining the presence of a solid phase in the slag formed in the ladle furnace was validated through laboratory experiments, where viscosity indicators of the slag were compared as the temperature decreased. It was observed that the solidification temperature of the heterogeneous slag is 200 °C higher than that of the homogeneous slag.

The calculated and experimental methods exhibited good convergence of results, with differences primarily arising in viscosity characteristics due to the presence of undissolved particles. This enables a preliminary assessment of slag properties formed in the electric arc furnace through calculation, with experimental research serving to confirm the set of slag calculations.

СПИСОК ЛИТЕРАТУРЫ / REFERENCES

1. Bigeev A.M., Bigeev V.A. Metallurgy of Steel. Theory and Technology of Steel Melting. Magnitogorsk: MSTU; 2000:544. (In Russ.).
Бигеев А.М., Бигеев В.А. Металлургия стали. Теория и технология плавки стали. Магнитогорск: МГТУ; 2000:544.
2. Fandrich R., Lungen H.-B., Wuppermann C.-D. Actual review on secondary metallurgys. *Revue de Metallurgie. Cahiers D'Informations Techniques*. 2008;105(7–8):364–374.
<https://doi.org/10.1051/metal:2008053>
3. Fandrich R., Luengen H.-B., Wuppermann C.-D. Secondary metallurgy – State of the art and research trends in Germany. *Stahl und Eisen*. 2008;128(2):45–53.
4. Cao Q., Pitts A., Nastac L. Numerical modelling of fluid flow and desulphurisation kinetics in an argon-stirred ladle furnace. *Ironmaking and Steelmaking*. 2018;45(3):280–287.
<http://doi.org/10.1080/03019233.2016.1262574>
5. Shen C., Liping W., Junbo G., Yuanwang P., Fei H. Industrial investigation of decarburization and desulphurization behaviour of 120 t new single snorkel degasser. *Ironmaking and Steelmaking*. 2020;47(7):713–721.
<http://doi.org/10.1080/03019233.2019.1580029>
6. Agapitov E.B., Lemeshko M.A., Sokolova M.S. Prospects for the use of hollow electrodes for deep desulfurization of steel in the ladle-furnace unit. *Materials Science Forum*. 2020;989:474–479.
<http://doi.org/10.4028/www.scientific.net/MSF.989.474>
7. Komolova O.A., Grigorovich K.V. Development of LF-software for modeling of refining processes in a ladle-furnace. *Journal of Physics: Conference Series*. 2019;1347:012066.
<http://doi.org/10.1088/1742-6596/1347/1/012066>
8. Metelkin A.A., Sheshukov O.Yu., Savel'ev M.V., Shevchenko O.I., Egiazar'yan D.K. On the issue of steel desulfurization of in a ladle-furnace unit. In: *Physico-Chemical Bases of Metallurgical Processes. The Int. Sci. Conf. named after Academician A.M. Samarin*. Moscow: IMET RAS; 2019:77. (In Russ.).
9. Metelkin A.A., Sheshukov O.Yu., Savel'ev M.V., Shevchenko O.I., Egiazar'yan D.K. Application of ionic theory to calculate sulfide capacity of slags. *Izvestiya. Ferrous Metallurgy*. 2021;64(2):104–111. (In Russ.).
<https://doi.org/10.17073/0368-0797-2021-2-104-111>
10. Savelyev M.V., Sheshukov O.Y., Egiazar'yan D.K., Metelkin A.A., Shevchenko O.I. Calculation of sulfur removal in ladle furnace unit by means of ionic theory of slags. In: *IOP Conference Series: Materials Science and Engineering*. 2020;966:012068.
<http://dx.doi.org/10.1088/1757-899X/966/1/012068>
11. Sommervil' I.D. Measurement, forecast and application of metallurgical slag tanks. In: *Injection Metallurgy '86*. Moscow: Metallurgiya; 1990:107–120. (In Russ.).
Соммервилль И.Д. Измерение, прогноз и применение емкостей металлургических шлаков / Пер. с англ. В кн.: *Инжекционная металлургия '86*. Москва: Металлургия; 1990:107–120.
12. Yavoiskii V.I., Kryakovskii Yu.V., Grigor'ev V.P., Nchkin Yu.M., Kravchenko V.F., Borodin D.I. Metallurgy of Steel. Moscow: Metallurgiya; 1983:584. (In Russ.).
Металлургия стали / В.И. Явойский, Ю.В. Кряковский, В.П. Григорьев, Ю.М. Нечкин, В.Ф. Кравченко, Д.И. Бородин. Москва: Металлургия; 1983:584.
13. Metelkin A.A., Sheshukov O.Y., Nekrasov I.V., Shevchenko O.I. Improving the Durability of Lining of Ladle-Furnace Units. *Nizhny Tagil: NTI (branch) UrFU*; 2015;144. (In Russ.).
Повышение стойкости футеровки агрегатов внепечной обработки стали / А.А. Метелкин, О.Ю. Шешуков, И.В. Некрасов, О.И. Шевченко. Нижний Тагил: НТИ (филиал) УрФУ; 2015;144.
14. Povolotskii D.Ya. Physico-Chemical Bases of Steelmaking. Chelyabinsk: SUSU; 2006;183.
Поволоцкий Д.Я. Физико-химические основы процессов производства стали. Челябинск: изд. ЮУрГУ; 2006;183.
15. Socha L., Hudzieczek Z., Michalek K., Pilka V., Piegza Z. Verification of physical modelling of steel desulphurization in the plant conditions of the homogenization station. In: *METAL 2014 – 23rd Int. Conf. on Metallurgy and Materials, Conference Proceedings*. 2014:64–71.
16. Socha L., Bažan J., Gryc K., Morávka J., Styrnal P., Pilka V., Piegza Z. Optimisation of the slag mode in the ladle during the steel processing of secondary metallurgy. *Materiali in Tehnologije*. 2013;47(5):673–678.
17. Sheshukov O.Yu., Nekrasov I.V., Metelkin A.A., Lozovaya E.Yu., Shevchenko O.I., Savel'ev M.V. Modern Steel: Theory and Technology: Textbook. Nizhny Tagil: NTI (branch) UrFU; 2020:400. (In Russ.).
Современная сталь: теория и технология: учебное пособие / О.Ю. Шешуков, И.В. Некрасов, А.А. Метелкин,

- Е.Ю. Лозовая, О.И. Шевченко, М.В. Савельев. Нижний Тагил: НТИ (филиал) УрФУ; 2020:400.
18. Novikov V.K., Nevidimov V.N. Polymeric Nature of Molten Slags. Yekaterinburg: UGTU – UPI; 2006:62. (In Russ.).
Новиков В.К., Невидимов В.Н. Полимерная природа расплавленных шлаков. Екатеринбург: изд. ВПО УГТУ – УПИ; 2006:62.
 19. Sheshukov O.Y., Mikheenkoy M.A., Nekrasov I.V., etc. Issues of Utilization of Refining Slags of Steelmaking Production. Nizhny Tagil: NTI (branch) UrFU; 2015:144. (In Russ.).
Вопросы утилизации рафинировочных шлаков сталеплавильного производства / О.Ю. Шешуков, М.А. Михеенков, И.В. Некрасов и др. Нижний Тагил: НТИ (филиал) УрФУ; 2015:144.
 20. Shtengel'meyer S.V. Electromagnetic vibration viscometer. *Zavodskaya laboratoriya*. 1964;(2):238–239. (In Russ.).
Штенгельмейер С.В. Электромагнитный вибрационный вискозиметр. *Заводская лаборатория*. 1964;(2):238–239.

Information about the Authors

Сведения об авторах

Vladimir A. Murysev, Chief Specialist of the Engineering and Technology Center, JSC "Vyksa Metallurgical Plant"

E-mail: murysev_va@vsw.ru

Oleg Yu. Sheshukov, Dr. Sci. (Eng.), Prof., Director of the Institute of New Materials and Technologies, Ural Federal University named after the first President of Russia B.N. Yeltsin; Chief Researcher of the Laboratory of Technogenic Formations Problems, Institute of Metallurgy, Ural Branch of the Russian Academy of Sciences

E-mail: o.j.sheshukov@urfu.ru

Vladimir M. Safonov, Dr. Sci. (Eng.), Prof. of the Chair of Electrometallurgy, Vyksa Branch of the National University of Science and Technology "MISIS"

E-mail: wmsafonov@gmail.com

Sergei A. Somov, Head of the Department of the Engineering and Technology Center, JSC "Vyksa Metallurgical Plant"

E-mail: somov_sa@vsw.ru

Anatolii A. Metelkin, Cand. Sci. (Eng.), Assist. Prof. of the Chair of Metallurgy of Iron and Alloys of the Institute of New Materials and Technologies, Ural Federal University named after the first President of Russia B.N. Yeltsin

E-mail: anatoliy82@list.ru

Denis K. Egiazar'yan, Cand. Sci. (Eng.), Assist. Prof. of the Chair of Metallurgy of Iron and Alloys of the Institute of New Materials and Technologies, Ural Federal University named after The First President of Russia B.N. Yeltsin; Senior Researcher, Head of the Laboratory of Technogenic Formations Problems, Institute of Metallurgy, Ural Branch of the Russian Academy of Sciences

ORCID: 0000-0002-9833-7191

E-mail: avari@mail.ru

Владимир Александрович Мурысев, главный специалист Инженерно-технологического центра, АО «Выксунский металлургический завод»

E-mail: murysev_va@vsw.ru

Олег Юрьевич Шешуков, д.т.н., профессор, директор Института новых материалов и технологий, Уральский федеральный университет имени первого Президента России Б.Н. Ельцина, главный научный сотрудник лаборатории Проблем техногенных образований, Институт металлургии Уральского отделения РАН

E-mail: o.j.sheshukov@urfu.ru

Владимир Михайлович Сафонов, д.т.н., профессор кафедры электрометаллургии, Выксунский филиал НИТУ «МИСиС»

E-mail: wmsafonov@gmail.com

Сергей Александрович Сомов, начальник отдела Инженерно-технологического центра, АО «Выксунский металлургический завод»

E-mail: somov_sa@vsw.ru

Анатолий Алексеевич Метелкин, к.т.н., доцент кафедры металлургии железа и сплавов Института новых материалов и технологий, Уральский федеральный университет имени первого Президента России Б.Н. Ельцина

E-mail: anatoliy82@list.ru

Денис Константинович Егиазарьян, к.т.н., доцент кафедры металлургии железа и сплавов Института новых материалов и технологий, Уральский Федеральное Университет имени первого Президента России Б.Н. Ельцина, заведующий лабораторией Проблем техногенных образований, старший научный сотрудник, Институт металлургии Уральского отделения РАН

ORCID: 0000-0002-9833-7191

E-mail: avari@mail.ru

Contribution of the Authors

Вклад авторов

V. A. Murysev – selection of industrial slags, analysis of laboratory tests, writing the text.

O. Yu. Sheshukov – formulation of the research problem, editing the text.

V. M. Safonov – formulation of the research problem, editing the text.

S. A. Somov – selection of industrial slags, analysis of laboratory tests.

A. A. Metelkin – summarising the results of laboratory and industrial tests, writing the text.

D. K. Egiazar'yan – carrying out laboratory tests, discussion of the results, writing the text.

В. А. Мурысев – отбор промышленных шлаков, анализ лабораторных испытаний, написание статьи.

О. Ю. Шешуков – постановка задачи исследований, редактирование статьи.

В. М. Сафонов – постановка задачи исследований, редактирование статьи.

С. А. Сомов – отбор промышленных шлаков, анализ лабораторных испытаний.

А. А. Метелкин – обобщение результатов лабораторных и промышленных испытаний, написание статьи.

Д. К. Егиазарьян – проведение лабораторных испытаний, обсуждение полученных результатов, написание статьи.

Received 08.11.2023

Revised 19.02.2024

Accepted 20.02.2024

Поступила в редакцию 08.11.2023

После доработки 19.02.2024

Принята к публикации 20.02.2024



UDC 669.162.221.2

DOI 10.17073/0368-0797-2024-2-148-154



Original article

Оригинальная статья

ESTIMATION OF ACCIDENT RATE OF BLAST FURNACE TUYERES

T. S. Stuk[✉], E. P. Pototskii

National University of Science and Technology “MISIS” (4 Leninskii Ave., Moscow 119049, Russian Federation)

✉ lazareva.ts@isis.ru

Abstract. In modern blast furnace production, even a short-term disruption of the technological process is associated with large productivity losses. In the practice of conducting blast furnace melting, there are often significant deviations from the optimal mode. They can lead not only to disruptions of the blast furnace, but also to accidents. In the operation of a blast furnace, typical deviations from the normal distribution of gas flow and charge materials include: peripheral, axial, channel passages; skewing of the backfill level; varying degrees and types of charge suspension. As a result, there are a cooling or excessive overheating of the furnace and violation of the melting operation. A serious consequence of the prolonged peripheral movement of gases is not only intensive wear of the lining, poor use of thermal and chemical energy of gases, but also stable cluttering of the hearth with formation of a deadman. Deadman is an ore-coke sinter formed in the tuyere zone of a blast furnace, as a result of cooling of its center. The paper describes the study and analysis of violations of blast furnace operation, analysis of the deadman causes and assessment of the accident rate of blast furnace tuyeres. Violation of gas distribution and hearth cluttering lead to formation of a deadman, which provokes mass burning of tuyeres and blast furnace refrigerators. The developed methodological foundations (mathematical model) allow us to estimate the maximum temperature of the tuyere zone and the resulting heat flow to the tuyere toe in presence of a deadman. It is shown that in large-volume blast furnaces, bubble outflow of the gas-coal flow prevails, contributing to growth of a deadman in the blast furnace.

Keywords: ferrous metallurgy, blast furnace production, blast furnace, tuyere, deadman, tuyere zone, temperature increase, resulting heat flow, burnout

For citation: Stuk T.S., Pototskii E.P. Estimation of accident rate of blast furnace tuyeres. *Izvestiya. Ferrous Metallurgy*. 2024;67(2):148–154.
<https://doi.org/10.17073/0368-0797-2024-2-148-154>

ОЦЕНКА АВАРИЙНОСТИ ДОМЕННЫХ ФУРМ

Т. С. Стук[✉], Е. П. Потоцкий

Национальный исследовательский технологический университет «МИСИС» (Россия, 119049, Москва, Ленинский пр., 4)

✉ lazareva.ts@isis.ru

Аннотация. В современном доменном производстве даже кратковременное нарушение технологического процесса связано с большими потерями производительности. В практике ведения доменной плавки нередко встречаются значительные отклонения от оптимального режима. Они могут приводить не только к расстройкам хода доменной печи, но и к авариям. В работе доменной печи к типичным отклонениям от нормального распределения потока газа и шихтовых материалов относят: периферийный, осевой, каналный ходы; перекося уровня засыпи; различной степени и вида подвеса шихты. Вследствие этого происходят похолодание или излишний перегрев печи, нарушение ровности хода. Тяжелым последствием длительного периферийного движения газов являются не только интенсивный износ кладки, слабое использование тепловой и химической энергии газов, но и стабильное загромождение горна с образованием тотермана. Тотерман – это рудно-коксый спек, образующийся в фурменной зоне доменной печи в результате похолодания ее центра. Данная работа посвящена исследованию и анализу нарушений работы доменной печи, анализу причин возникновения тотермана, оценке аварийности фурм доменной печи. Нарушение газораспределения и загромождение горна приводят к образованию тотермана, который провоцирует массовое горение фурм и холодильников доменной печи. Разработанные методические основы (математическая модель) позволяют оценить максимальную температуру фурменной зоны и результирующий тепловой поток на носок фурмы при наличии тотермана. Показано, что в доменных печах большого объема преобладает пузырьковый поток истечения газо-угольного потока, способствующий росту тотермана доменной печи.

Ключевые слова: черная металлургия, доменное производство, доменная печь, фурма, тотерман, фурменная зона, повышение температуры, результирующий тепловой поток, прогар

Для цитирования: Стук Т.С., Потоцкий Е.П. Оценка аварийности доменных фурм. *Известия вузов. Черная металлургия*. 2024;67(2): 148–154. <https://doi.org/10.17073/0368-0797-2024-2-148-154>

INTRODUCTION

As of today, the industrial safety policy of metallurgical companies is based on the assertion that accidents and emergencies at production facilities can be prevented. Therefore, to prevent accidents at enterprises, various methods for hazard analysis and risk assessment are actively implemented and used.

Despite the trend towards reducing the number of accidents, the frequency of incidents in metallurgical production remains consistently high. The number of accidents ranges from 4 to 9 annually, but their distribution across different metallurgical production processes varies¹ (Fig. 1). The most hazardous processes include blast furnace, oxygen converter, electric furnace steelmaking, and coke-chemical productions.

The most severe types of accidents in blast furnace production involve the removal of pig iron and/or slag from metallurgical units, breakthrough of the hearth, refrigerators, and air ducts of blast furnaces, as well as explosions in metallurgical units caused by the supply of charge materials and tuyere burnouts [1; 2].

According to the 2020 report by PJSC NLMK, blast furnace tuyeres failed more than 200 times (Fig. 2). Fig. 3 presents the statistics of blast furnace tuyere failures as a percentage.

Typical deviations from the normal distribution of gas flow and charge materials include peripheral, axial, and channel passages; skewing of the backfill level; and various degrees and types of charge suspension, including the so-called “tight” run [3; 4]. Consequently, the furnace may experience cooling or excessive overheating, overloading of the axial zone with mineral charge,

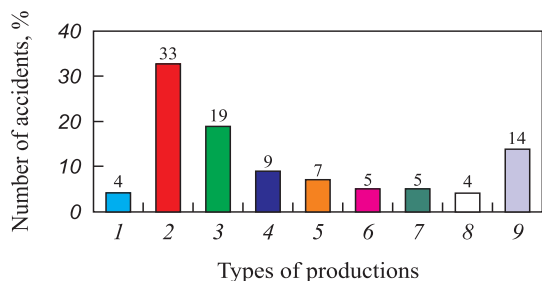


Fig. 1. Distribution of accidents by type of production:

1 – agglomeration; 2 – blast furnace; 3 – oxygen converter; 4 – coke-chemical; 5 – foundry; 6 – oxygen production; 7 – rolling; 8 – ferroalloy; 9 – electric furnace steelmaking

Рис. 1. Распределение аварий по видам производств:

1 – агломерационное; 2 – доменное; 3 – кислородно-конвертерное; 4 – коксохимическое; 5 – литейное; 6 – производство кислорода; 7 – прокатное; 8 – ферросплавное; 9 – электросталеплавильное

¹ Annual Report on the Activities of the Federal Service for Environmental, Technological, and Nuclear Supervision for the period from 2010 to 2020. URL: https://www.gosnadzor.ru/public/annual_reports/ (accessed on: January 25, 2024).

and violation of the melting operation. These conditions can lead to the cluttering of the hearth and frequent burning of the air tuyeres. Prolonged channel passages result in uneven burnout of the profile or stagnation of charge materials, leading to the formation of accretions [5].

Hearth cluttering in blast furnaces adversely affects the thermal mode, necessitating a reduction in ore loads. In the hearth, significant amounts of graphite form at lower temperatures [6]. The heating of the hearth deteriorates due to the formation of peripheral passages, as there is a decrease in heating when unprepared charge material is loaded [4]. Cold ferri-ferrous slag forms on the tuyeres.

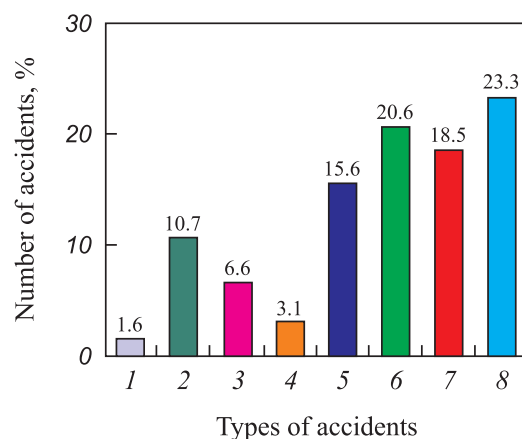


Fig. 2. Main types of accidents:

1 – rupture of blast furnace jacket; 2 – rupture of large diameter pipelines; 3 – explosion in metallurgical units; 4 – building collapse; 5 – fire; 6 – removal of cast iron and/or slag from metallurgical units; 7 – breakthrough of the hearth, refrigerators, air ducts of blast furnace; 8 – explosion in metallurgical units due to supply of raw charge and tuyeres burnout

Рис. 2. Основные виды аварий:

1 – разрыв кожуха доменной печи; 2 – разрыв трубопроводов большого диаметра; 3 – взрыв в металлургических агрегатах; 4 – обрушение здания; 5 – пожар; 6 – уход чугуна и/или шлака из металлургических агрегатов; 7 – прорывы горна, холодильников, воздухопроводов доменной печи; 8 – взрывы в металлургических агрегатах из-за подачи сырой шихты и прогара фурм

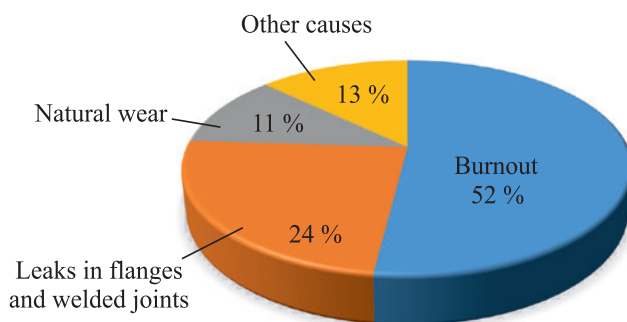


Fig. 3. Failure statistics of blast furnace tuyeres

Рис. 3. Статистика отказов доменных фурм

The infiltration of water vapor into the hearth through burnouts of cooling equipment is further exacerbated by the overloading of the low-mobility zone in the presence of low kinetic energy [7]. This deviation leads to the cluttering process in the tuyere belt of the blast furnace. As the cluttering zone expands, the burning of tuyere connections intensifies, as depicted in Fig. 4.

A severe disruption of the smelting process is the clogging of the hearth [4; 8]. It contributes to the deterioration of the gas dynamics of the process and significantly reduces the working space of the iron receiver. This hinders the movement of molten iron in the hearth and clogs the space in front of the tuyere nose. When the center of the blast furnace hearth cools, coke and slag begin to compress into a monolith due to the fine fraction of the charge material [9; 10]. This leads to poor filtration in the hearth, thus making it difficult for the smelting products to flow into the blast furnace iron receiver.

Despite the numerous developed and applied methods for assessing the risk of accidents in blast furnace production, a methodology is needed that can account for the specific operational characteristics of the blast furnace, considering the formation of the deadman in the tuyere zone and the increase in temperature in the tuyere zone with subsequent tuyere burnout, etc. Therefore, improving the methodology for assessing the accident risk of blast furnace tuyeres, taking into account the formation of the deadman, is currently a relevant task.

DESCRIPTION OF THE RESEARCH METHOD

A significant contribution to the study of tuyere zone cluttering has been made by the National University of Science and Technology MISiS (NUST MISiS)

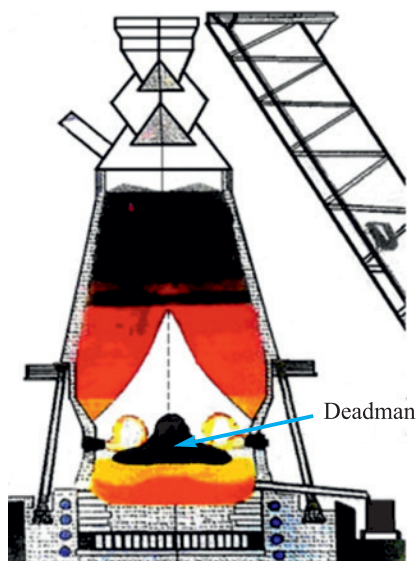


Fig. 4. Hearth cluttering with ore-coke sinter

Рис. 4. Процесс загромождения горна рудно-коксовым спеком

through the efforts of Zherebin B.N., Vegman E.F., Parenkov A.E., and others [1; 11]. It is known that large-volume blast furnaces (Blast Furnace No. 5 of the Kryvorizhstal plant) are prone to the formation of large scabs, including ore-coke sinter, in the central part of the hearth. The boulder-like formation (deadman), with its peak reaching the level of the bosh, consists of refractory carbides and carbonitrides. The deadman obstructs normal gas distribution and promotes the formation of a peripheral flow in the blast furnace [12; 13]. The tuyere blast reflects off the surface of the deadman onto the furnace lining and hearth refractory. This leads to a deterioration in the durability of the refractory and contributes to an emergency situation due to the breakthrough of high-temperature smelting products in the blast furnace.

This work proposes a methodology for assessing the accident rate of blast furnace tuyeres under the influence of a deadman.

In blast furnaces, two stable hydrodynamic outflow modes are realized: jet and bubble [14; 15]. The jet mode of flow is characteristic of normal gas distribution in the blast furnace, whereas the bubble mode of flow promotes the growth of the deadman.

The value of the Glinkov criterion G_n is determined by the formula

$$G_n = \frac{\rho_g w_g^2}{\rho_j g h_j}, \quad (1)$$

where ρ_g is the effective density of the flow, kg/m³; w_g is the gas velocity at the tuyere exit, m/s; ρ_j is the density of the melt in the tuyere zone, kg/m³; g is the acceleration due to gravity, m/s²; and h_j is the distance from the tuyere axis to the melt, m.

The effective density of the flow is calculated using the formula

$$\rho_g = Q_{\text{air}} \rho_{\text{hb}} + Q_{\text{ng}} \rho_{\text{ng}} + Q_{\text{coal}} \rho_{\text{coal}}, \quad (2)$$

where Q_{air} , Q_{ng} , Q_{coal} are the volumetric fractions of “air + oxygen,” natural gas, and pulverized coal; ρ_{hb} , ρ_{ng} , ρ_{coal} are the densities of hot blast, injected natural gas, and pulverized coal.

The density of the hot blast is calculated using the formula

$$\rho_{\text{hb}} = \rho_0 \frac{PT_0}{P_0 T_b}, \quad (3)$$

where ρ_{hb} is the density of the hot blast, kg/m³; ρ_0 is the density of air under normal conditions, kg/m³; P is the pressure of the hot blast, atm; P_0 is the atmospheric pressure, atm; T_0 is the ambient temperature, K; T_b is the blast temperature, K.

Density of the injected natural gas is determined using the formula

$$\rho_{ng} = \rho_0^{ng} \frac{P}{P_0}, \quad (4)$$

where ρ_0^{ng} is the density of natural gas, kg/m³.

If the Glinkov criterion is less than one, a bubble mode is present; if the Glinkov criterion exceeds three, the flow mode is jet. Intermediate values indicate a transitional flow mode.

The heat transfer from the deadman primarily occurs through radiation and convection. To calculate the resultant heat flow to the tuyere nose, it is necessary to determine the temperature of the internal blowing zone and the hydrodynamic blowing mode of the blast furnace. The temperature of the blowing zone corresponds to the surface temperature of the deadman [1].

The surface temperature of the deadman T_t can be calculated from the heat balance equation using the formula [16]

$$T_t = \frac{0.165T_f V_{bost}}{d_h^3} + 2.445(B - 483) + 2.91(T_j - 107) - 11.2(\eta_{CO} - 27.2) + 28.9(d_{proke} - 25.8) + 326, \quad (5)$$

where T_f is the theoretical combustion temperature, °C; V_{bost} is the volume of gas in the bosh, mm³/min; d_h is the diameter of the hearth, m; B is the fuel consumption, kg/t; T_j is the index of slag fluidity; η_{CO} is the CO content in the furnace center (from the shaft); d_{proke} is the diameter of coke particles in the deadman, mm.

The index of slag fluidity (T_j) is calculated using the formula

$$T_j = T_{mi} - \left\{ 342 \left(\frac{CaO}{SiO_2} \right) + 11.0[(Al_2O_3) + 1.4] + 819 \right\}, \quad (6)$$

where T_{mi} is the temperature of the molten iron, °C; $\left(\frac{CaO}{SiO_2} \right)$ is the basicity of the slag; and (Al_2O_3) concentration of Al_2O_3 in the slag, %.

The size of the blowing zone, i.e., the zone where the horizontal gas-liquid flow and the reaction zone are located, is determined using the formula

$$l_{bz} = 5.44d_0 \left(G_n \frac{H_0}{d_0} \right)^{0.24}, \quad (7)$$

where l_{bz} is the length of the blowing zone, m; H_0 is the height of the liquid bath, m; d_0 is the inner diameter of the tuyere nose, m.

The effective emissivity of the tuyere nose is calculated using the formula

$$\varepsilon_{ef} = \frac{1}{1 + \left(\frac{1}{\varepsilon_l} - 1 \right) \frac{S}{S_l}}, \quad (8)$$

where ε_{ef} is the effective emissivity of the tuyere nose; ε_l is the emissivity of the tuyere nose (assumed to be 0.6); S_l is the area of the inner surface of the blowing zone, m; S is the area of the metal casing of the tuyere nose, m².

The area of the metal casing of the tuyere nose S is determined using the formula

$$S = 0.785(d_n^2 - d_0^2), \quad (9)$$

where d_n is the outer diameter of the tuyere nose, m; d_0 is the inner diameter of the tuyere nose, m.

The area of the inner surface of the blowing zone S_l is calculated using the formula

$$S_l = \pi d_n l_{bz}, \quad (10)$$

where l_{bz} is the length of the blowing zone, m.

The resultant heat flow q^p to the tuyere nose [13] is calculated using the Stefan-Boltzmann law:

$$q^p = \varepsilon_{ef} \sigma (T_t^4 - T_l^4), \quad (11)$$

where ε_{ef} is the effective emissivity of the tuyere nose; σ is the Stefan-Boltzmann constant, equal to $5.67 \cdot 10^{-8}$ W/(m²·K⁴); T_t is the surface temperature of the deadman, K; T_l is the temperature of the multi-phase flow at the tuyere section, K.

CONDUCTED RESEARCH AND ANALYSIS OF ITS RESULTS

It is assumed that from the furnace throat to the bosh, there is a dense layer through which the ascending gases filter. The bubbling layer is located in the zone between the bosh and the hearth [15; 17]. The charge in the bubbling layer is in a liquid state. The blast streams, in addition to air, oxygen, and natural gas, carry pulverized coal particles [18]. According to Table 1, the Glinkov criterion was determined.

Using formulas (3) and (4), the values $\rho_{hb} = 0.61$ kg/m³, $\rho_{ng} = 2.08$ kg/m³ were determined. The effective density of the flow, calculated using formula (2), is 0.79 kg/m³, and the Glinkov criterion, using formula (1), is 0.27, indicating a bubble mode for the gas-coal flow in the blast furnace.

Next, the average surface temperature of the deadman was determined. The initial data for the calculation are presented in Table 2.

Using formula (6), the index of slag fluidity T_f was calculated to be 837 °C, and the surface temperature

Table 1. Initial data for calculating the Glinkov criterion

Таблица 1. Исходные данные для расчета критерия Глинкова

Title	Designation	Numerical value
Distance from the tuyere axis to the melt, m	h_j	5.8
Gas velocity at the tuyere exit, m/s	w_g	250
Blast temperature at the tuyere exit, °C	T_b	1255
Density of pulverized coal, kg/m ³	ρ_{coal}	1400
Density of air, kg/m ³	ρ_0	1.3
Hot blast pressure, atm	P	2.6
Ambient temperature, K	T_0	273
Density of natural gas, kg/m ³	ρ_0^{ng}	0.8
Air pressure, atm	P_0	1
Melt density in the tuyere zone, kg/m ³	ρ_j	3200
Acceleration due to gravity, m/s ²	g	9.8

of the deadman T_t using formula (5), was 2331 °C, which exceeds the theoretical combustion temperature by 231 °C.

To calculate the resultant heat flow on the tuyere nose of the blast furnace, we assume the following:

- the blowing zone is a cylindrical cavity with a diameter equal to the outer diameter of the tuyere;
- the surface temperature of the deadman T_t is 2331 °C;
- the output parameters of the tuyere, including the multiphase flow at this section, have a temperature T_1 of 800 °C;
- the gas flow in the blowing zone is filled with coal particles and melt droplets [18]. Radiation in this zone follows the laws of blackbody radiation.

The initial data for calculating the heat flux to the tuyere nose are presented in Table 3.

Table 3. Initial data for calculating the heat flow on tuyere toe

Таблица 3. Исходные данные для расчета теплового потока на носок фурмы

Title	Designation	Numerical value
Inner diameter of the tuyere nose, m	d_0	0.15
Outer diameter of the tuyere nose, m	d_n	0.25
Height of the liquid bath, m	H_0	5,8
Emissivity of the tuyere nose cut	ε_l	0,6
Surface temperature of the deadman, K	T_t	2573
Temperature of the multiphase flow at the tuyere section, K	T_1	1073

Table 2. Initial data for calculating the average deadman temperature

Таблица 2. Исходные данные для расчета средней температуры тотормана

Title	Designation	Numerical value
Theoretical combustion temperature, °C	T_f	2100
Volume of gas in the bosh, mm ³ /min	V_{bosh}	3.7
Diameter of the hearth, m	d_h	10.85
Fuel consumption, kg/t	B	500
CO content in the furnace center, %	η_{CO}	25 – 34
Diameter of coke particles in the deadman, mm	d_{proke}	up to 20
Temperature of molten iron, °C	T_{mi}	1250
Basicity of slag	(CaO/SiO ₂)	2 – 3
Concentration of Al ₂ O ₃ in slag, %	(Al ₂ O ₃)	6 – 10

The length of the blowing zone, determined using formula (7), is 1.43 m. The effective emissivity of the tuyere nose, calculated using formula (8), is 0.953. The area of the metal casing of the tuyere nose S , determined using formula (9), is 0.033 m², and the area of the inner surface of the blowing zone S_l using formula (10), is 1.123 m². The resultant heat flow q^p to the tuyere nose, determined using formula (12), is 2.3 MW/m².

In stationary mode (heating the tuyere), there is local contact between the tuyere nose and the pig iron. The allowable resultant flux on the tuyere nose should not exceed 2.1 MW/m² [19], indicating that further reducing the cooling water temperature for the tuyere is impractical and leads to thermal stresses. This reduction decreases the lifespan of the tuyere device and can provoke mass tuyere burnouts.

The increase in tuyere zone temperature for different volumes of blast furnaces indicates the need for additional measures to prevent tuyere burnouts. Fig. 5 shows this dependence.

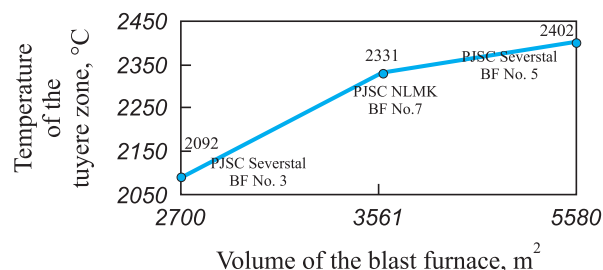


Fig. 5. Dependence of tuyere zone temperature on blast furnace volume

Рис. 5. Зависимость температуры фурменной зоны от объема доменной печи

Thus, the surface temperature of the deadman depends on the volume of the blast furnace. The temperature rise negatively impacts the safe operation of large-volume blast furnaces, increasing the likelihood of gas explosions and reducing the lifespan of tuyere devices.

Accidents involving mass tuyere burnouts are associated with intense vaporization. They are accompanied by a large amount of water entering the blast furnace [20]. The resulting steam breaches from beneath the layers of pig iron and slag cause chain-like thermal explosions.

RECOMMENDATIONS FOR PREVENTING TUYERE BURNOUT

The study proposes measures to prevent tuyere burnout depending on the volume of the blast furnace and the temperature of the tuyere zone.

For blast furnaces with a volume up to 2700 m³ and a tuyere zone temperature up to 2100 °C:

- automated analysis of retrospective data on the statistical properties of cooling water flow rate variations;
- analysis of silicon content in pig iron.

For blast furnaces with a volume of 2700 – 3500 m³ and a tuyere zone temperature of 2100 – 2300 °C:

- automated analysis of retrospective data on the statistical properties of cooling water flow rate variations;
- analysis of silicon content in pig iron;
- the nose of the air tuyere must be protected with refractory materials, including plasma spraying;
- the inner sleeve of the tuyere must be made of steel plate instead of copper, with additional lining of refractory materials.

For blast furnaces with a volume of 3500 – 5560 m³ and a tuyere zone temperature of 2300 – 2400 °C:

- automated analysis of retrospective data on the statistical properties of cooling water flow rate variations;
- analysis of silicon content in pig iron;
- the nose of the air tuyere must be protected with refractory materials, including plasma spraying;
- the inner sleeve of the tuyere must be made of steel plate instead of copper, with additional lining of refractory material;

– cooling water supply mode for the tuyere:

- a) technical water speed up to 11.6 m/s (normal water flow 4 – 5 m/s);
- b) water flow rate 30 m³/h (normal water flow 12 – 16 m³/h);
- c) water pressure 15 atm (normal water pressure 5 – 6 atm).

This regime requires the installation of high-pressure pumps and more robust equipment:

– the tuyere nose thickness should be no less than 40 – 50 mm;

– slag viscosity should not exceed 4 – 5 poise, and the loading of acidic pellets should be avoided.

CONCLUSIONS

It has been determined that the disruption of normal gas distribution and hearth cluttering leads to the formation of a blast furnace deadman, which provokes mass burning of tuyeres and refrigerators.

It is shown that in large-volume blast furnaces, the bubble flow of the gas-coal flow predominates, promoting the growth of the deadman, which can lead to increased accidents involving tuyere devices.

The proposed methodology (mathematical model) allows for the assessment of the maximum temperature of the tuyere zone and the resultant heat flow to the tuyere nose in the presence of a deadman.

Based on the calculated temperature of the tuyere zone, measures are proposed to prevent tuyere burnout depending on the volume of the blast furnace.

REFERENCES / СПИСОК ЛИТЕРАТУРЫ

1. Zharebin B.N., Paren'kov A.E. Malfunctions and Accidents in the Operation of Blast Furnaces. Novokuznetsk; 2001:275. (In Russ.).
Жеребин Б.Н., Пареньков А.Е. неполадки и аварии в работе доменных печей. Новокузнецк; 2001:275.
2. Pototskii E.P., Lazareva T.S. Analysis of stability and technological process of a blast furnace. In: "Energy-Efficient and Resource-Saving Technologies in Industry. Furnace Units. Ecology". Proceedings of the IX Int. Sci. and Pract. Conf. 2018, Moscow. Moscow: MISIS; 2018:169–173. (In Russ.).
Потоцкий Е.П., Лазарева Т.С. Анализ устойчивости и технологического процесса доменной печи. В кн.: Труды IX Международной научно-практической конференции «Энергоэффективные и ресурсосберегающие технологии в промышленности. Печные агрегаты. Экология». Москва: МИСиС; 2018:169–173.
3. Tarasov V.P., Khairtdinova O.T., Tomash A.A. On gas permeability of softening zone in conditions of blast furnace melting. *Izvestiya. Ferrous Metallurgy*. 2002;45(4):64–66. (In Russ.).
Тарасов В.П., Хайретдинова О.Т., Томаш А.А. О газопроницаемости зоны размягчения в условиях доменной плавки. *Известия вузов. Черная металлургия*. 2002;45(4):64–66.
4. Dmitriev A.N., Shumakov N.S., Leont'ev L.I., Onorin O.P. Fundamentals of Theory and Technology of Blast Furnace Melting. Yekaterinburg: UB RAS; 2005:547. (In Russ.).
Дмитриев А.Н., Шумаков Н.С., Леонтьев Л.И., Онорин О.П. Основы теории и технологии доменной плавки. Екатеринбург: УрО РАН; 2005:547.
5. Tarasov V.P., Tarasov P.V., Bykov L.V. Gas-dynamic parameters and performance indicators of blast furnaces with loading of BLT to carrier-loader. *Stal'*. 2005;(1):6–9. (In Russ.).

- Тарасов В.П., Тарасов П.В., Быков Л.В. Газодинамические параметры и показатели работы доменных печей с загрузкой БЗУ к ТЗУ. *Сталь*. 2005;(1):6–9.
6. Grigor'ev B.A., Tsvetkov F.F. Heat and Mass Transfer. Moscow: MEI; 2005:93. (In Russ.).
Григорьев Б.А., Цветков Ф.Ф. Тепломассообмен. Москва: МЭИ; 2005:93.
 7. Mastryukov B.S. Safety in Emergency Situations in Natural and Man-Made Sphere. Forecasting the Consequences. Moscow: Academy; 2015:368. (In Russ.).
Мастрюков Б.С. Безопасность в чрезвычайных ситуациях в природно-техногенной сфере. Прогнозирование последствий. Москва: ИЦ Академия; 2015:368.
 8. Hatano M.I. Influence of the method of loading the furnace profile, surface of the liquid phase on the gas flow in the blast furnace. Moscow: From Science; 2004:168.
 9. Power D.J. Web-based and model-driven decision support systems: concepts and issues. In: *AMCIS 2000, America's Conference on Information Systems*. California; 2000: 173–186.
 10. Anosov V.G., Fomenko A.P., Krutas N.V., Tsaplina T.S. On technology of blast furnace melting using pulverized coal fuel. *Metallurgiya. Naukovi pratsi ZDIA*. 2009;(20):37–43. (In Ukr.).
Аносов В.Г., Фоменко А.П., Крутас Н.В., Цаплина Т.С. О технологии доменной плавки при использовании пылеугольного топлива. *Металургия. Наукові праці ЗДІА*. 2009;(20):37–43.
 11. Vegman E.F., Zherebin B.N., Pokhvisnev A.N., Yusfin Yu.S., Kurunov I.F., Paren'kov A.E., Chernousov P.I. Ironmaking. Moscow: Akademkniga; 2004:774. (In Russ.).
Вегман Е.Ф., Жеребин Б.Н., Похвиснев А.Н., Юсфин Ю.С., Курунов И.Ф., Пареньков А.Е., Черноусов П.И. Металлургия чугуна. Москва: Академкнига; 2004:774.
 12. Gorban A.N., Zinovyev A.Y. Principal graphs and manifolds. In: *Handbook of Research on Machine Learning Applications and Trends: Algorithms, Methods, and Techniques. Chapter 2*. Hershey, PA; 2009:28–59.
<https://doi.org/10.4018/978-1-60566-766-9.ch002>
 13. Radyuk A.G., Titlyanov A.E., Sidorova T.Y. Modeling of the thermal state of air tuyeres of blast furnaces. *Izvestiya. Ferrous Metallurgy*. 2016;59(9):622–627. (In Russ.).
<https://doi.org/10.17073/0368-0797-2016-9-622-627>
 - Радюк А.Г., Титлянов А.Е., Сидорова Т.Ю. Моделирование теплового состояния воздушных фурм доменных печей. *Известия вузов. Черная Metallurgy*. 2016;59(9):622–627.
<https://doi.org/10.17073/0368-0797-2016-9-622-627>
 14. Dolinskii V.A., Nikitin L.D., Koverzin A.M., Portnov L.V., Bugaev S.F. Use of washing briquettes for improvement of the blast-furnace hearth operation. *Izvestiya. Ferrous Metallurgy*. 2013;56(2):33–36. (In Russ.).
<https://doi.org/10.17073/0368-0797-2013-2-33-36>
 - Долинский В.А., Никитин Л.Д., Коверзин А.М., Портнов Л.В., Бугаев С.Ф. Использование промывочных брикетов для улучшения работы горна доменной печи. *Известия вузов. Черная Metallurgy*. 2013;56(2):33–36.
<https://doi.org/10.17073/0368-0797-2013-2-33-36>
 15. Dai B., Long H.M., Ji Y.L., Rao J.T., Liu Y.C. Theoretical and practical research on relationship between blast air condition and hearth activity in large blast furnace. *Metallurgical Research and Technology*. 2020;117(1):113–117.
<https://doi.org/10.1051/metal/2020007>
 16. Pototskiy E. P., Lazareva T. S. Investigation of factors affecting the safety of a blast furnace operation. *CIS Iron and Steel Review*. 2022;(1):15–18.
<https://doi.org/10.17580/cisirs.2022.01.03>
 17. Song L., Xiaojie L., Qing L., Xusheng Z., Yana Q. Study on the appropriate production parameters of a gas-injection blast furnace. *High Temperature Materials and Processes*. 2020;39(1):10–25.
<https://doi.org/10.1515/htmp-2020-0005>
 18. Levitskii I.A., Radyuk A.G., Titlyanov A.E., Sidorova T.Yu. Influence of the method of natural gas supplying on gas dynamics and heat transfer in air tuyere of blast furnace. *Izvestiya. Ferrous Metallurgy*. 2018;61(5):357–363. (In Russ.).
<https://doi.org/10.17073/0368-0797-2018-5-357-363>
 - Левицкий И.А., Радюк А.Г., Титлянов А.Е., Сидорова Т.Ю. Влияние способа подачи природного газа на газодинамику и теплообмен в воздушной фурме доменной печи. *Известия вузов. Черная металлургия*. 2018;61(5):357–363.
<https://doi.org/10.17073/0368-0797-2018-5-357-363>
 19. Yasuo O. Blast Furnace Phenomena and Modelling. New York: Elsevier Applied Science; 1987:631.
 20. Feng Q., Wang L. Blast furnace hoist charging control system based on ActiveX technology. *WIT Transactions on Information and Communication Technologies*. 2014;46:1853–858.

Information about the Authors

Tat'yana S. Stuk, Leading Specialist on Occupational Safety, Postgraduate of the Chair of Technosphere Safety, National University of Science and Technology "MISIS"

E-mail: lazareva.ts@isis.ru

Evgenii P. Pototskii, Cand. Sci. (Eng.), National University of Science and Technology "MISIS"

E-mail: pep@disto.misis.ru

Сведения об авторах

Татьяна Сергеевна Стук, ведущий специалист по охране труда, аспирант кафедры техносферной безопасности, Национальный исследовательский технологический университет «МИСИС»

E-mail: lazareva.ts@isis.ru

Евгений Павлович Потоцкий, к.т.н., Национальный исследовательский технологический университет «МИСИС»

E-mail: pep@disto.misis.ru

Received 10.08.2023

Revised 17.10.2023

Accepted 11.12.2023

Поступила в редакцию 10.08.2023

После доработки 17.10.2023

Принята к публикации 11.12.2023



UDC 621.785

DOI 10.17073/0368-0797-2024-2-155-160



Original article

Оригинальная статья

INVESTIGATION OF CHANGES IN TEMPERATURE OF PRESSING TOOL DURING LASER PROCESSING

N. A. Chichenev¹, S. M. Gorbatyuk¹, K. N. Solomonov²,
S. A. Snitko³, O. N. Chicheneva¹

¹ National University of Science and Technology “MISIS” (4 Leninskii Ave., Moscow 119049, Russian Federation)

² Voronezh Branch of the Rostov State Transport University (75a Uritskogo Str., Voronezh 394026, Russian Federation)

³ Donetsk National Technical University (58 Artema Str., Donetsk, Donetsk People’s Republic 283001, Russian Federation)

✉ chich38@mail.ru

Abstract. The article is devoted to improving the wear resistance of forging tools, in particular punches for punching holes and cutting stamp dies. Low tool life leads to an increase in the cost of finished products, an increase in labor and material costs for replacing worn tools and adjusting them, a decrease in the productivity of pressing equipment and an increase in the number of defective products. A method is presented for theoretical research of solving the problem of calculating the temperature field of a stamp die tool during laser processing. A differential equation was compiled for a numerical solution of the problem. The authors proposed the modes of laser heat treatment of a punch for punching holes and a stamp die tool made of high-hardness steel. Field tests conducted in industrial conditions showed that the proposed laser heat treatment modes made it possible to increase resistance of the punch intended for punching holes by 2 – 3 times and the resistance of the stamp dies by 2.2 – 2.8 times.

Keywords: press forging, temperature field, punch, stamp die, laser

For citation: Chichenev N.A., Gorbatyuk S.M., Solomonov K.N., Snitko S.A., Chicheneva O.N. Investigation of changes in temperature of pressing tool during laser processing. *Izvestiya. Ferrous Metallurgy*. 2024;67(2):155–160. <https://doi.org/10.17073/0368-0797-2024-2-155-160>

ИССЛЕДОВАНИЕ ИЗМЕНЕНИЯ ТЕМПЕРАТУРЫ ПРЕССОВОГО ИНСТРУМЕНТА ПРИ ОБРАБОТКЕ ЛАЗЕРОМ

Н. А. Чиченев¹, С. М. Горбатьюк¹, К. Н. Соломонов²,
С. А. Снитко³, О. Н. Чиченева¹

¹ Национальный исследовательский технологический университет «МИСИС» (Россия, 119049, Москва, Ленинский пр., 4)

² Филиал Ростовского государственного университета путей сообщения в г. Воронеж (Россия, 394026, Воронеж, ул. Урицкого, 75а)

³ Донецкий национальный технический университет (Россия, Донецкая народная республика, 283001, Донецк, ул. Артема, 58)

✉ chich38@mail.ru

Аннотация. Работа посвящена повышению износостойкости кузнечно-прессового инструмента, в частности пуансонов для пробивки отверстий и вырубных штампов. Низкая стойкость инструмента приводит к повышению стоимости готовых изделий, увеличению трудовых и материальных затрат на замену изношенного инструмента и его наладку, снижению производительности прессового оборудования и повышению количества бракованной продукции. Представлена методика теоретического исследования для решения задачи по расчету температурного поля штампового инструмента при лазерной обработке. Составлено дифференциальное уравнение для численного решения поставленной задачи. Предложены режимы лазерной термообработки пуансона для пробивки отверстий и штампового инструмента из стали повышенной твердости. Натурные испытания, проведенные в промышленных условиях, показали, что рекомендованные режимы лазерной термообработки позволили повысить стойкость пуансона, предназначенного для пробивки отверстий, в 2 – 3 раза, а стойкость вырубных штампов в 2,2 – 2,8 раз.

Ключевые слова: кузнечно-прессовое производство, поле температур, пуансон, штамп, лазер

Для цитирования: Чиченев Н.А., Горбатьюк С.М., Соломонов К.Н., Снитко С.А., Чиченева О.Н. Исследование изменения температуры прессового инструмента при обработке лазером. *Известия вузов. Черная металлургия*. 2024;67(2):155–160.

<https://doi.org/10.17073/0368-0797-2024-2-155-160>

INTRODUCTION

One of the most widely used methods of cold metal working (CMW) by pressure is cold stamping [1–3], which allows for the production of high-precision parts in a wide range. Cold forming dies are used as tools for this process [4–6]. In recent years, the development of new domestic technologies aimed at improving the quality of manufactured products and reducing their cost has become highly relevant. This task can be efficiently solved by improving equipment and tools, including CMW [9; 10].

FORMULATION OF THE PROBLEM

One of the main reasons of the failure of stamping tools is the wear of their working surfaces. To improve the durability of cold metal working (CMW) tools, thermal, thermochemical, and thermomechanical treatments are applied [11–13]. These methods significantly increase the hardness of the tool's working surfaces and enhance the strength of the base metal from which the tool is made. Laser treatment is an effective method for improving the quality of CMW tools by processing their working surfaces. Laser treatment is characterized by a short exposure time to the treated surfaces and completely eliminates deformation. Only a thin surface layer of the processed part is heated when exposed to laser [14–16]. Numerous studies have shown that the thermal processes occurring during laser heating are similar to the results of heating metals by other methods. This allows for the application of classical equations of heat conduction theory to solve theoretical problems of laser processing, taking into account the specifics of laser heat treatment.

This work presents a solution to the problem of calculating the temperature field of a stamping tool when hardening its working surface using laser radiation.

METHOD OF THEORETICAL STUDY

OF TEMPERATURE FIELD DISTRIBUTION DURING LASER HARDENING

As it is known, the result of hardening tool steels [17; 18] significantly depends on distribution of the temperature field that forms during this process [19; 20]. To strengthen the surface layers, it is necessary to heat the working surface of the stamp above the austenitic transformation temperature T_a , after which it is rapidly cooled to a temperature below the pearlitic transformation temperature T_p . If a high-density laser beam is used for heat treatment, the surface layers of the tool will be heated to a temperature depending on the duration of the laser radiation and its power. After laser heating, the surface of the stamp quickly cools

down due to the transfer of heat from the heated surface to the other distant areas of the tool. Moreover, temperature of the heated areas depends on their distance from the stamp surface. The depth of the hardened layer can be estimated by studying the characteristics of the resulting temperature field [21; 22].

Let us provide a mathematical description of the temperature field for a cylindrical cutting punch (Fig. 1).

The change in temperature T over time t can be calculated by numerically solving a two-dimensional differential equation, which in a cylindrical coordinate system is given by [23–25]

$$\frac{\partial T}{\partial t} = a \left(\frac{\partial^2 T}{\partial r^2} + \frac{1}{r} \frac{\partial T}{\partial r} + \frac{\partial^2 T}{\partial z^2} \right).$$

Here, $T(r, z, t)$ is the temperature at an arbitrary point of the cutting punch at any given time t , characterized by cylindrical coordinates r and z ; a is the thermal conductivity coefficient of the material of the cutting punch; q is the power density of the external heat source (laser radiation) [26–28].

Let us define initial and boundary conditions:

– at the initial moment of deformation of the workpiece, the temperature of the cutting punch is assumed to be uniform throughout the entire volume, i.e.

$$T_0 = T(z, r, 0) = \text{const};$$

– on the free surfaces of the punch, heat exchange of convective and radiant types occurs with the environment

$$\frac{\partial T}{\partial t} = \alpha (T_{\text{surf}} - T_{\text{env}}) + \varepsilon \sigma \left[(T_{\text{surf}} - 273)^4 - (T_{\text{env}} - 273)^4 \right];$$

– radiant heat exchange occurs on the end (irradiated) surface of the punch

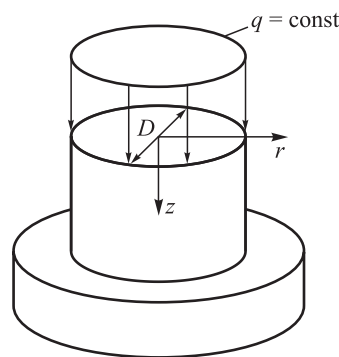


Fig. 1. Calculation scheme for temperature field of a cylindrical punch of diameter D

Рис. 1. Схема к расчету температурного поля цилиндрического пуансона диаметром D

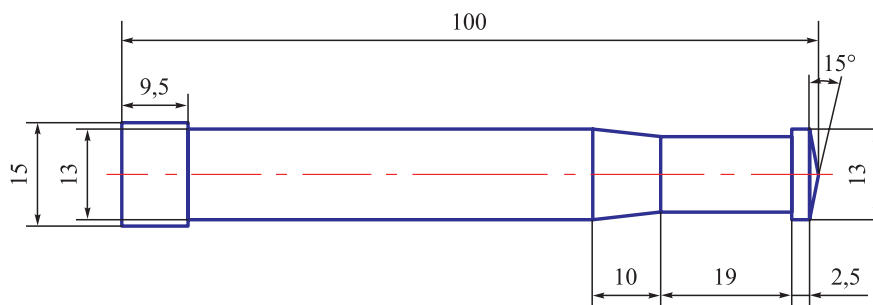


Fig. 2. Hole punch

Рис. 2. Пуансон для пробивки отверстий

$$\frac{\partial T}{\partial t} = q + \varepsilon \sigma \left[(T_{\text{surf}} - 273)^4 - (T_{\text{env}} - 273)^4 \right],$$

where α is the convective heat transfer coefficient; T_{surf} and T_{env} are the temperatures of punch surface and the environment, respectively; ε is the degree of emissivity of the punch surface; σ is the emissivity of an absolutely solid body.

EXPERIMENTAL RESULTS

According to the methodology described above, theoretical and experimental studies were conducted on a punch (Fig. 2) made of high-hardness chromium tool steel Kh12M¹ [29; 30] with a working surface diameter $D = 13$ mm.

Based on the analysis of the preliminary experiment results with samples made of Kh12M steel, which are consistent with known data from scientific and technical literature, the following thermal-physical parameters were used in further research:

- thermal conductivity coefficient $\lambda = 0.028$ W/(mm·°C);
- temperature conductivity coefficient $a = 7.78$ mm²/s;
- quenching temperature $T_q = 1000$ °C;
- melting temperature $T_m = 1280$ °C.

Fig. 3 shows the results of calculating the temperature field in axial and radial directions with $\lambda = \text{const}$ (solid lines) and $\lambda = f(T)$ (dashed lines) at a laser power of $P = 0.97$ kW, laser beam movement speed $v = 12$ mm/s, and laser spot diameter $d_{\text{sp}} = 4$ mm. Analysis of the obtained graphs shows that the difference in the punch temperature obtained with constant and variable λ values is insignificant. Therefore, when conducting engineering calculations, the average value of the thermal conductivity coefficient can be used.

ANALYSIS OF THE RESULTS

The analysis of the obtained research results served as the basis for conducting a full-scale experiment. Two experimental batches of punches and dies made of Kh12M steel were manufactured for various stamping operations. The first batch underwent traditional bulk thermal treatment, while the second batch received additional strengthening treatment using a CO₂ laser. Based on the data obtained, the following parameters of laser irradiation were recommended for efficient strengthening of the working surface of the stamping tool: with a laser spot diameter of $d_{\text{sp}} = 4$ mm, laser power $P = 0.95$ – 0.99 kW, and laser beam movement speed $v = 11$ – 13 mm/s.

Pilot tests have shown that the durability of stamping tools significantly increases after laser heat treatment. For example, the working lifespan of punching punches after traditional thermal processing is 10 – 12 h, while after additional strengthening laser treatment, the durability increased to 20 – 36 h, that is, doubled or tripled. Pilot tests of a sample batch of blanking dies, consisting of 20 pieces, demonstrated that the application of addi-

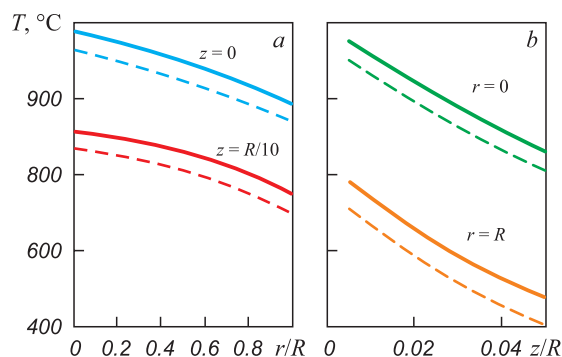


Fig. 3. Graphs of the punch temperature change in axial (a) and radial (b) directions at $\lambda = \text{const}$ (solid lines) and $\lambda = f(T)$ (dashed lines)

Рис. 3. Графики изменения температуры пуансона в осевом (a) и радиальном (b) направлении при $\lambda = \text{const}$ (сплошные линии) и $\lambda = f(T)$ (штриховые линии)

¹ Characteristics of Kh12M material / Grade Guide of steels and alloys. Available at URL: <http://www.splav-kharkov.com> (accessed 23.08.2023).

tional strengthening treatment with a CO₂ laser allows for a 2.2 – 2.8 times increase in their operational durability. The technical and economic efficiency of using laser strengthening is determined not only by saving on expensive tool steel but also by reducing labor costs due to aligning the replacement period of stamping tools with the schedule of preventive and repair works.

CONCLUSIONS

A methodology for theoretical analysis of the temperature field of a cylindrical punch formed during laser processing is proposed. The methodology is based on the numerical solution of a two-dimensional differential equation in cylindrical coordinates. As a result of the theoretical analysis, laser heat treatment modes have been proposed for stamping tools of various purposes made of Kh12M tool steel. Studies conducted in industrial conditions have shown that laser heat treatment carried out according to the proposed modes has allowed an increase in the operational durability of punches for hole punching by 2 – 3 times, and cutting dies by 2.2 – 2.8 times.

REFERENCES / СПИСОК ЛИТЕРАТУРЫ

1. Rogov V.A., Poznyak G.G. Mechanical Engineering Technology. Stamping and Foundry production: Textbook. Moscow: Yurait Publ.; 2022:319.
Рогов В.А., Позняк Г.Г. Технология машиностроения. Штамповочное и литейное производство: Учебник. Москва: Издательство Юрайт; 2022:319.
2. Konstantinov I.L., Sidel'nikov S.B. Press Forging: Textbook. Moscow: Scientific Research Center INFRA-M; 2021:464.
Константинов И.Л., Сидельников С.Б. Кузнечно-штамповочное производство: Учебник. Москва: НИЦ ИНФРА-М; 2021:464.
3. Semenov E.I. Forging and Hot Stamping: Textbook. Moscow: MSIU; 2011:414.
Семенов Е.И. Ковка и горячая штамповка: Учебник. Москва: МГИУ; 2011:414.
4. Bocharov Yu.A. Press Forging Equipment: Textbook. Moscow: Akademiya; 2008:479.
Бочаров Ю.А. Кузнечно-штамповочное оборудование: Учебник. Москва: Академия; 2008:479.
5. Zhivov L.I., Ovchinnikov A.G., Skladchikov E.N. Press Forging Equipment: Textbook. Moscow: N.E. Bauman MSTU Publ.; 2006:560.
Живов Л.И., Овчинников А.Г., Складчиков Е.Н. Кузнечно-штамповочное оборудование: Учебник / Под ред. Л.И. Живова. Москва: Изд-во МГТУ им. Н.Э. Баумана; 2006:560.
6. Efremov D.B., Stepanov V.M., Chicheneva O.N. Upgrading of the roll emergency lifting mechanism of the mill 2800 rolling stand of the JSC "Ural Steel". *Stal'*. 2020;(8):44–47. (In Russ.).
Ефремов Д.Б., Степанов В.М., Чиченева О.Н. Модернизация механизма быстрого отжима валков прокатной
7. Nefedov A.V., Svichkar V.V., Chicheneva O.N. Re-engineering of equipment to feed the melting furnace with aluminum charge. *Lecture Notes in Mechanical Engineering*. 2021: 1198–1204. https://doi.org/10.1007/978-3-030-54817-9_139
8. Nefedov A.V., Kitanov A.A., Chichenev N.A. Reengineering of the roller hardening machine of the sheet-rolling shop of JSC Ural Steel. *Chernye metally*. 2022;(3):22–26. (In Russ.).
Нефедов А.В., Китанов А.А., Чиченев Н.А. Реинжиниринг роликовой закалочной машины листопркатного цеха АО «Уральская Сталь». *Черные металлы*. 2022;(3):22–26.
9. Nefedov A.V., Tanchuk A.V., Chichenev N.A. Modernization of the tipper drive for ore trolleys at the Donskoy Mining and Processing Plant of TNK Kazchrome JSC. *Gornyi zhurnal*. 2022;(8):52–56. (In Russ.).
<https://doi.org/10.17580/gzh.2022.08.07>
Нефедов А.В., Танчук А.В., Чиченев Н.А. Модернизация привода опрокидывателя рудных вагонеток Донского ГОК АО «ТНК Казхром». *Горный журнал*. 2022;(8): 52–56. <https://doi.org/10.17580/gzh.2022.08.07>
10. Samusev S.V., Fadeev V.A., Sidorova T.Yu. Development of effective calibrations for forming blank for production of longitudinal welded pipes of small and medium diameters. *Metallurgist*. 2020;64(7–8):658–664.
<https://doi.org/10.1007/s11015-020-01042-4>
Самусев С.В., Фадеев В.А., Сидорова Т.Ю. Разработка эффективных калибровок формовки листовой заготовки для производства прямошовных электросварных труб малого и среднего диаметров. *Металлург*. 2020;(7):55–59.
11. Gorbatyuk S.M., Morozova I.G., Naumova M.G. Development of the working model of production reindustrialization of die steel heat treatment. *Izvestiya. Ferrous Metallurgy*. 2017;60(5):410–415. (In Russ.).
<https://doi.org/10.17073/0368-0797-2017-5-410-415>
Горбатюк С.М., Морозова И.Г., Наумова М.Г. Разработка рабочей модели процесса реиндустриализации производства термической обработки штамповых сталей. *Известия вузов. Черная металлургия*. 2017;60(5):410–415. <https://doi.org/10.17073/0368-0797-2017-5-410-415>
12. Metallurgy and Heat Treatment of Steel and Cast Iron: Reference Book. In 3 vols. T. 3. Thermal and Thermomechanical Processing of Steel and Cast Iron / Rakhshadt A.G., Kaputkina L.M., Prokoshkina S.D., Supova A.V. eds. Moscow: Internet Engineering; 2007:919.
Металловедение и термическая обработка стали и чугуна: справочник. В 3-х т. Т. 3. Термическая и термомеханическая обработка стали и чугуна / Под ред. Рахштадта А.Г., Капуткиной Л.М., Прокошкина С.Д., Супова А.В. Москва: Интернет Инжиниринг; 2007:919.
13. Steniko A., Tami V. Improvement of direct hardening process at the Nucor Tuscaloosa plant. *Chernye metally*. 2018;(12):41–43. (In Russ.).
Стенико А., Тами В. Совершенствование процесса прямой закалки на заводе компании Nucor Tuscaloosa. *Черные металлы*. 2018;(12):41–43.
14. Chichenev N.A., Gorbatyuk S.M., Naumova M.G., Morozova I.G. Using the similarity theory to describe laser hardening processes. *CIS Iron and Steel Review*. 2020;19:44–47.

15. Grigor'yants A.G., Shiganov I.N., Misyurov A.I. *Technological Processes of Laser Processing: Tutorial*. Moscow: N.E. Bauman MSTU Publ.; 2006:663.
Григорьянц А.Г., Шиганов И.Н., Мисюров А.И. *Технологические процессы лазерной обработки: Учебное пособие*. Москва: Изд-во МГТУ им. Н.Э. Баумана; 2006:663.
16. *Laser Technologies for Materials Processing: Modern Problems of Fundamental Research and Applied Developments*. Panchenko V.Ya. ed. Moscow: FIZMATLIT; 2009:664.
Лазерные технологии обработки материалов: современные проблемы фундаментальных исследований и прикладных разработок / Под ред. В.Я. Панченко. Москва: ФИЗМАТЛИТ; 2009:664.
17. Milenin A., Petrov P., Petrov M., Krutina E. Numerical model of fracture in magnesium alloys during forming processes. *Steel Research International*. 2012;(SPL. ISSUE):847–850.
18. Maksimov E.A., Shatalov R.L., Krutina E.V. Procedures for calculation of deformation and energy-power parameters for combined rotary drawing and cross rolling of wheel disks. *Proizvodstvo prokata*. 2019;(10):9–14. (In Russ.).
Максимов Е.А. Шаталов Р.Л., Крутина Е.В. Методика расчета деформационных и энергосиловых параметров при совмещенной ротационной вытяжке и поперечной прокатке дисков колес. *Производство проката*. 2019;(10):9–14.
19. Kiani-Rashid A.R., Rounaghi S.A. The new methods of graphite nodules detection in ductile cast iron. *Materials and Manufacturing Processing*. 2011;26(2):242–248.
<https://doi.org/10.1080/10426914.2010.520788>
20. Di Cocco V., Iacoviello F., Cavallini M. Damaging micro-mechanisms characterization of a ferritic ductile cast iron. *Engineering Fracture Mechanics*. 2010;77(11):2016–2023.
<https://doi.org/10.1016/j.engfracmech.2010.03.037>
21. Chaus A.S., Sojka J., Pokrovskii A.I. Effect of hot plastic deformation on microstructural changes in cast iron with globular graphite. *The Physics of Metals and Metallography*. 2013; 114(1):84–95. <https://doi.org/10.1134/S0031918X13010031>
22. Zhao X., Jing T.F., Gao Y.W., Qiao G.Y., Zhou J.F., Wang W. Morphology of graphite in hot compressed nodular iron. *Journal of Materials Science*. 2004;39(19):6093–6096.
<https://doi.org/10.1023/B:JMSC.0000041709.60100.56>
23. Carslaw H.S., Jaeger J.C. *Conduction of Heat in Solids*. London: Oxford University Press; 1947.
Карслоу Г., Егер Д. *Теплопроводность твердых тел*. Москва: Наука; 1964:487.
24. Tikhonov A.N., Samarskii A.A. *Equations of Mathematical Physics: Textbook*. Moscow: M.V. Lomonosov MSU; 2004:800.
Тихонов А.Н., Самарский А.А. *Уравнения математической физики: учебник*. Москва: МГУ им. М.В. Ломоносова; 2004:800.
25. Thambynayagam R. K. M. *The Diffusion Handbook: Applied Solutions for Engineers*. McGraw-Hill Professional; 2011:2048.
26. Tkachenko L.A., Repina A.V. *Heat Transfer Theory: Tutorial*. Kazan: Kazan University Publ.; 2017:151.
Ткаченко Л.А., Репина А.В. *Теория теплообмена: Учебное пособие*. Казань: Изд-во Казанского университета; 2017:151.
27. Ushakov I.V. Method of mechanical testing of laser treated metallic glass by indenters with different geometry. *Proceedings of SPIE – The International Society for Optical Engineering*. 2007;6597:659714. <https://doi.org/10.1117/12.726773>
28. Shinkaryov A.S., Ozherelkov D.Yu., Pelevin I.A., Eremin S.A., Anikin V.N., Burmistrov M.A., Chernyshikhin S.V., Gromov A.A., Nalivaiko A.Yu. Laser fusion of aluminum powder coated with diamond particles via selective laser melting: powder preparation and synthesis description. *Coatings*. 2021;11(10):1219.
<https://doi.org/10.3390/coatings11101219>
29. Ganzulenko O.Y., Petkova A.P. Simulation and approbation of the marking laser process on metal materials. *Journal of Physics: Conference Series*. 2021;1753(1):012016.
<https://doi.org/10.1088/1742-6596/1753/1/012016>
30. Pichuev A.V., Petrov V.L. Equivalent circuit for mine power distribution systems for the analysis of insulation leakage current. *Mining Science and Technology (Russia)*. 2023;8(1):78–86. (In Russ.).
<https://doi.org/10.17073/2500-0632-2023-01-72>
Пичуев А.В., Петров В.Л. Обоснование схемы замещения шахтной подземной электрической сети для анализа режимов утечки тока через изоляцию. *Горные науки и технологии*. 2023;8(1):78–86.
<https://doi.org/10.17073/2500-0632-2023-01-72>
31. Zhang Y.Q., Jiang S.Y., Zhao Y.N., Shan D.B. Isothermal precision forging of complex-shape rotating disk of aluminum alloy based on processing map and digitized technology. *Materials Science and Engineering: A*. 2013;580:294–304.
<https://doi.org/10.1016/j.msea.2013.05.059>
32. Zheng J.H., Lin J.G., Lee J., Pan R., Li C., Davies C.M. A novel constitutive model for multi-step stress relaxation ageing of a pre-strained 7xxx series alloy. *International Journal of Plasticity*. 2018;106:31–47.
<https://doi.org/10.1016/j.ijplas.2018.02.008>

Information about the Authors

Сведения об авторах

Nikolai A. Chichenev, Dr. Sci. (Eng.), Prof. of the Chair “Engineering of Technological Equipment”, National University of Science and Technology “MISIS”

ORCID: 0000-0002-9019-4675

E-mail: chich38@mail.ru

Sergei M. Gorbatyuk, Dr. Sci. (Eng.), Prof. of the Chair “Engineering of Technological Equipment”, National University of Science and Technology “MISIS”

ORCID: 0000-0002-4368-5965

E-mail: sgor02@mail.ru

Николай Алексеевич Чиченев, д.т.н., профессор кафедры инженеринга технологического оборудования, Национальный исследовательский технологический университет «МИСИС»

ORCID: 0000-0002-9019-4675

E-mail: chich38@mail.ru

Сергей Михайлович Горбатюк, д.т.н., профессор кафедры «Инженеринг технологического оборудования», Национальный исследовательский технологический университет «МИСИС»

ORCID: 0000-0002-4368-5965

E-mail: sgor02@mail.ru

Konstantin N. Solomonov, Dr. Sci. (Eng.), Prof. of the Chair of Social, Humanitarian, Natural Sciences and General Professional Discipline, Voronezh Branch of the Rostov State Transport University
E-mail: konssol@list.ru

Sergei A. Snitko, Dr. Sci. (Eng.), Assist. Prof., Head of the Chair "Metal Forming", Donetsk National Technical University
ORCID: 0000-0002-1099-5801
E-mail: snitko_sa@mail.ru

Ol'ga N. Chicheneva, Cand. Sci. (Eng.), Assist. Prof., National University of Science and Technology "MISIS"
E-mail: chich38@mail.ru

Константин Николаевич Соломонов, д.т.н., профессор кафедры социально-гуманитарных, естественно-научных и общепрофессиональных дисциплин, Филиал Ростовского государственного университета путей сообщения в г. Воронеж
E-mail: konssol@list.ru

Сергей Александрович Снитко, д.т.н., доцент, заведующий кафедрой «Обработка металлов давлением», Донецкий национальный технический университет
ORCID: 0000-0002-1099-5801
E-mail: snitko_sa@mail.ru

Ольга Николаевна Чиченева, к.т.н., доцент, Национальный исследовательский технологический университет «МИСИС»
E-mail: chich38@mail.ru

Contribution of the Authors

N. A. Chichenev – development of method for calculating the temperature field of a cylindrical body.
S. M. Gorbatyuk – analysis and generalization of the obtained modeling results.
K. N. Solomonov – formation of the article concept, setting the research goals and objectives, writing the text.
S. A. Snitko – technical justification of research tasks, justification of process parameters.
O. N. Chicheneva – graphic design of the obtained results.

Вклад авторов

Н. А. Чиченев – разработка методики расчета температурного поля цилиндрического тела.
С. М. Горбатюк – анализ и обобщение полученных результатов моделирования.
К. Н. Соломонов – формирование концепции статьи, определение цели и задачи исследования, подготовка текста.
С. А. Снитко – техническое обоснование задач исследования, обоснование параметров процесса.
О. Н. Чиченева – графическое оформление полученных результатов.

Received 17.09.2023
Revised 07.01.2024
Accepted 23.03.2024

Поступила в редакцию 17.09.2023
После доработки 07.01.2024
Принята к публикации 23.03.2024



UDC 669.15–198

DOI 10.17073/0368-0797-2024-2-161-166



Original article

Оригинальная статья

INFLUENCE OF ADDITIVES ON PROPERTIES OF HIGH-CARBON FERROCHROME SLAG

A. M. Akuov¹, B. S. Kelamanov², O. V. Zayakin³,
E. K. Samuratov¹, D. A. Yessengaliyev²

¹ Kazphosphate LLP (126 Abaya Str., Taraz, Zhambyl Region 080000, Republic of Kazakhstan)

² K. Zhubanov Aktobe Regional University (34 A. Moldagulova Ave., Aktobe 030000, Republic of Kazakhstan)

³ Institute of Metallurgy, Ural Branch of the Russian Academy of Sciences (101 Amundsena Str., Yekaterinburg 620016, Russian Federation)

✉ akuov.am@mail.ru

Abstract. Industrial slags produced by high-carbon ferrochrome are a material of complex composition consisting of an oxide part (Cr_2O_3 , CaO , MgO , FeO , SiO_2 , Al_2O_3) and “entangled” metal prills (Cr_{met}). In order to increase the degree of chromium utilization and reduce losses in the form of metal prills, we conducted the laboratory experiments to study changes in properties of the slag produced by high-carbon ferrochrome through the use of effective and affordable fluxing materials: expanded clay, calcium borate and refined ferrochrome slag. The effect of fluxing additives in the form of expanded clay, calcium borate and slag from the production of low-carbon ferrochrome on the properties of high-carbon ferrochrome slag was studied. Addition of up to 8 % of expanded clay and low-carbon ferrochrome slag leads to a stable decrease in the softening temperatures of the final slags. The greatest intensity of decrease in the softening temperature is observed when calcium borate is injected in an amount of 6 – 10 %. The greatest effect on reducing softening temperatures is exerted by the addition of 10 % calcium borate when introducing high-carbon ferrochrome into the slag, while the temperature of softening beginning decreases by 262 °C, and the temperature of softening end – by 135 °C. All the studied fluxing additives have a positive effect on reduction degree of the residual concentration of metallic chromium in the slag. The most intense decrease in the content of Cr_{met} in the slag is observed with the introduction of 2 % of fluxing materials. The best values for the residual content of 0.7 – 0.8 % Cr_{met} were achieved using 4 % of low-carbon ferrochrome slag and calcium borate. When using expanded clay, an additive in the amount of 10 % is required to achieve such indicators of Cr_{met} . In general, the effectiveness of using the studied fluxing materials to increase the degree of chromium extraction in the production of high-carbon ferrochrome is shown, its content in the slag is reduced by 84 %.

Keywords: metallurgy, ferrochrome, slag, metal prills, fluxing materials, expanded clay, calcium borate

For citation: Akuov A.M., Kelamanov B.S., Zayakin O.V., Samuratov E.K., Yessengaliyev D.A. Influence of additives on properties of high-carbon ferrochrome slag. *Izvestiya. Ferrous Metallurgy*. 2024;67(2):161–166. <https://doi.org/10.17073/0368-0797-2024-2-161-166>

ИЗУЧЕНИЕ ВЛИЯНИЯ ФЛЮСУЮЩИХ ДОБАВОК НА СВОЙСТВА ШЛАКА ВЫСОКОУГЛЕРОДИСТОГО ФЕРРОХРОМА

А. М. Акуов¹, Б. С. Келаманов², О. В. Заякин³,
Е. К. Самуратов¹, Д. А. Есенгалиев²

¹ ТОО Казфосфат (Казахстан, 080000, Жамбылская обл., Тараз, ул. Абая, 126)

² Актюбинский региональный университет им. К. Жубанова (Казахстан, 030000, Актюбинская обл., Актобе, пр. А. Молдагуловой, 34)

³ Институт металлургии Уральского отделения РАН (Россия, 620016, Екатеринбург, ул. Амундсена, 101)

✉ akuov.am@mail.ru

Аннотация. Промышленные шлаки высокоуглеродистого феррохрома имеют сложный состав. Они состоят из оксидной части (Cr_2O_3 , CaO , MgO , FeO , SiO_2 , Al_2O_3), а также «запутавшихся» металлических корольков ($\text{Cr}_{\text{мет}}$). С целью увеличения степени полезного использования хрома и снижения потерь в виде металлических корольков проведены эксперименты в лабораторных условиях по изучению изменения свойств шлака высокоуглеродистого феррохрома путем применения эффективных и доступных флюсующих материалов (керамзита, бората кальция и шлака рафинированного феррохрома). Изучено влияние флюсующих добавок в виде керамзита, бората кальция и шлака от произ-

водства низкоуглеродистого феррохрома на свойства шлака высокоуглеродистого феррохрома. Присадки до 8 % керамзита и шлака низкоуглеродистого феррохрома приводят к стабильному снижению температур размягчения конечных шлаков. При вводе 6 – 10 % бората кальция происходит интенсивное снижение температур начала размягчения. Наибольшее влияние на снижение температур размягчения оказывает добавка 10 % бората кальция при вводе в шлак высокоуглеродистого феррохрома, при этом наблюдается снижение температуры начала размягчения на 262 °С, конца размягчения – на 135 °С. Все исследованные флюсующие добавки оказывают положительное влияние на степень снижения остаточной концентрации металлического хрома в шлаке. При вводе 2 % флюсующих материалов наблюдается наиболее интенсивное снижение содержания $Cr_{мет}$ в шлаке. Наилучшие значения по остаточному содержанию 0,7 – 0,8 % $Cr_{мет}$ достигнуты при использовании 4 % шлака низкоуглеродистого феррохрома и бората кальция. При использовании керамзита для достижения таких показателей $Cr_{мет}$ необходима добавка в количестве 10 %. Показана эффективность использования исследованных флюсующих материалов при производстве высокоуглеродистого феррохрома для повышения степени извлечения хрома, содержание которого в шлаке снижается примерно на 84 %.

Ключевые слова: металлургия, феррохром, шлак, корольки металла, флюсующие материалы, керамзит, борат кальция

Для цитирования: Акуов А.М., Келаманов Б.С., Заякин О.В., Самуратов Е.К., Есенгалиев Д.А. Изучение влияния флюсующих добавок на свойства шлака высокоуглеродистого феррохрома. *Известия вузов. Черная металлургия*. 2024;67(2):161–166.

<https://doi.org/10.17073/0368-0797-2024-2-161-166>

INTRODUCTION

The operational characteristics of slag in the production of high-carbon ferrochrome depend on the nature of chrome ores, the content of main components (iron and chrome oxides), and slag-forming agents (SiO_2 , MgO , and Al_2O_3). Therefore, the phase diagram of the SiO_2 – MgO – Al_2O_3 system (Fig. 1) serves as the physicochemical basis for determining the optimal slag compositions [1 – 3].

The selected slag composition should ensure the overheating of high-carbon ferrochrome (HCFC) and create conditions for successful “droplet” (movement of metal droplets through the ore layer) and “bottom” (at the metal-slag interface) refining of carbon and silicon. The slag should have low viscosity and be sufficiently mobile for the precipitation of metal droplets (especially in the ladle during tapping from the furnace), easily separate from the metal ingot, and possess optimum electrical resistance

to facilitate deep insertion of electrodes into the charge and obtain standard metal in terms of sulfur and phosphorus content.

The temperature regime of the metal and slag during the smelting of high-carbon ferrochrome is primarily determined by the softening temperatures of the oxide material (SiO_2 concentration and MgO/Al_2O_3 ratio) as well as the ratio between chromium and carbon content in the alloy. The melting temperatures of the selected slag composition should be higher than the melting temperature of the metal by 100 – 150 °C since the heating of the metal during the smelting of high-carbon ferrochrome occurs through the slag, and the furnace operates in resistance mode. The slag obtained from processing chrome ores of the Kempirsaiskoe deposit has a high melting temperature and viscosity, which makes it difficult to remove from the furnace and contributes to excessive overheating of the metal. To lower the melting temperature and viscosity of the slag, silicon-containing

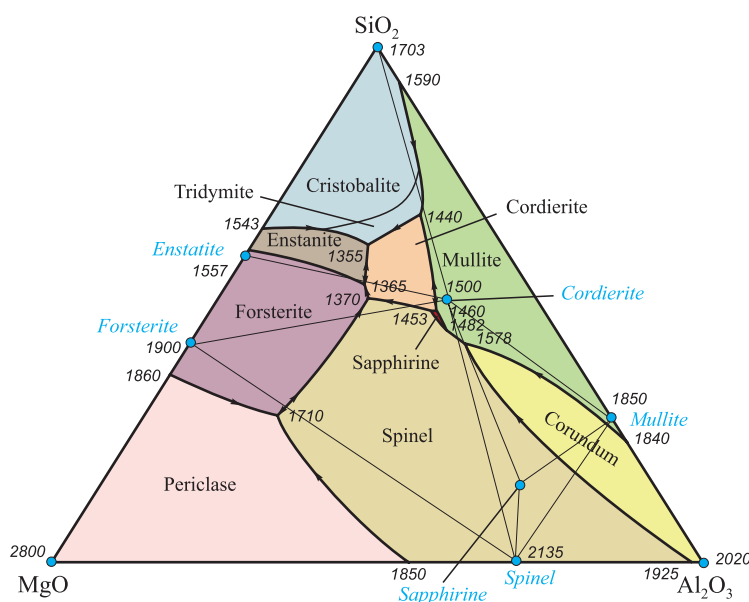


Fig. 1. State diagram of the SiO_2 – MgO – Al_2O_3 ternary system [1]

Рис. 1. Диаграмма состояния тройной системы SiO_2 – MgO – Al_2O_3 [1]

fluxing materials such as quartzite screenings or high-ash reducers are added to the charge.

Over the years of operation, as mining activities extended into deeper layers, ores from lower horizons began to be extracted. These ores had undergone less exposure to weathering processes, significantly impacting the composition of the host rock. There was an increase in magnesium oxide content and a decrease in aluminum oxide content. Consequently, the composition of chromite ores obtained by ferroalloy plants in recent years has undergone significant changes. The composition of the slag is determined by the composition of the chromite ores, thus their compositions have also shifted towards increased magnesium oxide content (from 28 – 32 % to 45 – 48 %) and decreased aluminum oxide content (from 28 – 29 % to 14 – 15 %), while the silicon dioxide content (SiO_2) has remained at the level of 29 – 34 %. This is evidenced by the dynamics of changes in the composition of the final slag of high-carbon ferrochrome, which indicates that the $\text{MgO}/\text{Al}_2\text{O}_3$ ratio has increased from 1.8 to 3.0 and higher over the past decades [4 – 6].

According to the chemical composition, significant changes have also occurred in the phase composition of the slag of high-carbon ferrochrome, which has shifted from the magnesioaluminate spinel field ($\text{MgO} \cdot \text{Al}_2\text{O}_3$) to the forsterite field ($2\text{MgO} \cdot \text{SiO}_2$). The proportion of the latter in the slag has increased from 35 to 70 % since the commissioning of the Kempirsaiskoe mine. The increase in magnesium content in the slag mainly occurred due to the supply of poorer chromite ores and the exploitation of new deposits with increased magnesium content.

Therefore, further growth in the production volume of chromium-containing ferroalloys necessitates the extensive utilization of the most common high-magnesia chromite ores with a magnesium oxide content of 18 – 22 % and an aluminum oxide concentration of 7 – 9 %.

Increasing the magnesium concentration in the slag leads to increased chromium losses. A significant amount of chromium is lost in the form of a metallic phase, which is associated with the deterioration of the physicochemical properties of the formed high-magnesia slags.

MATERIALS AND METHODS

In [7 – 9], it is demonstrated that the introduction of various fluxing and carbon-containing materials into the charge of high-carbon ferrochrome contributes to reducing the high melting point of the resulting oxide materials, thereby allowing for a reduction in chrome losses with the slag in the form of entangled metal droplets [10 – 12].

Laboratory experiments were conducted to reduce the softening temperatures of slags during the smelting of high-carbon ferrochrome by adding various fluxing materials for the deposition and coagulation of entangled metal droplets. Calcium borate [13 – 15], expanded clay, and stabilized low-carbon (refined) ferrochrome (RFC) slag were used as fluxing materials. Due to the different fractional compositions of the materials used, all samples were crushed and fractionated to obtain materials with a size of 1 – 3 mm. The chemical compositions of the considered fluxing materials and the initial HCFC slag are presented in the Table.

Experimental melts were carried out in a high-temperature resistance furnace according to Tamman. The technical characteristics of the furnace were as follows: power consumption – 40 kW; network voltage – 380 V; maximum voltage on the furnace buses – 15 V; maximum allowable temperature – 1800 °C; heating time to the maximum temperature – 30 min.

The weight of the initial HCFC slag for each experiment was 300 g. Fluxing additives were added in amounts of 2 – 10 % of the mass of the initial slag with a step of 2 %. At least two melts were carried out for each charging variant. The initial temperature (T_{ini}) and end temperature (T_{end}) of softening were determined in accordance with State standard GOST 26517-85. The pre-dosed mixture of slag and flux was poured into a crucible, then placed in the furnace and heated at a rate of 10 – 15 °C/min. Temperature measurements were made using a VR 5/20 tungsten-rhenium thermocouple.

RESULTS AND DISCUSSION

The introduction of fluxing additives has a multifaceted effect on the chemical composition and basicity of the processed slags [16 – 18]. According to the chemi-

Chemical compositions of the fluxing materials

Химические составы флюсующих материалов

Material	Content of elements, wt. %							
	Cr_{met}	Cr_2O_3	CaO	MgO	Al_2O_3	FeO	SiO_2	B_2O_3
Expanded clay	–	0.10	3.01	2.59	15.27	7.38	62.30	–
Calcium borate	–	–	37.20	0.50	0.05	–	–	43.80
RFC slag	1.3	8.60	46.80	12.80	5.80	1.90	22.90	0.30
HCFC slag	4.9	9.40	1.70	42.00	16.80	2.30	26.00	–

cal analysis data of the final slags, the introduction of expanded clay up to 10 % with a basicity of 0.09 leads to an increase in the concentration of SiO_2 oxide from 26.0 to 32.1 %, accompanied by a decrease in the basicity of the final slag by 0.28.

Adding high-basicity RFC slag up to 10 % leads to an increase in the basicity of the final slag by 0.12. The slag contains a minor concentration of B_2O_3 oxide at 0.01 %. It is necessary to note the additional positive impact of the addition of RFC slag, as waste from their own production is used and an additional 0.13 % of Cr metal is introduced. However, the high melting temperature of RFC slag when considering the option of introducing fluxing materials into the ladle requires a thermal balance calculation to determine the allowable amount of additives. In the case of adding fluxing materials directly into the furnace, one must consider the increase in the basicity of the final slag, which can affect both the lining of the furnace and the technological process of smelting high-carbon ferrochrome [19 – 21].

Adding calcium borate leads to an increase of up to 5 % CaO and 2.6 % B_2O_3 in the final slag. Considering that the B_2O_3 oxide belongs to “acidic” materials, it

can be said that the basicity of the slag changes insignificantly (increases by 0.02).

When selecting flux materials, their cost should be considered. It is promising to utilize waste from our own production (RFC slag).

The results of temperature measurement at the beginning of softening are presented in Fig. 2, *a*, and at the end of softening in Fig. 2, *b*.

For all tested samples, an increase of up to 8 % of flux additives from the mass of HCFC slag leads to a decrease in the temperature at the beginning of softening. Increasing the flux addition to 10 % has a contradictory effect on the values of T_{ini} (Fig. 2, *a*): it increases for expanded clay and RFC slag, but decreases sharply for calcium borate.

When adding up to 8 % of RFC slag, there is a gradual decrease in the temperatures at the beginning of softening (by 35 °C). Further increasing the RFC addition leads to a sharp increase in the value of T_{ini} . When introducing 10 % of RFC slag, the temperature at the beginning of softening exceeds the value of T_{ini} for the original HCFC slag.

For comparison, the high-carbon ferrochrome slag was melted without flux additives. Up to a temperature of 1650 °C, no changes in the state of the slag were observed, starting from 1660 °C, the slag enters a pasty state. At a temperature of 1677 °C, the slag becomes a dense viscous mass, and at 1705 °C, the slag completely melts. The slag is less fluid than when processed with fluxes.

When using calcium borate in an amount of up to 10 % of the slag mass, the temperatures at the beginning and end of slag softening decrease by 265 and 135 °C. In the case of expanded clay, these indicators are 39 and 80 °C. With additions of up to 10 % of stabilized RFC slag, the slag softening temperature increases by 2 °C above the softening temperature of the original HCFC slag.

Fig. 3 presents data on the residual content of metallic chromium in the slag after processing with fluxes.

The best results for precipitating chrome spinels were achieved with a consumption of 4 % calcium borate from the slag mass. The content of metallic Cr in the slag decreased by 83.7 %. For slags treated with expanded

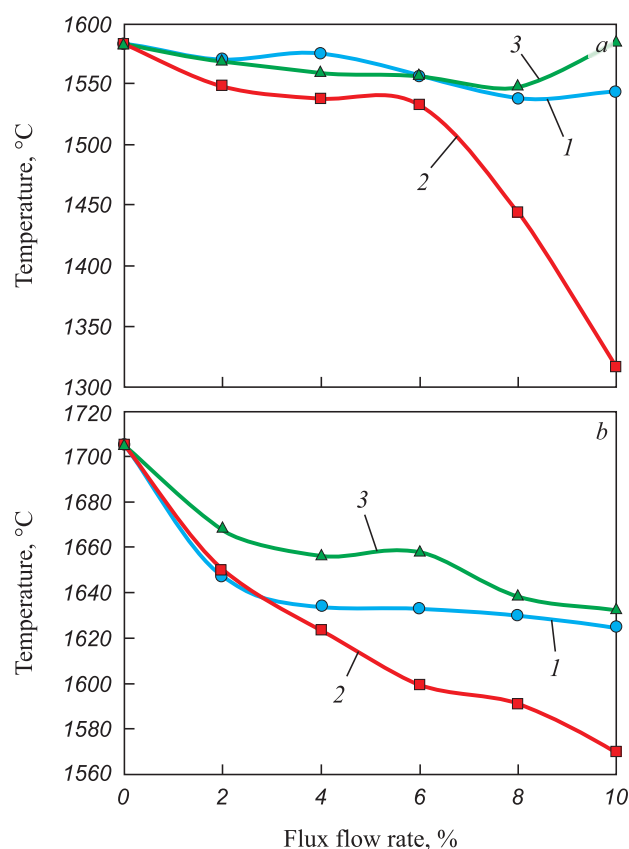


Fig. 2. Dependence of the temperature of beginning (*a*) and end (*b*) of slag softening on the flux flow rate:

1 – expanded clay; 2 – calcium borate; 3 – refined ferrochrome slag

Рис. 2. Зависимость температуры начала (*a*) и конца (*b*) размягчения шлака от расхода флюса:

1 – керамзит; 2 – борат кальция; 3 – шлак РФХ

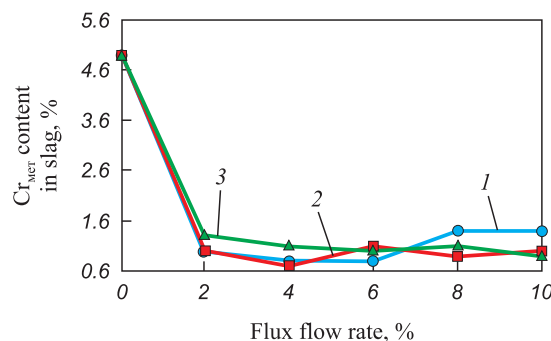


Fig. 3. Dependence of Cr_{met} content in the slag on the flux flow rate: 1 – calcium borate; 2 – refined ferrochrome slag; 3 – expanded clay

Рис. 3. Зависимость содержания $\text{Cr}_{\text{мет}}$ в шлаке от расхода флюса:

1 – борат кальция; 2 – шлак РФХ; 3 – керамзит

clay, this value is 81.7 % at a consumption rate of 10 % of the slag mass. In slags treated with stabilized RFC slag in an amount of 4 % of the slag mass, the content of Cr_{met} decreased by 85.7 %.

Significant reduction in the content of metallic chromium in the slag is observed when introducing 2 – 4 % of the tested flux materials.

Based on the reduction in the content of metallic Cr in the slag, it can be concluded that it is preferable to use expanded clay and RFC slag stabilized with boron. In industrial conditions, it is necessary to take into account the cost of each type of fluxing additives.

CONCLUSIONS

The influence of fluxing additives such as expanded clay, calcium borate, and slag from RFC production on the properties of high-carbon ferrochrome slag has been studied. It has been shown that the addition of up to 8 % expanded clay and low-carbon ferrochrome slag leads to a stable decrease in the softening temperatures of final slags. The most significant reduction in softening temperature onset is observed with the introduction of 6 – 10 % calcium borate. The greatest impact on reducing softening temperatures is achieved with the addition of calcium borate; with the addition of 10 % calcium borate to HCFC slag, the start of softening temperature is reduced by 262 °C, and the end of softening by 135 °C.

All studied fluxing additives have a positive influence on the degree of reduction in the residual concentration of metallic chromium in the slag. The most intense reduction in Cr_{met} content in the slag is observed with the addition of 2 % fluxing materials. The best values for residual content of 0.7 – 0.8 % Cr_{met} are achieved when using 4 % RFC slag and calcium borate. When using expanded clay to achieve such chromium content levels, an addition of 10 % is required.

The efficiency of using the studied fluxing materials to increase the extraction of chromium during the production of high-carbon ferrochrome is demonstrated, with the residual content in the slag reduced by approximately 84 %.

REFERENCES / СПИСОК ЛИТЕРАТУРЫ

1. Ryss M.A. Production of Ferroalloys. Moscow: Metallurgiya; 1985:344. (In Russ.).
Рысс М.А. Производство ферросплавов. Москва: Металлургия; 1985:344.
2. Bereznoi A.S. Multicomponent Systems of Oxides. Kyiv: Naukova dumka; 1970:544. (In Russ.).
Бережной А.С. Многокомпонентные системы окислов. Киев: Наукова думка; 1970:544.
3. Akberdin A., Konurov U., Kim A., Sultangaziyev R., Issagulov A. Viscosity and electric conductivity of melt system of $CaO-Al_2O_3-B_2O_3$. *Metallurgija*. 2016;55(3):313–316.

4. Kim A.S., Akberdin A.A., Sultangaziev R.B. Using basalt rocks for agglomeration of refractory chromite ores of Kazakhstan. *Metallurgist*. 2020;63(9–10):1005–1012.
<https://doi.org/10.1007/s11015-020-00919-8>
5. Abdullabekov E.E., Kaskin K.K., Nurumgaliev A.Kh. Theory and Technology of Chromium Alloys Production. Almaty: Respublikanskii izdatel'skii kabinet po uchebnoi i metodicheskoi literature; 2010:280. (In Russ.).
Абдуллабеков Е.Э., Каскин К.К., Нурумгалиев А.Х. Теория и технология производства хромистых сплавов. Алматы: Республиканский издательский кабинет по учебной и методической литературе; 2010:280.
6. Sariev O., Kelamaov B., Zhumagaliyev Ye., Kim S., Abdirashit A., Almagambetov M. Remelting the high-carbon ferrochrome dust in a direct current arc furnace. *Metallurgija*. 2020;59(4):533–536.
7. Kuatbay Ye., Nurumgaliev A., Zhuniskaliyev T., Smailov S., Yerzhanov A., Bulekova G. Development of carbon ferrochrome smelting technology using high-ash coal. *Metallurgija*. 2022;61(3-4):764–766.
8. Zhilo N.L., Ostretsova I.S., Mizin V.G., etc. Physico-chemical properties of carbon ferrochrome slags. *Stal'*. 1983;(3): 35–39. (In Russ.).
Жило Н.Л., Острцова И.С., Мизин В.Г. и др. Физико-химические свойства шлаков углеродистого феррохрома. *Сталь*. 1983;(3):35–39.
9. Kelamanov B., Samuratov Ye., Akuov A., etc. Thermodynamic-diagram analysis of Fe–Ni–C–O system. *Metallurgija*. 2022;61(1):261–264.
10. Yessengaliyev D., Kelamanov B., Zayakin O. Thermodynamic modeling of the recovery process of manganese by metallothermic method. *Journal of Chemical Technology and Metallurgy*. 2022;57(6):1230–1234.
11. Akberdin A., Kim A., Sultangaziyev R., Karbayev M. Thermodynamic modeling of the borbarium ferroalloy smelting technological process. *Metallurgija*. 2020;59(3):333–336.
12. Grinenko V.I., Tolymbekov M.Zh., Baisanov S.O., Musina I.B. Experience of using low-phosphorous fractionated coals in the production of high-carbon ferrochrome. *Stal'*. 1999;(6):34–35. (In Russ.).
Гриненко В.И., Толымбеков М.Ж., Байсанов С.О., Мусина И.Б. Опыт использования в производстве высокоуглеродистого феррохрома низкофосфористых фракционированных углей. *Сталь*. 1999;(6):34–35.
13. Akuov A., Samuratov Y., Kelamanov B., Zhumagaliyev Y., Taizhigitova M. Development of an alternative technology for the production of refined ferrochrome. *Metallurgija (Zagreb, Croatia)*. 2020;59(4):529–532.
14. Shabanov E.Zh., Baisanov A.S., Toleukadyr R.T., Inkarbekova I.S. Study of phase transformations during heating of briquetted mono-charge from chromium-containing materials and carbon reducing agents. *CIS Iron and Steel Review*. 2023;25(1):26–30.
<https://doi.org/10.17580/cisr.2023.01.05>
15. Kim A.S., Akberdin A.A., Sultangaziyev R.B., Orlov A.S., Adamova G.H. Features of the slag regime of smelting boron containing silicochrome. *Metallurgija*. 2023;62(2):194–196.
16. Li J.–L., Xu A.–J., He D.–F., Yang Q.–X., Tian N.–Y. Effect of FeO on the formation of spinel phases and chromium distribution in the $CaO-SiO_2-MgO-Al_2O_3-Cr_2O_3$ system.

International Journal of Minerals Metallurgy and Materials. 2013;20(3):253–258.

<http://dx.doi.org/10.1007/s12613-013-0720-9>

17. Ma J., Li W., Fu G., Zhu M. Effect of B_2O_3 on the melting temperature and viscosity of $CaO-SiO_2-MgO-Al_2O_3-TiO_2-Cr_2O_3$ slag. *Journal of Sustainable Metallurgy*. 2021;7(3):1190–1199.

<https://doi.org/10.1007/s40831-021-00413-8>

18. Zhdanov A.V., Nurmaganbetova B.N., Pavlov V.A. Effect of additives of aluminosilicate and silicate materials on softening temperatures of chromite ore. *Metals*. 2015;(4):3–8. (In Russ.).

Жданов А.В., Нурмаганбетова Б.Н., Павлов В.А. Изучение влияния добавок алюмосиликатных и силикатных материалов на температуры размягчения хромитовой руды. *Металлы*. 2015;(4):3–8.

19. Shabanov Y., Makhambetov Y., Saulebek Z., Toleukadyr R., Baisanov S., Nurgali N., Shotanov A., Dossekenov M.,

Zhumagaliyev Y. Pilot tests of pre-reduction in chromium raw materials from Donskoy ore mining and processing plant and melting of high-carbon ferrochromium. *Metals*. 2024;14(202):1–15.

<https://doi.org/10.3390/met14020202>

20. Panda C.R., Mishra K.K., Nayak B.D., Rao D.S., Nayak B.B. Release behaviour of chromium from ferrochrome slag. *International Journal of Environmental Technology and Management*. 2012;15(3-6):261–274.

<https://doi.org/10.1504/IJETM.2012.049227>

21. Esenzhulov A.B., Ostrovskii Ya.I., Afanas'ev V.I., Zayakin O.V., Zhuchkov V.I. Russian chromium ore in smelting high-carbon ferrochrome at OAO SZF. *Steel in Translation*. 2008;38(4): 315–317. <https://doi.org/10.3103/S096709120804013X>

Есенжулов А.Б., Островский Я.И., Афанасьев В.И., Заякин О.В., Жучков В.И. Использование российского хромородного сырья при выплавке высокоуглеродистого феррохрома в ОАО «СЗФ». *Сталь*. 2008;(4):32–36.

Information about the Authors

Сведения об авторах

Askhat M. Akuov, Cand. Sci. (Eng.), Process Engineer, Kazphosphate LLP

ORCID: 0000-0002-5163-5378

E-mail: akuov.am@mail.ru

Bauyrzhan S. Kelamanov, Cand. Sci. (Eng.), Assist. Prof., Prof. of the Chair of Metallurgy and Mining, K. Zhubanov Aktobe Regional University

ORCID: 0000-0001-7646-9153

E-mail: kelamanov-b@mail.ru

Oleg V. Zayakin, Corresponding Member of RAS, Dr. Sci. (Eng.), Chief Researcher, Head of the Laboratory of Steel and Ferroalloys, Institute of Metallurgy, Ural Branch of the Russian Academy of Sciences

ORCID: 0000-0002-9442-5928

E-mail: zferro@mail.ru

Yerulan K. Samuratov, Cand. Sci. (Eng.), Process Engineer, Kazphosphate LLP

ORCID: 0000-0001-8591-8547

E-mail: Samuratov.ek@mail.ru

Dauren A. Yessengaliyev, Cand. Sci. (Eng.), Assist. Prof. of the Chair of Metallurgy and Mining, K. Zhubanov Aktobe Regional University

ORCID: 0000-0003-0792-0822

E-mail: dauralga@mail.ru

Асхат Максотович Акуов, к.т.н., инженер-технолог, ТОО Казфосфат

ORCID: 0000-0002-5163-5378

E-mail: akuov.am@mail.ru

Бауыржан Сатыбалдыұлы Келаманов, к.т.н., ассоц. профессор, автор-корреспондент, профессор кафедры «Металлургия и горное дело», Актюбинский региональный университет им. К. Жубанова

ORCID: 0000-0001-7646-9153

E-mail: kelamanov-b@mail.ru

Олег Вадимович Заякин, член-корреспондент РАН, д.т.н., главный научный сотрудник, заведующий лабораторией стали и ферросплавов, Институт металлургии Уральского отделения РАН

ORCID: 0000-0002-9442-5928

E-mail: zferro@mail.ru

Ерулан Кауржанович Самуратов, к.т.н., инженер-технолог, ТОО Казфосфат

ORCID: 0000-0001-8591-8547

E-mail: Samuratov.ek@mail.ru

Даурен Амангельдиевич Есенгалиев, к.т.н., доцент кафедры «Металлургия и горное дело», Актюбинский региональный университет им. К. Жубанова

ORCID: 0000-0003-0792-0822

E-mail: dauralga@mail.ru

Contribution of the Authors

Вклад авторов

A. M. Akuov – conducting laboratory tests, data processing.

B. S. Kelamanov – review of the literary data, conducting calculations.

O. V. Zayakin – analysis of the research results, formulation of conclusions.

Ye. K. Samuratov – studying the residual chromium content in slags after laboratory experiments.

D. A. Yessengaliyev – formation of research goals and objectives, writing the text.

А. М. Акуов – проведение лабораторных исследований, обработка данных.

Б. С. Келаманов – обзор литературных данных, проведение расчетов.

О. В. Заякин – анализ результатов исследований, формирование выводов.

Е. К. Самуратов – изучение остаточного содержания хрома в шлаках после лабораторных экспериментов.

Д. А. Есенгалиев – формирование целей и задач исследования, подготовка текста.

Received 11.12.2023

Revised 12.02.2024

Accepted 19.02.2024

Поступила в редакцию 11.12.2023

После доработки 12.02.2024

Принята к публикации 19.02.2024



UDC 669:539.375.5

DOI 10.17073/0368-0797-2024-2-167-175



Original article

Оригинальная статья

INTERNAL STRESSES AND THEIR SOURCES IN STEELS WITH BCC LATTICE

N. A. Popova¹, E. L. Nikonenko^{1,2}, M. A. Porfir'ev³, R. E. Kryukov³

¹ Tomsk State University of Architecture and Building (2 Solyanaya Sqr., Tomsk 634003, Russian Federation)

² National Research Tomsk Polytechnic University (30 Lenina Ave., Tomsk, 634050, Russian Federation)

³ Siberian State Industrial University (42 Kirova Str., Novokuznetsk, Kemerovo Region – Kuzbass 654007, Russian Federation)

✉ natalya-popova-44@mail.ru

Abstract. The paper studies fine structure of industrial steels with BCC lattice (pearlite, ferrite-pearlite and martensite) using transmission diffraction electron microscopy. The internal structure of the grains was analyzed; the scalar density of dislocations in various parts of the material, the sources of internal stresses and their amplitude were determined. The use of a method based on the analysis of bending extinction contours allowed us to study internal stresses. We analyzed the internal stresses and their sources using the example of 0.76C–Cr–V–Fe rail steel with a lamellar pearlite structure after ultra long-term operation with the tonnage of 1770 million gross tons. The metal of the rails was examined along the central axis of symmetry (rolling surface) and the rounding radius (working fillet) of the railhead at distances of 0, 2 and 10 mm from the surface. As one approaches the head surface, regardless of the research direction (along the fillet rounding radius or along the axis of symmetry), the lamellar pearlite is gradually replaced by destroyed pearlite with formation of a ferrite-carbide mixture and formation of a fragmented structure. These processes occur more intensively in the working fillet. Along the entire central axis of symmetry of the rail head (rolling surface), there is a plastic bending-torsion of the crystal lattice, along the rounding radius of the rail head (working fillet) at a distance of 10 mm from the surface – also plastic, and at a distance from 0 to 2 mm – elastic-plastic. The main source of internal torque (long-acting) stresses in rail steel is the excessive density of dislocations. Using the example of 34CrNi3MoVN steel of the martensitic class, the type of bending extinction contour was determined using mathematical equations. At low degrees of plastic deformation, extinction contours are contours of bending or torsion, at high degrees they are of a mixed type.

Keywords: electron microscopy, BCC lattice, bending extinction contour, curvature-torsion, scalar dislocation density, excess dislocation density, internal stresses, sources

Acknowledgements: The work was carried out within the framework of the state task of the Ministry of Science and Higher Education of the Russian Federation (subject No. FEMN-2023-0003).

For citation: Popova N.A., Nikonenko E.L., Porfir'ev M.A., Kryukov R.E. Internal stresses and their sources in steels with BCC lattice. *Izvestiya. Ferrous Metallurgy*. 2024;67(2):167–175. <https://doi.org/10.17073/0368-0797-2024-2-167-175>

ВНУТРЕННИЕ НАПРЯЖЕНИЯ И ИХ ИСТОЧНИКИ В СТАЛЯХ С ОЦК-КРИСТАЛЛИЧЕСКОЙ РЕШЕТКОЙ

Н. А. Попова¹, Е. Л. Никоненко^{1,2}, М. А. Порфирьев³, Р. Е. Крюков³

¹ Томский государственный архитектурно-строительный университет (Россия, 634003, Томск, пл. Соляная, 2)

² Национальный исследовательский Томский политехнический университет (Россия, 634050, Томск, пр. Ленина, 30)

³ Сибирский государственный индустриальный университет (Россия, 654007, Кемеровская обл. – Кузбасс, Новокузнецк, ул. Кирова, 42)

✉ natalya-popova-44@mail.ru

Аннотация. Методом просвечивающей дифракционной электронной микроскопии выполнены исследования тонкой структуры сталей промышленного назначения, которые обладают ОЦК-кристаллической решеткой (перлитные, феррито-перлитные и мартенситные). Проанализирована внутренняя структура зерен, определены скалярная плотность дислокаций в различных участках материала, источники внутренних напряжений и их амплитуда. Использование метода, основанного на анализе изгибных экстинкционных контуров, позволяет изучать внутренние напряжения. Изучение внутренних напряжений и их источников проведено на примере рельсовой стали Э76ХФ со структурой пластинчатого перлита после сверхдлительной эксплуатации (пропущенный тоннаж – 1770 млн т брутто). Места проведения исследования металла рельсов: вдоль центральной оси симметрии (поверхность катания) и вдоль радиуса скругления (рабочая выкружка) головки рельса на расстояниях 0, 2 и 10 мм от поверхности. По мере приближения к поверхности головки, независимо от

направления исследований (вдоль радиуса скругления выкружки или вдоль оси симметрии) пластинчатый перлит постепенно заменяется на разрушенный с образованием феррито-карбидной смеси и формированием фрагментированной структуры, причем эти процессы более интенсивно протекают в рабочей выкружке. Вдоль всей центральной оси симметрии головки рельса (поверхность катания) имеет место пластический изгиб-кручение кристаллической решетки, вдоль радиуса скругления головки рельса (рабочая выкружка) на расстоянии 10 мм от поверхности – также пластический, а на расстоянии от 0 до 2 мм – упругопластический. Основным источником внутренних моментных (дальнодействующих) напряжений в рельсовой стали является избыточная плотность дислокаций. На примере стали мартенситного класса 34ХНЗМФА с использованием матричных уравнений определен тип изгибного экстинкционного контура. При малых степенях пластической деформации экстинкционные контуры являются контурами изгиба или кручения, при больших степенях – контурами смешанного типа.

Ключевые слова: электронная микроскопия, ОЦК-кристаллическая решетка, изгибной экстинкционный контур, кривизна-кручение, скалярная плотность дислокаций, избыточная плотность дислокаций, внутренние напряжения, источники

Благодарности: Работа выполнена в рамках государственного задания Министерства науки и высшего образования Российской Федерации (тема № FEMN-2023-0003).

Для цитирования: Попова Н.А., Никоненко Е.Л., Порфирьев М.А., Крюков Р.Е. Внутренние напряжения и их источники в сталях с ОЦК-кристаллической решеткой. *Известия вузов. Черная металлургия*. 2024;67(2):167–175. <https://doi.org/10.17073/0368-0797-2024-2-167-175>

INTRODUCTION

The investigation of internal stresses in metals and alloys has long captivated researchers [1 – 3] due to their critical role in several mechanical properties and behaviors. Internal stresses significantly influence yield strength [4 – 6], deformation strengthening [7 – 9], and crucially, the fracture of crystalline materials through the initiation [10 – 15] and propagation of microcracks [16 – 18]. They are also vital in the evolution of defect structures during various thermal treatments of metals, alloys, and steels [15; 19; 20], and in phase and structural transformations [5; 6; 15; 20 – 22]. Additionally, internal stresses are indispensable in the production of bulk nanostructured materials created via intensive plastic deformation [4; 24 – 26].

Internal stresses are categorized based on their localization: macro-, meso-, and microstresses. Macro stresses span the entire sample or a substantial part thereof. Mesoscopic internal stresses are localized within volumes ranging from tens to hundreds of micrometers, often confined to one or several grain volumes or part of a grain volume. Microscopic stress fields are confined to areas a few micrometers in size or smaller.

Methods for assessing internal stresses fall into two primary categories: destructive and non-destructive. Destructive methods include chemical, thermal, metallographic, and mechanical approaches [27], which may lead to the partial or complete destruction of the sample. These methods typically assess first-order stresses, which are crucial for determining the operational properties of materials.

Non-destructive techniques encompass magnetic, optical, and polarization-optical methods [28]. These allow for the measurement of elastic deformations within a component without altering its geometry.

Both non-destructive and destructive methods provide an integral assessment of stresses, with stress (first-order stress) averaging over centimeters.

Internal stresses can also be determined using X-ray structural analysis, which measures both first and second-order stresses [29 – 31] and is considered a non-destructive method [32 – 34]. This technique reduces the range of stress averaging to millimeters, although it is still relatively broad. X-ray structural analysis is particularly effective for evaluating the amplitude of mesoscopic internal stresses [35 – 38].

Presently, the most informative method for examining meso- and microscopic internal stress fields is transmission electron diffraction microscopy, which offers precise control over the locality of stress measurements, ranging from hundreds of nanometers to hundreds of micrometers [39]. In this study, internal stresses and their sources in FCC steels were investigated using transmission electron diffraction microscopy with a focus on bending extinction contours.

Measurements of meso- and microscopic internal stresses were derived from the material's structure, including the radius of curvature of dislocations in the slip plane [23], the spacing between dislocations, the parameters of dislocation clusters [40], and the characteristics of bending extinction contours [19; 39].

The aim of this study is to investigate internal stresses and their sources in FCC steels using a method based on the analysis of bending extinction contours.

MATERIALS AND METHODS

A study was conducted on samples of industrial-purpose steels with a BCC crystal lattice (pearlite, ferrite-pearlite, and martensite), which underwent heat treatment and various plastic deformation processes (stretching, compression, rolling). The research was carried out using transmission diffraction electron microscopy (TEM) on thin foils with EM-125K electron microscopes equipped with a goniometric attachment and EM-125, which offers higher resolution capabilities. Foils were prepared using the electropolishing method with special modes to obtain

larger areas for viewing in the electron microscope. The working magnification in the microscope column was set at 25,000 times. As a result of the conducted research, the internal grain structure was analyzed, and the scalar density of dislocations in different areas of the material was determined. Sources of internal stresses were identified, and their amplitude was measured. The scalar density of dislocations was determined using the intercept method [39].

ASSESSING INTERNAL STRESSES WITH TEM

The uncharged dislocation ensemble (i.e., an ensemble without excess dislocations) produces internal shear stress (stress fields created by the dislocation structure), determined by the equation [2; 6; 13 – 15; 20]

$$\sigma = m\alpha Gb\sqrt{\rho}, \quad (1)$$

where m is the orientation multiplier or Schmid factor [20]; α is the parameter dependent on the type of dislocation ensemble (for the uncharged dislocation ensemble, $\alpha = 0.05 \div 1.00$ [2; 6; 19]); G is the shear modulus; b is the Burgers vector; ρ is the scalar dislocation density.

In the case of a charged dislocation ensemble, when there is an excess dislocation density $\rho_{\pm} = \rho_+ - \rho_- \neq 0$, internal moment (or long-range) stresses are generated. The presence of excess dislocation density and, consequently, internal moment stresses are identified by the presence of bending extinction contours in the material. These contours result from diffraction contrast observed in electron microscopic images of a highly deformed crystal.

The bending of the crystal lattice can be [6; 12 – 15; 20; 23]: purely elastic, created by stress fields accumulated due to deformation incompatibility (for example, between grains in a polycrystal, matrix material, and non-deformable particles); plastic, if the bending is created by dislocation charges (i.e. by an excess density of dislocations localized within a certain volume of the material); elastoplastic, when both sources of fields are present in the material.

By observing bending extinction contours using the TEM method, it is possible to measure internal (moment or long-range) stresses. These stresses lead to the bending of the foil, corresponding to the curvature-torsion of the crystal lattice, if the foil retains its plate shape. The procedure for measuring the value of internal moment (long-range) stresses involves determining the curvature gradient of the foil (crystal lattice):

$$\chi = \frac{\partial\varphi}{\partial l}, \quad (2)$$

where $\partial\varphi = \Delta\varphi$ is the change in orientation of the reflecting foil surface; $\partial l = \Delta l$ is the displacement of the bending extinction contour.

The χ value is determined by shifting the extinction contour by Δl at a controlled angle of inclination of the foil $\Delta\varphi$ in the microscope column using a goniometer. Special experiments have shown that for BCC steels, the width of the contour in terms of disorientation is approximately 1° [6; 20]. This indicates that when the goniometer is turned by $\Delta\varphi \approx 1^\circ$, the bending extinction contour shifts a distance equal to its width, that is $\Delta l \approx l$.

To differentiate between cases of plastic, elastic, and elastoplastic bending, it is necessary to compare the scalar dislocation density (ρ) measured in a local area near the bending extinction contour with the excess dislocation density (ρ_{\pm}) measured locally based on the disorientation gradient [20; 23]:

$$\rho_{\pm} = \frac{1}{b} \frac{\partial\varphi}{\partial l} = \frac{\chi}{b}. \quad (3)$$

If in the investigated area of the foil, $\rho \geq \rho_{\pm}$, then the bending of the crystal lattice can be considered plastic. The amplitude of the curvature-twist of the crystal lattice determined by Eq. (2) is $\chi = \chi_{pl}$, and the amplitude of internal stresses created by plastic bending is given by

$$\sigma_d^{pl} = m\alpha Gb\sqrt{\rho_{\pm}} = m\alpha G\sqrt{b\chi_{pl}}, \quad (4)$$

where $\alpha = 0.05 \div 0.60$ is the parameter depending on the type of dislocation ensemble [23].

It should be noted that the value of α in Eq. (4) is practically independent of the material under study (metal, alloy, or steel) and is determined only by the type of substructure formed [23].

If in the investigated area of the foil near the bending extinction contour, $\rho = 0$, then the bending of the crystal lattice is purely elastic. The amplitude of the curvature-torsion of the crystal lattice, determined by Eq. (2), is $\chi = \chi_{el}$, and the amplitude of internal moment stresses created by elastic bending should be determined as follows [20; 23]

$$\sigma_{\alpha}^y = m\alpha_c Gt \frac{\partial\varphi}{\partial l} = m\alpha_c Gt\chi_{ymp}, \quad (5)$$

where $\alpha_s = 1.0 \div 1.5$ is the Strunin coefficient [20], calculated for a dislocation ensemble composed of dislocations of the same sign; t is the foil thickness.

If in the vicinity of the bending extinction contour $\rho < \rho_{\pm}$, then the bending of the crystal lattice is elastoplastic, and in this case, the value of ρ_{\pm} is conditional. In this case, the bending of the crystal lattice is divided into a plastic component, for which $\rho = \rho'_{\pm}$, and an elas-

tic component, for which $\rho_{\pm}'' = \rho_{\pm} - \rho_{\pm}'$. The amplitude of the curvature-torsion of the crystal lattice is

$$\chi = \chi_{pl} + \chi_{el}, \quad (6)$$

where χ is calculated by Eq. (2), $\chi_{pl} = b\rho_{\pm}' = b\rho$ and, thus

$$\chi_{el} = \chi - \chi_{pl}. \quad (7)$$

As a result, the amplitude of internal moment (long-range) stresses is determined as

$$\sigma_d = \sigma_d^{pl} + \sigma_d^{el}, \quad (8)$$

where σ_d^{pl} is determined by Eq. (4), and σ_d^{el} by Eq. (5):

$$\sigma = m\alpha G \sqrt{b\chi_{pl}} + m\alpha_s G t \chi_{el}. \quad (9)$$

RESULTS AND DISCUSSION

Sources of internal stresses in BCC steels

A single dislocation is inherently a source of internal stresses. The fields generated by individual dislocations extend only over small distances, much smaller than the distances between the nearest dislocations [39]. However, groups of dislocations are more effective sources of internal stresses as they cover the entire microlevel and create fields of significantly greater amplitude [40]. Such groups primarily consist of distributed dislocation charges (excess dislocations of one sign) [41]. Although large groups of dislocations of one sign are rare, materials more commonly contain unevenly distributed dislocations of different signs with an excess density. Despite internal screening, these formations generate internal stress fields [41].

Another significant type of dislocation formation that induces substantial internal stresses is various dislocation boundaries. Typically, these contain an unequal number of dislocations of different signs and can introduce misorientation. A key characteristic is that the dislocations in the boundaries are from different slip planes, in contrast to dislocation charges where dislocations reside on the same or closely related slip planes.

Other sources of internal stresses include grain boundaries, grain junctions, and steps on intergranular boundaries [41; 42]. The root cause of these stresses is primarily the incompatibility of deformation between neighboring grains. This incompatibility is always present, despite the action of accommodating slip systems. Moreover, lattice dislocations that enter the grain boundaries and sources of dislocations at these boundaries contribute further to internal stresses. Junction dislocations at grain junctions and steps on interphase boundaries are also significant sources of internal stresses [43].

These mentioned sources are primarily responsible for internal stresses of plastic origin.

On the other hand, sources of elastic origin internal stresses, which mainly arise from heterogeneous deformation of the material, include microcracks [6; 12 – 15; 41] and bainitic deformation [20], which occurs due to the distortion of the crystalline lattice during the $\gamma \rightarrow \alpha$ phase transformation in steels. These stresses can also arise in materials reinforced with non-deformable dispersed particles [23]. In cases where these fields partially relax through the multiplication and slip of dislocations, they acquire an elastoplastic character [12 – 15; 41]. Depending on the degree of interaction with surrounding dislocation structures, the resultant internal stresses can exhibit all three types. In real materials, especially after significant deformations, fields from different sources combine to form a complex three-dimensional field of internal stresses.

Sources and characteristics of internal stresses in rail steel

The study of internal stresses and their sources after long-term operation (with a passing tonnage of 1770 million tons gross) was conducted on rails made of 0.76C–Cr–V–Fe steel, which has a lamellar pearlite structure. The investigation focused on the rail metal along the central axis of symmetry (rolling surface) and the radius of curvature (working fillet) of the rail head at distances of 0, 2, and 10 mm from the surface.

The research revealed that rail operation led to significant structural transformations and complications, especially along the radius of the rail head. For example, at a distance of 10 mm from the rolling surface along the axis of symmetry, the volumetric fraction of lamellar pearlite was 95 %, and the ferrite-carbide mixture (degraded pearlite) was 5 %. However, in the surface layer, the fraction of lamellar pearlite dropped to 45 %, the ferrite-carbide mixture increased to 50 %, and a fragmented structure emerged (5 %). Similarly, at a distance of 10 mm from the surface along the radius of curvature, the volumetric fraction of lamellar pearlite remained at 95 %. But in the surface layer, it decreased to 25 %, with the fragmented structure also accounting for 25 %. Thus, as one approaches the head surface, regardless of the research direction (along the radius of the rail head or the axis of symmetry), lamellar pearlite gradually transforms into a degraded form, forming a ferrite-carbide mixture and fragmented structure, with these processes being more pronounced in the working fillet.

Fig. 1 illustrates the changes in the average quantitative parameters of the fine structure as we approach the head surface.

All characteristics increase as we approach the surface of the rail head, with the scalar (ρ) and especially

excess (ρ_{\pm}) dislocation densities intensifying. However, their behavior varies within different structural components. The scalar dislocation density in the entire material, regardless of the direction of investigation (along the radius of the fillet or along the axis of symmetry), increases almost uniformly as it approaches the surface. The excess dislocation density, determined by the width of the bending extinction contours, remains smaller than the scalar density along the central axis of symmetry (rolling surface), indicating plastic bending-torsion of the crystalline lattice: $\chi = \chi_{pl}$ and $\sigma_d = \sigma_d^{pl}$ (Fig. 1, *a – c*). Along the radius of the fillet, the condition $\rho > \rho_{\pm}$, is also met in the lamellar pearlite, but in the ferrite-carbide mixture and fragmented structure, $\rho = \rho_{\pm}$. This indicates that the dislocation structure is fully polarized in these regions of the material, and elastic-plastic bending of the crystalline lattice occurs: $\chi = \chi_{pl} + \chi_{el}$ and $\sigma_d = \sigma_d^{pl} + \sigma_d^{el}$. Despite the minor magnitude of the elastic component (Fig. 1, *e, f*), these areas are critical in the material structure as they are likely initiation points

for failure. Thus, excess dislocation density is a primary source of internal momentary (long-range) stresses in rail steel. However, other sources of internal stresses include the ferrite and cementite phase boundaries, as well as boundaries of fragments and cementite particles located at the boundaries and within the fragments (Fig. 2).

Impact of plastic deformation on the curvature–torsion of the crystalline lattice in BCC steel

It is known [6; 23] that with the progression of deformation, the curvature-torsion gradient along the material intensifies. This phenomenon is evidenced both by the variation in the width of extinction contours along their length and by their overall bending. The type of contours also transforms. Generally, the curvature-torsion value of the crystal lattice, χ , is recognized as a second-rank tensor [6; 44; 45]. This tensor encapsulates components of both curvature and torsion of the crystal lattice. Utilizing matrix equations [6], it becomes fea-

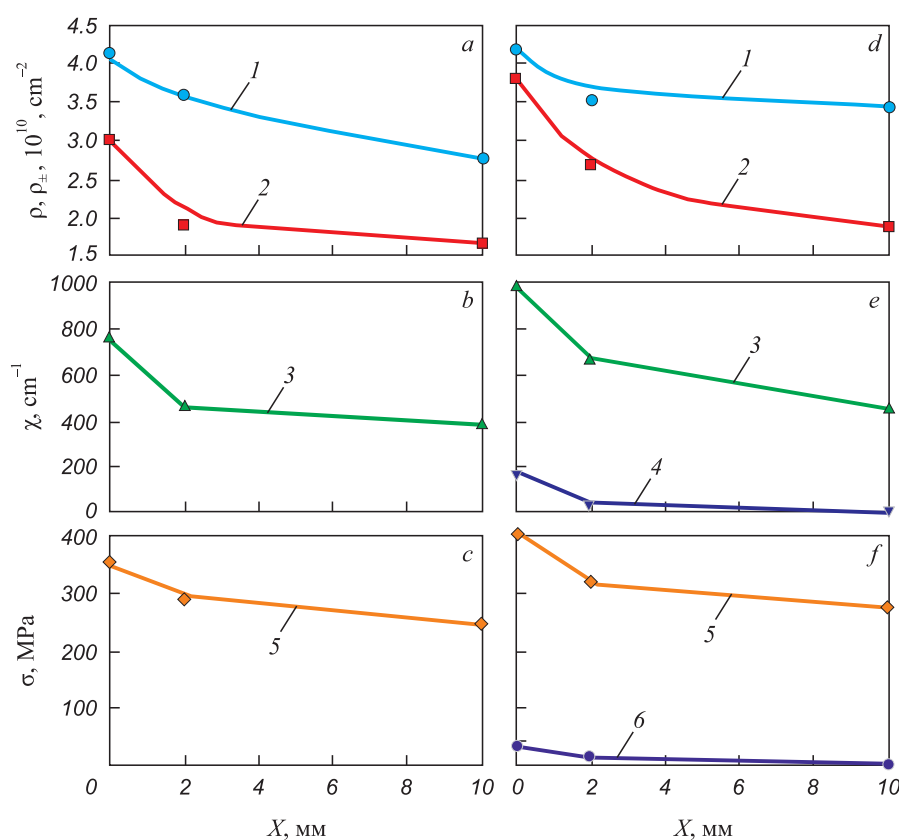


Fig. 1. Changes in the average quantitative parameters of fine structure of the 0.76C–Cr–V–Fe rail steel after ultra-long operation as it moves away from the surface:

a – c – rolling surface; *d – f* – working fillet; 1 and 2 – scalar and excessive dislocation density; 3 and 4 – amplitude of plastic χ_{pl} and elastic χ_{el} curvature-torsion of crystal lattice; 5 and 6 – amplitude of internal momentous σ_{pl} plastic and elastic σ_{el} stresses

Рис. 1. Изменение средних количественных параметров тонкой структуры рельсовой стали Э76ХФ после сверхдлительной эксплуатации по мере удаления от поверхности:

a – c – поверхность катания; *d – f* – рабочая выкружка; 1 и 2 – скалярная ρ и избыточная ρ_{\pm} плотность дислокаций; 3 и 4 – амплитуда пластической χ_{pl} и упругой χ_{el} кривизны-кручения кристаллической решетки; 5 и 6 – амплитуда внутренних моментных пластических σ_{pl} и упругих σ_{el} напряжений

sible to categorize the type of contour. This method was applied to the 34C–1Cr–3Ni–1Mo–1V–Fe martensitic steel, where prior to deformation, extinction contours were identified either as curvature (bending/tilting) contours (Fig. 3, curve 1) or torsion contours (Fig. 3, curve 2). The prevalence of curvature contours was significant, accounting for up to 85 % of observations. As the degree of plastic deformation increased, the contour configuration became more complex, with mixed-type contours emerging. When the deformation reached $\varepsilon \geq 0.2$, all bending contours transitioned to mixed-type contours (Fig. 3, curve 3).

CONCLUSIONS

An analysis of the sources of internal stresses in rail steels has been conducted. It has been determined that

these sources can be categorized into three types: plastic, elastic, and elastoplastic origin.

TEM analysis of 0.76C–Cr–V–Fe steel rails, which have endured a cumulative gross tonnage of 1770 million tons, revealed significant microstructural transformations as the surface of the rail head is approached. The lamellar pearlite gradually transforms into a structure featuring a ferrite-carbide mixture and fragmented structure. This process is notably more pronounced in the working fillet. Along the entire central axis of symmetry of the rail head, plastic bending-torsion of the crystal lattice is observed, while along the radius of curvature at distances up to 2 mm, the bending-torsion exhibits elastoplastic characteristics. The primary source of internal moment stresses is identified as the excess density of dislocations.

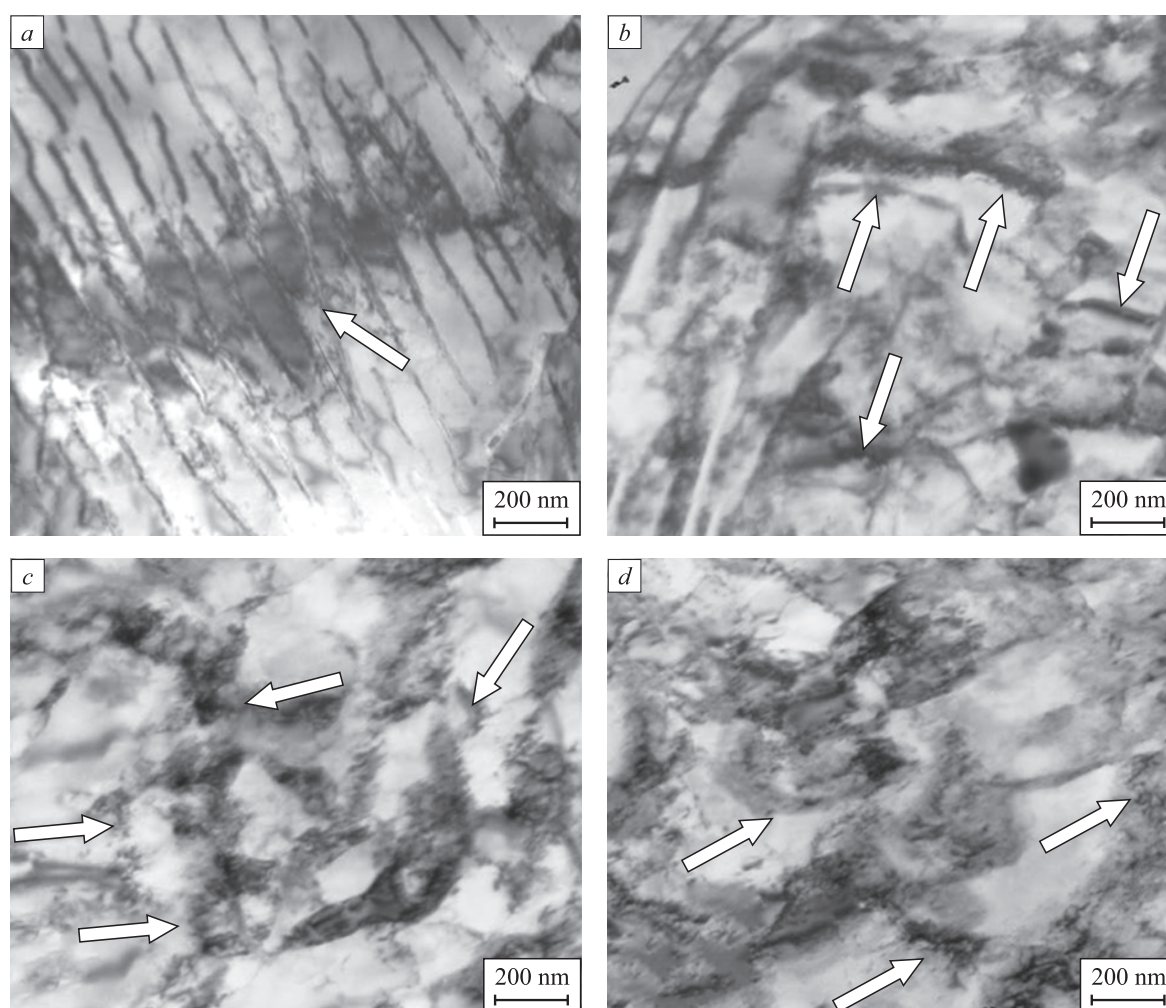


Fig. 2. TEM images of bending extinction contours (indicated by arrows) in different parts of the material from different sources:
a – boundaries between ferrite and cementite; *b* – boundaries between fragments;
c – globular particles at fragment boundaries; *d* – globular particles in the volume of fragments

Рис. 2. ПЭМ-изображения изгибных экстинкционных контуров (указаны стрелками)
 в различных участках материала от различных источников:

a – границы раздела феррита и цементита; *b* – границы раздела фрагментов;
c – частицы глобулярной формы на границах фрагментов; *d* – частицы глобулярной формы в объеме фрагментов

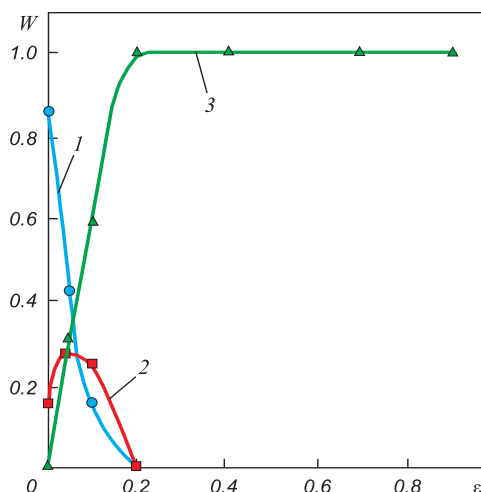


Fig. 3. Change in the volume fraction of bending extinction contours of curvature (1), torsion (2), and mixed type (3) on degree of plastic deformation in rolled tempered steel 34CrNi3MoVN

Рис. 3. Изменение объемной доли изгибных экстинкционных контуров кривизны (1), кручения (2) и смешанного типа (3) от степени пластической деформации в катаной отпущенной стали 34ХН3МФА

In studies of 34C–1Cr–3Ni–1Mo–1V–Fe martensitic steel, it has been observed that at low degrees of deformation, extinction contours are either bending or torsion contours. However, at higher degrees of deformation, all contours evolve into a mixed type.

REFERENCES / СПИСОК ЛИТЕРАТУРЫ

1. Koneva N.A., Kozlov E.V., Trishkina L.I. Internal field sources, their screening and the flow stress. *Materials Science and Engineering: A*. 2001;319–321:156–159. [https://doi.org/10.1016/S0921-5093\(01\)00945-5](https://doi.org/10.1016/S0921-5093(01)00945-5)
2. Koneva N.A., Kozlov E.V. Dislocation structure and physical mechanisms of hardening of metal materials. In: *Promising Materials. Structure and Methods of Research (Tutorial)*. Merson D.L. ed. Tula: TGU; Moscow: MISiS; 2006:267–320. (In Russ.).
Конева Н.А., Козлов Э.В. Дислокационная структура и физические механизмы упрочнения металлических материалов. В кн.: *Перспективные материалы. Структура и методы исследования (учебное пособие)* / Под ред. Д.Л. Мерсона. Тула: ТГУ; Москва: МИСиС; 2006:267–320.
3. Ovid'ko I.A., Valiev R.Z., Zhu Y.T. Review on superior strength and enhanced ductility of metallic nanomaterials. *Progress in Materials Science*. 2018;94:462–540. <https://doi.org/10.1016/j.pmatsci.2018.02.002>
4. Tyumentsev A.N., Korotaev A.D., Ditenberg I.A., Pinzhin Yu.P., Chernov V.M. Patterns of Plastic Deformation in High-Strength and Nanocrystalline Metallic Materials. Novosibirsk: SB RAS Nauka; 2018:256. (In Russ.).
Закономерности пластической деформации в высокопрочных и нанокристаллических металлических материалах / А.Н. Тюменцев, А.Д. Коротаев, И.А. Дитенберг, Ю.П. Пинжин, В.М. Чернов. Новосибирск: СО РАН Наука; 2018:256.

5. Yang M., Pan Yu., Yuan F., Zhu Yu., Wu X. Back stress strengthening and strain hardening in gradient structure. *Materials Research Letters*. 2016;4(3):145–151. <https://doi.org/10.1080/21663831.2016.1153004>
6. Koneva N., Kiseleva S., Popova N. Evolution of the Structure and Internal Stress Fields. Austenitic Steel. Germany: LAP LAMBER Academic Publishing; 2017:156. (In Russ.).
Конева Н., Киселева С., Попова Н. Эволюция структуры и внутренние поля напряжений. Аустенитная сталь. Германия: LAP LAMBER Academic Publishing; 2017:156.
7. Kundu A., Field D.P. Geometrically necessary dislocation density evolution in interstitial free steel at small plastic strains. *Metallurgical and Materials Transactions A*. 2018;49:3274–3282. <https://doi.org/10.1007/s11661-018-4693-1>
8. Kundu A., Field D.P., Chakraborti P.C. Effect of strain and strain rate on the development of deformation heterogeneity during tensile deformation of a solution annealed 304 LN austenitic stainless steel: An EBSD study. *Materials Science and Engineering: A*. 2019;773:138854. <https://doi.org/10.1016/j.msea.2019.138854>
9. Muñoz J.A., Komissarov A. Back stress and strength contributions evolution of a heterogeneous austenitic stainless steel obtained after one pass by equal channel angular sheet extrusion (ECASE). *The International Journal of Advanced Manufacturing Technology*. 2020;109:607–617. <https://doi.org/10.1007/s00170-020-05630-1>
10. Ivanov Yu.F., Gromov V.E., Yuriev A.A., Kormyshev V.E., Rubannikova Yu.A., Semin A.P. Deformation strengthening mechanisms of rails in extremely long-term operation. *Journal of Materials Research and Technology*. 2021;11:710–718. <https://doi.org/10.1016/J.JMRT.2020.12.107>
11. Yuriev A.A., Ivanov Yu.F., Gromov V.E., Rubannikova Yu.A., Starostenkov M.D., Tabakov P.Y. Structure and properties of lengthy rails after extreme long-term operation. *Materials Research Foundations*. MRF; 2021;106:193. <https://doi.org/10.21741/9781644901472>
12. Ivanov Yu.F., Gleser A.M., Kuznetsov R.V., Gromov V.E., Shliarova Yu.A., Semin A.P., Sundeev R.V. Fine structure formation in rails under ultra long-term operation. *Materials Letters*. 2022;309(4):131378. <https://doi.org/10.1016/j.matlet.2021.131378>
13. Smirnov A.N., Kozlov E.V. Substructure, Internal Stress Fields and the Problem of Destruction of Steam Pipelines Made of 12Kh1MF Steel. Kemerovo: Kuzbassvuzizdat; 2004:163. (In Russ.).
Смирнов А.Н., Козлов Э.В. Субструктура, внутренние поля напряжений и проблема разрушения паропроводов из стали 12Х1МФ. Кемерово: Кузбассвузиздат; 2004:163.
14. Smirnov A.N., Knyaz'kov A.F., Knyaz'kov V.L., etc. Modulated Current Welding. Structural-Phase State and Internal Stress Fields in Welded Joints of Structural Steels. Moscow: Innovatsionnoe mashinostroenie; Kemerovo: Sibirskaya izdatel'skaya gruppa; 2017:328. (In Russ.).

Сварка модулированным током. Структурно-фазовое состояние и поля внутренних напряжений в сварных соединениях конструкционных сталей / А.Н. Смирнов, А.Ф. Князьков, В.Л. Князьков и др. Москва: Инновационное машиностроение; Кемерово: Сибирская издательская группа; 2017:328.

15. Smirnov A.N., Knyaz'kov A.F., Knyaz'kov V.L., etc. Structural-Phase State, Control and Testing of Welded Joints of Austenitic Stainless Steels. Kemerovo: Sibirskaya izdatel'skaya gruppy; 2021:248. (In Russ.).
Смирнов А.Н., Князьков А.Ф., Князьков В.Л. и др. Структурно-фазовое состояние, контроль и испытания сварных соединений аустенитных нержавеющей сталей. Кемерово: Сибирская издательская группа; 2021:248.
16. Panin V.E., Egorushkin V.E. Fundamental role of local curvature of crystal structure in plastic deformation and fracture of solids. *Physical Mesomechanics of Multilevel Systems 2014: AIP Conference Proceedings*. 2014;1623(1):475–478. <https://doi.org/10.1063/1.4898985>
17. Panin V.E., Panin A.V., Elsuikova T.F., Popkova Yu.F. The fundamental role of the curvature of the crystal structure in the plasticity and strength of solids. *Fizicheskaya mezomekhanika*. 2014;17(6):7–18. (In Russ.).
Панин В.Е., Панин А.В., Елсуикова Т.Ф., Попкова Ю.Ф. Фундаментальная роль кривизны кристаллической структуры в пластичности и прочности твердых тел. *Физическая мезомеханика*. 2014;17(6):7–18.
18. Cattivelli A., Roy M.J., Burke M.G., Dthers J., Lee T.L., Francis J.A. Internal stresses in a clad pressure vessel steel during post weld heat treatment and their relevance to underclad cracking. *International Journal of Pressure Vessels and Piping*. 2021;193:104448. <https://doi.org/10.1016/j.ijpvp.2021.104448>
19. Fang X.-Y., Zhang H.-N., Ma D.-W., Wu Z.-J., Huang W. Influence of welding residual stress on subsurface fatigue crack propagation of rail. *Engineering Fracture Mechanics*. 2022;271:108642. <https://doi.org/10.1016/j.engfracmech.2022.108642>
20. Kozlov E.V., Popova N.A., Kabanina O.V., Klimashin S.I., Gromov V.E. Evolution of Phase Composition, Defective Structure, Internal Stresses and Carbon Redistribution during Tempering of Cast Structural Steel. Novokuznetsk: SibSIU; 2007:177. (In Russ.).
Эволюция фазового состава, дефектной структуры, внутренних напряжений и перераспределение углерода при отпуске литой конструкционной стали / Э.В. Козлов, Н.А. Попова, О.В. Кабанина, С.И. Климашин, В.Е. Громов. Новокузнецк: изд. СибГИУ; 2007:177.
21. Kassner M.E., Geantil P., Levine L.E. Long range internal stresses in single-phase crystalline materials. *International Journal of Plasticity*. 2013;45:44–60. <https://doi.org/10.1016/j.ijplas.2012.10.003>
22. Zhang Y., Yu T., Xu R., Thorborg J., Liu W., Tischler J., Godfrey A., Jensen D.J. Local residual stresses and microstructure within recrystallizing grains in iron. *Materials Characterization*. 2022;191:112113. <https://doi.org/10.1016/j.matchar.2022.112113>
23. Glezer A.M., Kozlov E.V., Koneva N.A., Popova N.A., Kurzina I.A. Plastic Deformation of Nanostructured Materials. Boca Raton, London, New York: CRC Press, Taylor & Francis Group; 2017:334. <http://dx.doi.org/10.1201/9781315111964>
24. Valiev R.Z., Zhilyaev A.P., Langdon T.G. Bulk Nanostructured Materials: Fundamentals and Applications. Hoboken: Wiley/TMS; 2014:440. <https://doi.org/10.1002/9781118742679>
25. Vinogradov A., Estrin Y. Analytical and numerical approaches to modelling severe plastic deformation. *Progress in Materials Science*. 2018;95:172–242. <https://doi.org/10.1016/j.pmatsci.2018.02.001>
26. Wilde G., Divinski S. Grain boundaries and diffusion phenomena in severely deformed materials. *Materials Transactions*. 2019;60(7):1302–1315. <https://doi.org/10.2320/matertrans.MF201934>
27. Burkin S.P., Shimov G.V., Andryukova E.A. Residual Stresses in Metal Products. Ekaterinburg: izd. Ural'skogo universiteta; 2015:248. (In Russ.).
Буркин С.П., Шимов Г.В., Андрюкова Е.А. Остаточные напряжения в металлопродукции. Екатеринбург: изд. Уральского университета; 2015:248.
28. Handbook on Experimental Mechanics. 2nd ed. Kobayashi A. ed. VCH; 1993:1074.
Экспериментальная механика. В 2-х книгах / Пер. с англ.; под ред. А. Кобаяси. Москва: Мир; 1990.
29. Reynolds A.P., Tang W., Gnaupel-Herold T., Prask H. Structure, properties, and residual stress of 304L stainless steel friction stir welds. *Scripta Materialia*. 2003;48(9):1289–1294. [https://doi.org/10.1016/S1359-6462\(03\)00024-1](https://doi.org/10.1016/S1359-6462(03)00024-1)
30. Cihak U., Staron P., Clemens H., Homeyer J., Stockinger M., Tockner J. Characterization of residual stresses in turbine discs by neutron and high-energy X-ray diffraction and comparison to finite element modeling. *Materials Science and Engineering: A*. 2006;437(1):75–82. <https://doi.org/10.1016/j.msea.2006.04.049>
31. Withers P.J. Mapping residual and internal stress in materials by neutron diffraction. *Comptes Rendus Physique*. 2007; 8(7-8):806–820. <https://doi.org/10.1016/j.crhy.2007.09.015>
32. Withers P.J., Turski M., Edwards L., Bouchard P.J., Buttle D.J. Recent advances in residual stress measurement. *International Journal of Pressure Vessels and Piping*. 2008; 85(3):118–127. <https://doi.org/10.1016/j.ijpvp.2007.10.007>
33. Sekimoto K. Internal stress as a link between macroscale and mesoscale mechanics. In: *Chemomechanical Instabilities in Responsive Materials*. 2009:241–250. https://doi.org/10.1007/978-90-481-2993-5_10
34. Wong S.L., Dawson P.R. Evolution of the crystal stress distributions in face-centered polycrystals subjected to cyclic loading. *Acta Materialia*. 2011;59(18):6901–6916. <https://doi.org/10.1016/j.actamat.2011.07.042>
35. McNelis K.P., Dawson P.R., Miller M.P. A two-scale methodology for determining the residual stresses in polycrystalline solids using high energy X-ray diffraction data. *Journal of the Mechanics and Physics of Solids*. 2013;61(2):428–449. <https://doi.org/10.1016/j.jmps.2012.09.015>
36. Demir E., Park J.-S., Miller M.P., Dawson P.R. A computational framework for evaluating residual stress distributions from diffraction-based lattice strain data. *Computer Methods in Applied Mechanics and Engineering*. 2013;265:120–135. <https://doi.org/10.1016/j.cma.2013.06.002>
37. Skrotzki W. Deformation heterogeneities in equal channel angular pressing. *Materials Transactions*. 2019;60(7): 1331–1343. <https://doi.org/10.2320/matertrans.MF201926>
38. Yildirim C., Jessop C., Ahlström J., Detlefs C., Zhang Y. 3D mapping of orientation variation and local residual stress within individual grains of pearlitic steel using synchrotron dark field X-ray microscopy. *Scripta Materialia*. 2021;197: 113783. <https://doi.org/10.1016/j.scriptamat.2021.113783>
39. Hirsch P.B., Howrie A., Nicholson R.B., Pashley D.W., Whelan M.J. Electron Microscopy of Thin Crystals. London: Butterworths; 1965:549.

40. Mader S., Zeeger A., Leitts K. Deformation hardening and dislocation distribution in HCC metals. In: *Proceedings of the Conf. "Structure and Mechanical Properties of Metals"*, Teddington, Middlesex, January 7 – 9, 1963. Moscow: Metallurgiya; 1967:9–41. (In Russ.).
Мадер С., Зеегер А., Лейтц К. Деформационное упрочнение и распределение дислокаций в ГЦК металлах. В кн.: *Материалы конференции «Структура и механические свойства металлов», Тедингтон, Мидлсекс, 7–9 января 1963 г.* Москва: Металлургия; 1967:384.
41. Koneva N.A., Trishkina L.I., Zhdanov A.N., Perevalova O.B., Popova N.A., Kozlova E.V. Sources of stress fields in deformed polycrystals. *Fizicheskaya mezomekhanika*. 2006;9(3):93–102. (In Russ.).
Конева Н.А., Тришкина Л.И., Жданов А.Н., Перевалова О.Б., Попова Н.А., Козлова Э.В. Источники полей напряжений в деформированных поликристаллах. *Физическая мезомеханика*. 2006;9(3):93–102.
42. Gromova A.V., Yur'ev A.B., Ivanov Yu.F., Chinokalov V.Ya. Formation of long-range stress fields during wire drawing. *Izvestiya. Ferrous Metallurgy*. 2006;49(2):27–31. (In Russ.).
Громова А.В., Юрьев А.Б., Иванов Ю.Ф., Чинокалов В.Я. Формирование дальнедействующих полей напряжений при волочении проволоки. *Известия вузов. Черная металлургия*. 2006;49(2):27–31.
43. Rybin V.V. Patterns of mesostructure formation during development of plastic deformation. *Voprosy materialovedeniya*. 2002;29(1):11–33. (In Russ.).
Рыбин В.В. Закономерности формирования мезоструктур в ходе развития пластической деформации. *Вопросы материаловедения*. 2002;29(1):11–33.
44. Calcaynotto M., Ponge D., Demir E., Raabe D. Orientation gradients and geometrically necessary dislocations in ultrafine grained dual-phase steels studied by 2D and 3D EBSD. *Materials Science and Engineering: A*. 2010;527(10–11):2738–2746.
<https://doi.org/10.1016/j.msea.2010.01.004>
45. Kundu A., Field D.P. Influence of plastic deformation heterogeneity on development of geometrically necessary dislocation density in dual phase steel. *Materials Science and Engineering: A*. 2016;667:435–443.
<https://doi.org/10.1016/j.msea.2016.05.022>

Information about the Authors

Сведения об авторах

Natal'ya A. Popova, Cand. Sci. (Eng.), Research Associate of the Scientific and Educational Laboratory "Nanomaterials and Nanotechnologies", Tomsk State University of Architecture and Building

ORCID: 0000-0001-8823-4562

E-mail: natalya-popova-44@mail.ru

Elena L. Nikonenko, Cand. Sci. (Phys.-Math.), Assist. Prof. of the Chair of Physics, Chemistry, Theoretical Mechanics, Tomsk State University of Architecture and Building; Senior Lecturer, National Research Tomsk Polytechnic University

ORCID: 0000-0002-0396-9541

E-mail: vilatomsk@mail.ru

Mikhail A. Porfir'ev, Research Associate of Department of Scientific Researches, Siberian State Industrial University

ORCID: 0000-0003-3602-5739

E-mail: mporf372@gmail.com

Roman E. Kryukov, Dr. Sci. (Eng.), Assist. Prof. of the Chair of Ferrous Metallurgy, Siberian State Industrial University

ORCID: 0000-0002-3394-7941

E-mail: rek_nzrmk@mail.ru

Наталья Анатольевна Попова, к.т.н., научный сотрудник научно-учебной лаборатории «Наноматериалы и нанотехнологии», Томский государственный архитектурно-строительный университет

ORCID: 0000-0001-8823-4562

E-mail: natalya-popova-44@mail.ru

Елена Леонидовна Никоненко, к.ф.-м.н., доцент кафедры физики, химии, теоретической механики, Томский государственный архитектурно-строительный университет; старший преподаватель, Национальный исследовательский Томский политехнический университет

ORCID: 0000-0002-0396-9541

E-mail: vilatomsk@mail.ru

Михаил Анатольевич Порфирьев, научный сотрудник управления научных исследований, Сибирский государственный индустриальный университет

ORCID: 0000-0003-3602-5739

E-mail: mporf372@gmail.com

Роман Евгеньевич Крюков, д.т.н., доцент кафедры металлургии черных металлов, Сибирский государственный индустриальный университет

ORCID: 0000-0002-3394-7941

E-mail: rek_nzrmk@mail.ru

Contribution of the Authors

Вклад авторов

N. A. Popova – formation of the article main concept, conducting TEM studies in rail and martensitic steel.

E. L. Nikonenko – literature review, writing the draft.

M. A. Porfir'ev – estimation of quantitative parameters of internal stresses for rail steel.

R. E. Kryukov – estimation of quantitative parameters of internal stresses for martensitic steel.

Н. А. Попова – формирование общей концепции статьи, проведение ПЭМ исследований в рельсовой и мартенситной стали.

Е. Л. Никоненко – обзор литературы, написание чернового варианта статьи.

М. А. Порфирьев – оценка количественных параметров внутренних напряжений для рельсовой стали.

Р. Е. Крюков – оценка количественных параметров внутренних напряжений для мартенситной стали.

Received 14.02.2023

Revised 01.09.2023

Accepted 10.01.2024

Поступила в редакцию 14.02.2023

После доработки 01.09.2023

Принята к публикации 10.01.2024



UDC 669.017.15

DOI 10.17073/0368-0797-2024-2-176-184



Original article

Оригинальная статья

EVOLUTION OF DISLOCATION STRUCTURE AND PHASE COMPOSITION OF DEFORMED $Al_{0.3}CoCrFeNi$ HIGH-ENTROPY ALLOY DURING HEATING

I. V. Ivanov¹, S. A. Akkuzin², D. E. Safarova¹,I. Yu. Litovchenko², I. A. Bataev¹¹Novosibirsk State Technical University (20 K. Marksa Ave., Novosibirsk 630073, Russian Federation)²Institute of Strength Physics and Materials Science, Siberian Branch of the Russian Academy of Sciences (2/4 Akademicheskii Ave., Tomsk 634055, Russian Federation)

✉ i.ivanov@corp.nstu.ru

Abstract. When choosing compositions of high-entropy alloys, one of the parameters taken into account is thermal stability. The paper considers the structural transformations of the deformed $Al_{0.3}CoCrFeNi$ high-entropy alloy occurring during its annealing. The material was obtained by argon-arc melting with a mixture of pure single-element components. In order to homogenize the structure, the resulting ingot was subjected to thermomechanical processing according to a scheme combining cold rolling with a compression ratio of 50 % and low-temperature annealing (400 °C for 100 h). In the future, the homogenized billet was rolled in a cold state with a compression ratio of 80 %. The structure of the materials was studied directly during heating (*in-situ* mode) using the method of synchrotron X-ray diffraction. The heating rate of the samples was 20 °C/min, the maximum heating temperature was 1000 °C. The parameters of the alloy dislocation structure (density of screw dislocations, spatial distribution of dislocations) during heating were determined using the modified Williamson–Hall and Warren–Averbach methods. According to the data obtained, the temperature of beginning of formation of a high-entropy phase with a primitive cubic lattice is 560 °C. In the process of heating the material up to this temperature, an increase in density of screw dislocations and formation of a disordered dislocation structure are observed. The nature of change in dislocation density correlates well with the increase in the alloy microhardness. At an initial value of $406 \pm 13 HV_{0.1}$ (for the deformed material), the microhardness during heat treatment increases up to $587 \pm 10 HV_{0.1}$.

Keywords: high-entropy alloy, $Al_{0.3}CoCrFeNi$, plastic deformation, heat treatment, dislocation structure, transmission electron microscopy, synchrotron X-ray diffraction

Acknowledgements: The work was supported by the Russian Science Foundation, research project No. 20-73-10215 “*In-situ* study of evolution of dislocation structure of plastically deformed high-entropy alloys under high-pressures and temperatures using synchrotron radiation”.

For citation: Ivanov I.V., Akkuzin S.A., Safarova D.E., Litovchenko I.Yu., Bataev I.A. Evolution of dislocation structure and phase composition of deformed $Al_{0.3}CoCrFeNi$ high-entropy alloy during heating. *Izvestiya. Ferrous Metallurgy*. 2024;67(2):176–184.
<https://doi.org/10.17073/0368-0797-2024-2-176-184>

ЭВОЛЮЦИЯ ДИСЛОКАЦИОННОЙ СТРУКТУРЫ И ФАЗОВОГО СОСТАВА В ПРОЦЕССЕ НАГРЕВА ДЕФОРМИРОВАННОГО ВЫСОКОЭНТРОПИЙНОГО СПЛАВА $Al_{0.3}CoCrFeNi$

И. В. Иванов¹, С. А. Аккузин², Д. Э. Сафарова¹,И. Ю. Литовченко², И. А. Батаев¹¹Новосибирский государственный технический университет (Россия, 630073, Новосибирск, пр. Карла Маркса, 20)²Институт физики прочности и материаловедения Сибирского отделения РАН (Россия, 634055, Томск, пр. Академический, 2/4)

✉ i.ivanov@corp.nstu.ru

Аннотация. При выборе составов высокоэнтروпийных сплавов одним из учитываемых параметров является термическая стабильность. В работе рассматриваются структурные преобразования деформированного высокоэнтропийного сплава $Al_{0.3}CoCrFeNi$, происходящие в процессе его отжига. Материал получен методом аргондуговой плавки смеси чистых одноэлементных компонентов. С целью гомогенизации структуры полученный слиток подвергался термомеханической обработке по схеме, сочетающей холодную прокатку

со степенью обжатия 50 % и низкотемпературный отжиг (400 °C в течение 100 ч). В дальнейшем гомогенизированная заготовка прокатывалась в холодном состоянии со степенью обжатия 80 %. Структуру материалов исследовали непосредственно в процессе нагрева (в режиме *in-situ*) с использованием метода дифракции синхротронного рентгеновского излучения. Скорость нагрева образцов составляла 20 °C/мин, максимальная температура нагрева – 1000 °C. Параметры дислокационной структуры сплава (плотность винтовых дислокаций, пространственное распределение дислокаций) в процессе нагрева определяли с использованием модифицированных методов Вильямсона–Холла и Уоррена–Авербаха. Согласно полученным данным, температура начала формирования высокоэнтропийной фазы, обладающей примитивной кубической решеткой, составляет 560 °C. В процессе нагрева материала вплоть до температуры начала формирования этой фазы наблюдаются увеличение плотности винтовых дислокаций и формирование разупорядоченной дислокационной структуры. Характер изменения плотности дислокаций хорошо коррелирует с ростом микротвердости сплава. При начальном значении в $406 \pm 13 \text{ HV}_{0.1}$ (для деформированного материала) микротвердость в процессе термической обработки повышается до $587 \pm 10 \text{ HV}_{0.1}$.

Ключевые слова: высокоэнтропийные сплавы, сплав $\text{Al}_{0.3}\text{CoCrFeNi}$, пластическая деформация, термическая обработка, дислокационная структура, просвечивающая электронная микроскопия, дифракция синхротронного рентгеновского излучения

Благодарности: Исследование выполнено при финансовой поддержке Российского Научного Фонда в рамках проекта № 20-73-10215 «*In-situ* исследование эволюции дислокационной структуры пластически деформированных высокоэнтропийных сплавов в условиях действия высоких давлений и температур с применением синхротронного излучения».

Для цитирования: Иванов И.В., Аккузин С.А., Сафарова Д.Э., Литовченко И.Ю., Батаев И.А. Эволюция дислокационной структуры и фазового состава в процессе нагрева деформированного высокоэнтропийного сплава $\text{Al}_{0.3}\text{CoCrFeNi}$. *Известия вузов. Черная металлургия*. 2024;67(2):176–184. <https://doi.org/10.17073/0368-0797-2024-2-176-184>

INTRODUCTION

Thermal stability is a crucial parameter often considered when selecting compositions for high-entropy alloys (HEAs) [1 – 4]. For HEAs within multicomponent systems, the formation of both ordered and disordered crystalline phases is typical. Disordered phases are characterized by a random distribution of atoms within the unit cell, typically exhibiting a face-centered cubic (FCC) or body-centered cubic (BCC) lattice, occupying the largest fraction of the alloy volume [5]. However, during melting and subsequent heat treatment of HEAs, the formation of ordered phases with a primitive cubic lattice is possible [6]. Undoubtedly, the formation of such phases leads to changes in the properties of the alloys.

Among the numerous known compositions of HEAs, the $\text{Al}_x\text{CoCrFeNi}$ system is often highlighted [7 – 11]. The peculiarity of alloys within this system lies in the ability to control the phase composition of the alloy by varying the aluminum content. For instance, at $x = 0.3$, the alloys' structure consists solely of the BCC phase. Within the range of x values from 0.3 to 0.6, a second phase with an FCC lattice forms alongside the BCC phase in the alloy's structure. Increasing the parameter x to values of 0.6 – 2.0 is accompanied by the formation of a single-phase FCC structure.

Experimental studies and thermodynamic calculations confirm the correspondence of the structural and phase state to the indicated composition ranges of high-entropy alloys [12]. However, it is known that the formation of additional phases in alloys of the $\text{Al}_x\text{CoCrFeNi}$ system can be significantly influenced by pre-thermomechanical processing. For instance, plastic deformation of alloys with x equal to 0.3, 0.6, and 0.9 at 930 °C is accompanied by the precipitation of AlNi particles along grain boundaries [13]. Additionally, research indicates that the formation of an intermetallic phase

in $\text{Al}_x\text{CoCrFeNi}$ alloys can occur during dry friction at 900 °C. Deformation and annealing processes result in the formation of ordered high-entropy phases. For example, plastic deformation of the $\text{Al}_{0.3}\text{CoCrFeNi}$ alloy with a compression degree of 20 % followed by annealing at 550 °C leads to the formation of a phase with an L1_2 structure (characterized by a primitive cubic lattice). Increasing the annealing temperature to 700 °C is accompanied by the formation of the AlNi intermetallic and B2 phases, both possessing a primitive cubic lattice. Furthermore, the B2 phase is observed after annealing of samples deformed by the high-pressure torsion method [16]. Cold rolling of the $\text{Al}_{0.3}\text{CoCrFeNi}$ alloy with a compression degree of 50 % followed by annealing at 800 °C leads to the formation of the B2 phase [17]. The significant influence of annealing temperature on the mechanical properties of deformed HEA blanks is also noted [17].

From the analysis of available publications, several conclusions can be drawn. Firstly, alloys of the $\text{Al}_x\text{CoCrFeNi}$ system are characterized by the formation of not only high-entropy disordered phases but also multi-component phases with ordered structures. Secondly, the phase composition of these materials is largely determined by the scheme and modes of thermomechanical processing. The combination of plastic deformation and high-temperature annealing promotes the formation of ordered high-entropy phases. By varying the parameters of temperature-force exposure, it is possible to change the temperature at which the ordered phases begin to precipitate. Finally, a number of studies indicate the possibility of changing the mechanical properties of high-entropy alloys depending on the annealing temperature.

The questions regarding the thermal stability of HEAs, the formation of ordered phases in them, and changes in their mechanical properties depending on temperature effects are important not only for controlling the structure

and properties of the final product but also for understanding the conditions under which this product can function. While acknowledging the significance of this issue, it should be noted that there is a lack of experimental data revealing the peculiarities of the formation of new phases in the analyzed HEAs under deformation and thermal conditions. In this work, the method of synchrotron *X*-ray diffraction *in situ* was employed to analyze the changes in the structure of the deformed $\text{Al}_{0.3}\text{CoCrFeNi}$ alloy during heating. This method, combined with profile analysis of recorded diffraction patterns, allowed for the calculation of lattice parameter changes, identification of the temperature at which the formation of ordered high-entropy phase begins, and estimation of the density of dislocations during material heating. Additionally, the structure of the materials was investigated using transmission electron microscopy, and the hardness of the samples was evaluated using the Vickers method.

MATERIALS AND METHODS

A high-entropy alloy ingot $\text{Al}_{0.3}\text{CoCrFeNi}$ was produced by argon arc melting of pure elemental components. The melting process took place in a Bühler ArcMelter AM furnace at an argon pressure of $2 \cdot 10^{-2}$ bar ($2 \cdot 10^3$ Pa). To ensure a homogeneous chemical composition, the material underwent ten cycles of remelting. Additional thermomechanical treatment of the alloy was also conducted for the same purpose. The resulting ingot underwent cold rolling with a reduction degree of 50 % and was held at 400 °C for 100 h. This thermal treatment regime was employed to prevent the formation of ordered phases in the alloy structure [18].

The prepared billet was utilized for investigations aimed at studying the influence of heating temperature on the structural and phase transformations of the alloy deformed by cold rolling. The total reduction degree of the billet, amounting to 80 %, was achieved through multiple passes. Each pass involved a 2 % reduction in thickness relative to the initial billet thickness. Samples cut from the cold-deformed sheet were placed in a Bähr DIL 805 A/D dilatometer furnace and heated at a rate of 20 °C/min, with the maximum heating temperature reached 1000 °C.

The analysis of the material structure during heating was conducted using the *in-situ* synchrotron *X*-ray diffraction method. The investigations were carried out at the P07 (“High Energy Materials Science”) beamline of the DESY: PETRA III source in Hamburg. The wavelength of the *X*-ray radiation used was 0.014235 nm, corresponding to a photon energy of 87.1 keV. A 2D scintillation detector PerkinElmer XRD 1621 with a resolution of 2048×2048 pixels and an area of 409.6 mm^2 was employed to record the diffraction patterns, with the distance from the sample to the detector being 1.05 m.

The diffraction patterns were recorded in transverse direction and were converted into one-dimensional form by azimuthal integration using the pyFAI library [19].

To perform profile analysis, the one-dimensional diffraction patterns were described by the following function:

$$I_{\text{pattern}}(2\theta) = \sum_{i=1}^{10} I_i(2\theta) + \sum_{j=0}^7 a_j(2\theta)^j. \quad (1)$$

The first sum in Eq. (1) determines the contribution of ten diffraction maxima to the intensity, while the second represents the 7th order polynomial describing the background of the diffraction pattern. In turn, the profile of each of the diffraction maxima was described by a pseudo-Voigt function as follows:

$$I_i(2\theta) = I_0[\eta L(2\theta) + (1 - \eta)G(2\theta)], \quad (2)$$

where I_0 is the maximum intensity of diffraction maximum; η is the contribution of the Lorentz function; $L(2\theta)$ and $G(2\theta)$ are Lorentz and Gaussian functions, respectively, defined as:

$$L(2\theta) = \frac{[0,5\beta(1-A)]^2}{[0,5\beta(1-A)]^2 + (2\theta - 2\theta_0)^2}, \quad (3)$$

$$G(2\theta) = \exp \left\{ \frac{-\pi(2\theta - 2\theta_0)^2}{\left[0,5\beta(1-A)\sqrt{\frac{\pi}{\ln 2}} \right]^2} \right\}, \quad (4)$$

where $2\theta_0$ is the angular position corresponding to the maximum intensity of the peak; β is the full width at half maximum of the diffraction peak; A is the asymmetry parameter of the diffraction peak ($-1 \leq A \leq 1$).

The parameters of the dislocation structure (density of screw dislocations, spatial arrangement of dislocations) corresponding to a specific stage of alloy heating were determined using modified Williamson–Hall and Warren–Averbach methods. A detailed description of these methods is presented in [20 – 23].

In addition to experiments analyzing the structure using synchrotron *X*-ray radiation, a series of samples was prepared to evaluate the microhardness of cold-deformed HEA after heating to 100 – 900 °C (in intervals of 50 °C), including 875 and 900 °C. The materials were analyzed using the Vickers method on a semi-automatic hardness tester WolpertGroup 402MVD. The load on the four-sided diamond indenter was 0.98 N, with a dwell time under load of 10 s. The fine structure of samples thermally treated at 550, 650, and 900 °C was examined using a transmission electron microscope JEOL JEM-2100 at an accelerating voltage of 200 kV.

RESULTS AND DISCUSSION

In previous publications, various data on the characteristics of phase transformations occurring during the heating of $\text{Al}_{0.3}\text{CoCrFeNi}$ alloy have been presented. It has been noted that one of the factors determining the temperature at which ordered phases start to precipitate is the degree of pre-deformation of the material. For example, in [17], it was demonstrated that the temperature at which the B2 phase starts to form in $\text{Al}_{0.3}\text{CoCrFeNi}$ alloy, cold-rolled to 50 %, falls within the range of 600–800 °C. However, the exact value of this temperature could not be determined accurately in the *ex-situ* experiment. An undeniable advantage of the *in-situ* approach implemented in this study is the ability to precisely determine the temperatures of phase and structural transformations occurring during the heating of the alloy. Fig. 1 displays a diffraction pattern corresponding to the heating process of the cold-rolled $\text{Al}_{0.3}\text{CoCrFeNi}$ alloy. Throughout the entire temperature range, diffraction peaks of the FCC phase are observed. However, starting from around 600 °C, peaks of a phase with a primitive cubic lattice emerge. To more accurately determine the temperature at which it starts to form, an analysis of the intensity change of the (310) diffraction peak was conducted (Fig. 2).

The data presented indicate a non-monotonic change in the intensity of the peak (310) of the phase with a primitive cubic lattice (Fig. 2, *a*). A characteristic feature of this parameter is its gradual increase with temperature followed by a decrease. The analyzed phase begins to form at 560 °C (Fig. 2, *b*).

Figure 3 illustrates the results of changes in the material lattice parameter and linear expansion of the sample.

Upon heating to approximately 750 °C, the rate of change of both parameters becomes close to linear. A weakly pronounced change in the relationship between the magnitude ΔL and the heating temperature is observed in the temperature range of 450–600 °C (Fig. 3, *b*). This observed effect may be explained by the restructuring of the dislocation structure of the alloy. Upon heating the alloy to above 850 °C, the lattice parameter growth rate increases from $0.07 \cdot 10^{-4}$ to $0.125 \text{ \AA}/^\circ\text{C}$. In the temperature range of 750–900 °C, the rate of growth of the parameter ΔL gradually decreases, and in the temperature interval of 900–1000 °C, a sample compression effect is manifested.

Fig. 4 displays the results of profile analysis of experimentally recorded diffraction patterns. Using modified Williamson–Hall and Warren–Averbach methods, the values of screw dislocation density (ρ_{screw}) and Wilkens parameter (M) were calculated. The parameter M characterizes the spatial configuration features of dislocations. A decrease in M indicates the formation of dislocation walls in the alloy, while an increase in M is a sign of the formation of a disordered dislocation structure. According to the obtained data, up to the onset of ordered phase precipitation (560 °C), there is a simultaneous increase in dislocation density and disordering of the dislocation structure.

The change in dislocation density correlates well with the increase in microhardness of the analyzed samples. In the initial state (before heating), the microhardness of the cold-deformed sample is $406 \pm 13 \text{ HV}_{0.1}$. The maximum microhardness value at $587 \pm 10 \text{ HV}_{0.1}$ is recorded in samples thermally treated at 550–600 °C. According to the results of profile analysis, at these temperatures, the values of dislocation density are also at their

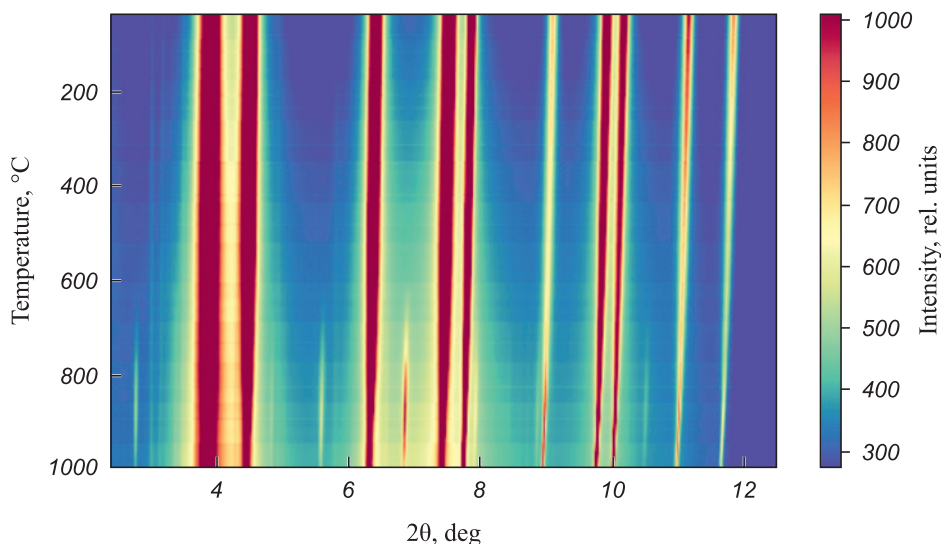


Fig. 1. X-ray diffraction pattern of heating of the cold rolled $\text{Al}_{0.3}\text{CoCrFeNi}$ alloy

Рис. 1. Дифракционная карта процесса нагрева холоднокатанного сплава $\text{Al}_{0.3}\text{CoCrFeNi}$

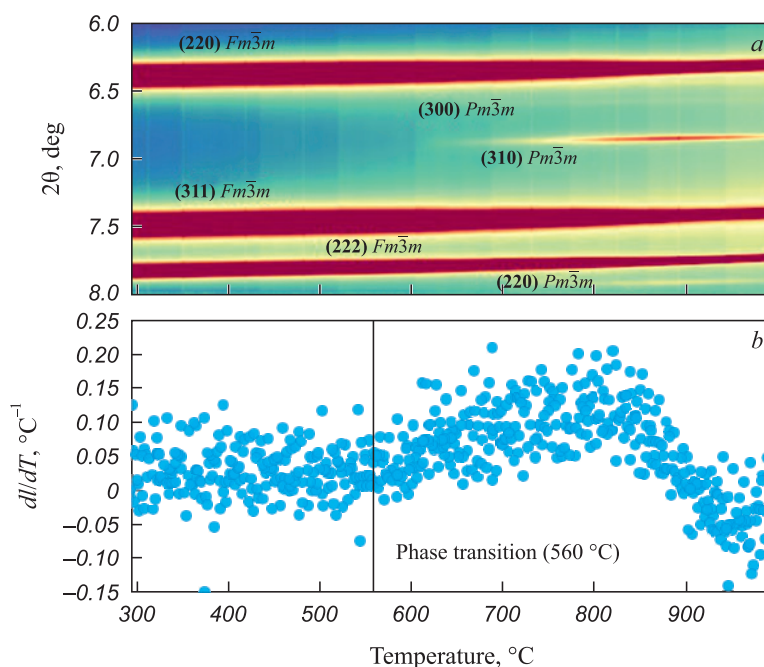


Fig. 2. Change in intensity of diffraction maxima of the disordered and ordered phases in $\text{Al}_{0.3}\text{CoCrFeNi}$ high-entropy alloy (a) and change in intensity derivative according to temperature of diffraction maximum (310) of the phase with a primitive cubic lattice (b)

Рис. 2. Изменение интенсивности дифракционных максимумов разупорядоченной и упорядоченной фаз высокоэнтропийного сплава $\text{Al}_{0.3}\text{CoCrFeNi}$ (a) и изменение производной интенсивности по температуре дифракционного максимума (310) фазы с примитивной кубической решеткой (b)

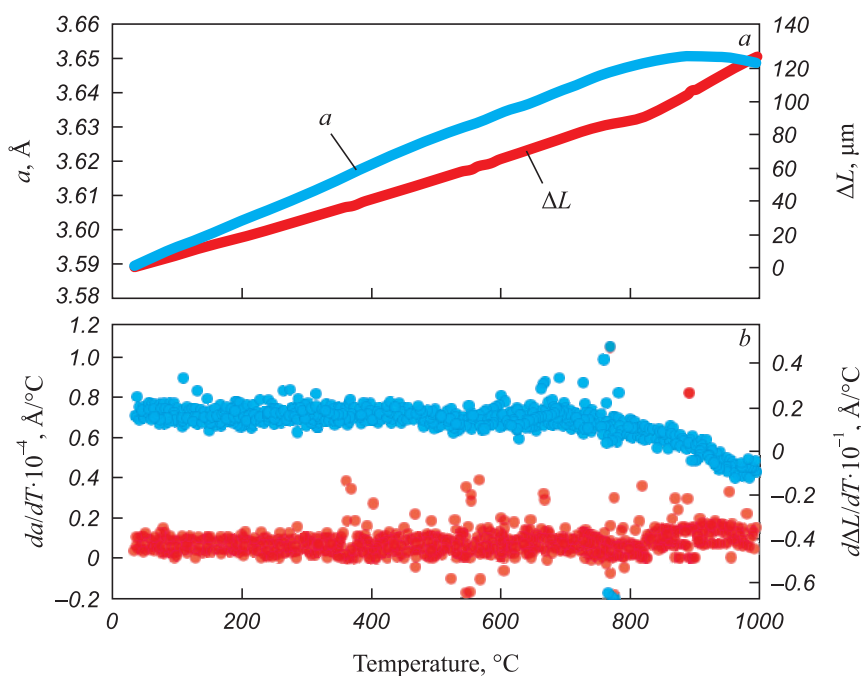


Fig. 3. Change in the lattice parameter a (●) and thermal expansion of the plastically deformed sample ΔL (●) of $\text{Al}_{0.3}\text{CoCrFeNi}$ alloy during heating (a) and change in derivatives da/dT (●) and $d\Delta L/dT$ (●) (b)

Рис. 3. Изменение параметра решетки a (●) и термическое расширение пластически деформированного образца ΔL (●) из сплава $\text{Al}_{0.3}\text{CoCrFeNi}$ в процессе его нагрева (a) и изменение производных da/dT (●) и $d\Delta L/dT$ (●) (b)

maximum level. As the temperature is further increased, the dislocation density and microhardness level decrease to $395 \pm 16 \text{ HV}_{0.1}$.

The authors of [23] have previously discussed the changes in structure and properties of the $\text{Al}_{0.3}\text{CoCrFeNi}$ alloy depending on the heat treatment

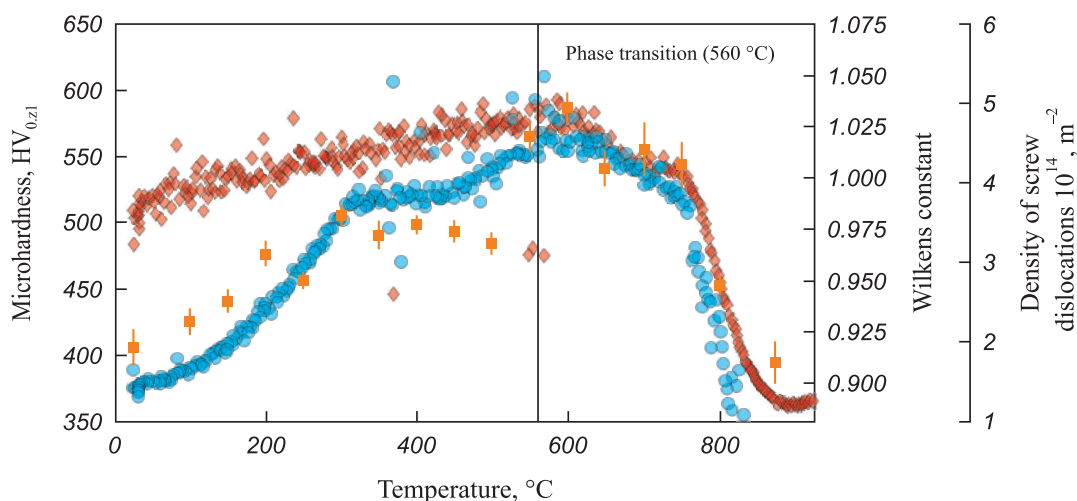


Fig. 4. Change in density of screw dislocations (●), the Wilkens parameter (◆) and microhardness (■) during heating of deformed $\text{Al}_{0.3}\text{CoCrFeNi}$ alloy

Рис. 4. Изменение плотности винтовых дислокаций (●), параметра Вилкенса (◆) и микротвердости (■) при нагреве деформированного сплава $\text{Al}_{0.3}\text{CoCrFeNi}$

temperature. In [24], it was noted that plastic deformation followed by annealing of the high-entropy alloy $\text{Al}_{0.3}\text{CoCrFeNi}$ leads to the the formation of an ordered phase with a primitive cubic lattice on subgrain boundaries or in areas of high local defect density. However, the issue regarding the increase in dislocation density during the heating process of high-entropy alloys has not been discussed in publications before and requires further research.

Analysis of Fig. 4 allows us to conclude that exceeding the temperature values corresponding to the onset of ordered phase precipitation is accompanied by a decrease in both dislocation density and the Wilkens parameter. This fact indicates the activation of processes associated with polygonization and recrystallization of the alloy structure. The results of the research conducted using transmission electron microscopy (Fig. 5) also indicate the development of recrystallization processes. Analysis of the presented images shows an increased degree of structural defects in the material in the cold-deformed state (Fig. 5, *a*), as well as after heating to 550 and 650 °C (Fig. 5, *b*, *c*).

Despite the fact that, according to synchrotron radiation diffraction data, the formation of the phase with a primitive cubic lattice begins at 560 °C, even after heating to a temperature of 650 °C, no particles of this phase were detected using transmission electron microscopy (Fig. 5, *c*). This can be explained by the fact that at the initial stage of particle formation, the analyzed phase particles are small in size and are separated from the original matrix in such a way that they are not visible using diffraction contrast. However, in samples thermally treated at 900 °C, particles of the ordered phase are clearly visible (Fig. 5, *d*).

Thus, the results of the research conducted using transmission electron microscopy correspond to the experimental data obtained during X-ray structural analysis. The analysis carried out in this work indicates that the intensive decrease in dislocation density and the Wilkens parameter (when heating the alloy to 750 °C) (Fig. 4) is due to the onset of recrystallization processes. The observed decrease in linear expansion rate (ΔL) at heating temperatures above 750 °C is likely also related to the development of recrystallization processes and the accompanying annihilation of crystal structure defects. It can be expected that with further increase in temperature, the linear expansion rate of the sample will reach a plateau, and then the material will begin to expand, but at a different rate. A similar effect was observed in a study [25] that examined the structure of friction-welded samples. The experimentally observed deviation of the $\Delta L - T$ dependence from linearity by the authors of this work was associated with recrystallization processes and changes in residual stresses. Similar phenomena were also observed in [26; 27].

CONCLUSIONS

Using synchrotron X-ray radiation diffraction, it was determined that the temperature at which the formation of a high-entropy phase with a primitive cubic lattice begins in a cold-rolled sample of $\text{Al}_{0.3}\text{CoCrFeNi}$ alloy is 560 °C.

Heating the deformed alloy to 560 °C is accompanied by an increase in the density of screw dislocations (ρ_{screw}) and an increase in the degree of disorder in the dislocation structure, expressed by the growth of the Wilkens parameter M .

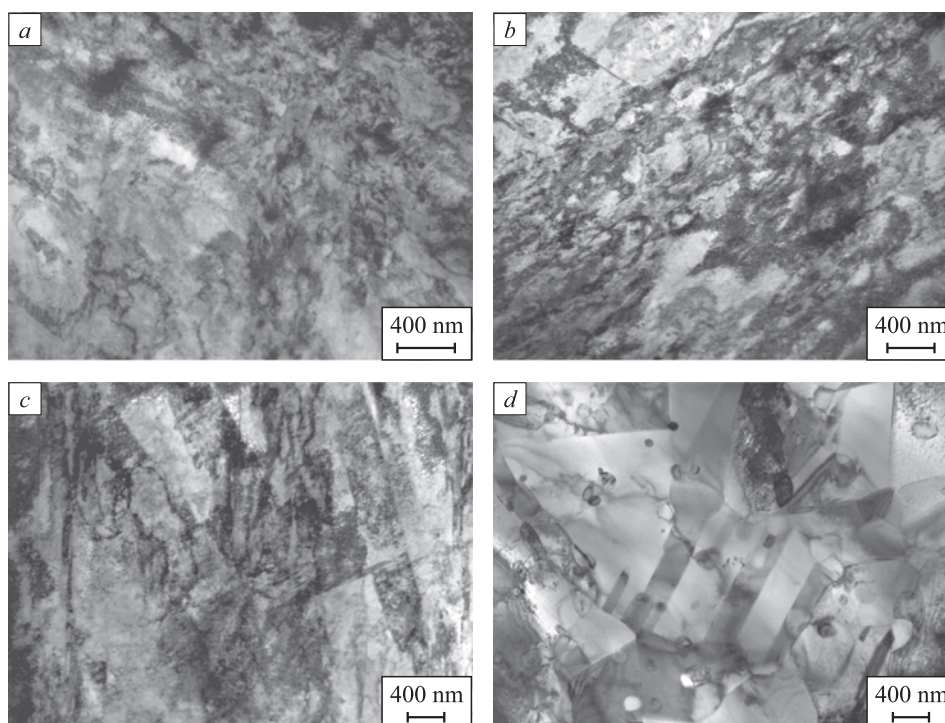


Fig. 5. Results of transmission electron microscopy of $\text{Al}_{0.3}\text{CoCrFeNi}$ alloy after cold rolling (a) and after rolling and annealing at 550 (b), 650 (c) and 900 °C (d)

Рис. 5. Результаты структурных исследований сплава $\text{Al}_{0.3}\text{CoCrFeNi}$ методом просвечивающей электронной микроскопии после холодной прокатки (a), а также после прокатки и отжига при 550 (b), 650 (c) и 900 °C (d)

The change in dislocation density correlates with the nature of the change in microhardness of the $\text{Al}_{0.3}\text{CoCrFeNi}$ alloy. Heating the cold-worked material from room temperature to 600 °C, accompanied by an increase in dislocation density, leads to an increase in microhardness from 406 ± 13 to $587 \pm 10 \text{ HV}_{0.1}$. The decrease in dislocation density that occurs during further annealing at higher temperatures leads to a decrease in the microhardness of the alloy to $395 \pm 16 \text{ HV}_{0.1}$.

Dilatometric analysis of the $\text{Al}_{0.3}\text{CoCrFeNi}$ alloy indicates a non-linear relationship between the lattice parameter a and the elongation of the sample ΔL with the heating temperature. In the temperature range from 25 to 850 °C, the rate of lattice parameter growth is $0.07 \cdot 10^{-4} \text{ Å/°C}$ and increases to 0.125 Å/°C when heated above 850 °C. An increase in temperature from 750 to 900 °C is accompanied by a gradual decrease in the rate of linear expansion of the sample. In the temperature range of 900 – 1000 °C, compression is observed. This observed effect may be associated with a decrease in the number of defects in the crystal lattice, accompanying the development of recrystallization processes.

REFERENCES / СПИСОК ЛИТЕРАТУРЫ

1. Thirathipviwat P., Song G., Jayaraj J., Bednarcik J., Wendrock H., Gemming T., Freudenberger J., Nielsch K., Han J. A comparison study of dislocation density, recrystalliza-

tion and grain growth among nickel, FeNiCo ternary alloy and FeNiCoCrMn high entropy alloy. *Journal of Alloys and Compounds*. 2019;790:266–273.

<https://doi.org/10.1016/j.jallcom.2019.03.052>

2. Karati A., Guruvidyathri K., Hariharan V.S., Murty B.S. Thermal stability of AlCoFeMnNi high-entropy alloy. *Scripta Materialia*. 2019;162:465–467. <https://doi.org/10.1016/j.scriptamat.2018.12.017>
3. Pacheco V., Lindwall G., Karlsson D., Cedervall J., Fritze S., Ek G., Berastegui P., Sahlberg M., Jansson U. Thermal stability of the HfNbTiVZr high-entropy alloy. *Inorganic Chemistry*. 2019;58(1):811–820. <https://doi.org/10.1021/acs.inorgchem.8b02957>
4. Bataeva Z.B., Ruktuev A.A., Ivanov I.V., Yurgin A.B., Bataev I.A. Review of alloys developed using the entropy approach. *Obrabotka metallov (Metal Working and Material Science)*. 2021;23(2):116–146. (In Russ.). <https://doi.org/10.17212/1994-6309-2021-23.2-116-146>
Батаева З.Б., Руктуев А.А., Иванов И.В., Юргин А.Б., Батаев И.А. Обзор исследований сплавов, разработанных на основе энтропийного подхода. *Обработка металлов (технология, оборудование, инструменты)*. 2021;23(2):116–146. <https://doi.org/10.17212/1994-6309-2021-23.2-116-146>
5. Gromov V.E., Konovalov S.V., Ivanov Yu.F., Osintsev K.A. Structure and Properties of High-Entropy Alloys. Berlin: Springer; 2021;107:110. <https://doi.org/10.1007/978-3-030-78364-8>
6. Ivanov I.V., Yurgin A.B., Nasennik I.E., Kuper K.E. Residual stress estimation in crystalline phases of high-entropy alloys of the $\text{Al}_x\text{CoCrFeNi}$ system. *Obrabotka metallov (Metal Working and Material Science)*. 2022;23(2):

- 116–146. (In Russ.).
<http://dx.doi.org/10.17212/1994-6309-2022-24.4-181-191>
- Иванов И.В., Юргин А.Б., Насенник И.Е., Купер К.Э. Оценка остаточных напряжений в кристаллических фазах высокоэнтропийных сплавов системы $\text{Al}_x\text{CoCrFeNi}$. *Обработка металлов (технология, оборудование, инструменты)*. 2022;24(4):181–191.
<http://dx.doi.org/10.17212/1994-6309-2022-24.4-181-191>
7. Wang W.-R., Wang W.-L., Yeh J.-W. Phases, microstructure and mechanical properties of $\text{Al}_x\text{CoCrFeNi}$ high-entropy alloys at elevated temperatures. *Journal of Alloys and Compounds*. 2014;589:143–152.
<https://doi.org/10.1016/j.jallcom.2013.11.084>
8. Osintsev K., Konovalov S., Gromov V., Panchenko I., Chen X. Phase composition prediction of Al-Co-Cr-Fe-Ni high entropy alloy system based on thermodynamic and electronic properties calculations. *Materials Today: Proceedings*. 2021;46-2:961–965.
<https://doi.org/10.1016/j.matpr.2021.01.079>
9. Osintsev K., Gromov V., Ivanov Y., Konovalov S., Panchenko I., Vorobyev S. Evolution of structure in AlCoCrFeNi high-entropy alloy irradiated by a pulsed electron beam. *Metals*. 2021;11(8):1228. <https://doi.org/10.3390/met11081228>
10. Osintsev K.A., Konovalov S.V., Glezer A.M., Gromov V.E., Ivanov Yu.F., Panchenko I.A., Sundeev R.V. Research on the structure of $\text{Al}_{2.1}\text{Co}_{0.3}\text{Cr}_{0.5}\text{FeNi}_{2.1}$ high-entropy alloy at submicro- and nano-scale levels. *Materials Letters*. 2021;294:129717.
<https://doi.org/10.1016/j.matlet.2021.129717>
11. Gromov V.E., Ivanov Yu.F., Konovalov S.V., Osintsev K.A. Effect of electron beam treatment on the structure and properties of AlCoCrFeNi high-entropy alloy. *CIS Iron and Steel Review*. 2021;22:72–76.
<https://doi.org/10.17580/cisirs.2021.02.13>
12. Gao M.C., Yeh J.-W., Liaw P.K., Zhang Y. High-Entropy Alloys. Cham: Springer International Publishing; 2016;1:516.
<https://doi.org/10.1007/978-3-319-27013-5>
13. Annasamy M., Haghdadi N., Taylor A., Hodgson P., Fabijanic D. Dynamic recrystallization behaviour of $\text{Al}_x\text{CoCrFeNi}$ high entropy alloys during high-temperature plane strain compression. *Materials Science and Engineering: A*. 2019;745:90–106. <https://doi.org/10.1016/j.msea.2018.12.102>
14. Joseph J., Haghdadi N., Shamlaye K., Hodgson P., Barnett M., Fabijanic D. The sliding wear behaviour of CoCrFeMnNi and $\text{Al}_x\text{CoCrFeNi}$ high entropy alloys at elevated temperatures. *Wear*. 2019;428–429:32–44.
<https://doi.org/10.1016/j.wear.2019.03.002>
15. Gwalani B., Soni V., Choudhuri D., Lee M., Hwang J.Y., Nam S.J., Ryu H., Hong S.H., Banerjee R. Stability of ordered L_{12} and B_2 precipitates in face centered cubic based high entropy alloys- $\text{Al}_{0.3}\text{CoFeCrNi}$ and $\text{Al}_{0.3}\text{CuFeCrNi}_{2.1}$. *Scripta Materialia*. 2016;123:130–134.
<https://doi.org/10.1016/j.scriptamat.2016.06.019>
16. Tang Q.H., Huang Y., Huang Y.Y., Liao X.Z., Langdon T.G., Dai P.Q. Hardening of an $\text{Al}_{0.3}\text{CoCrFeNi}$ high entropy alloy via high-pressure torsion and thermal annealing. *Materials Letters*. 2015;151:126–129.
<https://doi.org/10.1016/j.matlet.2015.03.066>
17. Ivanov I.V., Emurlaev K.I., Kuper K.E., Safarova D.E., Bataev I.A. Structural transformations during annealing of cold-worked high-entropy alloy $\text{Al}_{0.3}\text{CoCrFeNi}$. *Izvestiya. Ferrous Metallurgy*. 2022;65(8):539–547. (In Russ.).
<https://doi.org/10.17073/0368-0797-2022-8-539-547>
- Иванов И.В., Эмурлаев К.И., Купер К.Э., Сафарова Д.Э., Батаев И.А. Структурные преобразования при отжиге холоднодеформированного высокоэнтропийного сплава $\text{Al}_{0.3}\text{CoCrFeNi}$. *Известия вузов. Черная Металлургия*. 2022;65(8):539–547.
<https://doi.org/10.17073/0368-0797-2022-8-539-547>
18. Asadikiya M., Yang S., Zhang Y., Lemay C., Apelian D., Zhong Y. A review of the design of high-entropy aluminum alloys: a pathway for novel Al alloys. *Journal of Materials Science*. 2021;56(21):12093–12110.
<https://doi.org/10.1007/s10853-021-06042-6>
19. Ashiotis G., Deschilde A., Nawaz Z., Wright J.P., Karkoulis D., Piccaci F.E., Kieffer J. The fast azimuthal integration Python library: pyFAI. *Journal of Applied Crystallography*. 2015;48-2:510–519.
<https://doi.org/10.1107/S1600576715004306>
20. Ungár T., Borbély A. The effect of dislocation contrast on X-ray line broadening: A new approach to line profile analysis. *Applied Physics Letters*. 1996;69(21):3173–3175.
<https://doi.org/10.1063/1.117951>
21. Ungár T., Tichy G. The effect of dislocation contrast on X-ray line profiles in untextured polycrystals. *Physica Status Solidi (a)*. 1999;171(2):425–434.
[https://doi.org/10.1002/\(SICI\)1521-396X\(199902\)171:2<425::AID-PSSA425>3.0.CO;2-W](https://doi.org/10.1002/(SICI)1521-396X(199902)171:2<425::AID-PSSA425>3.0.CO;2-W)
22. Ungár T., Dragomir I., Révész Á., Borbély A. The contrast factors of dislocations in cubic crystals: the dislocation model of strain anisotropy in practice. *Journal of Applied Crystallography*. 1999;32(5):992–1002.
<https://doi.org/10.1107/S0021889899009334>
23. Dong W., Zhou Z., Zhang L., Zhang M., Liaw P.K., Li G., Liu R. Effects of Y, GdCu, and Al addition on the thermoelectric behavior of CoCrFeNi high entropy alloys. *Metals*. 2018;8(10):781. <https://doi.org/10.3390/met8100781>
24. Dasari S., Sarkar A., Sharma A., Gwalani B., Choudhuri D., Soni V., Manda S., Samajdar I., Banerjee R. Recovery of cold-worked $\text{Al}_{0.3}\text{CoCrFeNi}$ complex concentrated alloy through twinning assisted B_2 precipitation. *Acta Materialia*. 2021;202:448–462.
<https://doi.org/10.1016/j.actamat.2020.10.071>
25. Khosravi J., Givi M.K.B., Barmouz M., Rahi A. Microstructural, mechanical, and thermophysical characterization of Cu/WC composite layers fabricated via friction stir processing. *The International Journal of Advanced Manufacturing Technology*. 2014;74:1087–1096. <https://doi.org/10.1007/s00170-014-6050-x>
26. Boso D.P., Lefik M., Schrefler B.A. Thermal and bending strain on rmNb_3rmSn strands. *IEEE Transactions on Applied Superconductivity*. 2006;16(2):1823–1827.
<https://doi.org/10.1109/TASC.2005.864255>
27. Panigrahi B.B., Dabhade V.V., Godkhindi M.M. Thermal expansion behaviour of nanocrystalline titanium powder compacts. *Materials Letters*. 2005;59(19-20):2539–2541.
<https://doi.org/10.1016/j.matlet.2005.03.041>

Information about the Authors

Сведения об авторах

Ivan V. Ivanov, Cand. Sci. (Eng.), Research Associate of the Research Laboratory of Physical and Chemical Technologies and Functional Materials, Novosibirsk State Technical University

ORCID: 0000-0001-5021-0098

E-mail: i.ivanov@corp.nstu.ru

Sergei A. Akkuzin, Junior Researcher of the Laboratory of Materials Science of Shape Memory Alloys, Institute of Strength Physics and Materials Science, Siberian Branch of the Russian Academy of Sciences

ORCID: 0000-0002-2078-4194

E-mail: s.akkuzin@ispms.ru

Dar'ya E. Safarova, MA Student of the Chair "Materials Science in Mechanical Engineering", Novosibirsk State Technical University

ORCID: 0000-0002-2811-8292

E-mail: safarova10ab@mail.ru

Igor' Y. Litovchenko, Dr. Sci. (Phys.-Math.), Assist. Prof., Head of the Laboratory of Materials Science of Shape Memory Alloys, Institute of Strength Physics and Materials Science, Siberian Branch of the Russian Academy of Sciences

ORCID: 0000-0002-5892-3719

E-mail: litovchenko@ispms.ru

Ivan A. Bataev, Dr. Sci. (Eng.), Assist. Prof., Head of the Research Laboratory of Physical and Chemical Technologies and Functional Materials, Novosibirsk State Technical University

ORCID: 0000-0003-2871-0269

E-mail: i.bataev@corp.nstu.ru

Иван Владимирович Иванов, к.т.н., научный сотрудник научно-исследовательской лаборатории физико-химических технологий и функциональных материалов, Новосибирский государственный технический университет

ORCID: 0000-0001-5021-0098

E-mail: i.ivanov@corp.nstu.ru

Сергей Александрович Аккузин, младший научный сотрудник лаборатории материаловедения сплавов с памятью формы, Институт физики прочности и материаловедения Сибирского отделения РАН

ORCID: 0000-0002-2078-4194

E-mail: s.akkuzin@ispms.ru

Дарья Эйнуллаевна Сафарова, магистрант кафедры материаловедения в машиностроении, Новосибирский государственный технический университет

ORCID: 0000-0002-2811-8292

E-mail: safarova10ab@mail.ru

Игорь Юрьевич Литовченко, д.ф.-м.н., доцент, заведующий лабораторией материаловедения сплавов с памятью формы, Институт физики прочности и материаловедения Сибирского отделения РАН

ORCID: 0000-0002-5892-3719

E-mail: litovchenko@ispms.ru

Иван Анатольевич Батаев, д.т.н., доцент, заведующий научно-исследовательской лабораторией физико-химических технологий и функциональных материалов, Новосибирский государственный технический университет

ORCID: 0000-0003-2871-0269

E-mail: i.bataev@corp.nstu.ru

Contribution of the Authors

Вклад авторов

I. V. Ivanov – development of the concept of scientific research, processing and analysis of results, writing the text.

S. A. Akkuzin – samples preparation for research by transmission electron microscopy, analysis of the materials structure by transmission electron microscopy.

I. Yu. Litovchenko – analysis of the materials structure by transmission electron microscopy, description of results.

D. E. Safarova – smelting of samples, conducting experiments on plastic deformation.

I. A. Bataev – scientific guidance, development of the concept of scientific research, writing the text.

И. В. Иванов – разработка концепции научного исследования, обработка и анализ полученных результатов, написание текста статьи.

С. А. Аккузин – пробоподготовка образцов для проведения исследований методом просвечивающей электронной микроскопии, анализ структуры материалов методом просвечивающей электронной микроскопии.

И. Ю. Литовченко – анализ структуры материалов методом просвечивающей электронной микроскопии, описание полученных результатов.

Д. Э. Сафарова – выплавка образцов, проведение экспериментов по пластической деформации.

И. А. Батаев – руководство научным исследованием, разработка первоначальной концепции научного исследования, написание статьи.

Received 16.02.2023

Revised 16.05.2023

Accepted 11.09.2023

Поступила в редакцию 16.02.2023

После доработки 16.05.2023

Принята к публикации 11.09.2023



UDC 536.425:539.25:539.351

DOI 10.17073/0368-0797-2024-2-185-194



Original article

Оригинальная статья

FORMATION OF THE GRADIENT OF STRUCTURAL-PHASE STATES OF HIGH-SPEED STEEL DURING SURFACING. PART 2. THE ROLE OF THE MULLINS–SEKERKA INSTABILITY IN FORMATION OF CRYSTALLIZATION STRUCTURES

S. A. Nevskii¹ , L. P. Bashchenko¹, V. E. Gromov¹,
O. A. Peregudov², A. N. Gostevskaya¹, T. V. Volodin¹

¹ Siberian State Industrial University (42 Kirova Str., Novokuznetsk, Kemerovo Region – Kuzbass 654007, Russian Federation)

² Omsk State Technical University (11 Mira Ave., Omsk 644050, Russian Federation)

nevskiy.sergei@yandex.ru

Abstract. The authors studied the crystallization process of the Fe–W system, which is the basis of heat-resistant high-speed steel used in plasma arc surfacing on the surface of rolls and various cutting tools. The structure of this material consists of two components: cellular and dendritic. Histogram of the structural elements distribution shows the presence of a single maximum. The most probable size takes a value in the range of 10 – 15 μm . The paper considers the morphological instability of crystallization front (the Mullins-Sekerka instability). The model includes the equations of convective thermal conductivity and diffusion. The Stefan conditions for temperature were set at interface of the phases. Linear analysis of this instability is carried out for two cases: when the convective term in the equations of thermal conductivity and diffusion can be neglected; when convection prevails over diffusion processes. In all cases, it was assumed that the value $(1 - k_s)$ was close to zero, which corresponds to a concentration of the alloying element approximately equal to or exceeding the eutectic one, and a short-wave approximation was also used. In the first case, the analytical view of dependence of the wavelength, which accounts for the maximum rate of interface disturbances growth, coincides with generally accepted concepts. In the second case, the value of this wavelength is directly proportional to square root of the interphase boundary velocity. The limits of applicability of these approximations for various mechanisms of crystal growth were determined. In the case of normal growth, both approximations provide an adequate explanation for the formation of structural elements up to 5 μm in size at a crystallization front velocity of about 2 m/s. For the case of growth due to screw dislocations, the wavelength value corresponding to the fastest-growing perturbation mode in the first case coincides with experimental data at a crystallization front velocity of the order of 10^{-7} m/s, whereas in the convective approximation such a coincidence is observed at 10^{-4} m/s. Further development of the model consists in simultaneous consideration of the convective and diffusion components. The results obtained will serve as a material for the research of the Mullins-Sekerka instability for two interface boundaries.

Keywords: Fe – W system, the Mullins–Sekerka morphological instability, equation of thermal conductivity, mobile boundaries of phase transformations

Acknowledgements: The research was supported by the Russian Science Foundation (grant No. 23-19-00186), <https://rscf.ru/project/23-19-00186/>.

For citation: Nevskii S.A., Bashchenko L.P., Gromov V.E., Peregudov O.A., Gostevskaya A.N., Volodin T.V. Formation of the gradient of structural-phase states of high-speed steel during surfacing. Part 2. The role of the Mullins-Sekerka instability in formation of crystallization structures. *Izvestiya. Ferrous Metallurgy*. 2024;67(2):185–194. <https://doi.org/10.17073/0368-0797-2024-2-185-194>

ФОРМИРОВАНИЕ ГРАДИЕНТА СТРУКТУРНО-ФАЗОВЫХ СОСТОЯНИЙ БЫСТРОРЕЖУЩЕЙ СТАЛИ ПРИ НАПЛАВКЕ. Часть 2. Роль неустойчивости Маллинза–Секерки в образовании структур кристаллизации

С. А. Невский¹, Л. П. Башенко¹, В. Е. Громов¹, О. А. Перегудов²,
А. Н. Гостевская¹, Т. В. Володин¹

¹ Сибирский государственный индустриальный университет (Россия, 654007, Кемеровская обл. – Кузбасс, Новокузнецк, ул. Кирова, 42)

² Омский государственный технический университет (Россия, 644050, Омск, пр. Мира, 11)

✉ nevskiy.sergei@yandex.ru

Аннотация. Изучен процесс кристаллизации системы Fe–W, которая лежит в основе теплостойкой быстрорежущей стали, применяемой в процессе плазменно-дуговой наплавки на поверхность валков и различных режущих инструментов. Исследования структуры данного материала показали, что структура состоит из двух составляющих: ячеистой и дендритной. Гистограмма распределения структурных элементов показывает наличие одного максимума. Наиболее вероятный размер находится в диапазоне 10 – 15 мкм. В работе рассматривается морфологическая неустойчивость фронта кристаллизации (неустойчивость Маллинза–Секерки). Модель включает в себя уравнения конвективной теплопроводности и диффузии. На границе раздела фаз задавались условия Стефана для температуры. Линейный анализ данной неустойчивости проводится для двух случаев: когда конвективным членом в уравнениях теплопроводности и диффузии можно пренебречь; когда конвекция преобладает над диффузионными процессами. Во всех случаях предполагается, что величина $(1 - k_s)$ близка к нулю, что соответствует концентрации легирующего элемента, примерно равной эвтектической или превышающей ее, а также используется коротковолновое приближение. В первом случае аналитический вид зависимости длины волны, на которую приходится максимум скорости роста возмущений межфазной границы, совпадает с общепринятыми представлениями. Во втором случае значение данной длины волны прямо пропорционально квадратному корню из скорости движения межфазной границы. Определены границы применимости данных приближений для различных механизмов роста кристаллов. В случае нормального роста оба приближения дают адекватное объяснение образованию структурных элементов размерами до 5 мкм при скорости фронта кристаллизации порядка 2 м/с. Для случая роста за счет винтовых дислокаций значение длины волны, соответствующей наиболее быстрорастущей моде возмущений в первом случае, совпадает с экспериментальными данными при скорости фронта кристаллизации порядка 10^{-7} м/с, тогда как в конвективном приближении такое совпадение наблюдается при 10^{-4} м/с. Дальнейшее развитие модели заключается в одновременном учете конвективной и диффузионной составляющих. Полученные результаты послужат материалом для исследования неустойчивости Маллинза–Секерки для двух границ раздела.

Ключевые слова: система железо – вольфрам, морфологическая неустойчивость Маллинза–Секерки, уравнение теплопроводности, подвижные границы фазовых превращений

Благодарности: Исследование выполнено при финансовой поддержке Российского научного фонда (грант № 23-19-00186), <https://rscf.ru/project/23-19-00186/>.

Для цитирования: Невский С.А., Башенко Л.П., Громов В.Е., Перегудов О.А., Гостевская А.Н., Володин Т.В. Формирование градиента структурно-фазовых состояний быстрорежущей стали при наплавке. Часть 2. Роль неустойчивости Маллинза–Секерки в образовании структур кристаллизации. *Известия вузов. Черная металлургия*. 2024;67(2):185–194. <https://doi.org/10.17073/0368-0797-2024-2-185-194>

INTRODUCTION

High-speed steels are increasingly used as wear-resistant coating materials, applied by plasma spraying onto the working surfaces of mining and metallurgical equipment subjected to abrasive wear conditions [1]. These steels exhibit high mechanical properties such as hardness and wear resistance. However, the spraying process can lead to the formation of structures that cause cracks and reduce hardness, preventing the full utilization of the high-performance characteristics of high-alloy, heat-resistant alloys [2]. To maintain the high mechanical properties of the resulting coating, additional heat treatments [3] or adjustments to the spraying parameters [4] are necessary. Optimal spraying parameters require an understanding of the material crystallization processes and

the associated structural-phase transformations. The formation of specific structures (cellular or dendritic) during the action of concentrated energy fluxes is explained by the morphological instability of the crystallization front, known as Mullins–Sekerka instability [5; 6].

Currently, various authors are studying this instability [7 – 10]. In [7], the instability was examined for binary alloys. Criteria for absolute and relative stability of a spherical crystallization nucleus were formulated for these alloys, and it was demonstrated that as the particle size increases, the initial concentration in the diluted binary melt initially suppresses and then enhances the morphological stability of the particle. The critical concentration at which this effect begins was also determined. The work described in [8] focuses on studying

the influence of an incoming melt flow on the crystallization front of supercooled liquids with a two-phase layer. It was found that the incoming melt flow plays a crucial role in the changes in the parameters of the two-phase layer and its internal structure. The proportion of the solid phase in this layer and its thickness significantly increase, while its permeability and average distance between dendrites decrease with increasing intensity of the incoming melt flow. In [9], the verification of results from linear stability analysis using the phase field method in multi-component melts with a planar solidification front demonstrated that, despite using a unified set of equations for linear stability analysis under various solidification conditions, theoretical differences between directional and isothermal solidification should be noted. Specifically, in the case of directional solidification, if considering the steady-state solution of the planar problem, the equilibrium compositions at the interface are invariant with respect to the choice of the diffusion coefficient matrix, thus allowing the change in concentration gradients ahead of the interface, which affect instability behavior, to be easily determined since the interface velocity is known [9]. Conversely, in isothermal solidification, the planar problem does not have a steady-state solution characterized by a constant system velocity. The growth rate of the interface and the equilibrium compositions depend on the choice of the diffusion coefficient matrix as well as the alloy composition. These characteristics of phase transition affect the growth of morphological perturbations and thus influence the choice of length scales of the microstructure. In [10], similar investigations were conducted on a particle with spherical geometry, taking into account non-stationary terms in the diffusion equations and a complete representation of the diffusion coefficient matrix. This allowed the establishment that stability criteria are not reduced to low velocities as previously thought [11]. The stability of the growing sphere can be considered at high perturbation growth rates, which correspond to high supersaturation. The results clearly show that the threshold values for the destabilization of the growing sphere interface strongly depend on the growth rate. It was also found that the degree of spherical harmonics at which stability is not maintained increases with increasing growth rate. The role of surface tension in the melt is not sufficiently addressed in the presented works [7–11], while it can significantly shift the values of the wavelength corresponding to the maximum mode of perturbations [12; 13]. In [12], the dependence of this wavelength on surface tension and crystal growth mechanism is established. It is shown that for most binary compositions considered by the author, the growth mechanism occurs through screw dislocations, and the dependence of λ on $V^{-1/2}$ is practically linear and coincides with experimental data. Surface tension, according to the data from [13], has a significant influence on the kinetic coefficient in the growth model through screw dislocations.

Thus, when constructing mathematical models of crystallization of materials under plasma exposure and formulating stability criteria for the interface between the melt and crystal, in addition to concentration supercooling, it is necessary to take into account the role of surface tension and crystal growth mechanisms. As indicated in [14], the instability of Mullins–Sekerka should be studied in several stages: 1 – determine the nature of perturbations of the interface and assess the influence of its curvature on the liquidus temperature; 2 – calculate the temperature and concentration fields in the solid and liquid phases; 3 – find the dependencies of the growth rate of perturbations from conditions at the phase transition boundary. In this study, attention is given to the first and third stages of research, assuming a cylindrical shape of the crystallization front. To verify the obtained results, investigations of the structure of coatings made of high-speed steels after surfacing were conducted using scanning electron microscopy.

MATERIALS AND METHODS

Plasma coating of high-speed steel R18Yu was performed in reverse polarity within a nitrogen protective and alloying environment using non-conductive additive powder wire, as established in [15]. The chemical composition of the steel (wt. %) includes C 0.87; Cr 4.41; W 17.00; Mo 0.10; V 1.50; Ti 0.35; Al 1.15; N 0.06. This composition ensured optimal conditions for wetting the surface of the product with the deposited metal and defect-free formation of the deposited layer. Samples were taken from the upper parts of the deposited layer and subsequently sectioned on an electric spark cutting machine using kerosene for metallographic studies. The samples were then mechanically leveled using fine emery paper and diamond paste, followed by etching of the deformed layer and leveling by an electrolytic method. Studies were conducted using a KYKY-EM6900 scanning electron microscope with a thermionic tungsten cathode equipped with a microprobe attachment. The operating parameters were an accelerating voltage of 20 kV, an emission current of 150 μ A, and a filament saturation point of 2.4 A. The working distance between the sample and the objective lens was set at 15 mm. The sizes of the structural elements were determined using the random sectioning method [16].

RESULTS OF THE EXPERIMENT

Fig. 1 illustrates the microstructure of the surface layer of the plasma-coated high-speed steel, revealing two morphological components: cellular and dendritic. The grain sizes range from 3 to 45 μ m, with the most common sizes between 10 to 15 μ m, (Fig. 1, b).

The analysis of the histogram (Fig. 1, b) highlights that the instability of the crystallization front exhibits a single peak, corresponding to the wavelength that matches the most probable grain size. The presence of two distinct

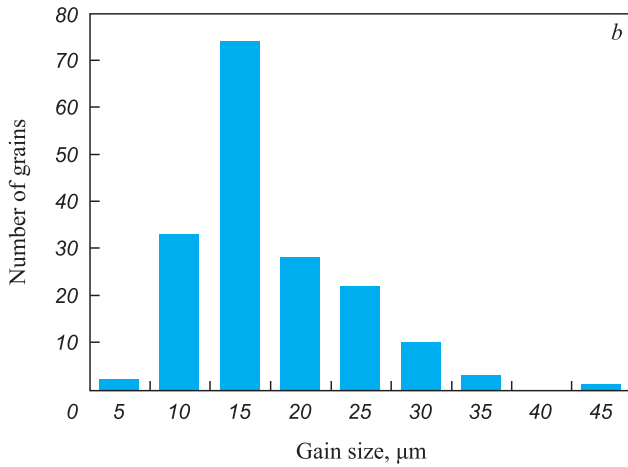
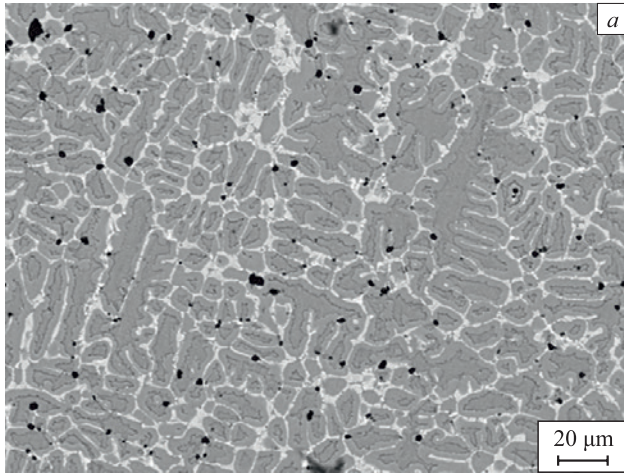


Fig. 1. Microstructure of high-speed steel coating after surfacing (a) (electron microscopical image) and histogram of grain size distribution (b)

Рис. 1. Микроструктура покрытия из быстрорежущей стали после наплавки (a) (электронно-микроскопическое изображение) и гистограмма распределения зерен по размеру (b)

morphological components indicates two types of instabilities: “soft”, associated with the cellular structure, and “hard” linked to the dendritic structure.

FORMULATION OF THE PROBLEM

Let’s examine the stability of the cylindrical crystallization front concerning small harmonic disturbances (Fig. 2).

For the sake of further calculations’ convenience, we introduce the following dimensionless variables, as in [12]:

$$T_l = \frac{T_{lr}}{T_0}, T_s = \frac{T_{sr}}{T_0}, C_l = \frac{C_{lr}}{C_0}, r = \frac{r_r}{a}, z = \frac{z_r}{a},$$

$$t = \frac{\chi_0}{a^2} t_r, D_l = \frac{D_{lr}}{\chi_0}, \chi_l = \frac{\chi_{lr}}{\chi_0}, \chi_s = \frac{\chi_{sr}}{\chi_0},$$

where T_{lr} , T_{sr} , C_{lr} , r_r , z_r , D_{lr} , χ_{lr} , χ_{sr} are the dimensional temperatures of the liquid and solid phases, impurity concentrations in the liquid phase, radial and longitu-

dinal coordinates, diffusion coefficient of the impurity in the liquid, thermal diffusivity of the liquid and solid phases, respectively; T_0 is the phase transition temperature (assumed equal to the liquidus temperature); C_0 is the initial impurity concentration, a is the initial radius of the cylindrical nucleus ($\sim 1 \mu\text{m}$); χ_0 is the characteristic value of the thermal diffusivity coefficient ($\sim 10^{-5} \text{ m}^2/\text{s}$).

Let us express the latent heat of phase transition ΔH in dimensionless form $\varepsilon = \frac{\Delta H}{c_0 T_0}$ (where c_0 is the heat capacity of the substance under study at the phase transition temperature). We will now formulate the equations of thermal conductivity and diffusion in dimensionless form for the solid and liquid phases:

$$\begin{aligned} \frac{\partial T_l}{\partial t} - V \frac{\partial T_l}{\partial r} &= \chi_l \left(\frac{\partial^2 T_l}{\partial r^2} + \frac{1}{r} \frac{\partial T_l}{\partial r} + \frac{\partial^2 T_l}{\partial z^2} \right); \\ \frac{\partial T_s}{\partial t} - V \frac{\partial T_s}{\partial r} &= \chi_s \left(\frac{\partial^2 T_s}{\partial r^2} + \frac{1}{r} \frac{\partial T_s}{\partial r} + \frac{\partial^2 T_s}{\partial z^2} \right); \\ \frac{\partial C_l}{\partial t} - V \frac{\partial C_l}{\partial r} &= D_l \left(\frac{\partial^2 C_l}{\partial r^2} + \frac{1}{r} \frac{\partial C_l}{\partial r} + \frac{\partial^2 C_l}{\partial z^2} \right). \end{aligned} \quad (1)$$

Boundary conditions:

$$\left. \begin{aligned} \chi_s \frac{\partial T_s}{\partial r} - \chi_l \frac{\partial T_l}{\partial r} &= \varepsilon V; \\ D_l \frac{\partial C_l}{\partial r} &= (1 - k_s) C_l V; \\ T_l &= T_s; V = V(T, C); \end{aligned} \right\} \text{ at } r = a + \xi(r, z); \quad (2)$$

$$C_l = 1; T_l = T_{00}; r \rightarrow \infty.$$

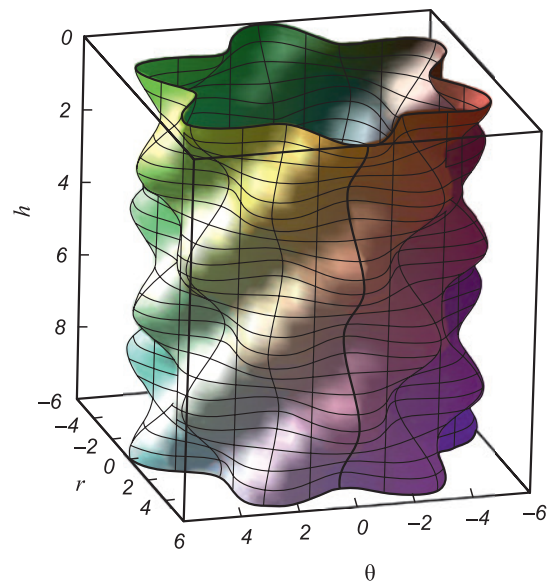


Fig. 2. Geometry of the problem of occurrence of cylindrical crystallization front instability

Рис. 2. Геометрия задачи о возникновении неустойчивости цилиндрического фронта кристаллизации

To analyze the stability of the crystallization front, we express solution (1) as a sum of stationary and disturbed components:

$$\begin{aligned} T_l &= T_{0l}(r) + T_{l1}(r, z, t); \\ T_s &= T_{0s}(r) + T_{s1}(r, z, t); \\ C_l &= C_{0l}(r) + C_{l1}(r, z, t); \\ V &= V_s + V_1(r, z, t). \end{aligned} \quad (3)$$

For the stationary component, we have:

$$\begin{aligned} \frac{\partial^2 T_{0l}}{\partial r^2} + \left(\frac{1}{r} + \frac{V_s}{\chi_l} \right) \frac{\partial T_{0l}}{\partial r} &= 0; \\ \frac{\partial^2 T_{0s}}{\partial r^2} + \left(\frac{1}{r} + \frac{V_s}{\chi_s} \right) \frac{\partial T_{0s}}{\partial r} &= 0; \\ \frac{\partial^2 C_{0l}}{\partial r^2} + \left(\frac{1}{r} + \frac{V_s}{D} \right) \frac{\partial C_{0l}}{\partial r} &= 0. \end{aligned} \quad (4)$$

Considering Eq. (3), the boundary conditions for Eq. (4) will be as follows:

$$\left. \begin{aligned} T_{0l} &= T_{0s}; \\ \chi_s \frac{\partial T_{0s}}{\partial r} - \chi_l \frac{\partial T_{0l}}{\partial r} &= \varepsilon V_s; \\ D_l \frac{\partial C_{0l}}{\partial r} &= (1 - k_s) C_{0l} V_s; \\ \chi_s \frac{\partial T_{0s}}{\partial r} &= I_0; \end{aligned} \right\} \text{ at } r = a; \quad (5)$$

$$\begin{aligned} C_{0l} &= 1, \quad T_l = T_{00}, \quad r \rightarrow \infty; \\ T_{0s} &= T_0, \quad r = r_0. \end{aligned}$$

The interface perturbation equations will be as follows:

$$\begin{aligned} \frac{\partial T_{l1}}{\partial t} - V_s \frac{\partial T_{l1}}{\partial r} - V_1 G_l &= \chi_l \left(\frac{\partial^2 T_{l1}}{\partial r^2} + \frac{1}{r} \frac{\partial T_{l1}}{\partial r} + \frac{\partial^2 T_{l1}}{\partial z^2} \right); \\ \frac{\partial T_{s1}}{\partial t} - V_s \frac{\partial T_{s1}}{\partial r} - V_1 G_s &= \chi_s \left(\frac{\partial^2 T_{s1}}{\partial r^2} + \frac{1}{r} \frac{\partial T_{s1}}{\partial r} + \frac{\partial^2 T_{s1}}{\partial z^2} \right); \\ \frac{\partial C_{l1}}{\partial t} - V_s \frac{\partial C_{l1}}{\partial r} - V_1 G_c &= D_l \left(\frac{\partial^2 C_{l1}}{\partial r^2} + \frac{1}{r} \frac{\partial C_{l1}}{\partial r} + \frac{\partial^2 C_{l1}}{\partial z^2} \right). \end{aligned} \quad (6)$$

Accordingly, boundary conditions (2) will be as follows:

$$\left. \begin{aligned} T_{l1} &= T_{s1}; \\ \chi_s \frac{\partial T_{s1}}{\partial r} - \chi_l \frac{\partial T_{l1}}{\partial r} &= \varepsilon V_s; \\ D_l \frac{\partial C_{l1}}{\partial r} &= (1 - k_s)(V_s C_{l1} + C_{0l} V_1); \end{aligned} \right\} \text{ at } r = a; \quad (7)$$

$$\begin{aligned} C_{l1} &= 0; \quad T_{l1} = 0; \quad r \rightarrow \infty; \\ T_{s1} &= 0; \quad r \rightarrow 0. \end{aligned}$$

Analyzing linear stability requires knowledge of the analytical form of the unperturbed temperature gradients included in equation (6). To obtain them, we need to solve the boundary value problem (4), (5). Let's present the solutions to this problem in the form:

$$\begin{aligned} T_{0l} &= T_{00} + \left(\frac{T_0 - T_{00}}{Ei\left(\frac{V_s a}{\chi_l}\right)} + \frac{I_0 a}{\chi_s} \exp\left(\frac{V_s a}{\chi_s}\right) \left[Ei\left(\frac{V_s r_0}{\chi_s}\right) - Ei\left(\frac{V_s a}{\chi_s}\right) \right] \right) Ei\left(\frac{V_s r}{\chi_l}\right); \\ T_{0s} &= T_0 + \frac{I_0 a}{\chi_s} \exp\left(\frac{V_s a}{\chi_s}\right) \left[Ei\left(\frac{V_s r_0}{\chi_s}\right) - Ei\left(\frac{V_s a}{\chi_s}\right) \right]; \\ C_{0l} &= 1 + \frac{V_s a(1 - k_s) Ei\left(\frac{V_s r}{D_l}\right)}{V_s a(k_s - 1) Ei\left(\frac{V_s a}{D_l}\right) + D_l \exp\left(-\frac{V_s a}{D_l}\right)}. \end{aligned} \quad (8)$$

Let us proceed to solve the boundary value problem (6) and (7) for perturbations of temperature, concentration, and velocity of the crystallization front. We will seek its solution in the following form:

$$\begin{aligned} T_{l1}(r, z, t) &= T_{m1}(r) \exp(\omega t + kz); \\ T_{s1}(r, z, t) &= T_{m2}(r) \exp(\omega t + kz); \\ C_{l1}(r, z, t) &= C_m(r) \exp(\omega t + kz); \\ V_1 &= V_m(r) \exp(\omega t + kz), \end{aligned} \quad (9)$$

where $\omega = \omega_1 + i\omega_2$; $k = k_1 + ik_2$.

Then, equations (6) will take the form:

$$\begin{aligned} \frac{d^2 T_{m1}}{dr^2} + \left(\frac{1}{r} + \frac{V_s}{\chi_l} \right) \frac{dT_{m1}}{dr} + \frac{\chi_l k^2 - \omega}{\chi_l} T_{m1} &= -\frac{V_m}{\chi_l} G_l; \\ \frac{d^2 T_{m2}}{dr^2} + \left(\frac{1}{r} + \frac{V_s}{\chi_s} \right) \frac{dT_{m2}}{dr} + \frac{\chi_s k^2 - \omega}{\chi_s} T_{m2} &= -\frac{V_m}{\chi_s} G_s; \\ \frac{d^2 C_m}{dr^2} + \left(\frac{1}{r} + \frac{V_s}{D_l} \right) \frac{dC_m}{dr} + \frac{D_l k^2 - \omega}{D_l} C_m &= -\frac{V_m}{D_l} G_c. \end{aligned} \quad (10)$$

Accordingly, the boundary conditions (7) take the form (where the prime denotes the derivative with respect to the radial coordinate):

$$\begin{aligned} T_{m1}(a) &= T_{m2}(a); \\ \chi_s T_{m2}(a)' - \chi_l T_{m1}(a)' &= \varepsilon V_m(a); \\ D_l C_m(a)' &= (k_s - 1)[V_s C_m(a) + C_{0l} V_m(a)]; \\ C_m &= 0; \quad T_{m1} = 0; \quad r \rightarrow \infty; \quad T_{m2} = 0; \quad r \rightarrow 0. \end{aligned} \quad (11)$$

As in equation [1], the amplitude of interphase boundary velocity disturbances as a function of maximum temperature and concentration disturbances is as follows:

$$V_m(a) = \theta T_{m1}(a) + \gamma C_m(a), \quad (12)$$

$$\text{where } \theta = \frac{\partial V}{\partial T}; \gamma = \frac{\partial V}{\partial C}.$$

DISPERSION EQUATION OF PERTURBATIONS OF PHASE TRANSITION BOUNDARY

Equations (10) are degenerate inhomogeneous hypergeometric equations whose solutions are Kummer functions. Obtaining and analyzing the dispersion equation, which includes these functions, is a complex and non-trivial task. Therefore, we will limit ourselves to considering special cases. In the first case, we neglect the convective term in equation (1). Then, stationary solutions are as follows:

$$\begin{aligned} T_{0l} &= T_{00} + \frac{a \ln\left(\frac{r}{b_l}\right) (I_0 - \varepsilon V_s)}{\chi_l}; \\ T_{0s} &= T_0 + \frac{a \ln\left(\frac{r}{b}\right) I_0}{\chi_s}; \\ C_{0l} &= 1 + \frac{(k_s - 1) V_s a \ln\left(\frac{r}{b_l}\right)}{(1 - k_s) a V_s \ln\left(\frac{r}{b_l}\right) + D_l}. \end{aligned} \quad (13)$$

Accordingly, equation (10) are as follows:

$$\begin{aligned} \frac{d^2 T_{m1}}{dr^2} + \frac{1}{r} \frac{dT_{m1}}{dr} - S_1^2 T_{m1} &= 0; \\ \frac{d^2 T_{m2}}{dr^2} + \frac{1}{r} \frac{dT_{m2}}{dr} - S_2^2 T_{m2} &= 0; \\ \frac{d^2 C_m}{dr^2} + \frac{1}{r} \frac{dC_m}{dr} - S_3^2 C_m &= 0, \end{aligned} \quad (14)$$

$$\text{where } S_1^2 = \frac{\omega}{\chi_l} - k^2; S_2^2 = \frac{\omega}{\chi_s} - k^2; S_3^2 = \frac{\omega}{D_l} - k^2.$$

Solutions (14) are as follows:

$$\begin{aligned} T_{m1} &= A_1 I_0(S_1 r) + A_2 K_0(S_1 r); \\ T_{m2} &= A_3 I_0(S_2 r) + A_4 K_0(S_2 r); \\ C_m &= A_5 I_0(S_3 r) + A_6 K_0(S_3 r). \end{aligned} \quad (15)$$

Substituting equations (15) into boundary conditions (11) and subsequent transformations, taking into account equation (12), lead to the following dispersion equation:

$$\begin{aligned} &\left(\frac{K_0(S_1 a) I_1(S_2 a) S_2}{I_0(S_2 a)} \chi_2 + \chi_1 K_1(S_1 a) S_1 - \varepsilon \theta K_0(S_1 a) \right) \times \\ &\times \left[(1 - k_s) K_0(S_3 a) (C_0 \gamma + V_s) - D_l K_1(S_3 a) S_3 \right] + \\ &+ (1 - k_s) \varepsilon \gamma C_0 K_0(S_3 a) K_0(S_1 a) \theta = 0. \end{aligned} \quad (16)$$

At an impurity concentration approximately equal to the eutectic, the value $(1 - k_s)$ is close to zero, therefore, these terms in dependence (16) can be neglected. As a result, we have:

$$\frac{I_1(S_2 a)}{I_0(S_2 a)} S_2 \chi_2 + \frac{K_1(S_1 a)}{K_0(S_1 a)} S_1 \chi_1 - \varepsilon \theta = 0. \quad (17)$$

The value of θ , as in [1], is considered equal to $\frac{\Lambda \omega}{\Lambda \Gamma k^2 - \omega}$ (where $\Lambda = \frac{\partial V}{\partial \Delta T}$ is a coefficient depending on the crystal growth mechanism; $\Gamma = \alpha \Gamma_r$; Γ_r is the ratio of the product of surface tension and phase transition temperature to the volumetric latent energy of phase transformation; $\alpha = 1/(a T_0)$).

In the case of short waves, where $S_{1,2} \gg 1$, the approximate values of the Bessel functions can be represented as

$$I_0(S_2 a) \approx I_1(S_2 a) \approx \frac{\exp(S_2 a)}{\sqrt{2\pi S_2 a}}$$

$$K_0(S_1 a) \approx K_1(S_1 a) \approx \frac{\pi \exp(-S_1 a)}{\sqrt{2\pi S_1 a}}.$$

Then, equation (17) is as follows

$$S_2 \chi_2 + S_1 \chi_1 - \varepsilon \theta = 0. \quad (18)$$

We assume that $k_1 = 0$ and $\omega_2 = 0$, then $S_1 = \sqrt{k_2^2 + \frac{\omega_1}{\chi_l}}$, $S_2 = \sqrt{k_2^2 + \frac{\omega_1}{\chi_s}}$. Let us substitute as follows: $\omega_1 = \frac{\delta V_s^2}{D_l}$, $k_2^2 = \frac{V_s^2}{D_l^2} Y$. Then, $S_1 = \frac{V_s}{D_l} \sqrt{Y + \frac{\delta D_l}{\chi_l}}$, $S_2 = \frac{V_s}{D_l} \sqrt{Y + \frac{\delta D_l}{\chi_s}}$. Provided that $Y \gg \frac{\delta D_l}{\chi_s}$ and at $\delta \sim Y$ the maximum growth rate will be observed at the wavelength

$$\lambda = \frac{2\pi(\chi_l + \chi_s)}{\varepsilon \Lambda} (1 + \Lambda \Gamma). \quad (19)$$

Thus, it can be concluded that equation (19) completely coincides with the dependency obtained in [12]. This allows us to infer that in the short-wave approximation, considering only diffusion terms, the problem of finding the wavelength at which the growth rate maximum occurs simplifies for cylindrical geometry to a problem on a plane.

In the second case, we neglect the diffusion term in equation (6). Then the equation takes the form:

$$\begin{aligned} \frac{\partial T_{l1}}{\partial t} - V_s \frac{\partial T_l}{\partial r} - V_l G_l &= 0; \\ \frac{\partial T_{s1}}{\partial t} - V_s \frac{\partial T_{s1}}{\partial r} - V_l G_s &= 0; \\ \frac{\partial C_{l1}}{\partial t} - V_s \frac{\partial C_{l1}}{\partial r} - V_l G_c &= 0. \end{aligned} \quad (20)$$

Substitution of solutions (22) into boundary conditions (11), subsequent transformations taking into account (12) lead to the following dispersion equation:

$$\begin{aligned} \frac{dT_{m1}}{dr} - \frac{\omega}{V_s} T_{m1} &= 0; \quad \frac{dT_{m2}}{dr} - \frac{\omega}{V_s} T_{m2} = 0; \\ \frac{dC_m}{dr} - \frac{\omega}{V_s} C_m &= 0. \end{aligned} \quad (21)$$

The solutions are as follows:

$$\begin{aligned} T_{m1} &= A_1 \exp\left(\frac{\omega r}{V_s}\right); \quad T_{m2} = A_2 \exp\left(\frac{\omega r}{V_s}\right); \\ C_m &= A_3 \exp\left(\frac{\omega r}{V_s}\right). \end{aligned} \quad (22)$$

Substituting solutions (22) into boundary conditions (11), subsequent transformations taking into account (12), lead to the following dispersion equation:

$$\begin{aligned} \left(\frac{(\chi_s - \chi_l)\omega}{V_s} - \varepsilon\theta \right) \left(\frac{D_l\omega}{V_s} - (k_s - 1)(V_s + C_0\gamma) \right) - \\ - \gamma\varepsilon(k_s - 1)C_0\theta = 0. \end{aligned} \quad (23)$$

Also, as in the previous case, in equation (23) we neglect the terms that contain $(k_s - 1)$. As a result, we get

$$\frac{(\chi_s - \chi_l)\omega}{V_s} - \varepsilon\theta = 0. \quad (24)$$

The maximum growth rate of disturbances is observed at a wavelength

$$\lambda = \frac{2\pi\sqrt{\varepsilon V_s \Lambda (\chi_s - \chi_l)(1 + \Gamma\Lambda)}}{\varepsilon \Lambda V_s}. \quad (25)$$

During normal crystal growth, the crystallization front velocity is directly proportional to the degree of undercooling $V_s = h\Delta T$ [12; 13] (where h is the proportionality coefficient; ΔT is undercooling). Then $\Lambda = h$. According to model [13], the dimensional value of the coefficient h is determined as

$$h_r = \frac{\beta D_l \Delta H M}{\Delta I R T_{rL}^2}, \quad (26)$$

where M is the molar weight; R is the universal gas constant; ΔI is the disturbance amplitude of the interface (approximately 0.1 nm); T_{rL} is the liquidus temperature; β is the coefficient that accounts for the difference between the mean free path of molecules in the liquid phase and the period of the crystalline lattice, as well as the symmetry of the molecules (for symmetric molecules $\beta \sim 10$).

According to the data from the Table in equation (26), it follows that with an initial nucleus size of 1 μm , the value of the coefficient h_r is 0.558 m/(s·K).

The transition to dimensional variables in equation (19) gives

$$\lambda_r = \frac{2\pi(\chi_{lr} + \chi_{sr})}{\frac{\Delta H}{c_0} h_r} \left(1 + h_r \frac{\Gamma_r}{\chi_0} \right). \quad (27)$$

The crystallization front velocity is determined based on the data from reference [14] as follows $V_{sr} = \frac{\Delta a}{\Delta t}$, knowing the undercooling, we determine h_r . Reference [14] indicates that $\Delta a = 10^{-8}$ m, and $\Delta t = 4.4118$ ns, then $V_{sr} = 2.27$ m/s and $h_r = 0.757$ m/(a·K) for an undercooling of 3 K. The coefficient Γ_r is determined as $\Gamma_r = \frac{\gamma T_{Lr}}{\Delta H \rho} = 1.71 \cdot 10^{-6}$ K·m. Calculation according to equation (27) shows that in the case when h_r is 0.558 m/(s·K), $\lambda = 0.382$ μm . With $h_r = 0.757$ m/(s·K), calculation according to equation (27) leads to $\lambda = 0.291$ μm . Calculation based on equation (25) shows that for $h_r = 0.558$ m/(s·K), $\lambda = 0.324$ μm , and for $h_r = 0.757$ m/(s·K), $\lambda = 0.242$ μm . Comparison of the obtained results with the grain sizes in Fig. 1, *b* shows that both convective and diffusive approximations provide an explanation for grain size formation through the mechanism of normal growth

Characteristics of the Fe–W system

Характеристики системы железо – вольфрам

Properties of material	Symbol	Value
Liquidus point, K	T_{Lr}	1806
Specific heat of melting, kJ/kg	ΔH	270
Density, kg/m ³	ρ	6980
Diffusion coefficient, m ² /s	D_r	10^{-8}
Specific heat capacity, J/(kg·K)	c_0	611
Thermal diffusivity of the liquid phase, m ² /s	χ_1	$6.8 \cdot 10^{-6}$
Thermal diffusivity of the solid phase, m ² /s	χ_2	$6.9 \cdot 10^{-6}$
Surface tension, N/m	γ	1.788

up to 5 μm , although the maximum is found at sizes of 10 – 15 μm . This suggests that under these conditions, the normal growth model is not adequate. Let us consider the growth mechanism through screw dislocations. The crystallization front velocity in this case is directly proportional to the square of the undercooling. In this case $\Lambda = 2\sqrt{hV_s}$ [12], equation (19) will take the form:

$$\lambda = \frac{\pi(\chi_l + \chi_s)}{\varepsilon\sqrt{hV_s}} \left(1 + 2\sqrt{hV_s}\Gamma\right). \quad (28)$$

Returning to the dimensional variables in equation (28), we obtain

$$\lambda_r = \frac{\pi(\chi_{lr} + \chi_{sr})}{\frac{\Delta H}{c_0}\sqrt{h_r V_{sr}}} \left(1 + 2\sqrt{h_r V_{sr}} \frac{\Gamma_r}{\chi_0}\right). \quad (29)$$

For the growth mechanism through screw dislocations, the value of the kinetic coefficient h_r is determined as

$$h_r = \frac{\beta(1 + 2g^{1/2})D_{lr}(\Delta HM)^2}{4\pi gRT_{rL}^3\gamma V_m}, \quad (30)$$

where $g = 2\pi^4 n^3 \exp\left(-\frac{\pi^2 n}{2}\right)$; n is the number of molecular layers [16]; V_m is the molar volume.

For metallic materials, when $n \sim 6$, $g \sim 5.99 \cdot 10^{-9}$. The value of the kinetic coefficient h_r , calculated from the table data for the growth model through screw dislocations, is 433 $\text{m}/(\text{s} \cdot \text{K}^2)$. The value of the wavelength, calculated using equation (30) with this value of h_r and a crystallization front velocity of about 10^{-7} m/s , is 14.8 μm , which coincides with the most probable grain size values in Fig. 1, b. In the convective approximation, calculation using equation (25) shows that the wavelength takes values of the order of 10^4 μm . This suggests a predominance of diffusion processes at these crystallization front velocities. When the crystallization velocity is increased by three orders of magnitude, $\lambda = 14.9$ μm , which matches the experimental data. Thus, the convective approximation is significant for crystallization velocities greater than 10^{-4} m/s . Based on the above, it can be concluded that the Mullins–Sekerka instability provides an adequate explanation for the formation of cellular structures with sizes of about 10 μm at $V_s < 1$ m/s and undercooling degrees of about $\sim 10^{-5}$ K. When a volumetric heat source acts on the surface of the irradiated material, as shown in [17; 18], obtained using the phase-field method, the transformation front velocity can range from 10^{-7} to 10^3 m/s , depending on the power density of the source and the characteristics of the medium. These works [19; 20] indicate that the action of this source leads to the occurrence of large temperature gradients in the surface layers of the material and, as a result, to the emergence of thermocapillary

effects. This allows us to conclude that to build a crystallization model, in addition to the Mullins–Sekerka morphological instability, it is necessary to take into account other instabilities (thermocapillary and concentration-capillary) that occur in the molten material. Analysis of the dispersion equations obtained in [21; 22] for these instabilities showed that for the Fe–W system under consideration, the wavelength corresponding to the maximum disturbances is 12 μm , which also coincides with experimental data.

CONCLUSIONS

The theoretical study conducted on the formation of cellular structures during the crystallization process of the iron-tungsten system, by analyzing the dispersion equation characterizing the morphological instability of the crystallization front (the Mullins–Sekerka instability), revealed that the mechanism of normal crystal growth provides an adequate explanation for the formation of cells with sizes up to 5 μm when the convective term can be neglected. Additionally, the growth mechanism through screw dislocations leads to $\lambda = 14.8$ μm , coinciding with experimental data under the condition that the crystallization front velocity is less than 1 m/s and the undercooling degree is about $\sim 10^{-5}$ K. Further development of the presented model involves incorporating thermocapillary and concentration-capillary effects.

REFERENCES / СПИСОК ЛИТЕРАТУРЫ

1. Mozgovoi I.V., Shneider E.A. High-Speed Steel Surfacing. Omsk: izd. OmGTU; 2016:200. (In Russ.).
Мозговой И.В., Шнейдер Е.А. Наплавка быстрорежущей стали. Омск: изд. ОмГТУ; 2016:271.
2. Wang Yu., Mao B., Chu S., Chen S., Xing H., Zhao H., Wang S., Wang Y., Zhang J., Sun B. Advanced manufacturing of high-speed steels: A critical review of the process design, microstructural evolution, and engineering performance. *Journal of Materials Research and Technology*. 2023;24: 8198–8240. <https://doi.org/10.1016/j.jmrt.2023.04.269>
3. Lavrentiev A.Yu., Dozhdelev A.M. Improvement of the structure of the zone of thermal influence of a deposited bimetallic tool. *Scientific and Technical Bulletin of St. Petersburg State University. Natural and Engineering Sciences*. 2017;23(3):118–126. (In Russ.).
<https://doi.org/10.18721/JEST.230311>
4. Лаврентьев А.Ю., Дожделев А.М. Совершенствование структуры зоны термического влияния наплавленного биметаллического инструмента. *Научно-технические ведомости СПбПУ. Естественные и инженерные науки*. 2017;23(3):118–126. <https://doi.org/10.18721/JEST.230311>
4. Cao H.T., Dong X.P., Pan Z., Wu X.W., Huang Q.W., Pei Y.T. Surface alloying of high-vanadium high-speed steel on ductile iron using plasma transferred arc technique: Microstructure and wear properties. *Materials & Design*. 2016;100: 223–234. <https://doi.org/10.1016/j.matdes.2016.03.114>

5. Sekerka R.F. Morphological stability. *Journal of Crystal Growth*. 1968;3-4:71–81.
[https://doi.org/10.1016/0022-0248\(68\)90102-4](https://doi.org/10.1016/0022-0248(68)90102-4)
6. Merchant G.J., Davis S.H. Morphological instability in rapid directional solidification. *Acta Metallurgica et Materialia*. 1990;38(12):2683–2693.
[https://doi.org/10.1016/0956-7151\(90\)90282-L](https://doi.org/10.1016/0956-7151(90)90282-L)
7. Chen M.W., Wang Z.D. The evolution and morphological stability of a particle in a binary alloy melt. *Journal of Crystal Growth*. 2023;607:127113.
<https://doi.org/10.1016/j.jcrysgro.2023.127113>
8. Alexandrov D.V., Toropova L.V. The role of incoming flow on crystallization of undercooled liquids with a two-phase layer. *Scientific Reports*. 2022;12:17857.
<https://doi.org/10.1038/s41598-022-22786-w>
9. Lahiri A., Choudhury A. Theoretical and numerical investigation of diffusive instabilities in multicomponent alloys. *Journal of Crystal Growth*. 2017;459:1–12.
<http://dx.doi.org/10.1016/j.jcrysgro.2016.11.046>
10. Guillemot G., Gandin C.-A. Morphological stability of spherical particles – Extension of the Mullins-Sekerka criteria to multi-component alloys under a non-stationary diffusive regime. *Acta Materialia*. 2021;205:116539.
<https://doi.org/10.1016/j.actamat.2020.116539>
11. Colin J., Voorhees P.W. Morphological instability of a solid sphere of dilute ternary alloy growing by diffusion from its melt. *Journal of Crystal Growth*. 2016;448:17–20.
<https://doi.org/10.1016/j.jcrysgro.2016.03.041>
12. Gus'kov A.P. Dependence of structure period on interphase boundary velocity during eutectics crystallization. *Zhurnal tekhnicheskoi fiziki*. 2003;73(5):46–52. (In Russ.).
Гуськов А.П. Зависимость периода структуры от скорости межфазной границы при кристаллизации эвтектик. *Журнал технической физики*. 2003;73(5):46–52.
13. Gus'kov A.P., Orlov A.D. Dependence of period of macrostructures on kinetic parameters under directed crystallization. *Computational Materials Science*. 2002;24(1-2):93–98.
[https://doi.org/10.1016/S0927-0256\(02\)00169-6](https://doi.org/10.1016/S0927-0256(02)00169-6)
14. Nevskii S.A., Bashchenko L.P., Peregudov O.A. Formation of the gradient of structural-phase states of high-speed steel during surfacing. Part 1. Solving the Stefan problem with two movable boundaries. *Izvestiya. Ferrous Metallurgy*. 2023;66(5):587–593.
<https://doi.org/10.17073/0368-0797-2023-5-587-593>
Невский С.А., Башченко Л.П., Перегудов О.А. Формирование градиента структурно-фазовых состояний быстрорежущей стали при наплавке. Часть 1. Решение задачи Стефана с двумя подвижными границами. *Известия вузов. Черная металлургия*. 2023;66(5):587–593.
<https://doi.org/10.17073/0368-0797-2023-5-587-593>
15. Malushin N.N., Romanov D.A., Kovalev A.P., Osetkovskii V.L., Bashchenko L.P. Structural-phase state of a heat-resistant alloy of high hardness formed by plasma surfacing in nitrogen medium and high-temperature tempering. *Izvestiya vuzov. Fizika*. 2019;62(10(742)):106–111. (In Russ.).
Малушин Н.Н., Романов Д.А., Ковалев А.П., Осетковский В.Л., Башченко Л.П. Структурно-фазовое состояние теплостойкого сплава высокой твердости, сформированного плазменной наплавкой в среде азота и высокотемпературным отпуском. *Известия вузов. Физика*. 2019;62(10(742)):106–111.
16. Cahn J.W., Hillig W.B., Sears G.W. The molecular mechanism of solidification. *Acta Metallurgica*. 1964;12(12):1421–1439.
[https://doi.org/10.1016/0001-6160\(64\)90130-0](https://doi.org/10.1016/0001-6160(64)90130-0)
17. Slyadnikov E.E., Turchanovskii I.Yu. The order parameter and kinetics of a nonequilibrium phase transition stimulated by the action of a volumetric heat source. *Izvestiya vuzov. Fizika*. 2016;59(9):125–133. (In Russ.).
Слядников Е.Е., Турчановский И.Ю. Параметр порядка и кинетика неравновесного фазового перехода, стимулированного воздействием объемного теплового источника. *Известия вузов. Физика*. 2016;59(9):125–133.
18. Slyadnikov E.E., Khon Yu.A., Kaminskii P.P., Turchanovskii I.Yu. Kinetics of nonequilibrium melting of a macrosystem initiated by the action of a volumetric heat source on it. *Inzhenerno-fizicheskii zhurnal*. 2020;93(2):403–415. (In Russ.).
Слядников Е.Е., Хон Ю.А., Каминский П.П., Турчановский И.Ю. Кинетика неравновесного плавления макросистемы, инициированного воздействием на нее объемного теплового источника. *Инженерно-физический журнал*. 2020;93(2):403–415.
19. Mirzade F.Kh. Wave instability of a molten metal layer formed by intense laser irradiation. *Technical Physics*. 2005;50(8):993–998. <http://dx.doi.org/10.1134/1.2014528>
20. Das K.S., Ward C.A. Surface thermal capacity and its effects on the boundary conditions at fluid-fluid interfaces. *Physical Review E*. 2007;75:065303.
<http://dx.doi.org/10.1103/PhysRevE.75.065303>
21. Nevskii S., Sarychev V., Kononov S., Granovskii A., Grovov V. Formation mechanism of micro- and nanocrystalline surface layers in titanium and aluminum alloys in electron beam irradiation. *Metals*. 2020;10(10):1399.
<https://doi.org/10.3390/met10101399>
22. Nevskii S.A. The mechanism of formation of micro- and nanocrystalline surface layers of titanium and aluminum alloys during electron beam processing. *Fundamental'nye problemy sovremennogo materialovedeniya*. 2020;17(10):385–395.
Невский С.А. Механизм образования микро- и нанокристаллических поверхностных слоев титановых и алюминиевых сплавов при электронно-пучковой обработке. *Фундаментальные проблемы современного материаловедения*. 2020;17(10):385–395.

Information about the Authors

Сведения об авторах

Sergei A. Nevskii, Dr. Sci. (Eng.), Assist. Prof. of the Chair of Science named after V.M. Finkel', Siberian State Industrial University
ORCID: 0000-0001-7032-9029
E-mail: nevskiy_sa@physics.sibsiu.ru

Сергей Андреевич Невский, д.т.н., доцент кафедры естественно-научных дисциплин им. профессора В.М. Финкеля, Сибирский государственный индустриальный университет
ORCID: 0000-0001-7032-9029
E-mail: nevskiy_sa@physics.sibsiu.ru

Lyudmila P. Bashchenko, Cand. Sci. (Eng.), Assist. Prof. of the Chair "Thermal Power and Ecology", Siberian State Industrial University
ORCID: 0000-0003-1878-909X
E-mail: luda.baschenko@gmail.com

Viktor E. Gromov, Dr. Sci. (Phys.-Math.), Prof., Head of the Chair of Science named after V.M. Finkel', Siberian State Industrial University
ORCID: 0000-0002-5147-5343
E-mail: gromov@physics.sibsiu.ru

Oleg A. Peregudov, Cand. Sci. (Eng.), Vice-Rector for Youth Policy and Educational Activities, Omsk State Technical University
ORCID: 0000-0001-5154-5498
E-mail: olegomgtu@mail.ru

Anastasia N. Gostevskaya, Postgraduate of the Chair of Science named after V.M. Finkel', Siberian State Industrial University
ORCID: 0000-0002-7328-5444
E-mail: lokon1296@mail.ru

Taras V. Volodin, Head of the Department of Scientific Research, Siberian State Industrial University
E-mail: volodin_tv@sibsiu.ru

Людмила Петровна Бащенко, к.т.н., доцент кафедры теплоэнергетики и экологии, Сибирский государственный индустриальный университет
ORCID: 0000-0003-1878-909X
E-mail: luda.baschenko@gmail.com

Виктор Евгеньевич Громов, д.ф.-м.н., профессор, заведующий кафедрой естественнонаучных дисциплин им. профессора В.М. Финкеля, Сибирский государственный индустриальный университет
ORCID: 0000-0002-5147-5343
E-mail: gromov@physics.sibsiu.ru

Олег Александрович Перегудов, к.т.н., проректор по молодежной политике и воспитательной деятельности, Омский государственный технический университет
ORCID: 0000-0001-5154-5498
E-mail: olegomgtu@mail.ru

Анастасия Николаевна Гостевская, аспирант кафедры естественнонаучных дисциплин им. профессора В.М. Финкеля, Сибирский государственный индустриальный университет
ORCID: 0000-0002-7328-5444
E-mail: lokon1296@mail.ru

Тарас Витальевич Володин, начальник управления научных исследований, Сибирский государственный индустриальный университет
E-mail: volodin_tv@sibsiu.ru

Contribution of the Authors

S. A. Nevskii – problem statement, obtaining and analyzing the dispersion equation, discussion and verification of modeling results.

L. P. Bashchenko – conducting calculations, discussion of the results, design of the article.

V. E. Gromov – analysis and discussion of the results of analysis of the structure of deposited high-speed steel by scanning electron microscopy.

O. A. Peregudov – discussion of the results, analysis of literary sources on the Mallins-Sekerki instability.

A. N. Gostevskaya – conducting research using scanning electron microscopy of deposited high-speed steel, discussion of the results.

T. V. Volodin – conducting research using scanning electron microscopy of deposited high-speed steel, discussion of the results.

Вклад авторов

С. А. Невский – постановка задачи, получение и анализ дисперсионного уравнения, обсуждение и верификация результатов моделирования.

Л. П. Бащенко – проведение расчетов, обсуждение результатов, оформление статьи.

В. Е. Громов – анализ и обсуждение результатов исследования структуры наплавленной быстрорежущей стали методами сканирующей электронной микроскопии.

О. А. Перегудов – обсуждение результатов, анализ литературных источников по неустойчивости Маллинза–Секерки.

А. Н. Гостевская – проведение исследований методами сканирующей электронной микроскопии наплавленной быстрорежущей стали, обсуждение результатов.

Т. В. Володин – проведение исследований методами сканирующей электронной микроскопии наплавленной быстрорежущей стали, обсуждение результатов.

Received 11.09.2023
 Revised 25.09.2023
 Accepted 18.12.2023

Поступила в редакцию 11.09.2023
 После доработки 25.09.2023
 Принята к публикации 18.12.2023



UDC 621.78.084:620.186

DOI 10.17073/0368-0797-2024-2-195-204



Original article

Оригинальная статья

EFFECT OF HEAT TREATMENT MODES ON STRUCTURE AND PROPERTIES OF 08KH18N6AG10S STEEL

A. I. Gordienko¹, E. V. Abdulmenova¹, T. V. Kozlova¹, Yu. F. Gomorova¹,
I. V. Vlasov¹, I. A. Fotin¹, K. N. Kayurov², S. P. Buyakova¹

¹ Institute of Strength Physics and Materials Science, Siberian Branch of Russian Academy of Sciences (2/4 Akademicheskii Ave., Tomsk 634055, Russian Federation)

² LLK Scientific Production Enterprise of Geophysical Equipment “Luch” (49 Geological str., Novosibirsk 630010, Russian Federation)

✉ mirantil@ispms.ru

Abstract. The paper studies the influence of heat treatment modes on the structure and properties of austenitic steel grade 08Kh18N6AG10S. Austenitic structure with twinned boundaries was preserved after quenching at 1040 and 1100 °C. At the same time, the average size of austenitic grains decreased from $42.3 \pm 6 \mu\text{m}$ (supply condition) to 38.1 ± 5.0 and $39.0 \pm 4.5 \mu\text{m}$, respectively. Quenching at 1040 °C leads to release of excess carbide phases at the grain boundaries. Mainly manganese and silicon oxides were found after quenching at 1100 °C. Quenching at 1040 °C leads to a slight decrease in microhardness (by 12 %) compared to the condition of supply (from 3285 ± 80 to 2895 ± 70 MPa). The hardness decreases less after quenching at 1100 °C (up to 3090 ± 80 MPa). Quenching at 1040 and 1100 °C has significantly improved the fracture toughness of steel. Values of impact strength of the steel increased to 223 ± 10 and $240 \pm 5 \text{ J/cm}^2$ compared to the condition of supply (55 J/cm^2). The authors found that the steel samples demonstrate a comparable level of wear resistance during tests for abrasive wear compared to the condition of supply after quenching at 1040 and 1100 °C. The mass loss after passing the roller distance of 4309 m for all steel conditions is approximately 8.0 %. The authors concluded that the most optimal heat treatment of 08Kh18N6AG10S steel is quenching at 1100 °C, which improves the fracture toughness of steel while maintaining microhardness and wear resistance.

Keywords: non-magnetic austenitic steel, hardening, microstructure, phase composition, fracture toughness, microhardness, abrasive wear

Acknowledgements: The work was performed within the framework of the state task of the Institute of Strength Physics and Materials Science, Siberian Branch of Russian Academy of Sciences, project No. FWRW-2021-0009. The authors express their gratitude to V.N. Eremin for providing material for research, I.N. Sevostyanova for assistance in preparing samples for microstructural studies and mechanical tests, A.A. Neumann for conducting structural studies using scanning electron microscopy, V.V. Shmakov for assistance in conducting abrasive tests.

For citation: Gordienko A.I., Abdulmenova E.V., Kozlova T.V., Gomorova Yu.F., Vlasov I.V., Fotin I.A., Kayurov K.N., Buyakova S.P. Effect of heat treatment modes on structure and properties of 08Kh18N6AG10S steel. *Izvestiya. Ferrous Metallurgy*. 2024;67(2):195–204.

<https://doi.org/10.17073/0368-0797-2024-2-195-204>

ВЛИЯНИЕ РЕЖИМОВ ТЕРМИЧЕСКОЙ ОБРАБОТКИ НА СТРУКТУРУ И СВОЙСТВА СТАЛИ 08Х18Н6АГ10С

А. И. Гордиенко¹, Е. В. Абдульменова¹, Т. В. Козлова¹, Ю. Ф. Гоморова¹,
И. В. Власов¹, И. А. Фотин¹, К. Н. Каюров², С. П. Буякова¹

¹ Институт физики прочности и материаловедения Сибирского отделения РАН (Россия, 634055, Томск, пр. Академический, 2/4)

² ООО Научно-производственное предприятие геофизической аппаратуры «Луч» (Россия, 630010, Новосибирск, ул. Гео-логическая, 49)

✉ mirantil@ispms.ru

Аннотация. Исследовано влияние режимов термической обработки на структуру и свойства аустенитной стали марки 08Х18Н6АГ10С. После закалки от 1040 и 1100 °C сохранилась аустенитная структура с двойникованными границами, при этом произошло уменьшение среднего размера аустенитных зерен с $42,3 \pm 6 \text{ мкм}$ (состояние поставки) до $38,1 \pm 5,0$ и $39,0 \pm 4,5 \text{ мкм}$ соответственно. После закалки от 1040 °C происходит выделение избыточных карбидных фаз на границах зерен. После закалки от 1100 °C обнаружены преимущественно оксиды

марганца и кремния. Закалка стали от температуры 1040 °C приводит к незначительному снижению микротвердости (на 12 %) по сравнению с состоянием поставки (с 3285 ± 80 до 2895 ± 70 МПа). После закалки от 1100 °C твердость снижается в меньшей степени (до 3090 ± 80 МПа). Проведение закалки от 1040 и 1100 °C позволило существенно улучшить ударную вязкость разрушения стали. Значения ударной вязкости стали возросли до 223 ± 10 и 240 ± 5 Дж/см² по сравнению с состоянием поставки (55 Дж/см²). При проведении испытаний на абразивный износ обнаружено, что образцы стали после закалки от 1040 и 1100 °C демонстрируют сопоставимый уровень износостойкости по сравнению с состоянием поставки. Потеря массы после прохождения дистанции ролика 4309 м для всех состояний стали составляет примерно 8,0 %. Сделано заключение, что оптимальной термической обработкой стали марки 08X18H6AG10C является закалка от температуры 1100 °C, которая позволяет улучшить вязкость разрушения стали при сохранении микротвердости и износостойкости.

Ключевые слова: немагнитная аустенитная сталь, закалка, микроструктура, фазовый состав, ударная вязкость разрушения, микротвердость, абразивный износ

Благодарности: Работа выполнена в рамках государственного задания Института физики прочности и материаловедения Сибирского отделения РАН, тема номер FWRW-2021-0009. Авторы благодарят В.Н. Еремина за предоставление материала для исследований, И.Н. Севостьянову за помощь в подготовке образцов для микроструктурных исследований и механических испытаний, А.А. Неймана за проведение структурных исследований с помощью растровой электронной микроскопии, В.В. Шмакова за помощь в проведении абразивных испытаний.

Для цитирования: Гордиенко А.И., Абдульменова Е.В., Козлова Т.В., Гоморова Ю.Ф., Власов И.В., Фотин И.А., Каюров К.Н., Буякова С.П. Влияние режимов термической обработки на структуру и свойства стали 08X18H6AG10C. *Известия вузов. Черная металлургия*. 2024;67(2):195–204. <https://doi.org/10.17073/0368-0797-2024-2-195-204>

INTRODUCTION

In recent years, oil-producing companies have shown increased interest in fields with hard-to-recover (HTR) oil reserves. According to 2021 statistics, extraction from hard-to-recover oil reserves accounts for about 44 % of produced oil, and approximately 25 % of gas is extracted from HTR natural gas reserves [1; 2]. Modern directionally drilling technology – rotary steerable systems (RSS) – is used to develop HTR oil reserves with both horizontally and directionally well profiles [3; 4].

The RSS operates in direct contact with the aggressive liquid medium of the drilling agent, which contains salt solutions and a suspension of silicate sand particles, leading to accelerated corrosion and water-abrasive wear of the RSS components. Recesses were made in the RSS housing on the outer surface to accommodate telemetry and gamma-ray logging systems for carrying out geophysical research during drilling [5]. For stable and reliable RSS operation, its components must be made of non-magnetic, corrosion-resistant materials with high hardness and resistance to water-abrasive wear.

The most suitable materials for manufacturing RSS components are non-magnetic austenitic steels since their high strength, corrosion resistance, and significant wear resistance [6]. It was noted in [7] that steels with a high chromium content successfully combine strength, wear resistance, fracture toughness and creep resistance. Therefore, it is advisable to use them in conditions of increased abrasion. The study [8] revealed that steels containing 25 wt. % Mn are exceptionally ductile and strong as deformation twins form at room temperature [9; 10]. Joint alloying with nickel and chromium increases the ductility and fracture toughness of steel. Obtained steels, for example, 08Kh18N10, 02Kh18N11, 12Kh18N10T are well processed by cold and hot deformation. To enhance the performance of these steels at temperatures above 450 °C, they are additionally

alloyed with nitrogen [11 – 13], which improves their strength properties. At the same time, the plastic properties of nitrogen-containing steels are rather high [3; 14]. Nitrogen is a strong austenite-forming element; it replaces expensive nickel and manganese and reduces magnetic permeability [4; 11]. Alloying austenitic steels with nitrogen enhances their resistance to local corrosion [5; 12]. The physical and mechanical properties of steels alloyed with nitrogen improve due to the precipitation of fine and homogeneously distributed chromium and vanadium nitrides instead of coarser carbide precipitates [15]. Alloying with nitrogen leads to structural and phase transformations in steel which significantly affect the mechanical properties [16; 17].

Based on the above, the non-magnetic 08Kh18N6AG10S steel alloyed with chromium, nickel, manganese, and nitrogen can be selected as RSS housing elements material. Complex steel alloying should ensure the RSS operation in an aggressive environment.

Complex steel alloying should ensure the RSS operation in an aggressive environment. To obtain optimal mechanical characteristics required for the material operating in aggressive environments, austenitic nitrogen steels are subjected to thermal and thermomechanical treatments [18]. Heat treatment of chromium-nickel and chromium-manganese-nickel austenitic steels involves quenching in water at temperatures from 1050 to 1100 °C. Heating to the temperatures should ensure the chromium carbides dissolution, while rapid cooling should maintain the supersaturated solid solution state. Despite numerous publications on the heat treatment effect on the nitrogen austenitic steel structure, phase composition, and mechanical properties, information on the 08Kh18N6AG10S steel used for the RSS protective components is rather limited.

The purpose of the work is to study the impact of heat treatment modes on the structure, phase composition, and mechanical properties of 08Kh18N6AG10S steel.

MATERIALS AND METHODS

The industrial 08Kh18N6AG10S steel in as-forged (condition of supply) with the following chemical composition, wt. %: C < 0.06, 8.5 – 10.0 Mn, 0.6 – 1.2 Si, P < 0.03, S < 0.03, 16.0 – 18.0 Cr, 5.0 – 6.0 Ni, Al < 0.02, 0.01 – 0.02 Ca, N > 0.4 and Fe-rest, was investigated. The steel was heat treated in a SNOL 185/1200 electric chamber furnace in an argon atmosphere at temperatures of 1040 and 1100 °C for 40 min, followed by quenching in water. For structural studies, samples were cut by electrical discharge machining into rectangular plates with dimensions of 10×10×3 mm.

The sample surfaces were ground on abrasive paper with a gradual reduction in abrasive grain size and polished with diamond pastes of varying dispersion. Grain boundaries were etched with a solution of nitric (HNO₃) and hydrochloric (HCl) acids in a volume ratio of 25:75. Microstructural studies were conducting using an Altami MET 1M optical microscope and a scanning electron microscope (SEM) (LEO EVO 50) equipped with an energy-dispersive spectrometer.

Methods of *X*-ray phase and *X*-ray diffraction analysis were employed to determine the fine crystal structure (size of the coherent scattering region (CSR), lattice parameter), and phase composition of the steel. *X*-ray diffraction patterns were obtained using a diffractometer with filtered CuK_α radiation. The *X*-ray was performed in the angle range from 40 to 120° with a step of 0.05° and exposure for each point was set to ensure a statistical accuracy of a minimum of 0.5 %. Phases were identified by comparing the peaks of the *X*-ray diffraction patterns with the PDF-2 ICDD structural database. The parameters of the crystal cells were determined based on the interplanar distances (*d*) for all reflections in the angle range from 40 to 120°. The full width at half maximum (FWHM) of the *X*-ray lines was determined by approximating the diffraction lines using the Lorentz function. The coherent scattering region was calculated using the Scherrer equation [19] for the most intense lines of the *X*-ray spectra. Microstresses of 08Kh18N6AG10S steel were assessed according to the *X*-ray data based on [20], using calculated microdistortions and literature data on Young's modulus. The microdistortion was determined using the Stokes–Wilson equation [21]. Microstresses in the γ-Fe phase were calculated based on the last most distinguishable diffraction reflection with a plane index (222) under the assumption that microdistortion is the main factor determining the diffraction width at far angles.

Steel microhardness was measured using the Vickers method on a PMT-3 at a load of 0.98 N and using the Rockwell method on a TK-TM N1916 at a load of 98.7 N. Samples of 10×10×55 mm *V*-shaped notched of IX type

according to GOST 6996 – 66 underwent impact bending tests at room temperature using a KM-300-M-Sh pendulum impact testing machine. Macroimages of destroyed samples were received using an Altami SM0870 stereographic microscope. Fracture micromechanisms were studied using a LEO EVO 50 scanning electron microscope.

The samples were subjected to abrasive wear tests according to the ASTM G65-04 standard [22]. Plates were fixed in the holder of the abrasive wear unit, oriented so that the rubber roller touched the sample at its center. Quartz sand with a fraction size of 200 – 300 μm was supplied to the point of contact of the sample with a rubber roller at a speed of 400 g/min. The roller rotation speed was 100 rpm. Tests were conducted following method D of the ASTM G65-04 standard, wherein the roller distance was 4309 m, and the roller clamping force was 45 N. After completion of the test, as well as at intervals of linear continuous contact between the sample and the roller of 1000, 2000, 3000, and 4309 m, the samples were removed from the holder and weighed on an analytical laboratory balance AV-120-01 with an accuracy of 0.0001 g, followed by the relative weight loss control.

RESULTS AND DISCUSSION

Microstructural studies

Fig. 1 illustrates the microstructures of 08Kh18N6AG10S steel in the supply conditions and after quenching at 1040 and 1100 °C. The steel structure in the supply conditions features large austenitic grains (Fig. 1, *a*) with an average size of $42.3 \pm 6 \mu\text{m}$ with a large number of twins characterized for austenite (Fig. 1, *a*, indicated by arrows) [23]. Quenching at temperature of 1040 and 1100 °C resulted in grain refinement, the average grain size reduced to $38.1 \pm 5.0 \mu\text{m}$ and $39 \pm 4.5 \mu\text{m}$, respectively (Fig. 1, *b*, *c*). The reduction in grain size is likely due to the high cooling rate during quenching. The austenitic structure with twin boundaries remains intact. Additionally, dark areas were observed at the boundaries of austenite grains in the microstructure after quenching at 1040 °C (Fig. 1, *d*). Higher magnification revealed numerous inclusions within the dark areas of the grain boundaries (inset in the bottom corner, Fig. 1, *d*). Energy dispersive analysis during SEM enabled the detection of carbon segregations in the boundary regions (inset in the upper corner, Fig. 1, *d*). This phenomenon is attributed to incomplete dissolution of all alloying elements during heating to 1040 °C, leading to carbide precipitation at grain boundaries. During rapid cooling, particle segregation at grain boundaries can result in microcracks. These particle segregations and microcracks in steel after quenching at 1040 °C are considered as structural defects that can affect the properties of the steel. The authors [13]

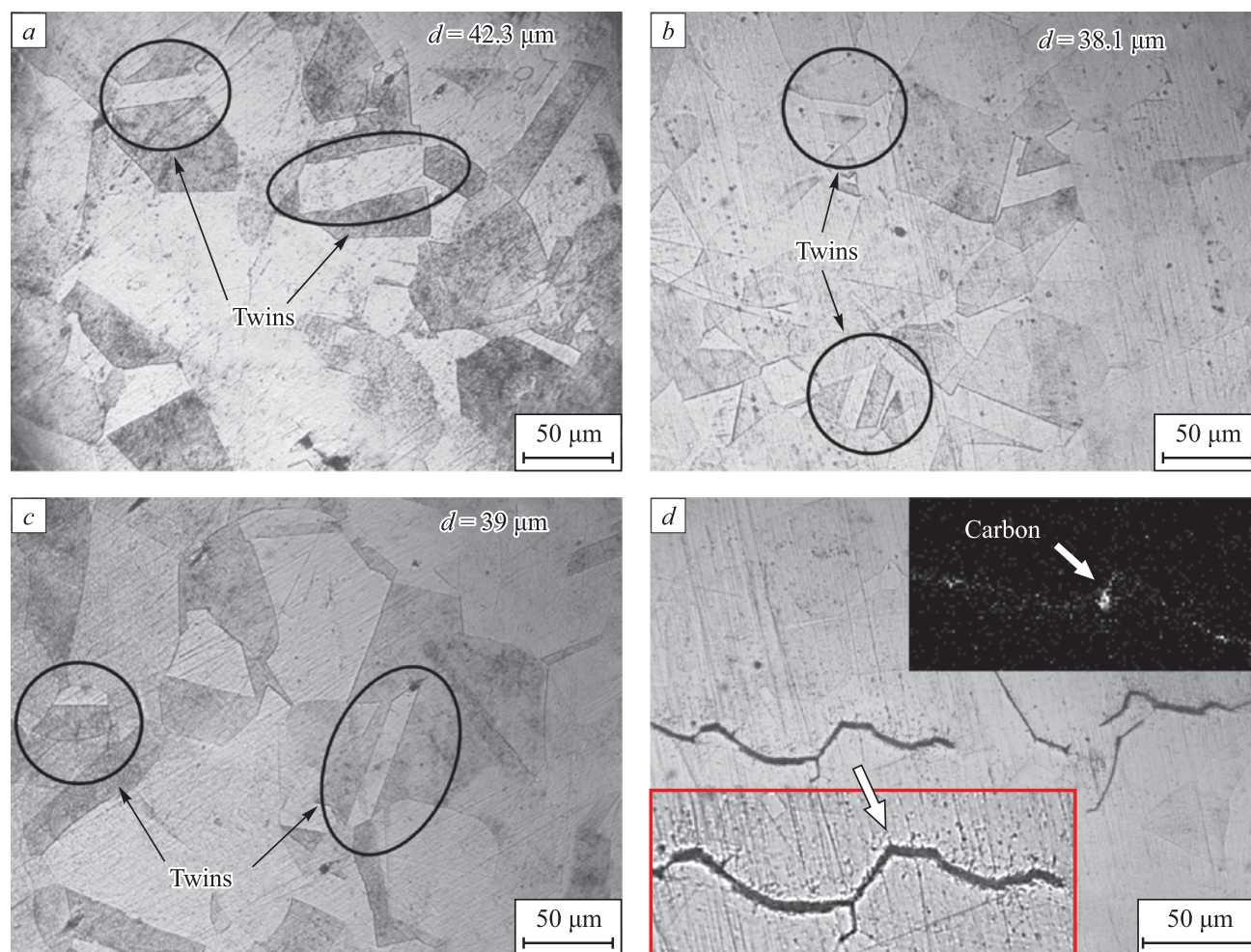


Fig. 1. Microstructure of 08Kh18N6AG10S steel in condition of supply (a), after quenching at 1040 °C (b, d) and 1100 °C (c)

Рис. 1. Микроструктура стали марки 08X18N6AG10C в состоянии поставки (a), после закалки от 1040 °C (b, d) и от 1100 °C (c)

noted that as carbide phases precipitated along grain boundaries, the susceptibility to intergranular corrosion of steel increased.

Fig. 2 presents the X-ray diffraction patterns of 08Kh18N6AG10S steel in the condition of supply and after quenching at 1040 and 1100 °C. All X-ray diffraction patterns exhibit lines corresponding to the γ -Fe phase with a face-centered cubic lattice. Quenching of the steel resulted in a decrease in the full width at half maximum (FWHM) of the γ -Fe phase diffraction lines compared to the X-ray diffraction pattern of the steel in the condition of supply. For instance, the FWHM of the diffraction reflection (111) decreased from 0.2496 to 0.1797° at a quenching temperature of 1040 °C and from 0.2496 to 0.2080° at a quenching temperature of 1100 °C. This trend aligns with the findings of [24], where heat treatment of Fe – Cr – Mn – C – N steel resulted in a decrease in FWHM of diffraction lines from 1.1 to 0.89°. The reduction in FWHM of diffraction lines may stem from an

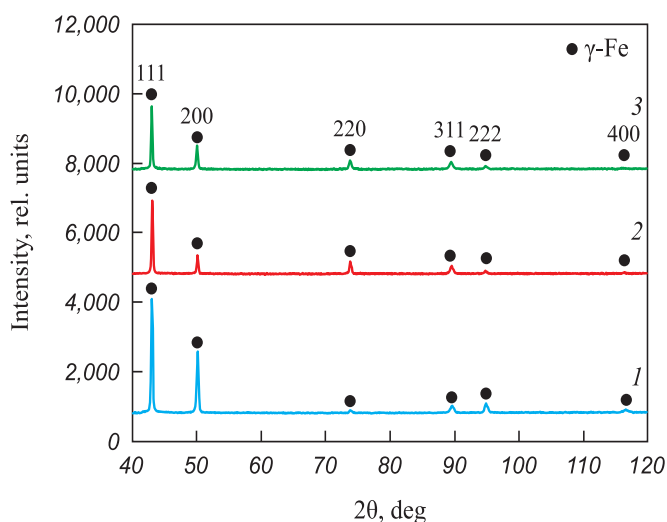


Fig. 2. X-ray images of 08Kh18N6AG10S steel in condition of supply (1), after quenching at 1040 °C (2) and 1100 °C (3)

Рис. 2. Рентгенограммы стали марки 08X18N6AG10C в состоянии поставки (1), после закалки от 1040 °C (2) и 1100 °C (3)

increased size of coherent scattering regions and changes in microstress values due to quenching.

The X-ray diffraction patterns of all studied conditions show no lines characteristic of free carbon or carbides (Fig. 2), indicating that the proportion of the carbide phase is insignificant relative to the austenitic matrix.

The cell parameter of the γ -Fe phase of steel in the condition of supply was measured at $0.3629 \pm 5 \cdot 10^{-4}$ nm. After quenching the cell parameter of the γ -Fe phase changed insignificantly to $0.3631 \pm 5 \cdot 10^{-4}$ nm after quenching at 1040 °C and $0.3633 \pm 5 \cdot 10^{-4}$ nm after quenching at 1100 °C.

Calculation of type II stresses revealed that after quenching at 1040 °C, microstresses present in the initial steel structure relaxed. Type II stresses decreased from 0.27 GPa in the supply condition to 0.24 GPa after quenching at 1040 °C. Quenching at 1100 °C led to the microstress value increased to 0.32 GPa, likely due to the formation of a fine-grained structure and better dissolution of alloying components in the solid solution.

Mechanical properties of steel

Table 1 displays the microhardness values and the results of impact tests for steel 08Kh18N6AG10S conducted at room temperature. The microhardness of the steel in the condition of supply was 3285 ± 80 MPa, which aligns well with literature data [25]. After quenching the microhardness decreased to 2895 ± 70 MPa (equivalent to 30 ± 1 HRC) at 1040 °C and to 3090 ± 80 MPa (equivalent to 32 ± 1 HRC) at 1100 °C. Notably, the microhardness values of steel after quenching at 1040 °C are lower compared to those after quenching at 1100 °C. This suggests that the heating temperature of 1040 °C may not be sufficient for all alloying elements to enter the solid solution, leading to carbide precipitation at grain boundaries (Fig. 1, d). Consequently, the effect of solid solution hardening is more pronounced in steel after quenching at 1100 °C. This aligns with the type II stresses calculation results, showing an increase in microstress to 0.32 GPa after quenching at 1100 °C.

The hardness of chromium-manganese-nickel austenitic steels decreases during quenching as carbides of alloying elements dissolve and the supersaturated solid solution is maintained during rapid cooling. Additionally, recrystallization processes during quenching eliminate the effect of dislocation hardening due to plastic deformation under forging.

The fracture toughness of steel in the condition of supply is 55 J/cm^2 . Fractures of the steel samples in the condition of supply exhibit minimal tightening of the side faces, and shear lips are practically absent (Fig. 3, a), indicating that macroplastic deformation preceding destruction is not significant.

The fracture micromechanism of steel in the condition of supply is mixed, featuring large pits characteristic of ductile fracture, as well as areas of brittle fracture with typical cleavage facets and microcracks (Fig. 3, a, inset). Cracking is observed within large austenite grains. Energy dispersive analysis revealed that second-phase inclusions in large pits consist of manganese and iron carbides, silicon, and aluminum oxides (Table 2, with areas of energy dispersive analysis indicated in Fig. 3 as an example). The size of round particles ranges from 3.2 to 5.0 μm .

After quenching at 1040 °C, the fracture toughness of the steel is significantly higher (Table 1) compared to the condition of supply. Concurrently, the tightening of the side faces and the width of the shear lip areas at the fractures (Fig. 3, b, marked with an arrow), which characterize the degree of plastic deformation as the crack develops, increased. The destruction micromechanism of the samples is entirely ductile and dimple-shaped, without signs of brittle fracture (Fig. 3, b, inset).

Round and elongated particles, with shapes close to plates, were detected in the pits. The size of round particles ranged from 1.5 to 5.5 μm , while the size of elongated particles reached $3 \times 15 \mu\text{m}$.

After quenching at 1100 °C, the impact strength of the steel is the highest among those presented, reaching $240 \pm 5 \text{ J/cm}^2$ (Table 1). The fractures of the samples are characterized by a high degree of tightening (Fig. 3, c, marked with an arrow) and sophisticated surface topogra-

Table 1. Microhardness and results of impact tests of 08Kh18N6AG10S steel at room temperature

Таблица 1. Микротвердость и результаты ударных испытаний, проведенных при комнатной температуре, стали марки 08X18H6AG10C

Steel condition	Hardness		Fracture toughness, J/cm^2	Fracture energy, J
	according to Vickers, MPa	HRC		
Supply	3285 ± 80	35 ± 1	55 ± 11	44 ± 11
Quenching at 1040 °C	2895 ± 70	30 ± 1	223 ± 10	178 ± 10
Quenching at 1100 °C	3090 ± 80	32 ± 1	240 ± 5	192 ± 5

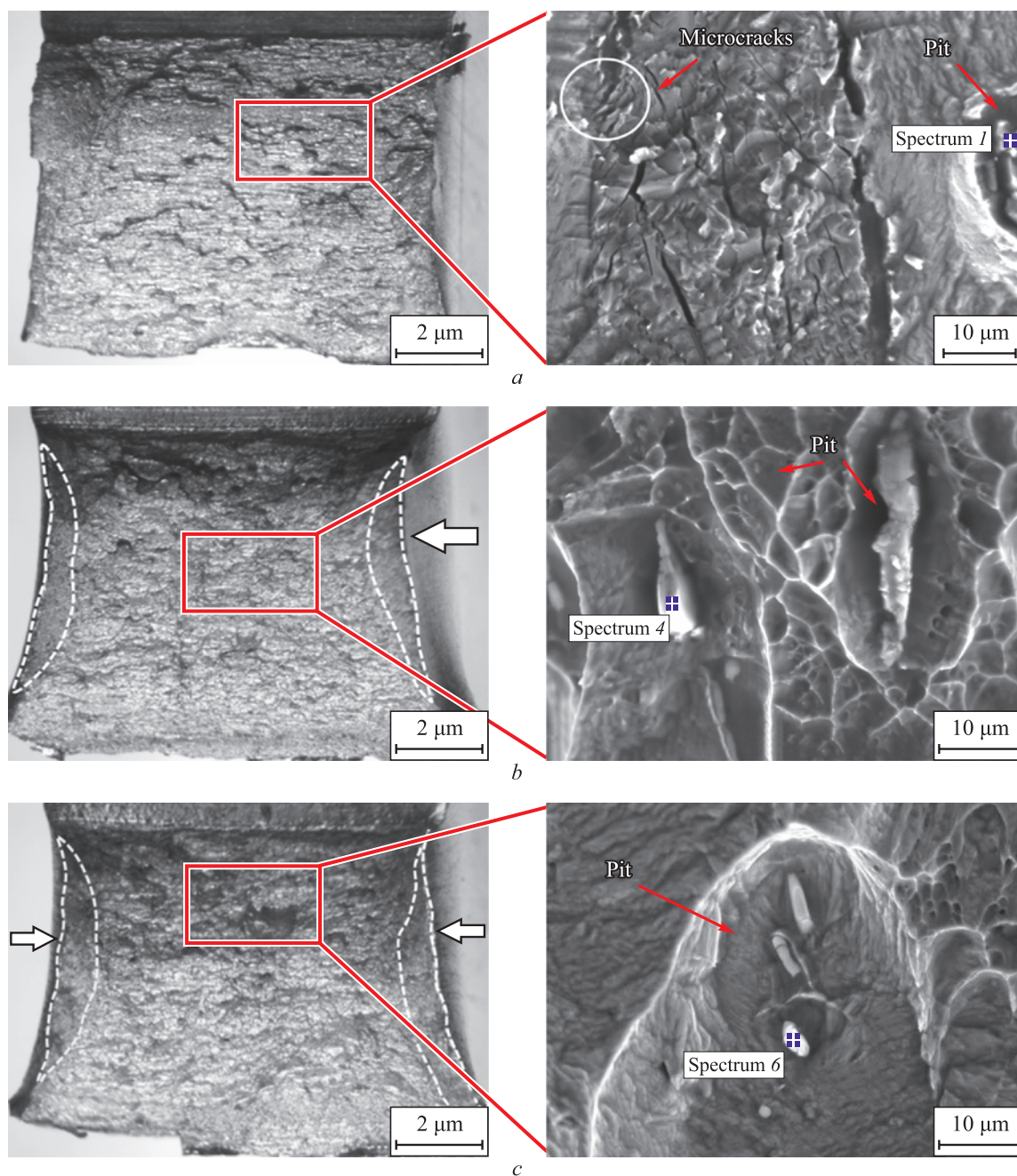


Fig. 3. Fracture surfaces of 08Kh18N6AG10S steel in condition of supply (a), after quenching at 1040 °C (b) and 1100 °C (c)

Рис. 3. Поверхности разрушения стали марки 08X18H6AG10C в состоянии поставки (a), после закалки от 1040 °C (b) и 1100 °C (c)

phy. Large pores on the fracture surface indicate the ductile nature of the fracture. Particles of different morphologies and sizes were found in the pores (Fig. 3, c). These include round particles, ranging in size from 3.5 to 5.0 μm, dispersed particles with sizes of 0.8 – 1.5 μm, and elongated particles measuring 1.5 × 7.0 μm. According to the energy dispersive analysis data, the particles in the pits are primarily oxides of manganese and silicon (Table 2). The proportion of carbide inclusions in the steel after quenching at 1100 °C is significantly smaller. This confirms the earlier conclusions that when heated to 1100 °C, most of the alloying elements enter

the solid solution, leading to a reduction in the carbide inclusions of in the steel. The smaller proportion of carbide particles and their smaller size account for the higher fracture toughness of the steel in this structural condition (Table 1).

During the abrasive wear testing of the steel in different structural conditions, marked traces of abrasive wear and changes in the geometry of the samples are observed after the roller covers a distance of 4309 m (the traces of abrasive wear of the sample in the supply condition are shown as an example, Fig. 4, a).

Table 2. Result of X-ray energy dispersive microanalysis obtained from fractures of 08Kh18N6AG10S steel**Таблица 2. Результаты энергодисперсионного микроанализа, полученные с изломов стали марки 08X18H6AГ10C**

Spectrum	Element content, at. %							
	C	O	Mg	Al	Si	Cr	Mn	Fe
Supply condition								
Spectrum 1	45.1	–	–	–	–	4.6	42.3	8.0
Spectrum 2	14.9	46.0	8.5	21.5	–	3.8	4.1	1.2
Quenching at 1040 °C								
Spectrum 3	50.7	–	–	–	0.5	1.2	46.0	1.6
Spectrum 4	19.3	46.5	5.6	–	11.9	0.6	15.2	0.9
Quenching at 1100 °C								
Spectrum 5	7.9	51.9	8.6	–	13.9	0.8	15.7	1.2
Spectrum 6	15.5	49.5	2.0	–	11.1	1.8	17.0	3.1

In all three cases, the maximum decrease in the sample height is approximately 1.5 mm and observed at the center, corresponding to 15 % of the total sample height. Fig. 4, *b* depicts the dependence of mass loss on the roller path during the testing of 08Kh18N6AG10S steel. The dependencies for all samples are linear. Steels in the condition of supply and after quenching at 1040 °C exhibit comparable weight loss values, approximately 7.7 %. After quenching at 1100 °C, the weight loss is slightly greater about 8.5 %. It can be concluded that quenching and changes in the structural condition of the steel do not significantly alter the wear resistance.

Thus, when 08Kh18N6AG10S steel is utilized to manufacture the RSS housing, quenching at 1100 °C is recom-

mended. Suggested heat treatment can notably enhance the fracture toughness of the steel without compromising wear resistance and hardness. Additionally, quenching at a temperature of 1100 °C results in a decrease in the proportion of carbide inclusions with magnetic properties, which are unacceptable when conducting geophysical research during drilling.

CONCLUSIONS

After quenching 08Kh18N6AG10S steel at 1040 and 1100 °C, an austenitic structure forms with grain sizes of 38.1 ± 5.0 and 39 ± 4.5 μm , respectively. It was observed that quenching at 1040 °C leads to the precipitation of excess carbide phases at grain boundaries due to incomplete austenitization.

According to energy dispersive analysis, the proportion of carbide inclusions decreases after quenching at 1100 °C with the main inclusions being manganese and silicon oxides.

The research revealed that quenching at 1040 and 1100 °C significantly increases the fracture toughness of 08Kh18N6AG10S steel to 223 – 240 J/cm² compared to the condition of supply values of 55 J/cm².

Abrasive wear tests demonstrated that despite decreased hardness and increased fracture toughness steel samples after quenching at 1040 and 1100 °C exhibit approximately the same wear resistance as the as-supplied steel.

Therefore, we recommend quenching at 1100 °C for 08Kh18N6AG10S steel used in RSS housing manufacturing as it provides the required mechanical properties and helps to reduce the proportion of magnetic inclusions in the material.

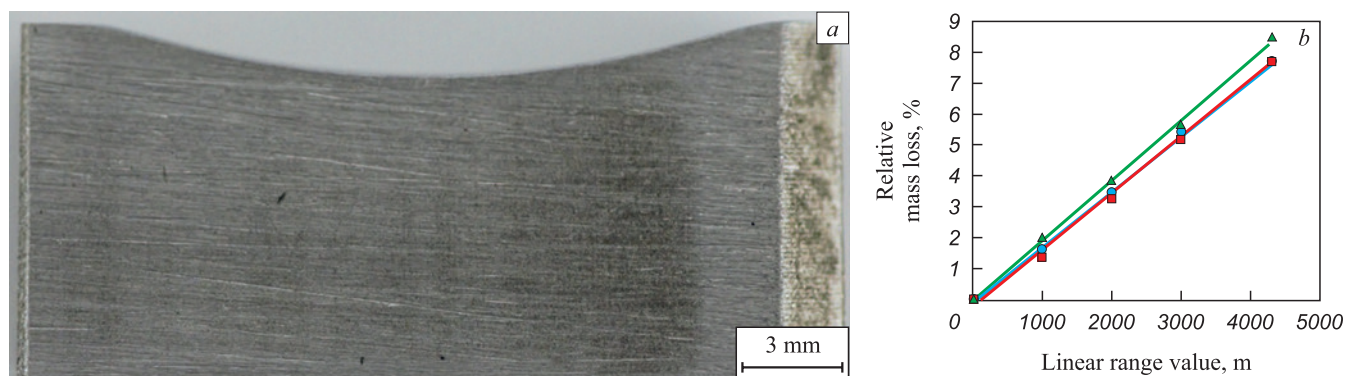


Fig. 4. Macrograph of lateral side of the steel sample in condition of supply after passing the distance from the roller of 4309 m (*a*), dependences of the mass loss on the roller path during abrasive wear tests 08Kh18N6AG10S steel (*b*):

● – in condition of supply; ■ and ▲ – after quenching at 1040 and 1100 °C

Рис. 4. Макрофотография боковой стороны образца стали в состоянии поставки после прохождения дистанции ролика 4309 м (*a*), зависимость потери массы от пути ролика при испытаниях на абразивный износ стали марки 08X18H6AГ10C (*b*):

● – в состоянии поставки; ■ и ▲ – после закалки от 1040 и 1100 °C

REFERENCES / СПИСОК ЛИТЕРАТУРЫ

1. Brook B.W., Alonso A., Meneley D.A., Misak J., Bles T., van Erp J.B. Why nuclear energy is sustainable and has to be part of the energy mix. *Sustainable Materials and Technologies*. 2014;1-2:8–16.
<https://doi.org/10.1016/j.susmat.2014.11.001>
2. Jia C., Pang X., Song Y. The mechanism of unconventional hydrocarbon formation: Hydrocarbon self-sealing and intermolecular forces. *Petroleum Exploration and Development*. 2021;48(3):507–526.
[https://doi.org/10.1016/s1876-3804\(21\)60042-3](https://doi.org/10.1016/s1876-3804(21)60042-3)
3. Shevchenko I.A. Drilling wells with a large departure from the vertical, using a rotary-driven systems with control geophysical parameters in real-time. *Modern Science: Actual Problems of Pheory and practice. Series: Natural and Technical Sciences*. 2014;(1-2):36–39. (In Russ.).
Шевченко И.А. Бурение скважин с большим отходом от вертикали с использованием роторных управляемых систем при контроле геофизических параметров в режиме реального времени. *Современная наука: актуальные проблемы теории и практики. Серия: естественные и технические науки*. 2014;(1-0):36–39.
4. Zakirov A.Ya. The first test results of Russian-made rotary-controlled systems. *Proneft'. Professionally about oil*. 2016;(2(2)):43–47. (In Russ.).
Закиров А.Я. Первые результаты испытаний роторно-управляемых систем российского производства. *Пронефть. Профессионально о нефти*. 2016;(2(2)):43–47.
5. Zhang C., Zou W., Cheng N. Overview of rotary steerable system and its control methods. In: *Proceedings of 2016 IEEE Int. Conf. on Mechatronics and Automation*. 2016: 1559–1565. <https://doi.org/10.1109/icma.2016.7558796>
6. Kushnereva D.S., Sapozhnikov G.V. Properties investigations of the new high-strength stainless steels. *Chemical Physics and Mesoscopy*. 2019;21(1):39–44. (In Russ.).
<https://doi.org/10.15350/17270529.2019.1.6>
Кушнерева Д.С., Сапожников Г.В. Исследование свойств новых высокопрочных нержавеющей сталей. *Химическая физика и мезоскопия*. 2019;21(1):39–44.
<https://doi.org/10.15350/17270529.2019.1.6>
7. Foldyna V., Kubon Z., Filip M., Mayer K.-H., Berger C. Evaluation of structural stability and creep resistance of 9–12 % Cr steels. *Steel Research*. 1996;67(9):375–381.
<https://doi.org/10.1002/srin.199605504>
8. Grässel O., Krüger L., Frommeyer G., Meyer L.W. High strength Fe–Mn–(Al, Si) TRIP/TWIP steels development – properties – application. *International Journal of Plasticity*. 2000;16(10-11):1391–1409.
[https://doi.org/10.1016/S0749-6419\(00\)00015-2](https://doi.org/10.1016/S0749-6419(00)00015-2)
9. Brück U., Frommeyer G., Grässel O., Meyer L.W., Weise A. Development and characterization of high strength impact resistant Fe–Mn–(Al, Si) TRIP/TWIP steels. *Steel Research*. 2002;73(6-7):294–298.
<https://doi.org/10.1002/srin.200200211>
10. Frommeyer G., Brück U., Neumann P. Supra-ductile and high-strength manganese-TRIP/TWIP steels for high energy absorption purposes. *ISIJ International*. 2002;43(3):438–446.
<https://doi.org/10.2355/isijinternational.43.438>
11. Kostina M.V., Bannykh O.A., Blinov V.M. Features of nitrogen-alloyed steels. *Metallovedenie i termicheskaya obrabotka metallov*. 2000;(12):3–6. (In Russ.).
Костина М.В., Банньих О.А., Блинов В.М. Особенности сталей, легированных азотом. *Металловедение и термическая обработка металлов*. 2000;(12):3–6.
12. Mudali U.K., Dayal R.K. Influence of nitrogen addition on the crevice corrosion resistance of nitrogen-bearing austenitic stainless steels. *Journal of Materials Science*. 2000;35(7):1799–1803.
<https://doi.org/10.1023/A:1004740905317>
13. Kostina M.V., Rigina L.G. Nitrogen-containing steels and methods of their production. *Izvestiya. Ferrous Metallurgy*. 2020;63(8):606–622. (In Russ.).
<https://doi.org/10.17073/0368-0797-2020-8-606-622>
Костина М.В., Ригина Л.Г. Азотосодержащие стали и способы их производства. *Известия вузов. Черная металлургия*. 2020;63(8):606–622.
<https://doi.org/10.17073/0368-0797-2020-8-606-622>
14. Naumenko V.V., Shlyamnev A.P., Filipov G.A. Nitrogen in austenitic stainless steels of various alloying systems. *Metalurg*. 2011;(6):46–53. (In Russ.).
Науменко В.В., Шлямнев А.П., Филипов Г.А. Азот в аустенитных нержавеющих сталях различных систем легирования. *Металлург*. 2011;(6):46–53.
15. Klotz U.E., Solenthaler C., Ernst P., Uggowitzer P.J., Speidel M.O. Alloy compositions and mechanical properties of 9–12 % chromium steels with martensitic-austenitic microstructure. *Materials Science and Engineering: A*. 1999;272(2):292–299.
[https://doi.org/10.1016/S0921-5093\(99\)00490-6](https://doi.org/10.1016/S0921-5093(99)00490-6)
16. Rawers J.C. Characterizing alloy additions to carbon high-nitrogen steel. *Journal of Materials: Design and Applications*. 2004;218(3):239–246.
<https://doi.org/10.1177/146442070421800309>
17. Rawers J.C. Alloying effects on the microstructure and phase stability of Fe–Cr–Mn steels. *Journal of Materials Science*. 2008;43(10):3618–3624.
<https://doi.org/10.1007/s10853-008-2576-3>
18. Mushnikova S.Yu., Kostin S.K., Sagaradze V.V., Kataeva N.V. Structure, properties, and resistance to stress-corrosion cracking of a nitrogen-containing austenitic steel strengthened by thermomechanical treatment. *Physics of Metals and Metallography*. 2017;118(11):1155–1166.
<https://doi.org/10.1134/S0031918X17110096>
19. Scherrer P. Bestimmung der Größe und der inneren Struktur von Kolloidteilchen mittels Röntgenstrahlen. *Nachrichten von der Gesellschaft der Wissenschaften zu Göttingen, Mathematisch-Physikalische Klasse*. 1918;1918(2):98–101. (In Germ.).
20. Timoshenko S.P., Goodier J.N. Theory of Elasticity. New York – Toronto – London: McGraw-Hill book company; 1951:519.
21. Stokes A.R., Wilson A.J.C. The diffraction of X rays by distorted crystal aggregates. *Proceedings of the Physical Society*. 1944;56(3):174–181.
<https://doi.org/10.1088/0959-5309/56/3/303>
22. ASTM G65. Standard Test Method for Measuring Abrasion Using the Dry Sand/Rubber Wheel Apparatus ASTM. 2016:14.

23. Yuan X., Chen L., Zhao Y., Di H., Zhu F. Influence of annealing temperature on mechanical properties and microstructures of a high manganese austenitic steel. *Journal of Materials Processing Technology*. 2015;217:278–285. <https://doi.org/10.1016/J.JMATPROTEC.2014.11.027>
24. Lee E., Mishra B., Palmer B.R. Effect of heat treatment on wear resistance of Fe–Cr–Mn–C–N high-interstitial stainless steel. *Wear*. 2016;368–369:70–74. <https://doi.org/10.1016/j.wear.2016.09.008>
25. Speidel M.O. Nitrogen containing austenitic stainless steels. *Materials Science and Engineering Technology*. 2006;37(10):875–880. <https://doi.org/10.1002/mawe.200600068>

Information about the Authors

Сведения об авторах

Antonina I. Gordienko, Cand. Sci. (Eng.), Research Associate of the Laboratory of Physical Mesomechanics and Non-Destructive Control Methods, Institute of Strength Physics and Materials Science, Siberian Branch of Russian Academy of Sciences

ORCID: 0000-0002-4361-8906

E-mail: mirantil@ispms.ru

Ekaterina V. Abdulmenova, Cand. Sci. (Eng.), Junior Research of the Laboratory of Molecular Imaging and Photoacoustics, Institute of Strength Physics and Materials Science, Siberian Branch of Russian Academy of Sciences

ORCID: 0000-0002-9594-5706

E-mail: Ekaterina.V.Abdulmenova@yandex.ru

Tanzilya V. Kozlova, Cand. Sci. (Phys.-Math.), Junior Research of the Laboratory of Physical Mesomechanics and Non-Destructive Control Methods, Institute of Strength Physics and Materials Science, Siberian Branch of Russian Academy of Sciences

ORCID: 0000-0003-0890-9983

E-mail: kozlovatv@ispms.ru

Yulia F. Gonorova, Cand. Sci. (Eng.), Research Associate of the Laboratory of Physical Mesomechanics and Non-Destructive Control Methods, Institute of Strength Physics and Materials Science, Siberian Branch of Russian Academy of Sciences

ORCID: 0000-0002-0880-2898

E-mail: gomjf@ispms.ru

Ilya V. Vlasov, Cand. Sci. (Eng.), Research Associate of the Laboratory of Physical Mesomechanics and Non-Destructive Control Methods, Institute of Strength Physics and Materials Science, Siberian Branch of Russian Academy of Sciences

ORCID: 0000-0001-9110-8313

E-mail: viv@ispms.ru

Igor' A. Fotin, Engineer of the Laboratory of Physical Mesomechanics and Non-Destructive Control Methods, Institute of Strength Physics and Materials Science, Siberian Branch of Russian Academy of Sciences

ORCID: 0000-0001-5185-6405

E-mail: i.fotin2010@gmail.com

Konstantin N. Kayurov, General Director, LLK Scientific Production Enterprise of Geophysical "Luch"

ORCID: 0000-0001-9545-5400

E-mail: kayurov@looch.ru

Svetlana P. Buyakova, Dr. Sci. (Eng.), Prof., Deputy Director for Research, Head of the Laboratory of Physical Mesomechanics and Non-Destructive Control Methods, Institute of Strength Physics and Materials Science, Siberian Branch of Russian Academy of Sciences

ORCID: 0000-0002-6315-2541

E-mail: sbuyakova@ispms.ru

Антонина Ильдаровна Гордиенко, к.т.н., научный сотрудник лаборатории физической мезомеханики и неразрушающих методов контроля, Институт физики прочности и материаловедения Сибирского отделения РАН

ORCID: 0000-0002-4361-8906

E-mail: mirantil@ispms.ru

Екатерина Владимировна Абдульменова, к.т.н., младший научный сотрудник лаборатории молекулярного имиджинга и фотоакустики, Институт физики прочности и материаловедения Сибирского отделения РАН

ORCID: 0000-0002-9594-5706

E-mail: Ekaterina.V.Abdulmenova@yandex.ru

Танзиля Вакильевна Козлова, к.ф.-м.н., младший научный сотрудник лаборатории физической мезомеханики и неразрушающих методов контроля, Институт физики прочности и материаловедения Сибирского отделения РАН

ORCID: 0000-0003-0890-9983

E-mail: kozlovatv@ispms.ru

Юлия Федоровна Гоморова, к.т.н., научный сотрудник лаборатории физической мезомеханики и неразрушающих методов контроля, Институт физики прочности и материаловедения Сибирского отделения РАН

ORCID: 0000-0002-0880-2898

E-mail: gomjf@ispms.ru

Илья Викторович Власов, к.т.н., научный сотрудник лаборатории физической мезомеханики и неразрушающих методов контроля, Институт физики прочности и материаловедения Сибирского отделения РАН

ORCID: 0000-0001-9110-8313

E-mail: viv@ispms.ru

Игорь Андреевич Фотин, инженер лаборатории физической мезомеханики и неразрушающих методов контроля, Институт физики прочности и материаловедения Сибирского отделения РАН

ORCID: 0000-0001-5185-6405

E-mail: i.fotin2010@gmail.com

Константин Николаевич Каюров, генеральный директор, ООО научно-производственное предприятие геофизической аппаратуры «Луч»

ORCID: 0000-0001-9545-5400

E-mail: kayurov@looch.ru

Светлана Петровна Буйкова, д.т.н., профессор, заместитель директора по научной работе, заведующий лабораторией физической мезомеханики и неразрушающих методов контроля, Институт физики прочности и материаловедения Сибирского отделения РАН

ORCID: 0000-0002-6315-2541

E-mail: sbuyakova@ispms.ru

Contribution of the Authors

Вклад авторов

A. I. Gordienko – literary review, writing the text, conducting steel quenching, analysis of experimental data.

E. V. Abdulmenova – literary review, writing the text, conducting and analyzing X-ray diffraction studies.

T. V. Kozlova – literary review, writing the text, microhardness measurement, processing results and data analysis.

Yu. F. Gonorova – revision of the text, carrying out structural studies by optical microscopy and the study of fracture surfaces after mechanical testing by scanning electron microscopy.

I. V. Vlasov – carrying out impact bending tests, describing the results of impact tests.

I. A. Fotin – testing of steel samples for abrasive wear, numerical analysis of experimental results.

K. N. Kayurov – formation of the main problem in the field of rotary steerable systems, discussion of the results.

S. P. Buyakova – formation of the main concept, goals and objectives of the study; finalization of the text.

А. И. Гордиенко – литературный обзор публикаций по теме статьи, написание текста рукописи, проведение закалки стали, анализ экспериментальных данных.

Е. В. Абдульменова – литературный обзор публикаций по теме статьи, написание текста рукописи, проведение и анализ рентгеноструктурных исследований.

Т. В. Козлова – литературный обзор публикаций по теме статьи, написание текста рукописи, измерение микротвердости, обработка результатов и анализ данных.

Ю. Ф. Гоморова – доработка текста, проведение структурных исследований методами оптической микроскопии, изучение поверхностей изломов образцов после механических испытаний методом растровой электронной микроскопии.

И. В. Власов – проведение испытаний на ударный изгиб, описание результатов ударных испытаний.

И. А. Фотин – проведение испытаний образцов стали на абразивный износ и численный анализ экспериментальных результатов.

К. Н. Каюров – формирование основной проблемы в области роторных управляемых систем, обсуждение полученных результатов.

С. П. Буякова – формирование основной концепции, цели и задач исследования; доработка текста рукописи.

Received 10.10.2023

Revised 01.11.2023

Accepted 10.01.2024

Поступила в редакцию 10.10.2023

После доработки 01.11.2023

Принята к публикации 10.01.2024

PHYSICO-CHEMICAL BASICS
OF METALLURGICAL PROCESSESФИЗИКО-ХИМИЧЕСКИЕ ОСНОВЫ
МЕТАЛЛУРГИЧЕСКИХ ПРОЦЕССОВ

UDC 669.046.584.2

DOI 10.17073/0368-0797-2024-2-205-210



Original article

Оригинальная статья

EFFECT OF BASICITY ON PHYSICAL PROPERTIES
OF LADLE SLAGS OF $\text{CaO} - \text{SiO}_2 - \text{Ce}_2\text{O}_3 - \text{Al}_2\text{O}_3 - \text{MgO}$ SYSTEMA. G. Upolovnikova[✉], R. R. Shartdinov, A. N. Smetannikov

Institute of Metallurgy, Ural Branch of the Russian Academy of Sciences (101 Amundsena Str., Yekaterinburg 620016, Russian Federation)

[✉ upol.ru@mail.ru](mailto:upol.ru@mail.ru)

Abstract. The authors studied the physical properties of the slags of $\text{CaO}-\text{SiO}_2-\text{Al}_2\text{O}_3-\text{MgO}$ system containing cerium oxide. The developed slags are based on a calcium silicate system, the basicity $(\text{CaO})/(\text{SiO}_2)$ of which has a great influence on the slag properties. Generalization of the performed studies results allowed obtaining new data on the effect of basicity in cerium-containing slags of the studied oxide system on viscosity, temperature of crystallization onset and structure. Experimental studies of the physical properties of cerium-containing slags showed that with an increase in basicity of 2.0 – 5.0, an increase in temperature of crystallization onset and viscosity is observed associated with structure of the formed slags. An increase in basicity from 2.0 to 5.0 contributes to an increase in viscosity from 0.20 to 0.41 Pa·s at 1500 °C and an increase in the crystallization temperature from 1397 to 1497 °C. The structural analysis showed that the structure of the cerium-containing slag is influenced by both the Si^{4+} ion and the Al^{3+} ion, which are grid-forming agents. Silicon ions in this system are present in the form of $[\text{SiO}_4]$ -tetrahedra, whereas aluminum ions are present in form of $[\text{AlO}_4]$ -tetrahedra and $[\text{AlO}_6]$ -octahedra. With an increase in basicity 2.0 to 2.5, the silicon structure becomes more complicated, and then at a basicity of 3.5 – 5.0 it becomes simpler, whereas the aluminate one becomes more complicated due to an increase in the content of CaO , which participates in charge compensation of polymerized structural units $[\text{AlO}_4]$ -tetrahedra with the formation of a more stable tetrahedral structure, and as a result of increased slag viscosity. Slags of the studied oxide system containing 15 % Ce_2O_3 are characterized by a sufficiently high liquid mobility in the considered basicity range.

Keywords: viscosity, crystallization temperature, Raman spectroscopy, cerium oxide, slag, phase composition, slag structure

Acknowledgements: The research was supported by the Russian Science Foundation, grant No. 22-29-00975, <https://rscf.ru/project/22-29-00975/>.

For citation: Upolovnikova A.G., Shartdinov R.R., Smetannikov A.N. Effect of basicity on physical properties of ladle slags of $\text{CaO} - \text{SiO}_2 - \text{Ce}_2\text{O}_3 - \text{Al}_2\text{O}_3 - \text{MgO}$ system. *Izvestiya. Ferrous Metallurgy*. 2024;67(2):205–210. <https://doi.org/10.17073/0368-0797-2024-2-205-210>

ВЛИЯНИЕ ОСНОВНОСТИ НА ФИЗИЧЕСКИЕ СВОЙСТВА
КОВШЕВЫХ ШЛАКОВ СИСТЕМЫ
 $\text{CaO} - \text{SiO}_2 - \text{Ce}_2\text{O}_3 - \text{Al}_2\text{O}_3 - \text{MgO}$ А. Г. Уполовникова[✉], Р. Р. Шартдинов, А. Н. Сметанников

Институт металлургии Уральского отделения РАН (Россия, 620016, Свердловская обл., Екатеринбург, ул. Амундсена, 101)

[✉ upol.ru@mail.ru](mailto:upol.ru@mail.ru)

Аннотация. Исследованы физические свойства шлаков системы $\text{CaO}-\text{SiO}_2-\text{Ce}_2\text{O}_3-\text{Al}_2\text{O}_3-\text{MgO}$, содержащих оксид церия. В основе разработанных шлаков кальций-силикатная система, основность $(\text{CaO})/(\text{SiO}_2)$ которой оказывает большое влияние на свойства шлака. Обобщение результатов выполненных исследований позволило получить новые данные о влиянии основности в церийсодержащих шлаках изучаемой оксидной системы на вязкость, температуру начала кристаллизации и структуру. Экспериментальные исследования физических свойств этих шлаков показали, что с ростом основности от 2,0 до 5,0 наблюдается рост температуры начала кристаллизации и вязкости, что связано со структурой формируемых шлаков. Повышение основности способствует повышению вязкости от 0,20 до 0,41 Па·с при температуре 1500 °C и повышению температуры кристаллизации от 1397 до 1497 °C. Полученные результаты показали, что на структуру церийсодержащего шлака влияют как ион Si^{4+} , так и ион Al^{3+} , которые являются сеткообразователями. Ионы кремния в рассматриваемой системе присутствуют в виде $[\text{SiO}_4]$ -тетраэдров, тогда как ионы алюминия присутствуют в виде $[\text{AlO}_4]$ -тетраэдров и $[\text{AlO}_6]$ -октаэдров. С повышением основности от 2,0 до 2,5 кремниевая структура усложняется, а затем при основ-

ности 3,5 – 5,0 упрощается. Аллюминатная структура усложняется за счет повышения содержания оксида CaO, который участвует в компенсации заряда полимеризованных структурных единиц $[AlO_4]$ -тетраэдров с образованием более стабильной тетраэдрической структуры, и, как следствие, повышенной вязкости шлака. Шлаки изучаемой оксидной системы, содержащие 15 % Ce_2O_3 , характеризуются в рассматриваемом диапазоне основности достаточно высокой жидкоподвижностью.

Ключевые слова: вязкость, температура начала кристаллизации, рамановская спектроскопия, оксид церия, шлак, фазовый состав, структура шлака

Благодарности: Исследование выполнено за счет гранта Российского научного фонда № 22-29-00975, <https://rscf.ru/project/22-29-00975/>.

Для цитирования: Уполовникова А.Г., Шартдинов Р.Р., Сметанников А.Н. Влияние основности на физические свойства ковшевых шлаков системы $CaO-SiO_2-Ce_2O_3-Al_2O_3-MgO$. *Известия вузов. Черная металлургия*. 2024;67(2):205–210. <https://doi.org/10.17073/0368-0797-2024-2-205-210>

INTRODUCTION

Viscosity stands out as one of the most crucial physical properties of slag, as metallurgical processes hinge on phenomena influenced by heat and mass transfer within both slag and metal [1; 2]. Exploring the utilization of rare earth element (REE) oxides represents a promising avenue for decreasing the viscosity of refining slags. Investigations into the impact of cerium oxide additives on slag's physical properties have revealed that cerium oxide reduces both viscosity and crystallization temperature [3 – 5]. Recent studies have demonstrated that incorporating rare earth oxides into slag can diminish the activity of Al_2O_3 oxide in the slag while enhancing the slag's adsorption capacity for Al_2O_3 inclusions in the metal [6 – 8]. Additionally, the equilibrium between refining slag containing Ce_2O_3 and molten steel deoxidized with aluminum hints at the potential for introducing a small amount of cerium, which may transfer into the steel [9 – 11], thereby facilitating micro-alloying and modification [12]. However, to date, the influence of basicity on the physical properties of cerium-containing ladle slags remains unexplored in both domestic and foreign literature.

This study aimed to investigate the physical properties of slags within the $CaO-SiO_2-Ce_2O_3-Al_2O_3-MgO$ system. By consolidating research findings, we sought to generate new insights into the impact of basicity on the viscosity, temperature of crystallization onset, and structure of cerium-containing slags within the studied oxide system.

RESEARCH METHODS

The slags of the $CaO-SiO_2-Ce_2O_3-Al_2O_3-MgO$ oxide system were melted in a resistance furnace using graphite crucibles under an argon atmosphere. Analytical grade oxides were calcined for 2 – 3 h at a temperature of 800 °C prior to melting. Viscosity measurements of the slags were conducted in graphite crucibles using an electric vibrating viscometer, with continuous cooling of the melt from a homogeneous-liquid to a solid state [13]. A molybdenum rod with a diameter of 1.5 mm served as the measuring spindle. The temperature of the slag was monitored using a VR 5/20 tungsten-rhenium thermocouple. The crystallization temperature of the slags was determined according to Frenkel's theory of viscous flow. For this purpose, graphs were plotted in coordinates $\ln \eta - 1/T$, with breaks indicating the onset temperature of slag crystallization [14]. The results of viscosity and crystallization temperature measurements are presented in Table 1 and Fig. 1.

The structure of test slag samples was investigated using a Raman microscope spectrometer U 1000 with a laser having an excitation wavelength of 532 nm. The obtained spectra, within the wave number range of 450 – 1250 cm^{-1} , are depicted in Fig. 2. The observed lines in such spectra can be clearly attributed to vibrations of the molecules of the material under study. Depending on the frequency, intensity, and shape of these lines, conclusions about the structure of the slags can be drawn [15]. This transformation can be attributed to the characteristics of the slag structure. Fig. 2 displays

Table 1. Composition, temperature of crystallization onset and viscosity of experimental slags

Таблица 1. Состав, температура начала кристаллизации и вязкость экспериментальных шлаков

Oxide content, %					B	$t_{cr}, ^\circ C$	Viscosity, Pa·s, at $T, ^\circ C$	
CaO	SiO_2	Ce_2O_3	MgO	Al_2O_3			1500	1550
41.3	20.7	15	8	15	2.0	1397	0.20	0.16
44.8	17.2	15	8	15	2.5	1419	0.22	0.17
48.2	13.8	15	8	15	3.5	1463	0.26	0.18
51.7	10.3	15	8	15	5.0	1497	0.41	0.23

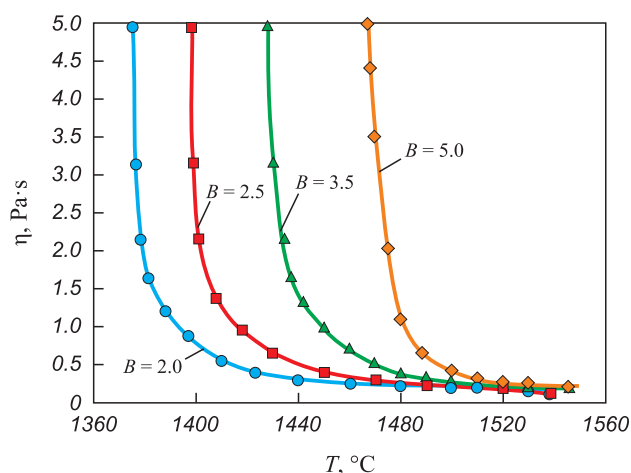


Fig. 1. Dependence of viscosity of the slags on temperature at basicity of 2.0 (●), 2.5 (■), 3.5 (▲) and 5.0 (◆)

Рис. 1. Зависимость вязкости шлаков от температуры при основности 2,0 (●), 2,5 (■), 3,5 (▲) и 5,0 (◆)

the Raman spectra of slag samples with varying basicity, featuring peaks: in the low-frequency region with wave numbers around 600 cm^{-1} , representing Al–O stretching vibrations in $[\text{AlO}_6]$ octahedra within the range of slag basicity from 2.0 to 2.5; as basicity increases to 3.5–5.0 units, peaks emerge in the region of about 550 cm^{-1} , attributed to the transverse motion of bridging oxygen inside the Al–O–Al bond; peaks in the range of $650–800\text{ cm}^{-1}$, reflecting Al–O stretching vibrations in $[\text{AlO}_4]$ tetrahedra. Peaks in the higher wave numbers region ($800–950\text{ cm}^{-1}$) are associated with the silicate structure ($[\text{SiO}_4]$ -tetrahedra). The intensity and shape of these peaks allow for the evaluation of the influence

of basicity on the structure of the formed slags and their viscosity.

For further quantitative determination of changes in structural units with different basicity of the slag, the Raman spectra (Fig. 2) were deconvoluted by the Gaussian method using the PeakFit software with the correlation coefficient of minimum 0.99. The results of deconvolution of the silicate region of Raman spectra are shown in Fig. 3 and Table 2.

RESULTS AND DISCUSSION

The viscosity dependence of the studied slags on temperature, within a basicity range of 2.0 to 5.0, is illustrated in Fig. 1. As basicity increases, slags transition gradually from fluid states with low crystallization temperatures to those with higher viscosity and crystallization onset temperatures (Table 1).

The slag structure formed at a basicity of 2.0 is low-polymerized. As noted earlier, it is characterized by the presence of $[\text{AlO}_6]$ -octahedra, which function as grid

Table 2. Proportion of structural elements

Таблица 2. Доли структурных элементов

Slag	B	Q_{Si}^0	Q_{Si}^1	BO
1	2.0	0.48	0.52	0.52
2	2.5	0.41	0.59	0.59
3	3.5	0.53	0.47	0.47
4	5.0	0.88	0.12	0.12

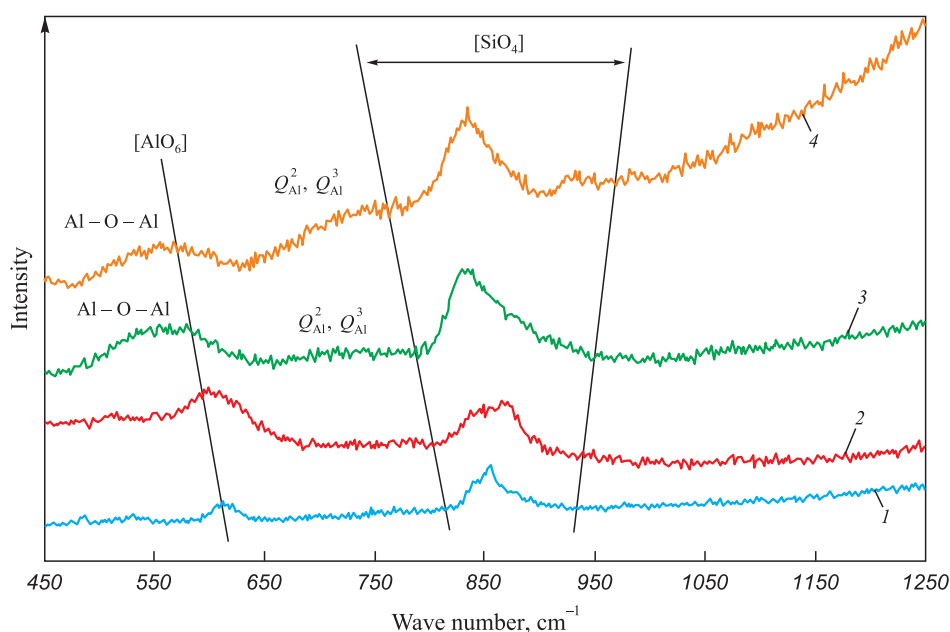


Fig. 2. Raman spectra of the slags at basicity of 2.0 (1), 2.5 (2), 3.5 (3) and 5.0 (4)

Рис. 2. Рамановские спектры изучаемых шлаков при основности 2,0 (1), 2,5 (2), 3,5 (3) и 5,0 (4)

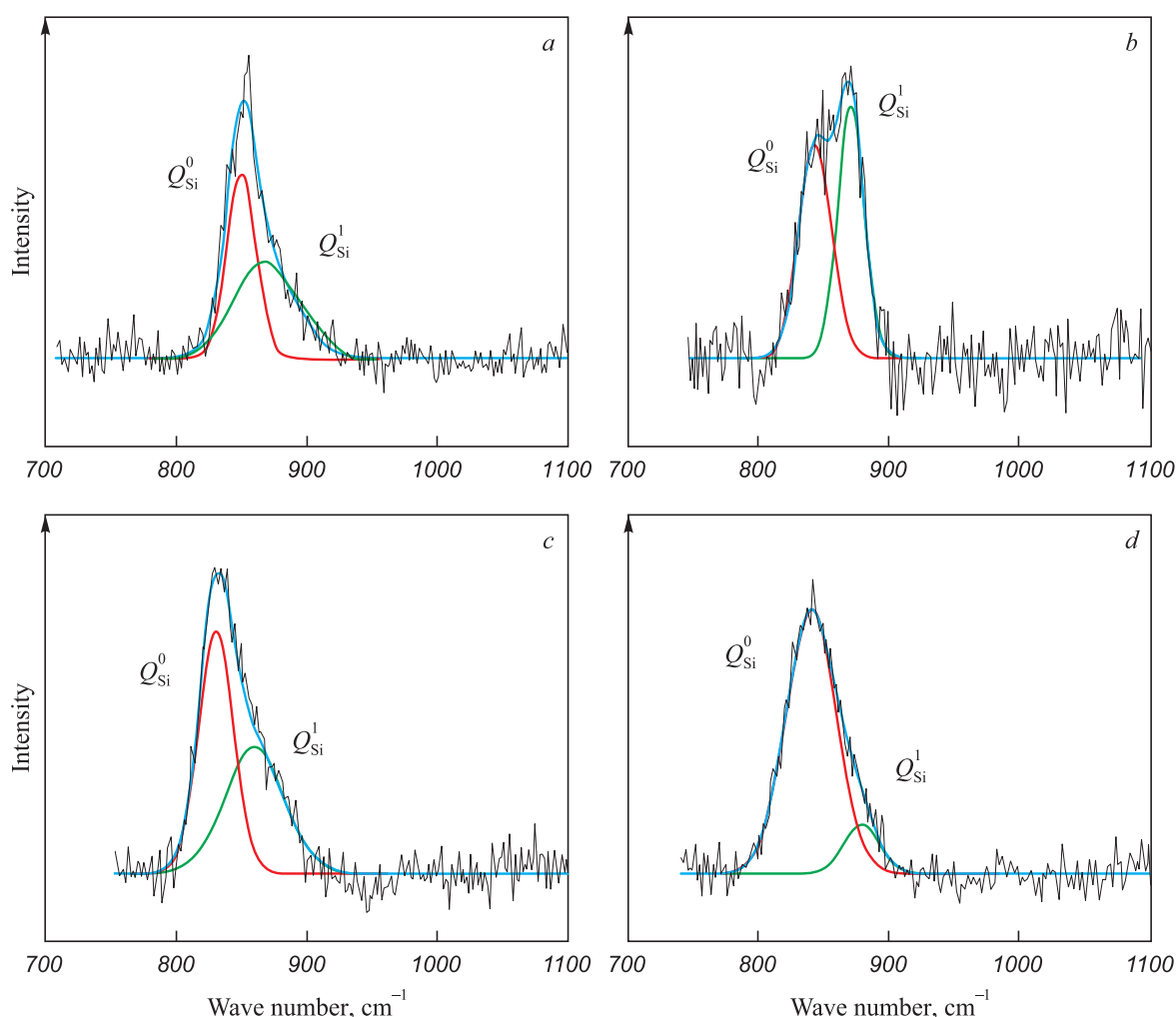


Fig. 3. Deconvolution of the silicate region at basicity of 2.0 (a), 2.5 (b), 3.5 (c) and 5.0 (d)

Рис. 3. Деконволюция силикатной области при основности 2,0 (a), 2,5 (b), 3,5 (c) и 5,0 (d)

modifier (Fig. 2), along with two depolymerized structural units of silicon: $[\text{SiO}_4]^{4-}$ with an increased proportion of non-bridging oxygen to 0.48 (Q_{Si}^0) and $[\text{Si}_2\text{O}_7]^{6-}$ with a proportion of one bridging oxygen increased to 0.52 (Q_{Si}^1) (Fig. 3, Table 2). This structure arises due to the presence of structure modifiers – calcium and cerium oxides – in the slag. Their dissociation in melts releases additional O^{2-} ions, which interact with $[\text{AlO}_4]^-$ and $[\text{SiO}_4]^-$ tetrahedra, disrupting the aluminate and silicate melt structures [16; 17]. Consequently, these slags exhibit a low crystallization temperature (1397 °C) and low viscosity (0.20 and 0.16 Pa·s) at temperatures of 1500 and 1550 °C (Table 1).

As the basicity increases to 2.5, the silicate structure becomes more complex. Its polymerization degree rises from 0.52 to 0.59, while the proportion of non-bridging oxygen decreases from 0.48 to 0.41, and the proportion with one bridging oxygen increases from 0.52 to 0.59 (Table 2). In high-basicity slags containing Al_2O_3 , Al^{3+} ions are absorbed by the silicate structure, acting as grid-forming agents, thus enhancing the complexity

of the silicate structure [18]. The increased complexity of the slag structure elevates the onset temperature of crystallization to 1419 °C and viscosity to 0.22 and 0.17 Pa·s at temperatures of 1500 and 1550 °C (Table 1).

As the basicity increases to 3.5 and 5.0, a peak emerges in the region of about 550 cm^{-1} , attributed to the transverse motion of bridging oxygen inside the Al–O–Al bond. The relative Al–O–Al intensity gradually increases with increasing basicity, while the opposite trend is observed for $[\text{AlO}_6]$ octahedra. This indicates an enhanced Al–O–Al bond and a decreased proportion of $[\text{AlO}_6]$ octahedra, leading to polymerization of the aluminate grid. Additionally, an increase in the slag basicity from 3.5 to 5.0 results in higher peak intensity in the region of wave numbers 650 – 800 cm^{-1} . This is attributed to symmetrical stretching vibrations $[\text{AlO}_3]^{3-}$ (Q_{Al}^2) and $[\text{Al}_2\text{O}_5]^{4-}$ (Q_{Al}^3) [16; 17], indicating that the aluminate structure in the molten slag (Fig. 2) has become more complex, resulting in an increase in the crystallization onset temperature to 1463 and 1497 °C. Viscosity increases to 0.26 and 0.18 Pa·s at temperatures of 1500 and 1550 °C and a basicity

of 3.50 and to 0.41 and 0.23 Pa·s at temperatures of 1500 and 1550 °C and a basicity of 5.0.

Alongside the polymerization of the aluminate structure at basicities of 3.5 and 5.0, the silicate structure becomes simpler, and the polymerization degree decreases from 0.47 to 0.12 (Table 2). CaO oxide can act not only as a grid modifier but also as a charge compensator due to the excess of Ca^{2+} ions formed with increasing basicity. Ca^{2+} cations will compensate for the polymerized structural units of $[\text{AlO}_4]$ -tetrahedra, leading to the formation of a more stable tetrahedral structure and resulting in increased slag viscosity [19; 20]. Cerium ions can act as charge compensators and stabilize the aluminate structure [3; 21; 22].

CONCLUSIONS

Experimental studies of the physical properties of the slags within the $\text{CaO}-\text{SiO}_2-\text{Ce}_2\text{O}_3-\text{Al}_2\text{O}_3-\text{MgO}$ oxide system have indicated that increasing the basicity from 2.0 to 5.0 leads to higher viscosity and temperature of crystallization onset. This phenomenon is attributed to the structure of the resulting slags. With the augmentation of basicity, the aluminate structure becomes more complex, while the silicate structure becomes simpler due to an excess of Ca^{2+} ions, which serve as charge compensators for the polymerized structural units of $[\text{AlO}_4]$ tetrahedra. Overall, the slags within the studied oxide system containing 15 % Ce_2O_3 exhibit sufficiently high fluidity within the considered basicity range.

REFERENCES / СПИСОК ЛИТЕРАТУРЫ

- Popel' S.I. Theory of Metallurgical Processes. Moscow: Metallurgiya; 1986:463. (In Russ.).
Попель С.И. Теория металлургических процессов. Москва: Металлургия; 1986:463.
- Sokolov G.A. Extra-Furnace Refining of Steel. Moscow: Metallurgiya; 1977:208. (In Russ.).
Соколов Г.А. Внепечное рафинирование стали. Москва: Металлургия; 1977:208.
- Wu C., Cheng G., Long H. Effect of Ce_2O_3 and $\text{CaO}/\text{Al}_2\text{O}_3$ on the phase, melting temperature and viscosity of $\text{CaO}-\text{Al}_2\text{O}_3-10 \text{ mass } \% \text{SiO}_2$ based slags. *High Temperature Materials and Processes*. 2014;33(1):77–84.
<http://dx.doi.org/10.1515/htmp-2013-0025>
- Liu C., Qi J., Sun J., Zhang X. Design and fluidity research of a new tundish flux for rare earth steel. *Journal of Sustainable Metallurgy*. 2022;8:1104–1116.
<https://doi.org/10.1007/s40831-022-00544-6>
- Zheng X., Liu C. Effect of Ce_2O_3 on the melt structure and properties of $\text{CaO}-\text{Al}_2\text{O}_3$ -based slag. *ISIJ International*. 2022;62(6):1091–1098.
<https://doi.org/10.2355/isijinternational.ISIJINT-2021-545>
- Wang L.J., Wang Q., Li J.M., Chou K.C. Dissolution mechanism of Al_2O_3 in refining slags containing Ce_2O_3 . *Journal of Mining and Metallurgy, Section B: Metallurgy*. 2016;52(1):35–40. <https://doi.org/10.2298/JMMB140706004W>
- Liu Y.Q., Wang L.J., Chou K.C. Dissolution behavior of Al_2O_3 in refining slags containing Ce_2O_3 . *ISIJ International*. 2014;54(4):728–733.
<http://dx.doi.org/10.2355/isijinternational.54.728>
- Cao J., Li Y., Lin W., Che J., Zhou F., Tan Y., Li D., Chen C., Dang J. Assessment of inclusion removal ability in refining slags containing Ce_2O_3 . *Crystals*. 2023;13(2):202.
<https://doi.org/10.3390/cryst13020202>
- Yang X., Long H., Cheng G., Wu C., Wu B. Effect of refining slag containing Ce_2O_3 on steel cleanliness. *Journal of Rare Earths*. 2011;29(11):1079–1083.
[https://doi.org/10.1016/S1002-0721\(10\)60602-3](https://doi.org/10.1016/S1002-0721(10)60602-3)
- Babenko A.A., Smirnov L.A., Upolovnikova A.G., Shartdinov R.R. Study of possibility of cerium reduction from slags of $\text{CaO}-\text{SiO}_2-\text{Ce}_2\text{O}_3-15\%\text{Al}_2\text{O}_3-8\%\text{MgO}$ system. In: *IOP Conference Series: Materials Science and Engineering*. 2020;966:012010.
<https://doi.org/10.1088/1757-899X/966/1/012010>
- Upolovnikova A.G., Babenko A.A., Smirnov L.A., Mikhailova L.Yu. Direct microalloying of steel with cerium under slags of $\text{CaO}-\text{SiO}_2-\text{Ce}_2\text{O}_3-15 \text{ } \%\text{Al}_2\text{O}_3-8 \text{ } \%\text{MgO}$ system with additional reducing agents. *Izvestiya. Ferrous Metallurgy*. 2021;64(8):581–587. (In Russ.).
<https://doi.org/10.17073/0368-0797-2021-8-581-587>
Уполовникова А.Г., Бабенко А.А., Смирнов Л.А., Михайлова Л.Ю. Прямое микролегирование стали церием под шлаками системы $\text{CaO}-\text{SiO}_2-\text{Ce}_2\text{O}_3-15 \text{ } \%\text{Al}_2\text{O}_3-8 \text{ } \%\text{MgO}$ дополнительными восстановителями. *Известия вузов. Черная Металлургия*. 2021;64(8):581–587.
<https://doi.org/10.17073/0368-0797-2021-8-581-587>
- Kudrin V.A. Extra-Furnace Treatment of Cast Iron and Steel. Moscow: Metallurgiya; 1992:336. (In Russ.).
Кудрин В.А. Внепечная обработка чугуна и стали. Москва: Металлургия; 1992:336.
- Shtengel'meier S.V., Prusov V.A., Bogachev V.A. Improvement of the viscosity measurement technique with a vibrating viscometer. *Zavodskaya laboratoriya*. 1985;51(9):56–57. (In Russ.).
Штенгельмейер С.В., Прусов В.А., Богачев В.А. Усовершенствование методики измерения вязкости вибрационным вискозиметром. *Заводская лаборатория*. 1985;51(9):56–57.
- Voskoboinikov V.G., Dunaev N.E., Mikhalevich A.G., Kukhtin T.I., Shtengel'meier S.V. Properties of Liquid Blast Furnace Slags. Moscow: Metallurgiya; 1975:180.
Воскобойников В.Г., Дунаев Н.Е., Михалевич А.Г., Кухтин Т.И., Штенгельмейер С.В. Свойства жидких доменных шлаков. Москва: Металлургия; 1975:180.
- Böcker J. Spektroskopie. Instrumentelle Analytik mit Atom- und Molekülspektrometrie. Würzburg: Vogel Buchverlag; 1997:519. (In Germ.).
Бёккер Ю. Спектроскопия. Москва: РИЦ Техносфера; 2009:528.
- Zhang R., Wang Z., Meng Y., Jiao S., Jia J., Min Y., Liu C. Quantitative insight into aluminum structures in $\text{CaO}-\text{Al}_2\text{O}_3-\text{SiO}_2$ system via Raman and ^{27}Al MAS-NMR spectroscopies. *Journal of Non-Crystalline Solids*. 2021;573:121116.
<https://doi.org/10.1016/j.jnoncrysol.2021.121116>

17. Kim T.S., Park J.H. Structure-viscosity relationship of low-silica calcium aluminosilicate melts. *ISIJ International*. 2014;54(9):2031–2038. <https://doi.org/10.2355/isijinternational.54.2031>
18. Gao J., Wen G., Huang T., Tang P., Liu Q. Effects of the composition on the structure and viscosity of the CaO–SiO₂-based mold flux. *Journal of Non-Crystalline Solids*. 2016;435: 33–39. <https://doi.org/10.1016/j.jnoncrysol.2016.01.001>
19. Zheng D.-L., Ma G.-J., Zhang X., Liu M.-K., Xu J. Effect of CaO/Al₂O₃ on structure, viscosity, and surface tension of electrosag remelting-type CeO₂-bearing slag. *Journal of Iron and Steel Research International*. 2023;30: 717–725. <https://doi.org/10.1007/s42243-022-00844-x>
20. Qi J., Liu C., Zhang C., Jiang M. Effect of Ce₂O₃ on structure, viscosity, and crystalline phase of CaO–Al₂O₃–Li₂O–Ce₂O₃. *Metallurgical and Materials Transactions B*. 2017;48:11–16. <https://doi.org/10.1007/s11663-016-0850-3>
21. Zheng X., Liu C. Investigation of CaO/Al₂O₃ mass ratio on the properties and structure of Ce₂O₃-containing CaO–Al₂O₃-based tundish flux. *ISIJ International*. 2022;62(3): 418–425. <https://doi.org/10.2355/isijinternational.ISIJINT-2021-438>
22. Lin S.-L., Hwang C.-S. Structures of CeO₂–Al₂O₃–SiO₂ glasses. *Japanese Journal of Applied Physics*. 1996;35(7R): 3975. <https://doi.org/10.1143/JJAP.35.3975>

Information about the Authors

Alena G. Upolovnikova, Cand. Sci. (Eng.), Senior Researcher of the Laboratory of Steel and Ferroalloys, Institute of Metallurgy, Ural Branch of the Russian Academy of Sciences

ORCID: 0000-0002-6698-5565

E-mail: upol.ru@mail.ru

Ruslan R. Shartdinov, Junior Researcher of the Laboratory of Steel and Ferroalloys, Institute of Metallurgy, Ural Branch of the Russian Academy of Sciences

ORCID: 0000-0003-0852-1161

E-mail: rr.shartdinov@gmail.com

Artem N. Smetannikov, Junior Researcher of the Laboratory of Steel and Ferroalloys, Institute of Metallurgy, Ural Branch of the Russian Academy of Sciences

ORCID: 0000-0001-9206-0905

E-mail: artem.smetannikov.89@mail.ru

Сведения об авторах

Алена Геннадьевна Уполовникова, к.т.н., старший научный сотрудник лаборатории стали и ферросплавов, Институт металлургии Уральского отделения РАН

ORCID: 0000-0002-6698-5565

E-mail: upol.ru@mail.ru

Руслан Рафикович Шартдинов, младший научный сотрудник лаборатории стали и ферросплавов, Институт металлургии Уральского отделения РАН

ORCID: 0000-0003-0852-1161

E-mail: rr.shartdinov@gmail.com

Артём Николаевич Сметанников, младший научный сотрудник лаборатории стали и ферросплавов, Институт металлургии Уральского отделения РАН

ORCID: 0000-0001-9206-0905

E-mail: artem.smetannikov.89@mail.ru

Contribution of the Authors

A. G. Upolovnikova – analysis and generalization of research results.

R. R. Shartdinov – study of the structure of experimental slag samples.

A. N. Smetannikov – experimental studies of physical properties of slags (temperatures of crystallization onset and viscosity).

Вклад авторов

А. Г. Уполовникова – анализ и обобщение результатов исследования.

Р. Р. Шартдинов – исследование структуры опытных образцов шлака.

А. Н. Сметанников – экспериментальные исследования физических свойств шлаков (температуры начала кристаллизации и вязкости).

Received 30.08.2023

Revised 12.10.2023

Accepted 16.10.2023

Поступила в редакцию 30.08.2023

После доработки 12.10.2023

Принята к публикации 16.10.2023

INNOVATION IN METALLURGICAL
INDUSTRIAL AND LABORATORY EQUIPMENT,
TECHNOLOGIES AND MATERIALSИННОВАЦИИ В МЕТАЛЛУРГИЧЕСКОМ
ПРОМЫШЛЕННОМ И ЛАБОРАТОРНОМ
ОБОРУДОВАНИИ, ТЕХНОЛОГИЯХ И МАТЕРИАЛАХ

UDC 621.74.045

DOI 10.17073/0368-0797-2024-2-211-218



Original article

Оригинальная статья

STRESS-STRAIN STATE OF CERAMIC SHELL MOLD DURING FORMATION OF SPHERICAL STEEL CASTING IN IT. PART 1

V. I. Odinokov[✉], A. I. Evstigneev, E. A. Dmitriev, A. N. Namokonov,
A. A. Evstigneeva, D. V. Chernyshova

■ Komsomolsk-on-Amur State University (27 Lenina Ave., Khabarovsk Territory, Komsomolsk-on-Amur 681013, Russian Federation)

✉ diss@knastu.ru

Abstract. The task of the present theoretical investigation was to determine the external factors at which a spherical shell mold will not fail due to temperature stresses occurring in it. The problem is formulated for determining the stress-strain state of the spherical shell mold formed in the support filler at cooling of solidifying spherical steel casting. The investigated axisymmetric rotational body has four zones: liquid metal, solid metal, shell mold, and support filler. To solve the problem, the equation of linear elasticity, the equation of heat capacity and a well-proven numerical method were used according to which the investigated zone is partitioned into elements by a system of orthogonal surfaces. For each element, a formulated system of equations is written in difference form, taking into account axial symmetry through the values of stresses and displacements along the element edges and the lengths of the ribs' arcs that limit its volume. The heat conduction equation is written in difference form for construction of a heat balance for an arbitrary orthogonal element, including both average temperature of the element and temperatures of the elements surrounding its volume. The authors found the solution of the difference analogue of heat equation by the "sweep" method according to the compiled iterative scheme. A difference analogue of the formulated system of differential equations of the linear theory of elasticity has the form of an algebraic system of equations. The algorithm for convolution of this system allows one to significantly reduce its rank. A general numerical scheme and algorithm for solving the problem are presented. The result of the solution is the magnitude of stresses, displacements on average along the edges of each element and average temperature in the element.

Keywords: investment casting, shell mold, stressed state, modeling, crack resistance

Acknowledgements: The research was supported by the Russian Science Foundation, grant No. 24-29-00214, <https://rscf.ru/project/24-29-00214/>.

For citation: Odinokov V.I., Evstigneev A.I., Dmitriev E.A., Namokonov A.N., Evstigneeva A.A., Chernyshova D.V. Stress-strain state of ceramic shell mold during formation of spherical steel casting in it. Part 1. *Izvestiya. Ferrous Metallurgy*. 2024;67(2):211–218. <https://doi.org/10.17073/0368-0797-2024-2-211-218>

НАПРЯЖЕННО-ДЕФОРМИРОВАННОЕ СОСТОЯНИЕ КЕРАМИЧЕСКОЙ ОБОЛОЧКОВОЙ ФОРМЫ ПРИ ФОРМИРОВАНИИ В НЕЙ СТАЛЬНОЙ ШАРООБРАЗНОЙ ОТЛИВКИ. ЧАСТЬ 1

В. И. Одиноков[✉], А. И. Евстигнеев, Э. А. Дмитриев, А. Н. Намоконов,
А. А. Евстигнеева, Д. В. Чернышова

■ Комсомольский-на-Амуре государственный университет (Россия, 681013, Хабаровский край, Комсомольск-на-Амуре, пр. Ленина, 27)

✉ diss@knastu.ru

Аннотация. Задачей настоящего теоретического исследования является определение внешних факторов, при которых сферическая оболочковая форма (ОФ) не будет разрушаться от возникающих в ней температурных напряжений. Сформулирована задача по определению напряженно-деформируемого состояния (НДС) ОФ, заформированной в опорный наполнитель (ОН), при охлаждении в ней затвердевающей шарообразной стальной отливки. Рассматриваемое осесимметричное тело вращения имеет четыре области (жидкий металл, твердый металл, оболочковая форма, опорный наполнитель). Для решения задачи авторы используют уравнение линейной теории упругости,

уравнение теплопроводности и апробированный численный метод, согласно которому исследуемая область разбивается системой ортогональных поверхностей на элементы. Для каждого элемента записана система уравнений в разностном виде с учетом осевой симметрии через напряжения и перемещения по граням элемента и длинам дуг ребер, ограничивающих его объем. Уравнение теплопроводности записано в разностном виде из построения теплового баланса для произвольного ортогонального элемента, включающее как среднюю температуру элемента, так и температуры элементов, окружающих его объем. Решение разностного аналога уравнения теплопроводности осуществляется методом «прогонки» по составленной итерационной схеме. Приведен разностный аналог сформулированной системы дифференциальных уравнений линейной теории упругости в виде алгебраической системы уравнений. Представленный алгоритм свертки этой системы позволяет значительно понизить ее ранг. Приводится общая численная схема и алгоритм решения задачи. Результатом решения являются величины напряжений, перемещений в среднем по граням каждого элемента и средняя температура в элементе.

Ключевые слова: литье по выплавляемым моделям, оболочковая форма, напряженное состояние, моделирование, трещинообразование

Благодарности: Исследование выполнено за счет гранта Российского научного фонда № 24-29-00214, <https://rscf.ru/project/24-29-00214/>.

Для цитирования: Одинокое В.И., Евстигнеев А.И., Дмитриев Э.А., Намоконов А.Н., Евстигнеева А.А., Чернышова Д.В. Напряженно-деформированное состояние керамической оболочковой формы при формировании в ней стальной шарообразной отливки. Часть 1. *Известия вузов. Черная металлургия*. 2024;67(2):211–218. <https://doi.org/10.17073/0368-0797-2024-2-211-218>

INTRODUCTION

Numerous analytical [1; 2] and theoretical studies [3 – 5] have investigated the crack resistance of a ceramic shell mold (CSM) after liquid metal is poured into it and the solidifying casting is cooled. A glass-shaped shell mold bounded by spherical and cylindrical surfaces was studied. It was established that the most dangerous stresses that arise when liquid metal is cooled in the shell mold are normal tensile stresses on the outer surface of the mold adjacent to the support filler. The researchers determined the optimal external force and temperature influences on the shell mold to guarantee its durability during steel casting production. Additionally, they studied the morphological structures of shell molds that can withstand the thermal stresses of cooled castings and proposed new designs.

Numerous theoretical and experimental studies have been conducted to establish the characteristics of the stress-strain state (SSS) of a ceramic shell mold and the resulting castings in investment casting, and the SSS dependence on factors such as the consumable pattern [6; 7], the shape and geometry of the ceramic shell mold [8; 9], mold wall thickness [10; 11], mold material [12; 13], geometry of castings [14 – 16], and methods of mold strength tests [17; 18].

Other works describe mathematical modeling of these processes, including modeling methods [19], research methods [20 – 22], studies based on numerical modeling [23 – 25], special mathematical models [26 – 28], and software [29; 30].

Further theoretical studies have shown that the durability of shell molds largely depends on their shape, which is organically related to the geometry of the casting formed in them.

However, practically no studies have investigated the modeling of the crack resistance of a ceramic shell mold based on the quantitative and qualitative indicators of its stress-strain state as a steel casting in the shape of a sphere (ball) is formed in it. This issue is addressed in our study.

We conducted a theoretical study related to steel casting production in a spherical shell mold. A variety of parts have spherical shapes, including spherical joints, which are crucial components in mechanical engineering and robotics.

The first theoretical results of the investigated manufacturing process were published in [31], where it was clearly shown that the stress-strain state in a spherical shell mold is drastically different from that in a cylindrical shell mold when producing a steel casting. However, the paper [31] does not present a mathematical model of the process.

This study shows that high-quality billets for spherical joints can be obtained using casting, which is much cheaper than metal treatment under pressure.

ENGINEERING PROBLEM STATEMENT

Liquid steel is poured into a spherical mold, where it crystallizes by removing heat through the shell mold walls via the support filler (Fig. 1, *a*). A spherical shell mold can be monolithic or consist of several layers [1], each with its own physical and mechanical properties. When steel is cooled in a shell mold, temperature stresses arise in the wall due to a large temperature gradient. Under certain external influences, these stresses can lead to wall destruction, resulting in the rejection of the steel casting. Therefore, the objective of this theoretical study is to determine the external factors under which the spherical shell mold will not be destroyed by the temperature stresses arising in it.

MATHEMATICAL PROBLEM STATEMENT

An axisymmetric rotational body is under consideration. The deformable material is considered isotropic, and the movement is deemed slow.

We have a four-component system (Fig. 1, *b*). The deformable medium includes the solidified metal (region *II*) and the mold (region *III*), both of which are isotropic materials. The process is non-stationary. Using the theory

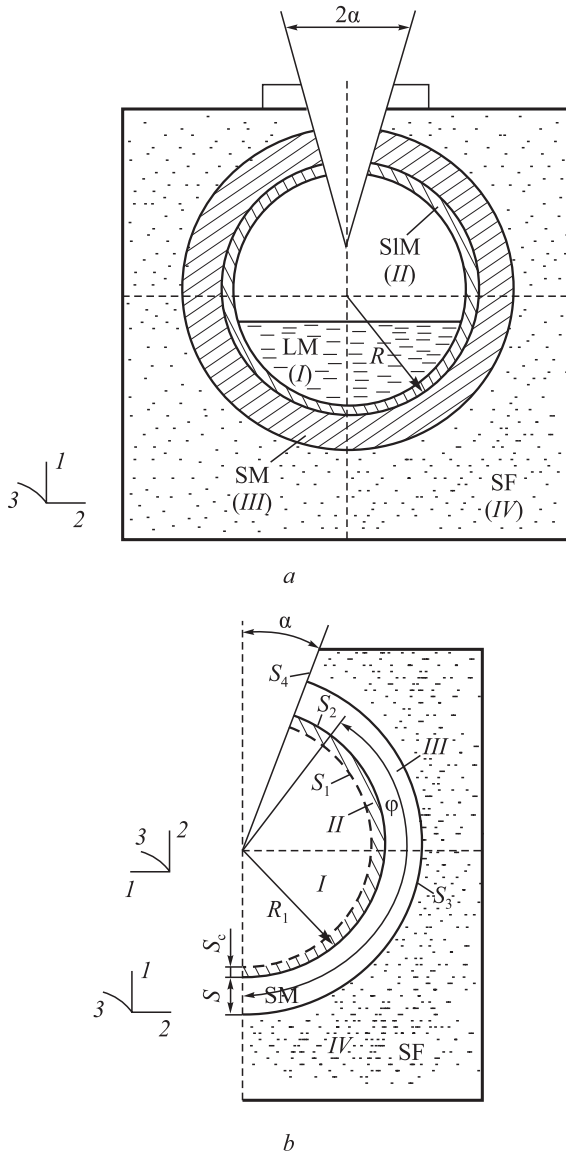


Fig. 1. General (a) and calculation (b) diagrams of a spherical shell mold (SM) molded in support filler and poured with liquid metal in accordance with the axial symmetry:

LM – liquid metal (area I); SIM – solid metal (area II); SM – shell mold (area III); SF – support filler (area IV); S_1 – inner contact surface of liquid and solidified metal; S_2 – inner contact surface of solidified metal and shell mold; S_3 – outer surface of the shell mold; S_4 – free surface of the end face of casting cup; R – radius of the spherical casting; S – thickness of shell mold; S_c – thickness of solidified metal crust; α – slope angle of casting cup; ϕ – angle of enclosing surface of shell mold with a support filler

Рис. 1. Общая (a) и расчетная (b) схемы шарообразной ОФ, заформованной в опорный наполнитель и залитой жидким металлом с учетом осевой симметрии:

LM – жидкий металл (область I); SIM – твердый металл (область II); SM – оболочковая форма (область III); SF – опорный наполнитель (область IV); S_1 – внутренняя поверхность контакта жидкого и затвердевшего металла; S_2 – внутренняя поверхность контакта затвердевшего металла и оболочковой формы; S_3 – внешняя поверхность оболочковой формы; S_4 – свободная поверхность торца литниковой чаши SM; R – радиус шарообразной отливки; S – толщина оболочковой формы; S_c – толщина корочки затвердевшего металла; α – угол наклона литниковой воронки; ϕ – угол охвата поверхности оболочковой формы опорным наполнителем

of elasticity and the Eulerian reference frame, we write a system of equations for each region:

– for region I:

$$\begin{aligned}\sigma_{11} = \sigma_{22} = \sigma_{33} = \sigma &= P; \\ P &= \gamma h; \quad \theta = \alpha_1 \Delta \theta;\end{aligned}\quad (1)$$

– for regions II, III:

$$\begin{cases} \sigma_{ij} = 0, \quad i, j = 1, 2, 3; \\ \sigma_{ij} - \sigma \delta_{ij} = 2G_p \varepsilon_{ij}^*; \quad \varepsilon_{ij}^* = \varepsilon_{ij} - \frac{1}{3} \varepsilon \delta_{ij}; \quad \varepsilon = \varepsilon_{ii}; \\ \varepsilon_{ii} = 3k_p \sigma + 3\alpha_p (\theta - \theta_p^*); \quad \varepsilon_{ij} = 0,5(U_{ij} + U_{ji}); \\ C_p \gamma \frac{\partial \theta}{\partial \tau} = \text{div}(\lambda \text{grad} \theta); \end{cases}\quad (2)$$

where σ_{ij} are the components of the stress tensor; σ is the hydrostatic stress; ε_{ij} are the components of the elastic strain tensor; h is the height of the liquid metal column; $k_p = \frac{1-2\mu}{E}$ is the coefficient of volume compressibility;

μ is Poisson's ratio; E is Young's modulus; G_p is the shear modulus in region p (II, III); α_p is the linear expansion coefficient; α_1 is the temperature conductivity coefficient in the region I; τ is time; θ is temperature; C_p is the specific heat in the region p ; γ is density; θ_p^* is the initial temperature in the region p ; $\lambda = \lambda(\theta)$ is heat conduction; $\sigma_{ij,j} = \frac{\partial \sigma_{ij}}{\partial x_j}$; $u_{i,j} = \frac{\partial u_i}{\partial x_j}$; and summation over repeated indices is performed.

In accordance with axial symmetry, we consider the meridian section (Fig. 1, b).

If $\theta_m \leq \theta_{cr}$ (θ_m and θ_{cr} are the temperatures of the metal and crystallization), as the liquid metal is cooled, its temperature is determined by the thickness of the solidified layer Δ_i from the solution of the interphase transition equation [5].

Initial statement of the problem:

$\Delta|_{\tau=0} = 0$ (absence of the metal solid phase);

$\theta|_{\tau=0} = 0 = \theta_m^*$ (temperature of the poured liquid metal);

$\theta_{III}|_{\tau=0} = \theta^*$ (initial mold temperature).

Boundary conditions of the problem (Fig. 1, b):

– on the axis of symmetry: $U_2 = 0$; $\sigma_{21} = 0$; $q_n = 0$;

– on surfaces S_1, S_3, S_4

$$\begin{aligned}\sigma_{11}|_{S_1} &= -P; \quad \sigma_{12}|_{S_1} = 0; \quad U_1|_{S_3} = 0; \quad \sigma_{22}|_{S_4} = 0; \\ \sigma_{12}|_{S_3} &= -\psi \frac{U_{ck}}{U^*} \text{con}(n_1 x_1); \quad \theta|_{S_3} = \theta^*;\end{aligned}\quad (3)$$

where U_{ck} is the sliding of the mold material relative to the sand; U^* is the normalizing displacement; and ψ is a parameter characterizing the friction conditions between the mold and the support filler.

The numerical method was used [32] to solve the system (2). According to this method, the deformation region is divided into a finite number of orthogonal curved elements (Fig. 2, *a*).

With axial symmetry, we have $\sigma_{31} = \sigma_{32} = 0$; $\sigma_{13} = \sigma_{23} = 0$; $U_3 = 0$.

In accordance with [32], the equations (2) and the values ε_{ij} taking into account axial symmetry, will be written as follows:

$$\begin{aligned} S_{13}\Delta S_{12}(\sigma_{11} - \sigma_{22}) + S_{12}S_{13}(\sigma_{11} - \sigma_{33}) + \\ + 0,5\Delta\sigma_{11}S_{12}S_{13} + 0,5\Delta\sigma_{12}S_{21}S_{23} + \\ + (S_{21}\Delta S_{23} + 2S_{23}\Delta S_{21})\sigma_{21} = 0; \\ S_{21}\Delta S_{23}(\sigma_{22} - \sigma_{33}) + S_{23}S_{21}(\sigma_{22} - \sigma_{11}) + \\ + 0,5\Delta\sigma_{22}S_{23}S_{21} + 0,5\Delta\sigma_{21}S_{12}S_{13} + \\ + (S_{12}\Delta S_{13} + 2S_{13}\Delta S_{12})\sigma_{21} = 0; \end{aligned} \quad (4)$$

$$\begin{aligned} \sigma_{11} - \sigma_{22} = 2G_p(\varepsilon_{11} - \varepsilon_{22}); \\ \sigma_{22} - \sigma_{33} = 2G_p(\varepsilon_{22} - \varepsilon_{33}); \end{aligned} \quad (5)$$

$$\varepsilon_{11} + \varepsilon_{22} + \varepsilon_{33} = 3k_p\sigma + 3\alpha_p(\theta - \theta_p^*); \quad (6)$$

$$\begin{aligned} \varepsilon_{11} = \frac{2\Delta U_1}{S_{21}} + \frac{2U_2}{S_{21}} \frac{\Delta S_{21}}{S_{12}}; \quad \varepsilon_{22} = \frac{2\Delta U_2}{S_{32}} + \frac{2U_1}{S_{12}} \frac{\Delta S_{12}}{S_{21}}; \\ \varepsilon_{33} = \frac{2U_1}{S_{13}} \frac{\Delta S_{13}}{S_{31}} + \frac{2U_2}{S_{23}} \frac{\Delta S_{23}}{S_{32}}; \end{aligned} \quad (7)$$

where $U_i = U_i^1 + U_i^2$, $\Delta U_i = U_i^2 - U_i^1$, ($i = 1, 2$); $S_{ij} = S_{ij}^1 + S_{ij}^2$; $\Delta S_{ij} = S_{ij}^2 - S_{ij}^1$.

The adopted symbols are described in [1; 7].

The equations (4) – (7) are written taking into account

that $\frac{\partial U_1}{\partial x_3} = 0$, $\frac{\partial \sigma_{3i}}{\partial x_3} = 0$; $i = 1, 2, 3$; for rotational bodies

$\Delta S_{31} = 0$; $\Delta S_{32} = 0$; $\frac{\Delta U_1}{S_3} = 0$; $\frac{\Delta U_2}{S_3} = 0$; $U_3 = 0$; on the sur-

face x_1x_3 : $S_2^+ - S_2^- = 0$; on the surface x_2x_3 : $S_1^+ - S_1^- = 0$; shift values ε_{ij} ($i \neq j$) shall be written for the node (0) (Fig. 2, *d*) in the form

$$\begin{aligned} \varepsilon_{12}^0 = \frac{2\Delta \bar{U}_2}{S_1} - 0,5\bar{U}_2 \frac{S_2^+ - S_2^-}{S_1S_2} + \\ + \frac{2\Delta \bar{U}_1}{S_2} - 0,5\bar{U}_1 \frac{S_1^+ - S_1^-}{S_1S_2}, \end{aligned} \quad (8)$$

where $S_i = S_i^1 + S_i^2$; $\Delta \bar{U}_i = \bar{U}_{i2} - \bar{U}_{i1}$; $S_i^+ = S_i^{1+} + S_i^{2+}$; $S_i^- = S_i^{1-} + S_i^{2-}$; \bar{U}_i is the average of the value U_i along the element edges.

The authors of [32] prove that if there are initial and boundary conditions, the difference analogue of the system (4) – (6), taking into account the equation (7), is

definable. The order of the system (4) – (6) is significantly reduced when the following operations are performed.

1. The differences $(\sigma_{ij} - \sigma_{jj})$ in equations (4) are expressed by formula (5).

2. The mass conservation equation is rewritten in the recurrent form, taking into account expressions (7), in the form $U_1^2 = U_1^1 + [A]$; where $[A]$ is an operator that does not contain U_1^2 ; direction of bypassing the area along $x_1(\rightarrow)$, along $x_2(\uparrow)$.

3. Shift expressions ε_{ij} ($i \neq j$) are determined based on internal grid nodes in accordance with formulas (8); $i = 1, j = 2$.

4. The values σ_{ij} ($i \neq j$) are determined based on the internal grid nodes from the equations of state $\sigma_{12}^0 = G_p^0 \varepsilon_{12}^0$.

5. The values σ_{ij} are determined based on the external grid nodes from the boundary conditions, and on the contact surfaces – from the friction law.

6. σ_{ij} are determined based on the element edges as the average of the values σ_{ij} at the edges' nodes.

7. The first equation (4) is rewritten in the recurrent form $\sigma_{11}^1 = \sigma_{11}^2 + [E]$; where $[E]$ is an operator that does not contain σ_{11}^1 ; direction of bypassing the area along $x_1(\leftarrow)$, along $x_2(\downarrow)$.

8. From the system of equations (the second equation in the system (4) and the equation $\sigma_{22} - \sigma_{11} = 2\lambda(\varepsilon_{11} - \varepsilon_{22})$) the values σ_{12}^1 and σ_{22}^2 for the element are determined, the equations of the form $F_3 = (\sigma_{22}^2)_{JJ} - (\sigma_{22}^1)_{JJ+1} = 0$ composed for the internal edges (where J is the element index on the coordinate x_2).

Thus, if we consider $X = \{U_2, U_1|_{x_1=0}, \sigma_{11}|_{x_1=x_1^*}\}$, independent variables, the sequence (1) – (7) can be used to determine the dependent variables through X (x_1^* is the final value of the coordinate x in the curved region).

The equivalent system of equations looks as follows

$$\begin{aligned} F_1 = (U_1^2 - U_1^*)|_{x_1=x_1^*} = 0; \\ F_2 = (\sigma_{11}^1 - \sigma_{11}^*)|_{x_1=0} = 0; \\ F_3 = 0; \end{aligned} \quad (9)$$

where U_1^* is known from the boundary conditions of displacement U_1 at the boundary of the region ($x_1 = x_1^*$); σ_{11}^* is known from the boundary conditions of stress σ_{11} at the boundary of the region ($x_1 = 0$).

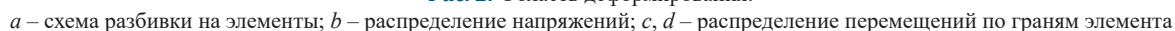
There are as many equations $F_1 = 0$ as there are unknown variables $\sigma_{11}|_{x_1=x_1^*}$, and as many equations $F_2 = 0$ as there are unknown variables $U_1|_{x_1=0}$.

The coefficients and free terms of the new equivalent system of equations (9) can be found using the following procedure.

Suppose the equivalent system of equations looks as follows

$$\bar{F}_i = \alpha_{ij}x_j + b_i = 0; \quad i, j = 1, \dots, n. \quad (10)$$

where θ_k^* is the average temperature in the k^{th} element at the beginning of the time step $\Delta\tau$; λ_k , θ_k , C_k , γ_k are the average heat conduction, temperature, heat capacity, and density in the k^{th} element at the end of the time step $\Delta\tau$; λ_i^- , θ_i^- and λ_i^+ , θ_i^+ , ($i = 1, 2$) are the heat conduction and tem-



perature in the element following the element k on the coordinate x_i in the negative and positive directions x_j ; $S_{21}^- = S_{21}^{1-} + S_{21}^{2-}$; $S_{21}^+ = S_{21}^{1+} + S_{21}^{2+}$; S_{ij}^{1+} ($i \neq j$; $i, j = 1, 2$) and S_{ij}^{1-} are the length of the arc S_{ij}^1 of the element following the element k in the positive and negative directions on the coordinate x_j .

The authors of [32] proved the iteration procedure convergence (11).

ALGORITHM FOR SOLVING THE PROBLEM

1. The cooling time τ^* is divided into a finite number of steps: $\tau^* = \sum \Delta\tau_n$; where n is the number of the time step.

2. The region under study is divided into a finite number of orthogonal elements.

3. The initial and boundary conditions for the elements forming the investigated region and the constants of the physical and mechanical properties of the materials are established.

4. The lengths of the elements' arcs are calculated S_{ik}^j ($i, k = 1, 2$; $i \neq k$; $j = 1, 2$).

5. The temperature field at the time step $\Delta\tau_n$ is determined by the numerical solution of the heat equation using the iterative formula (11) if there are initial and boundary conditions at the investigated time step.

6. If the temperature in the region I near the surface S_2 $\theta|_{S_2} \leq \theta_k$, the thickness Δ_n of the crystallized crust is calculated [5]. If $\theta|_{S_2} > \theta_k$, the following operation is performed.

7. The system of equations (2) is solved taking into account difference analogues (4) – (7) and the developed procedures [1; 32] described above. The fields of stress σ_{ij} and displacements U_i ($i, j = 1, 2$) are determined.

8. Time steps are taken; if $\sum \Delta\tau_n < \tau^*$, the operation 4 is performed; if $\sum \Delta\tau_n = \tau^*$ the calculation process is completed.

As the temperature problem was solved, boundary conditions of the first kind (3) were used. To determine $\theta_m(\tau)$ and $\theta^*(\tau)$, we will use the experimental data from [1]. Approximation of these values yields the following result:

$$\theta_m = 1550 - 1.666\tau - \frac{\tau(60 - \tau)}{10 + \tau^2};$$

$$\theta \leq \tau \leq 60 \text{ s};$$

$$\theta^* = 20 + 17.3\sqrt{\tau};$$

where τ is the cooling time, s.

The time τ does not exceed 60 s, since at $\tau \geq 60$ s the stresses in the shell mold plummet and cannot cause its destruction.

A mathematical model has been developed to determine the stress-strain state and temperature in the shell mold when a spherical casting is cooled in it. This model was used in a numerical solution of the problem on modeling the crack resistance of a spherical shell mold.

CONCLUSIONS

The first theoretical attempt was made to formulate and solve the problem of determining external factors at which a spherical shell mold will not fail due to temperature stresses occurring in it.

Based on the fundamental equations of the theory of elasticity and numerical methods, a numerical scheme and algorithm for solving the problem were developed.

The proposed method for modeling the crack resistance of a spherical shell can be recommended for other functional shells.

REFERENCES / СПИСОК ЛИТЕРАТУРЫ

1. Odinokov V.I., Dmitriev E.A., Evstigneev A.I., Sviridov A.V. Mathematical Modeling of the Processes of Obtaining Castings in Ceramic Shell Molds. Moscow: Innovatsionnoe mashinostroenie; 2020:224. (In Russ.).

Одинок В.И., Дмитриев Э.А., Евстигнеев А.И., Свиридов А.В. Математическое моделирование процессов получения отливок в керамические оболочковые формы. Москва: Инновационное машиностроение; 2020:224.

2. Evstigneev A.I., Odinokov V.I., Dmitriev E.A., Sviridov A.V., Ivankova E.P. The influence of external heat exposure on the stress state of shell forms by smelting models. *Matematicheskoe modelirovanie*. 2021;33(1):63–76. (In Russ.). <https://doi.org/10.20948/mm-2021-01-05>

Евстигнеев А.И., Одинок В.И., Дмитриев Э.А., Свиридов А.В., Иванкова Е.П. Влияние внешнего теплового воздействия на напряженное состояние оболочковых форм по выплавляемым моделям. *Математическое моделирование*. 2021;33(1):63–76.

<https://doi.org/10.20948/mm-2021-01-05>

3. Odinokov V.I., Dmitriev E.A., Evstigneev A.I., Sviridov A.V., Ivankova E.P. Choice of materials properties and of shell molds structure by investment models. *Izvestiya. Ferrous Metallurgy*. 2020;63(9):742–754. (In Russ.). <https://doi.org/10.17073/0368-0797-2020-9-742-754>

Одинок В.И., Дмитриев Э.А., Евстигнеев А.И. и др. Моделирование и оптимизация выбора свойств материалов и структур оболочковых форм по выплавляемым моделям. *Известия вузов. Черная металлургия*. 2020;63(9):742–754. <https://doi.org/10.17073/0368-0797-2020-9-742-754>

4. Odinokov V.I., Evstigneev A.I., Dmitriev E.A., Chernyshova D.V., Evstigneeva A.A. Influence of support filler and structure of shell mold on its crack resistance. *Izvestiya. Ferrous Metallurgy*. 2022;65(4):285–293. (In Russ.). <https://doi.org/10.17073/0368-0797-2022-4-285-293>

Одинок В.И., Дмитриев Э.А., Евстигнеев А.И. Чернышова Д.В., Евстигнеева А.А. Влияние опорного наполнителя и структуры оболочковой формы на ее трещиностойкость. *Известия вузов. Черная металлургия*. 2022;65(4):285–293.

<https://doi.org/10.17073/0368-0797-2022-4-285-293>

5. Evstigneev A.I., Dmitriev E.A., Chernysheva D.V., Odinokov V.I., Evstigneeva A.A., Ivankova E.P. Modeling of external force action on a shell mold for pouring steel. *Matematicheskoe modelirovanie*. 2022;34(5):61–72. (In Russ.). <https://doi.org/10.20948/mm-2022-05-04>

- Евстигнеев А.И., Дмитриев Э.А., Чернышева Д.В., Одинок В.И., Евстигнеева А.А., Иванкова Е.П. Моделирование внешнего силового воздействия на стойкость оболочковой формы при заливке в нее стали. *Математическое моделирование*. 2022;34(5):61–72.
<https://doi.org/10.20948/mm-2022-05-04>
6. Bansode S.N., Phalle V.M., Mantha S.S. Optimization of process parameters to improve dimensional accuracy of investment casting using Taguchi approach. *Advances in Mechanical Engineering*. 2019;11(4):1–12.
<https://doi.org/10.1177/1687814019841460>
7. Mittal Y.G., Kamble P., Gote G., Patil Y., Patel A. K., Bernard A., Karunakaran K.P. Mathematical modelling of pattern sublimation in rapid ice investment casting. *International Journal of Metalcasting*. 2022;16(2):1002–1009.
<http://dx.doi.org/10.1007/s40962-021-00665-w>
8. Kanyo J.E., Schafföner S., Uwanyuze R.S., Leary K.S. An overview of ceramic molds for investment casting of nickel superalloys. *Journal of the European Ceramic Society*. 2020;40(15):4955–4973.
<https://doi.org/10.1016/j.jeurceramsoc.2020.07.013>
9. Rafique M.M.A., Iqbal J. Modeling and simulation of heat transfer phenomena during investment casting. *International Journal of Heat and Mass Transfer*. 2009;52(7–8):2132–2139.
<http://doi.org/10.1016/j.ijheatmasstransfer.2008.11.007>
10. Singh R. Mathematical modeling for surface hardness in investment casting applications. *Journal of Mechanical Science and Technology*. 2012;26:3625–3629.
<http://dx.doi.org/10.1007/s12206-012-0854-0>
11. Jafari H., Idris M. H., Ourdjini A. Effect of thickness and permeability of ceramic shell mould on in situ melted AZ91D investment casting. *Applied Mechanics and Materials*. 2014;465–466:1087–1092.
<http://dx.doi.org/10.4028/www.scientific.net/AMM.465-466.1087>
12. Bansode S.N., Phalle V.M., Mantha S. Taguchi approach for optimization of parameters that reduce dimensional variation in investment casting. *Archives of Foundry Engineering*. 2019;19(1):5–12. <https://dx.doi.org/10.24425/afe.2018.125183>
13. Pattnaik S., Karunakar D.B., Jha P.K. Developments in investment casting process – A review. *Journal of Materials Processing Technology*. 2012;212(11):2332–2348.
<https://doi.org/10.1016/j.jmatprotec.2012.06.003>
14. Zhang J., Li K.W., Ye H.W., Zhang D.Q., Wu P.W. Numerical simulation of solidification process for impeller investment casting. *Applied Mechanics and Materials*. 2011;80–81:961–964.
<https://doi.org/10.4028/www.scientific.net/AMM.80-81.961>
15. Dong Y.W., Li X.L., Zhao Q., Jun Y., Dao M. Modeling of shrinkage during investment casting of thin walled hollow turbine blades. *Journal of Materials Processing Technology*. 2017;244:190–203.
<https://doi.org/10.1016/j.jmatprotec.2017.01.005>
16. Rakoczy Ł., Cygan R. Analysis of temperature distribution in shell mould during thinwall superalloy casting and its effect on the resultant microstructure. *Archives of Civil and Mechanical Engineering*. 2018;18(4):1441–1450.
<https://doi.org/10.1016/j.acme.2018.05.008>
17. Yameng W., Zhigang L. The design of testing methods for strength of ceramic shell mold in investment casting. *Proceedings of the Asia-Pacific Conf. on Intelligent Medical 2018 & Int. Conf. on Transportation and Traffic Engineering*. 2018;336–341. <https://doi.org/10.1145/3321619.3321686>
18. Kolczyk J., Zych J. High temperature strength of ceramic moulds applied in the investment casting method. *Archives of Foundry Engineering*. 2011;11(3):121–124.
19. Anglada E., Meléndez A., Maestro L., Domínguez I. Finite element model correlation of an investment casting process. *Materials Science Forum*. 2014;797:105–110.
<http://dx.doi.org/10.4028/www.scientific.net/MSF.797.105>
20. Liu C., Sun J., Lai X., He B., Li F. Influence of complex structure on the shrinkage of part in investment casting process. *The International Journal of Advanced Manufacturing Technology*. 2015;77:1191–1203.
<https://doi.org/10.1007/s00170-014-6523-y>
21. Liu C., Wang F., Jin S., Li F., Lai X. Permafrost analysis methodology (PAM) for ceramic shell deformation in the firing process. *International Journal of Metalcasting*. 2019;13(4):953–968. <http://dx.doi.org/10.1007/s40962-019-00317-0>
22. Everhart W.A., Lekakh S.N., Richards V., Chen J., Li H., Chandrashekhara K. Corner strength of investment casting shells. *International Journal of Metalcasting*. 2013;7:21–27.
<https://doi.org/10.1007/BF03355541>
23. Sabau A.S. Numerical simulation of the investment casting process. *Transactions of American Foundry Society*. 2005;113:407–417.
24. Zheng K., Lin Y., Chen W., Liu L. Numerical simulation and optimization of casting process of copper alloy water-meter shell. *Advances in Mechanical Engineering*. 2020;12(5):1–12. <http://dx.doi.org/10.1177/1687814020923450>
25. Manzari M.T., Gethin D.T., Lewis R.W. Optimisation of heat transfer between casting and mould. *International Journal of Cast Metals Research*. 2000;13(4):199–206.
<https://doi.org/10.1080/13640461.2000.11819402>
26. Rafique M.M.A., Shah U. Modeling and simulation of heat transfer phenomenon related to mold heating during investment casting. *Engineering*. 2020;12(5):291–314.
<http://dx.doi.org/10.4236/eng.2020.125024>
27. Dong Y., Bu K., Zhang D. Numerical simulation of displacement field of solidification process for investment casting. In: *2008 Asia Simulation Conf. – 7th Int. Conf. on System Simulation and Scientific Computing*. 2008:715–720.
<https://doi.org/10.1109/asc-icsc.2008.4675453>
28. Upadhyay G.K., Das S., Chandra U., Paul A.J. Modelling the investment casting process: a novel approach for view factor calculations and defect prediction. *Applied Mathematical Modelling*. 1995;19(6):354–362.
[https://doi.org/10.1016/0307-904X\(95\)90001-O](https://doi.org/10.1016/0307-904X(95)90001-O)
29. Khan M.A.A., Sheikh A.K. Simulation tools in enhancing metal casting productivity and quality: A review. *Proceedings of the Institution of Mechanical Engineers, Part B: Journal of Engineering Manufacture*. 2016;230(10):1799–1817.
<https://doi.org/10.1177/0954405416640183>
30. Banerjee S., Sutradhar G. Analysis of casting defects in investment casting by simulation. *Advances in Materials, Mechanical and Industrial Engineering: Selected Contributions from the First Int. Conf. on Mechanical Engineering, Jadavpur University, Kolkata, India*. Springer International Publishing. 2019:247–271.
http://dx.doi.org/10.1007/978-3-319-96968-8_12
31. Evstigneev A.I., Odinokov V.I., Dmitriev E.A., Chernyshova D.V., Evstigneeva A.A., Ivankova E.P. On the crack resistance of a ceramic shell mold according to smelted models when a spherical steel casting solidifies in it. *Liteinoe proizvodstvo*. 2022;(9):17–21. (In Russ.).

Евстигнеев А.И., Одинокое В.И., Дмитриев Э.А., Чернышова Д.В., Евстигнеева А.А., Иванова Е.П. О трещиностойкости керамической оболочковой формы по выплавляемым моделям при затвердевании в ней шарообразной стальной отливки. *Литейное производство*. 2022;(9):17–21.

32. Odinokov V.I., Kaplunov B.G., Peskov A.V., Bakov A.V. Mathematical Modeling of Complex Technological Processes. Moscow: Nauka; 2008:178. (In Russ.).

Одинокое В.И., Каплунов Б.Г., Песков А.В., Баков А.В. Математическое моделирование сложных технологических процессов. Москва: Наука; 2008:178.

Information about the Authors

Сведения об авторах

Valerii I. Odinokov, Dr. Sci. (Eng.), Prof., Chief Researcher of the Department of Research Activities, Komsomolsk-on-Amur State University
ORCID: 0000-0003-0200-1675
E-mail: 79122718858@yandex.ru

Aleksei I. Evstigneev, Dr. Sci. (Eng.), Prof., Chief Researcher of the Department of Research Activities, Komsomolsk-on-Amur State University
ORCID: 0000-0002-9594-4068
E-mail: diss@knastu.ru

Eduard A. Dmitriev, Dr. Sci. (Eng.), Assist. Prof., Rector, Komsomolsk-on-Amur State University
ORCID: 0000-0001-8023-316X
E-mail: rector@knastu.ru

Aleksandr N. Namokonov, Postgraduate, Komsomolsk-on-Amur State University
ORCID: 0009-0003-9269-7713
E-mail: namokonovsasha@mail.ru

Anna A. Evstigneeva, Student of the Chair "Applied Mathematics", Komsomolsk-on-Amur State University
ORCID: 0000-0003-0667-2468
E-mail: annka.ewstic@mail.ru

Dar'ya V. Chernyshova, Postgraduate of the Chair of Aircraft Engineering, Komsomolsk-on-Amur State University
ORCID: 0000-0001-5142-2455
E-mail: daracernysova744@gmail.com

Валерий Иванович Одинокое, д.т.н., профессор, главный научный сотрудник Управления научно-исследовательской деятельностью, Комсомольский-на-Амуре государственный университет
ORCID: 0000-0003-0200-1675
E-mail: 79122718858@yandex.ru

Алексей Иванович Евстигнеев, д.т.н., профессор, главный научный сотрудник Управления научно-исследовательской деятельностью, Комсомольский-на-Амуре государственный университет
ORCID: 0000-0002-9594-4068
E-mail: diss@knastu.ru

Эдуард Анатольевич Дмитриев, д.т.н., доцент, ректор, Комсомольский-на-Амуре государственный университет
ORCID: 0000-0001-8023-316X
E-mail: rector@knastu.ru

Александр Николаевич Намоконов, аспирант, Комсомольский-на-Амуре государственный университет
ORCID: 0009-0003-9269-7713
E-mail: namokonovsasha@mail.ru

Анна Алексеевна Евстигнеева, студент кафедры «Прикладная математика», Комсомольский-на-Амуре государственный университет
ORCID: 0000-0003-0667-2468
E-mail: annka.ewstic@mail.ru

Дарья Витальевна Чернышова, аспирант кафедры «Авиационное строительство», Комсомольский-на-Амуре государственный университет
ORCID: 0000-0001-5142-2455
E-mail: daracernysova744@gmail.com

Contribution of the Authors

Вклад авторов

V. I. Odinokov – scientific guidance, analysis of research results, editing and correction of the article final version.

A. I. Evstigneev – formation of the article concept, definition of the purpose and objectives of the study, analysis of research results, writing the text.

E. A. Dmitriev – conducting calculations and their analysis, writing and correction of the text.

A. N. Namokonov – conducting calculations, preparation of references, processing of graphic material.

A. A. Evstigneeva – conducting calculations, preparation of the text and graphic material.

D. V. Chernyshova – processing of calculated results, preparation of graphic material.

В. И. Одинокое – научное руководство, анализ результатов исследований, редактирование и корректировка финальной версии статьи.

А. И. Евстигнеев – формирование концепции статьи, определение цели и задачи исследования, анализ результатов исследования, подготовка текста.

Э. А. Дмитриев – проведение расчетов и их анализ, подготовка и корректировка текста.

А. Н. Намоконов – проведение расчетов, подготовка библиографического списка, обработка графического материала.

А. А. Евстигнеева – проведение расчетов, подготовка текстового и графического материала.

Д. В. Чернышова – обработка расчетных результатов, подготовка графического материала.

Received 19.01.2024
Revised 25.01.2024
Accepted 01.02.2024

Поступила в редакцию 19.01.2024
После доработки 25.01.2024
Принята к публикации 01.02.2024

ON THE MATERIALS OF THE INTERNATIONAL
CONFERENCE "SCIENTIFIC AND PRACTICAL
SCHOOL FOR YOUNG METALLURGISTS" – 2023ПО МАТЕРИАЛАМ МЕЖДУНАРОДНОЙ
КОНФЕРЕНЦИИ «НАУЧНО-ПРАКТИЧЕСКАЯ
ШКОЛА ДЛЯ МОЛОДЫХ МЕТАЛЛУРГОВ» – 2023

UDC 620.193:546.65

DOI 10.17073/0368-0797-2024-2-219-228



Original article

Оригинальная статья

INCREASING THE CORROSION PROPERTIES OF DUPLEX STEEL WITH REM MODIFICATION

V. S. Karasev¹, G. E. Kodzhaspirov¹, A. S. Fedorov¹,
A. A. Al'khimenko¹, A. I. Zhitenev²

¹ Peter the Great St. Petersburg Polytechnic University (29 Politekhnikeskaya Str., St. Petersburg 195251, Russian Federation)

² PJSC "Novolipetsk Metallurgical Plant" (2 Metallurgov Sqr., Lipetsk 398040, Russian Federation)

✉ karasev_vs@spbstu.ru

Abstract. Duplex stainless steels are a modern class of materials with a unique combination of high corrosion and mechanical properties. Due to this, they can be widely used in machine parts and aggregates in fields with aggressive oil and gas production conditions. One of the disadvantages of these materials is their tendency to local corrosion damage on non-metallic inclusions, other things being equal, formed during smelting and casting. To control the purity of steel in conditions of open induction smelting, it is effective to use modification with rare earth metals (REM). Therefore, the purpose of this work was to determine the optimal content of REM in duplex steel to increase corrosion properties. Thermodynamic modeling of the formation of nonmetallic inclusions in duplex corrosion-resistant steel S32750 was carried out and the results of calculations were compared with the experimental data. It is shown that there is an optimal concentration of REM at which contamination with inclusions is minimal due to favorable conditions for their removal, and with a further increase in consumption it increases due to coagulation of a large number of refractory oxides. Electrochemical tests were performed and parameters such as corrosion potential, pitting formation potential and the basis of pitting resistance of experimental steels were determined. Therefore, the corrosion properties of the investigated duplex steel are significantly improved when treated with REM. The electrochemical potentials of different types of inclusions are evaluated on a qualitative level. Based on the obtained results on corrosion resistance and contamination of the studied castings, the optimal amount of REM introduced for modifying inclusions is 0.05 % (0.65Ce + 0.35La).

Keywords: duplex stainless steels, thermodynamic modelling, deoxidation technology, modification, non-metallic inclusions, electrochemical tests

Acknowledgements: The work was supported by the Ministry of Science and Higher Education of the Russian Federation under the World Class Research Centre Program: Advanced Digital Technologies (Agreement No. 075-15-2022-311 dated 20.04.2022).

For citation: Karasev V.S., Kodzhaspirov G.E., Fedorov A.S., Al'khimenko A.A., Zhitenev A.I. Increasing the corrosion properties of duplex steel with REM modification. *Izvestiya. Ferrous Metallurgy*. 2024;67(2):219–228. <https://doi.org/10.17073/0368-0797-2024-2-219-228>

ПОВЫШЕНИЕ КОРРОЗИОННЫХ СВОЙСТВ ДУПЛЕКСНОЙ СТАЛИ С ПОМОЩЬЮ МОДИФИЦИРОВАНИЯ РЗМ

В. С. Карасев¹, Г. Е. Коджаспиров¹, А. С. Федоров¹,
А. А. Альхименко¹, А. И. Житенев²

¹ Санкт-Петербургский политехнический университет Петра Великого (Россия, 195251, Санкт-Петербург, ул. Политехническая, 29)

² ПАО «Новолипецкий металлургический комбинат» (Россия, 398040, Липецк, пл. Металлургов, 2)

✉ karasev_vs@spbstu.ru

Аннотация. Дуплексные коррозионностойкие стали – это современный класс материалов, обладающих уникальным сочетанием высоких коррозионных и механических свойств. Благодаря этому они могут получить широкое применение в деталях машин и агрегатов на месторождениях с агрессивными условиями добычи нефти и газа. Одним из недостатков этих материалов является их склонность к локальным коррозионным поражениям, при прочих равных условиях формирующихся на неметаллических включениях (НВ), которые образуются при выплавке и разливке. Для управления чистотой стали в условиях открытой индукционной выплавки эффективно приме-

нять модифицирование редкоземельными металлами (РЗМ). Поэтому целью настоящей работы являлось определение оптимального содержания РЗМ в дуплексной стали для повышения коррозионных свойств. Проведено термодинамическое моделирование образования НВ в дуплексной коррозионностойкой стали S32750. Результаты расчетов сопоставлены с экспериментальными данными. Показано, что существует оптимальная концентрация РЗМ, при которой загрязненность включениями минимальна из-за благоприятных условий для их удаления, а при дальнейшем увеличении расхода повышается из-за коагуляции большого количества тугоплавких оксидов. В результате электрохимических испытаний определены такие параметры, как потенциал коррозии, потенциал питтингообразования и базис питтингостойкости опытных сталей. Коррозионные свойства исследованной дуплексной стали значительно улучшаются при обработке РЗМ. На качественном уровне проведена оценка электрохимических потенциалов разных типов включений. На основании полученных результатов по коррозионной стойкости и загрязненности изученных отливок получено оптимальное количество РЗМ, вводимого для модифицирования включений, которое составляет 0,05 % (0,65Ce + 0,35La).

Ключевые слова: дуплексные коррозионностойкие стали, термодинамическое моделирование, технология раскисления, модифицирование, неметаллические включения, электрохимические исследования

Благодарности: Исследование выполнено при финансовой поддержке Министерства науки и высшего образования Российской Федерации в рамках программы Научного центра мирового уровня: Передовые цифровые технологии (соглашение № 075-15-2022-311 от 20.04.2022).

Для цитирования: Карасев В.С., Коджаспиров Г.Е., Федоров А.С., Альхименко А.А., Житенев А.И. Повышение коррозионных свойств дуплексной стали с помощью модифицирования РЗМ. *Известия вузов. Черная металлургия*. 2024;67(2):219–228.

<https://doi.org/10.17073/0368-0797-2024-2-219-228>

INTRODUCTION

Currently, the operational activities of oil and gas companies are shifting towards reservoirs with more aggressive extraction conditions, which continuously increase and tighten the requirements for the properties and quality of materials used in equipment manufacturing. One of the unique materials that has been effectively used abroad for a long time but is only now gradually being implemented in the domestic industry is duplex stainless steels (DS) [1; 2]. Due to their high level of chromium, nickel, molybdenum, and nitrogen alloying, these steels possess resistance to general corrosion at the level of traditional austenitic steels but allow for significant strength characteristics due to the simultaneous existence of austenite and ferrite. At the same time, these steels are highly vulnerable to local types of corrosion, such as pitting and crevice corrosion [3; 4].

Under equal conditions, non-metallic inclusions (NMIs) are the sites of formation of local corrosion damage, which occur during melting and casting processes. Therefore, it is necessary to minimize their quantity or modify them into types that have a weak effect on corrosion properties. Publications have shown the degree of negative influence of different types of NMIs [5; 6], their quantity, size, and morphology [7 – 9] on the properties of finished products made from DS.

It is well known that various two-stage processes of special electrometallurgy, such as vacuum induction melting of ingots–electrodes followed by electroslag remelting, are used to produce high-quality steels and alloys [10 – 12]. However, this technology is quite expensive and is also not suitable for obtaining shaped castings, which make up a significant part of the range of machine parts and units for oil and gas production. Such castings are usually produced by melting in an open induction furnace with very limited conditions for refi-

ning the melt. One effective way to control inclusions in these conditions is to use rare earth metals (REM) as modifiers for NMIs. Thus, the introduction of REM can lead to the formation of different types of NMIs, both increasing [13 – 16] and decreasing [16 – 19] the corrosion resistance of highly alloyed steels and alloys.

Therefore, the aim of this study is to investigate the influence of the consumption and concentration of REM on the formation of NMIs in DS in an open induction furnace and to study their effect on the pitting corrosion resistance of DS.

MATERIALS AND METHODS

The study investigated duplex stainless steel of the austenitic-ferritic class, type S32750, with varying amounts of rare earth metals (REM), obtained in an open induction furnace with a capacity of 20 kg. After complete melting of the charge, the steel was deoxidized with silicon and manganese, and then with titanium. It was then held in the furnace for 1 min to average the chemical composition and poured into an 80 mm diameter cast iron mold with a capacity of 10 kg. A portion of REM was added to the crucible, and the remaining melt was poured into a ladle, from which the second ingot was cast. In the second melt, both ingots were produced using REM, but with different amounts. Thus, four ingots weighing 10 kg each were obtained (Table 1). Since the ratio of cerium to lanthanum in all ingots was the same and corresponded to the chemical composition of the used alloy, for convenience, the total amount of REM was used for each ingot in Table 1 and onwards.

Therefore, the experiment was planned so that DS₁ steel without REM and DS₂ steel with a 0.02 % REM content were obtained in melt 1, while DS₃ and DS₄ steels with REM contents of 0.05 and 0.08 % respectively were obtained in melt 2. DS₁ and DS₃ steels were poured from

the furnace spout, while DS₂ and DS₄ steels were poured using a ladle. Since it is believed that pouring through a ladle allows for intensified metal mixing at the moment of pouring and increases the inclusion floatation time, this order of obtaining the ingots allowed for studying the influence of REM consumption and casting technology in two melts, excluding the influence of other melting features.

To obtain the required amount of ferrite (50 %) and eliminate secondary phases formed during slow cooling of selected section ingots, samples were quenched in water after isothermal holding at 1100 °C. The contamination assessment of experimental steels with inclusions was carried out using ASTM E 1245 method by field-by-field cumulative method. The volumetric inclusion content V , %, average diameter by Feret d , μm , and maximum diameter of the largest inclusions d_{max} , μm , were evaluated. The chemical composition of NMI was determined by X -ray spectral microanalysis using the TESCAN Mira-3M scanning electron microscope.

Thermodynamic simulation of inclusion formation was conducted according to the methodology presented in [20 – 22]. For the calculation of primary inclusions, the initial oxygen content interacting with deoxidizers during their introduction was taken into account. To calculate the equilibrium type of NMI for each deoxidizer concentration during steel cooling, solubility surfaces of components in metal (SSCM) were calculated [20], using temperature-dependent equilibrium constants and first-order interaction parameters for each considered reaction [23 – 25]. When forming tertiary inclusions, liquation was taken into account according to the Scheil equation [26].

The resistance of steels to pitting corrosion was evaluated by electrochemical method using VersaStat Princeton Applied Research potentiostat. The tests were conducted in a 5 % aqueous solution of NaCl, acidified with acetic acid to pH = 3 at 22 °C. During the experiment, the following parameters were determined:

– the steady-state corrosion potential E_{steady} , which was recorded after holding without external polarization for 1 h;

– the corrosion potential E_{cor} , indicating the potential of the metal at which anodic and cathodic reactions are in equilibrium under polarization conditions;

– the pitting potential E_{pit} , corresponding to the current at which pitting occurs as a result of local breakdown of metal passivity;

– the pitting resistance basis, calculated as the difference between the corrosion potential and the pitting potential.

RESULTS AND DISCUSSION

Thermodynamic simulation and assessment of NMIs

Fig. 1 shows the result of thermodynamic modeling of inclusion formation during deoxidation of experimental steel with titanium at 1550 °C. The initial oxygen content in equilibrium with non-deoxidized DS is 0.025 %. Upon introduction of titanium, up to a concentration of 0.01 %, deoxidation practically does not occur, the total oxygen content is equal to the sum of the amount of oxygen bound in a small number of primary inclusions and dissolved. In equilibrium with the melt, primary inclusions of the $[\text{FeO} \cdot \text{Cr}_2\text{O}_3]_{\text{solid sol.}}$ type are present. In the range of titanium concentrations from 0.010 to 0.023 %, the formation of a solid solution $[\text{Cr}_2\text{O}_3, \text{MnO}, \text{TiO}_2]_{\text{solid sol.}}$ becomes possible, while the solubility of oxygen in the steel begins to decrease. With further increase in titanium concentration to 0.027 %, the formation of titanium oxide Ti_3O_5 occurs, and when the titanium concentration reaches 0.075 %, Ti_2O_3 inclusions are formed.

To track the changes in the equilibrium phase composition in DS when introducing REM, SSCM was calculated for the studied steel in the $\lg[\text{Ce}] - \lg[\text{La}]$ coordinates (Fig. 2). Using this diagram, the combined influence of cerium and lanthanum on the type of formed non-metallic inclusions (NMI) can be assessed at a constant titanium concentration of 0.05 %, which corresponds to the experimental steels (Table 1, dashed line in Fig. 1). Let us consider the phases in equilibrium with the melt. In region I , the composition of the liquid

Table 1. Chemical compositions of the studied duplex steels

Таблица 1. Химический состав исследуемых дуплексных сталей

Sample	Melting	Pouring method	Elements, wt. %										
			C	Cr	Si	Mn	Ni	Mo	N	Cu	S	Ti	REM
DS ₁	1	From spout	0.027	24.000	0.300	1.000	7.600	3.400	0.100	0.700	0.012	0.050	–
DS ₂		Through ladle											0.020
DS ₃	2	From spout											0.050
DS ₄		Through ladle											0.080

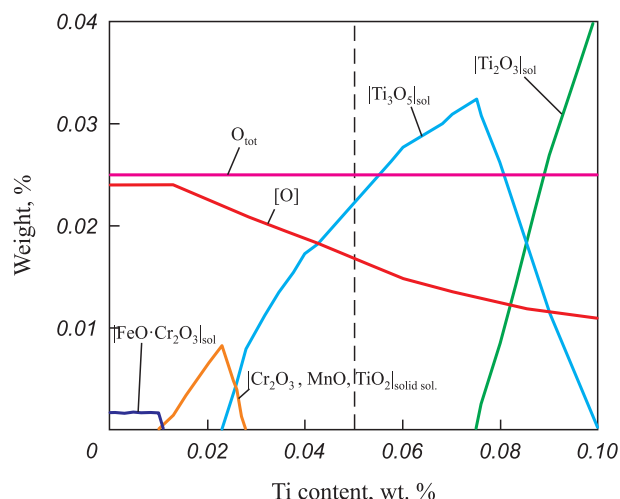


Fig. 1. Thermodynamic modeling of inclusions formation during deoxidation of experimental steel by titanium

Рис. 1. Термодинамическое моделирование образования включений при раскислении опытной стали титаном

metal is given, which is in equilibrium with solid particles $[\text{Ti}_3\text{O}_5]_{\text{sol}}$. Even with such a small amount of REM, the formation of inclusions $[\text{Cr}_2\text{O}_3, \text{MnO}, \text{TiO}_2]_{\text{solid sol.}}$, which appear during preliminary deoxidation with titanium, is completely suppressed. As the lanthanum content increases, the equilibrium phase becomes a solid solution of oxides $[\text{La}_2\text{O}_3, \text{CeO}_2]_{\text{solid sol.}}$ ($[\text{La}] \geq 0.000007\%$, region II), and with even higher concentration, lanthanum sulfide LaS is formed ($[\text{La}] \geq 0.0020\%$, region III). The formation of Ce_2O_3 type inclusions is possible at a concentration of $[\text{Ce}] \geq 0.0004\text{ wt. \%}$. The SSCM also includes a line representing the ratio of cerium and lanthanum concentrations in the mischmetal. Thus, when increasing the amount of the added REM, the change in the equilibrium type of inclusions will occur along this line.

Since the formation of inclusions occurs not only during deoxidation and modification, but also during cooling and solidification, modeling of these stages has been carried out. The results of the calculations for all four steels are shown in Fig. 3, where images and phase composition of the found inclusions in these ingots are also included for convenience of analysis. Table 2 presents the results of the assessment of the volumetric fraction and sizes of NMIs.

In DS_1 steel, pure titanium oxides Ti_3O_5 (Fig. 3, a) are formed initially as primary, and then as secondary and tertiary inclusions. However, in practice, complex oxides like $\text{Cr}_2\text{O}_3 - \text{MnO} - \text{TiO}_2$ have been found in this steel. The formation of these inclusions is associated with the time point of introducing titanium into the melt, when microvolumes with different concentrations are formed due to its uneven distribution in the furnace, leading to the possible formation of various oxides (Fig. 1). This

steel is the most contaminated with NMIs, with a volumetric fraction of 0.259 %, an average size of 1.8 μm , and the largest inclusion reaching 18 μm (Table 2).

When adding 0.02 % REM to DS_2 steel, in addition to primary titanium oxides, the formation of a solution $[\text{Ce}_2\text{O}_3 - \text{La}_2\text{O}_3]$ becomes possible (Fig. 3, d). Similar NMIs have been found experimentally in the metal (Fig. 3, f). However, besides these, large inclusions of $\text{Cr}_2\text{O}_3 - \text{MnO} - \text{TiO}_2$ have also been found in the same sample (Fig. 3, e). These inclusions, like in DS_1 steel, are products of preliminary deoxidation that do not have time to recrystallize into equilibrium inclusions, resulting in their volumetric fraction in this steel being lower than in DS_1 but still at a relatively high level (0.216 %). The average size of inclusions in this steel is almost the same, with the largest NMI size being 19 μm .

With an increase in REM concentration to 0.05 % (steel DS_3), the fraction of primary lanthanum and cerium-based inclusions increases, while the number of forming titanium oxides decreases accordingly (Fig. 3, g). Experimentally, a large number of $\text{Ce}_2\text{O}_3 - \text{La}_2\text{O}_3$ inclusions and a significantly smaller number of $\text{Cr}_2\text{O}_3 - \text{MnO} - \text{TiO}_2$ inclusions have been found in this steel. The contamination of NMIs in this steel is significantly lower, as primary REM inclusions are actively removed from the melt, with a fraction of 0.161 % and an average NMI size of 1.8 μm , with the largest inclusion size being 12 μm .

When introducing 0.08 % REM (DS_4 steel), the formation of primary titanium oxides is completely suppressed, as all initial oxidization is removed due

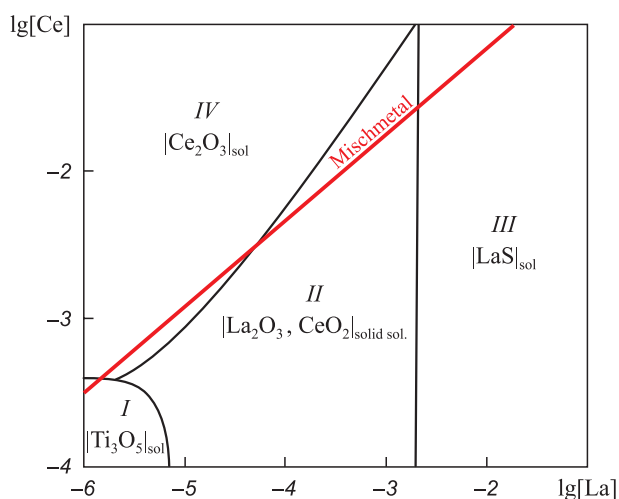


Fig. 2. Stability diagrams of nonmetallic inclusions (NMI) for the system 0.027C–24Cr–0.3Si–1.0Mn–7.6Ni–3.4Mo–0.1N–0.7Cu–0.012S at $T = 1550\text{ }^\circ\text{C}$, $P = 1\text{ atm}$

Рис. 2. Поверхности растворимости компонентов в металле для системы 0,027C–24Cr–0,3Si–1,0Mn–7,6Ni–3,4Mo–0,1N–0,7Cu–0,012S при $T = 1550\text{ }^\circ\text{C}$, $P = 1\text{ атм}$

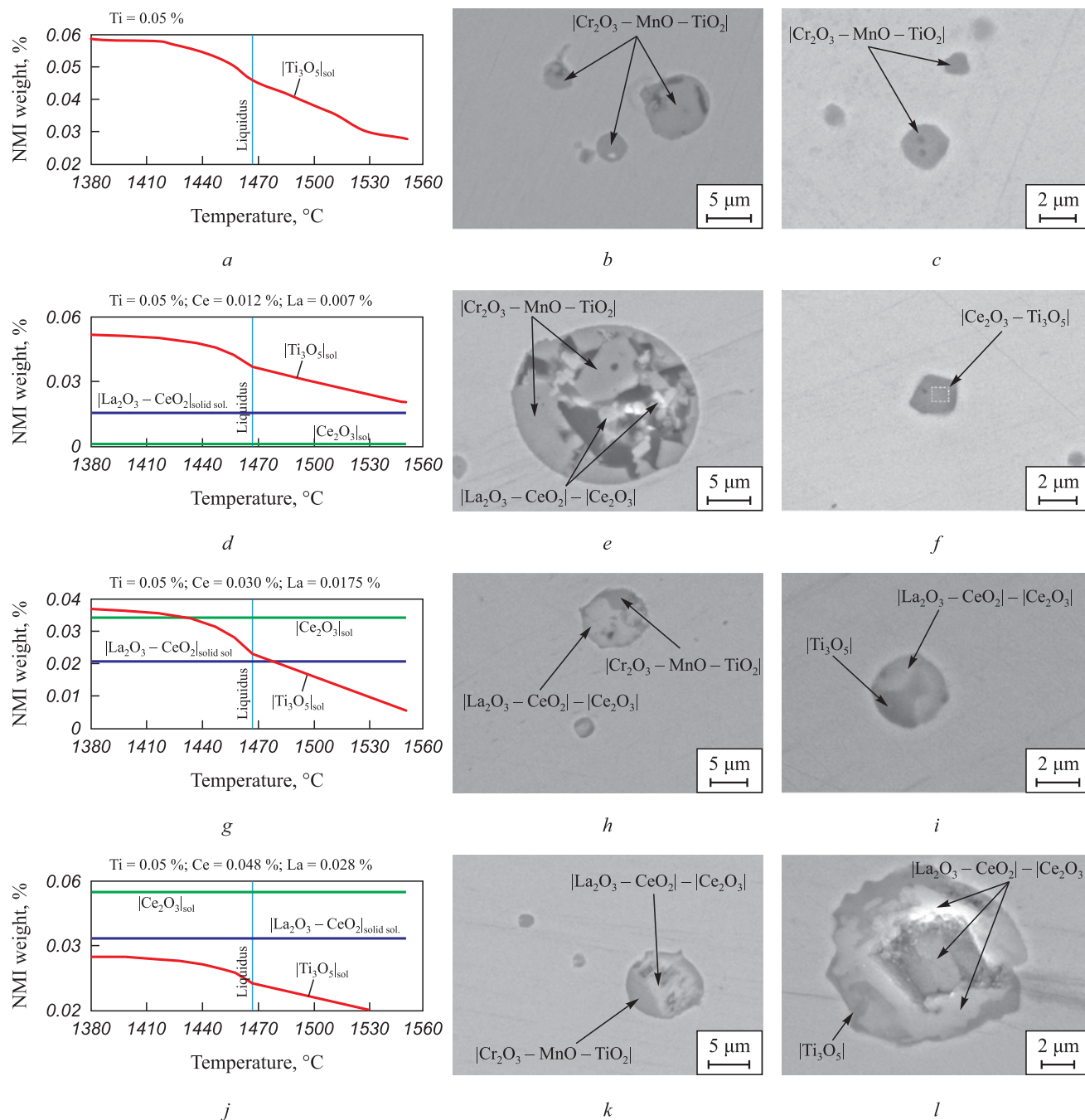


Fig. 3. Thermodynamic modeling and NMIs in experimental steel ingots:

DS₁ (a – c); DS₂ (d – f); DS₃ (g – i); DS₄ (j – l)

Рис. 3. Термодинамическое моделирование и экспериментально найденные НВ в опытных слитках сталей:

ДС₁ (a – c); ДС₂ (d – f); ДС₃ (g – i); ДС₄ (j – l)

Table 2. Results of the assessment of contamination with non-metallic inclusions (according to ASTM E1245)

Таблица 2. Результаты оценки загрязненности неметаллическими включениями (по ASTM E1245)

Sample	Melting	Pouring method	$V, \%$	$d, \mu\text{m}$	$d_{\text{max}}, \mu\text{m}$
DS ₁	1	From spout	0.259 ± 0.036	1.8 ± 0.1	18
DS ₂		Through ladle	0.216 ± 0.030	2.1 ± 0.3	19
DS ₃	2	From spout	0.161 ± 0.018	1.8 ± 0.2	12
DS ₄		Through ladle	0.179 ± 0.017	1.9 ± 0.2	15

to the formation of REM inclusions (Fig. 3, *j*). In this case, titanium oxides are formed as secondary and tertiary inclusions, making their removal from the melt difficult. Two-phase NMI containing cerium and lanthanum with a small amount of $\text{Cr}_2\text{O}_3\text{--MnO--TiO}_2$ oxides were found in a real DS_4 ingot (Fig. 3, *k*), as well as large inclusions based on cerium and lanthanum oxide and titanium oxide. By their morphology, it can be concluded that they are formed due to the coagulation of a large amount of refractory primary oxides (Fig. 3, *l*). The assessment results of contamination confirm this, as the volume fraction of NMI in this steel is higher than in DS_3 steel, at 0.179 %, with an average size of 1.9 μm and the largest NMI size of 15 μm .

Analysis of the data in Table 2 also allows us to conclude that in the treatment of REM, the pouring technology (From spout or Through ladle) does not have a significant effect on the contamination of NMI.

Thus, thermodynamic simulation efficiently describes the observed types of NMI and their quantities in experimental steels. However, even in steels with increased REM content, non-equilibrium products of primary deoxidation by titanium are found, as the amount of primary inclusions in DS steel is so high that even 0.08 % REM for complete modification is insufficient.

Influence of NMIs on corrosion resistance

The results of the evaluation of the corrosion properties of the studied steels are presented in Table 3. The steady-state corrosion potential E_{steady} for the steel deoxidized only by titanium (DS_1) is significantly lower than for the steels modified by REM. The addition of REM increased the value of E_{steady} , but there is no dependence between the specific amount of introduced REM and E_{steady} .

The values of the equilibrium corrosion potential for the steels modified by REM are approximately the same and significantly lower than the corresponding parameter for the steel without REM. The pitting resistance potentials slightly increase from the first steel to the fourth. In order to fully describe the range of potentials at which

the material exists in a passive state, the so-called pitting resistance basis is calculated. If the process of destruction of the oxide film begins at the corrosion potential, and its complete destruction occurs at the pitting potential, then the higher the value of the pitting resistance basis ($\Delta E = E_{\text{pit}} - E_{\text{cor}}$), the better the material's resistance to pitting corrosion. Thus, the addition of REM significantly increased the resistance to pitting corrosion of all steels treated with mischmetal.

The investigation of the pitting initiation sites was carried out on polished samples after electrochemical testing (Fig. 4). In steels DS_1 (Fig. 4, *a*) and DS_2 (Fig. 4, *b*) without REM or weakly modified by REM, numerous pits were found on $\text{Cr}_2\text{O}_3\text{--MnO--TiO}_2$ inclusions. In steels DS_3 (Fig. 4, *c*) and DS_4 (Fig. 4, *d*), it was found that in two-phase inclusions, the part consisting of oxides based on $\text{Cr}_2\text{O}_3\text{--MnO--TiO}_2$ is primarily damaged, while the part based on cerium and lanthanum oxides is retained.

There are several hypotheses about the mechanisms of inclusion influence on pitting initiation and development. The first hypothesis is based on the difference in the coefficient of thermal expansion (CTE) between the inclusion and the matrix [6]. If the CTE of the inclusion is higher than that of the matrix, compressive stresses are generated upon cooling, leading to the formation of microvoids. Conversely, if the CTE of the inclusion is lower, tensile stresses are generated. However, in this case, this mechanism is not applicable as no porosity or microvoids were observed at the inclusion-matrix interface before testing (Fig. 3). The second hypothesis, proposed in [27], suggests the formation of chromium-depleted zones around oxide inclusions based on chromium. However, other studies [6; 28] that have investigated the distribution of chromium around oxides do not confirm this hypothesis. Moreover, in the present study, an investigation of the element distribution across the NMI section (Fig. 5) shows no depletion zone around the $\text{Cr}_2\text{O}_3\text{--MnO--TiO}_2$ inclusion. Since the diffusion relaxation of reactants around a growing inclusion in liquid metal occurs within a few seconds [29], and the reactant concentrations quickly equilibrate, depletion can only occur during the growth of the inclu-

Table 3. Corrosion test results

Таблица 3. Результаты коррозионных испытаний

Sample	Steady corrosion potential E_{steady} , V	Equilibrium corrosion potential E_{cor} , V	Pitting formation potential E_{pit} , V	Pitting resistance basis ΔE , V
DS_1	0.109	−0.092	1.058	1.150
DS_2	0.191	−0.143	1.087	1.230
DS_3	0.190	−0.145	1.074	1.219
DS_4	0.190	−0.138	1.086	1.223

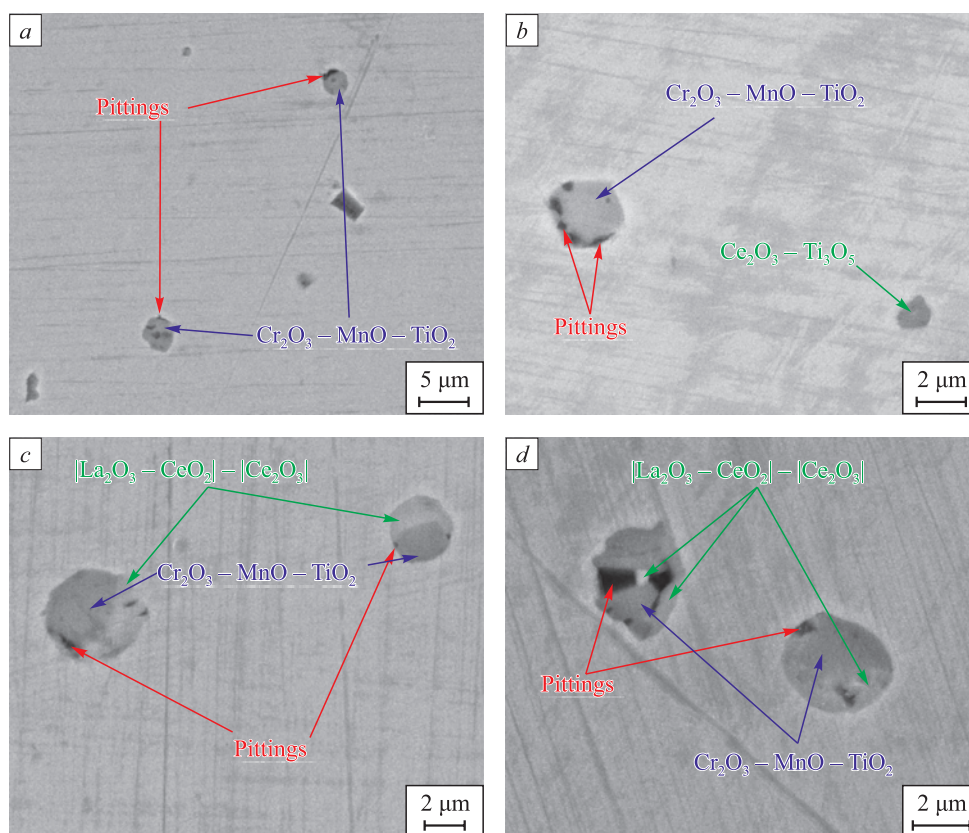


Fig. 4. NMIs in experimental steels after corrosion tests:

DS₁ (a); DS₂ (b); DS₃ (c); DS₄ (d)

Рис. 4. Неметаллические включения в опытных сталях после коррозионных испытаний:

ДС₁ (a); ДС₂ (b); ДС₃ (c); ДС₄ (d)

sion in solid metal, when the diffusion rate decreases by several orders of magnitude [30]. Due to the fact that $\text{Cr}_2\text{O}_3\text{--MnO--TiO}_2$ oxides are formed as primary inclusions (Fig. 1), the formation of a diffusion-depleted zone around them is impossible.

The third hypothesis is related to the dissolution of inclusions in the corrosive environment [7]. It is known that REM oxides form hydrolytically stable oxides in water [31]. However, these data should be cautiously applied to the considered electrolyte with a pH of 3. Direct studies on the nature of pitting formation (Fig. 4) only allow us to state the fact that cerium and lanthanum oxides have a higher potential in the chosen test medium, therefore, corrosion damage will primarily occur in the matrix. At the same time, pits were found specifically on the side of the $\text{Cr}_2\text{O}_3\text{--MnO--TiO}_2$ oxides in the vicinity of two-phase inclusions consisting of cerium and lanthanum oxides, and complex compounds of $\text{Cr}_2\text{O}_3\text{--MnO--TiO}_2$ oxides (Fig. 4, c, d). Therefore, the latter have a lower corrosion potential than the steel matrix. As shown above, as the REM content in the steel increases, the fraction of pure REM oxides increases while the fraction of complex NMIs, which are products of preliminary deoxidation, decreases. Therefore,

in steel containing a higher amount of cerium and lanthanum oxide inclusions, the potential for pitting formation E_{pit} and the basis ΔE are higher. The types of inclusions can be arranged in order of increasing potential

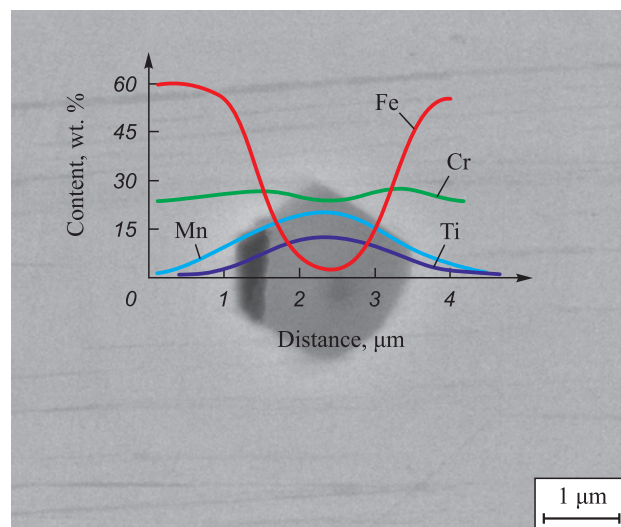


Fig. 5. Distribution of elements around $\text{Cr}_2\text{O}_3\text{--MnO--TiO}_2$ inclusion

Рис. 5. Распределение элементов в окрестности включения $\text{Cr}_2\text{O}_3\text{--MnO--TiO}_2$

in the selected electrolyte: $\text{Cr}_2\text{O}_3\text{--MnO--TiO}_2$ < steel matrix < $\text{La}_2\text{O}_3\text{--CeO}_2/\text{Ce}_2\text{O}_3$.

CONCLUSIONS

Taking into account the specific qualitative potential of the matrix and different types of inclusions, as well as the estimated quantity of inclusions and their sizes, the optimal amount of REM introduced for modifying inclusions in the studied DS is 0.05 %. At this content of REM, the best effect of modification can be achieved and the quantity and size of inclusions can be minimized, resulting in a significant improvement in corrosion properties. With a lower REM consumption, a large amount of primary oxidation products, which are more likely to form pitting, are preserved. On the other hand, with a significant increase in REM consumption, the volume fraction and size of inclusions increase due to intensified coagulation of primary refractory oxides. To increase the efficiency of modification and further reduce the required modifier consumption, measures should be taken to reduce the initial oxidation of the melt and decrease the quantity of primary inclusions.

REFERENCES / СПИСОК ЛИТЕРАТУРЫ

1. Franci R., Byrne G. Duplex stainless steels – alloys for the 21st century. *Metals*. 2021;11(5):836. <https://doi.org/10.3390/met11050836>
2. Kazakov A.A., Zhitenev A.I., Fedorov A.S., Fomina O.V. Development of duplex stainless steel compositions. *CIS Iron Steel Review*. 2019;(2):20–26. <https://doi.org/10.17580/cisirs.2019.02.04>
3. Practical Guidelines for the Fabrication of Duplex Stainless Steel. 3rd ed. IMO A; 2014:63.
4. Patra S., Agrawal A., Mandal A., Podder A.S. Characteristics and manufacturability of duplex stainless steel: A review. *The Indian Institute of Metals*. 2021;74(5):1089–1098. <https://doi.org/10.1007/s12666-021-02278-7>
5. Fedorov A., Zhitenev A., Karasev V., Alkhimenko A., Kovalev P. Development of a methodology for the quality management of duplex stainless steels. *Materials*. 2022; 15(17):6008. <https://doi.org/10.3390/ma15176008>
6. Karasev V.S., Kodzhaspirov G.E. Investigation of the influence of deoxidation technology and hot plastic deformation on the evolution of non-metallic inclusions in super duplex steel. In: *Int. Sci. Conf. "Modern Materials, Advanced Production Technologies and Equipment" SMPPTO-2023*. 2023:92–93. (In Russ.).
Карасев В.С., Коджаспиров Г.Е. Исследование влияния технологии раскисления и горячей пластической деформации на эволюцию неметаллических включений в супердуплексной стали. *Международная научная конференция «Современные материалы, передовые производственные технологии и оборудование для них» СМППТО-2023*. 2023:92–93.
7. Zhang Y., Hu Q., Dai M., Huang F., Frank Y.C., Liu J. Investigation of micro-electrochemical activities of oxide inclusions and microphases in duplex stainless steel and the implication on pitting corrosion. *Materials and Corrosion*. 2019;71(6):876–886. <https://doi.org/10.1002/maco.201911335>
8. Luo H., Li X., Dong C., Xiao K. Effect of solution treatment on pitting behavior of 2205 duplex stainless steel. *Arabian Journal of Chemistry*. 2017;10(1):90–94. <https://doi.org/10.1016/j.arabjc.2012.06.011>
9. Jeon S.H., Do H., Kim H., Park Y. Influence of oxygen content on the inclusion formation and pitting corrosion resistance of hyper duplex stainless steels. *Materials Transactions*. 2014;55(12):1872–1877. <https://doi.org/10.2320/matertrans.M2014164>
10. Utkina K.N., Levkov L.Ya., Fedorov A.S., Zhitenev A.I., Terekhin D.K., Kashirina Zh.K., Shipova E.V. Investigation of the influence of chemical composition and crystallization conditions on the formation of the structure of super duplex steels. In: *Physico-Chemical Fundamentals of Metallurgical Processes (FKhOMP 2022)*. 2022:248–256. (In Russ.).
Уткина К.Н., Левков Л.Я., Федоров А.С., Житенев А.И., Терехин Д.К., Каширина Ж.К., Шипова Е.В. Исследование влияния химического состава и условий кристаллизации на формирование структуры супердуплексных сталей. *Физико-химические основы металлургических процессов (ФХОМП 2022)*. 2022:248–256.
11. Dub V.S., Levkov L.Ya., Shurygin D.A., Tolstykh D.S., Klochhai V.V., Korzun E.L., Garchenko A.A. Electros slag remelting technology for contemporary engineering. retrospection and new possibilities. *Metallurgist*. 2018;62(5–6):511–520. <https://doi.org/10.1007/s11015-018-0688-9>
12. Orlov V., Levkov L., Dub V., Balikoev A., Shurygin D. New approach to development and manufacturing technologies of duplex steel. *E3S Web of Conferences*. 2019;121(6):04010. <https://doi.org/10.1051/e3sconf/201912104010>
13. Gupta C.K., Krishnamurthy N. Extractive metallurgy of rare earths. *International Materials Reviews*. 1992;37(1): 197–248. <https://doi.org/10.1179/imr.1992.37.1.197>
14. Kim S.T., Jeon S.H., Lee I.S., Park Y.S. Effects of rare earth metals addition on the resistance to pitting corrosion of super duplex stainless steel. Part 1. *Corrosion Science*. 2010;52(6): 1897–1904. <https://doi.org/10.1016/j.corsci.2010.02.043>
15. Wang X., Ha K., Zhou G., Wu H., Wu R. Effect of rare-earth on sulfides morphology and abrasive resistance of high sulfur steel. *Materials for Mechanical Engineering*. 2012; 36(5):33–37.
16. Mei Z., Wan T., Lou D. Influence of RE modifier on as-cast grain refinement of super-low carbon cast steel. *Special Casting & Nonferrous Alloys*. 2002;(2):3–4.
17. Yan H.H., Hu Y., Zhao D.W. Microstructure and properties of as-cast 30Mn steel. *AIP Advances*. 2018;8(12):125128. <https://doi.org/10.1063/1.5065444>
18. Wang H., Wang A., Li C., Yu X., Xie J., Liang T., Liu C. Effects of rare earth metals on microstructure, mechanical properties, and pitting corrosion of 27% Cr hyper duplex stainless steel. *Reviews on Advanced Materials Science*. 2022;61(1):873–887. <https://doi.org/10.1515/rams-2022-0284>
19. Ha H.Y., Park C.J., Kwon H.S. Effects of misch metal on the formation of non-metallic inclusions and the associated resistance to pitting corrosion in 25% Cr duplex stainless steels. *Scripta Materialia*. 2006;55(11):991–994. <https://doi.org/10.1016/j.scriptamat.2006.08.014>

20. Mikhailov G.G., Leonovich B.I., Kuznetsov Yu.S. Thermodynamics of Metallurgical Processes and Systems. MISIS; 2009:520. (In Russ.).
Михайлов Г.Г., Леонович Б.И., Кузнецов Ю.С. Термодинамика металлургических процессов и систем. Москва: ИД МИСиС; 2009:520.
21. Kazakov A.A., Kovalev P.V., Ryaboshchuk S.V., Mileikovskii A.B., Malakhov N.V. Investigation of the temperature-time nature of nonmetallic inclusions in order to improve the metallurgical quality of high-strength pipe steels. *Chernye metally*. 2009;(12):5–11. (In Russ.).
Казаков А.А., Ковалев П.В., Рябошчук С.В., Милейковский А.Б., Малахов Н.В. Исследование термовременной природы неметаллических включений с целью повышения металлургического качества высокопрочных трубных сталей. *Черные металлы*. 2009;(12):5–11.
22. Kazakov A.A., Urazgil'deev A.Kh., Gusev A.A. Algorithmic model of formation of nonmetallic inclusions in liquid and solidifying steel. *Izv. AN SSSR. Metally*. 1989;(3):60–65. (In Russ.).
Казаков А.А., Уразгильдеев А.Х., Гусев А.А. Алгоритмическая модель образования неметаллических включений в жидкой и затвердевающей стали. *Известия АН СССР. Металлы*. 1989;(3):60–65.
23. Kulikov I.S. Deoxidation of Metals. Metallurgiya; 1975:504. (In Russ.).
Куликов И.С. Раскисление металлов. Москва: Металлургия; 1975:504.
24. Turkdogan E.T. Physical Chemistry of High-Temperature Processes. Academic Press; 1980:447.
Туркдоган Е.Т. Физическая химия высокотемпературных процессов. Москва: Металлургия; 1985:344.
25. Grigoryan V.A., Stomakhin A.YA., Ponomarenko A.G., etc. Physico-Chemical Calculations of Electric Steelmaking Processes: Tutorial for Universities. Metallurgiya; 1989:288. (In Russ.).
Григорян В.А., Стомахин А.Я., Пономаренко А.Г. и др. Физико-химические расчеты электросталеплавильных процессов: Учебное пособие для вузов. Москва: Металлургия; 1989:288.
26. Kurz W., Fisher D., Rappaz M. Fundamentals of Solidification. Trans. Tech. Publications; 2023:353.
27. Ha H., Park C., Kwon H. Effects of non-metallic inclusions on the initiation of pitting corrosion in 11% Cr ferritic stainless steel examined by micro-droplet cell. *Corrosion Science*. 2007;49(3):1266–1275.
<https://doi.org/10.1016/j.corsci.2006.08.017>
28. Meng Q., Frankel G.S., Colijn H.O., Goss S.H. Stainless-steel corrosion and MnS inclusions. *Nature*. 2003;424:389–390. <https://doi.org/10.1038/424389b>
29. Kang Y., Lee H. Thermodynamic analysis of Mn-depleted zone near Ti oxide inclusions for intragranular nucleation of ferrite in steel. *ISIJ International*. 2010;50(4):501–508.
30. Kazakov A.A. Non-metallic inclusions in steel. Theory and its applications. In: *Advanced Materials*. TSU; 2017:203–275. (In Russ.).
Казаков А.А. Неметаллические включения в стали. Теория и ее приложения. *Перспективные материалы*. ТГУ; 2017:203–275.
31. Rabinovich V.A., Khavin Z.Ya. Brief Chemical Reference. 2nd ed. Leningrad: Khimiya; 1978:392. (In Russ.).
Рабинович В.А., Хавин З.Я. Краткий химический справочник. Издание 2-е., исправленное и дополненное. Ленинград: Химия; 1978:392.

Information about the Authors

Сведения об авторах

Vladimir S. Karasev, Engineer of the Scientific and Educational Center “Severstal-Polytech”, Peter the Great St. Petersburg Polytechnic University

ORCID: 0009-0006-9622-7243

E-mail: karasev_vs@spbstu.ru

Georgii E. Kodzhaspirov, Dr. Sci. (Eng.), Prof. of the Higher School of Physics and Technology of Materials, Peter the Great St. Petersburg Polytechnic University

E-mail: kodzhaspirov@spbstu.ru

Aleksandr S. Fedorov, Engineer of the Scientific and Technological Complex “New Technologies and Materials”, Peter the Great St. Petersburg Polytechnic University

ORCID: 0000-0003-2571-060X

E-mail: fedorov_as@spbstu.ru

Aleksei A. Al'khimenko, Director of the Scientific and Technological Complex “New Technologies and Materials”, Peter the Great St. Petersburg Polytechnic University

ORCID: 0000-0001-6701-1765

E-mail: a.alkhimenko@spbstu.ru

Andrei I. Zhitenev, Cand. Sci. (Eng.), Head of Technological Projects, Directorate for Research and Development of New Products, Department of “Electrotechnical Steels”, PJSC “Novolipetsk Metallurgical Plant”

ORCID: 0000-0002-4817-4048

E-mail: zhitenev.ai1991@gmail.com

Владимир Сергеевич Карасев, инженер научно-образовательного центра «Северсталь-Политех», Санкт-Петербургский политехнический университет Петра Великого

ORCID: 0009-0006-9622-7243

E-mail: karasev_vs@spbstu.ru

Георгий Ефимович Коджаспиров, д.т.н., профессор Высшей школы физики и технологий материалов, Санкт-Петербургский политехнический университет Петра Великого

E-mail: kodzhaspirov@spbstu.ru

Александр Сергеевич Федоров, инженер Научно-технологического комплекса Новые технологии и материалы, Санкт-Петербургский политехнический университет Петра Великого

ORCID: 0000-0003-2571-060X

E-mail: fedorov_as@spbstu.ru

Алексей Александрович Альхименко, директор Научно-технологического комплекса «Новые технологии и материалы», Санкт-Петербургский политехнический университет Петра Великого

ORCID: 0000-0001-6701-1765

E-mail: a.alkhimenko@spbstu.ru

Андрей Игоревич Житенев, к.т.н., руководитель технологических проектов, Дирекция по исследованиям и разработке новых продуктов, управление «Электротехнические стали», ПАО «Новолипецкий металлургический комбинат»

ORCID: 0000-0002-4817-4048

E-mail: zhitenev.ai1991@gmail.com

Contribution of the Authors

Вклад авторов

V. S. Karasev – formation of the research main idea, participation in experimental melting, thermodynamic modeling, analysis of the research results.

G. E. Kodzhaspirov – scientific guidance, task setting, development of the research plan.

A. S. Fedorov – formation of the research main idea, management of experimental melting, conducting electrochemical studies and interpretation of their results.

A. A. Al'khimenko – organization of the research work, conducting electrochemical studies and interpretation of their results.

A. I. Zhitenev – formation of the research main idea, scientific guidance, analysis of the research results.

В. С. Карасев – формирование основной идеи исследований, участие в опытных плавках, термодинамическое моделирование, анализ результатов исследований.

Г. Е. Коджаспиров – научное руководство, постановка задач, разработка плана исследования.

А. С. Федоров – формирование основной идеи исследований, руководство ведением опытных плавков, проведение электрохимических исследований и интерпретация их результатов.

А. А. Альхименко – организация комплекса исследования, проведение электрохимических исследований и интерпретация их результатов.

А. И. Житенев – формирование основной идеи исследований, научное руководство, анализ результатов исследований.

Received 10.10.2023

Revised 09.02.2024

Accepted 04.03.2024

Поступила в редакцию 10.10.2023

После доработки 09.02.2024

Принята к публикации 04.03.2024

ON THE MATERIALS OF THE INTERNATIONAL
CONFERENCE "SCIENTIFIC AND PRACTICAL
SCHOOL FOR YOUNG METALLURGISTS" – 2023ПО МАТЕРИАЛАМ МЕЖДУНАРОДНОЙ
КОНФЕРЕНЦИИ «НАУЧНО-ПРАКТИЧЕСКАЯ
ШКОЛА ДЛЯ МОЛОДЫХ МЕТАЛЛУРГОВ» – 2023

UDC 620.193:669.1.017

DOI 10.17073/0368-0797-2024-2-229-236



Original article

Оригинальная статья

APPROACHES TO THE SELECTION OF MATERIAL DESIGN OF INFRASTRUCTURE FACILITIES FOR TRANSPORT AND INJECTION OF CO₂

A. S. Rovbo¹, I. A. Golubev¹, N. O. Shaposhnikov¹,
A. V. Penigin², A. S. Fedorov¹

¹ Peter the Great St. Petersburg Polytechnic University (29 Politekhnicheskaya Str., St. Petersburg 195251, Russian Federation)

² Gazprom Neft Scientific and Technical Center (75–79 D Moika Quay, St. Petersburg 190000, Russian Federation)

✉ harchenko.annna@yandex.ru

Abstract. The article is devoted to the study of dependence of carbon dioxide corrosion rate on the microstructure of material design of the pipeline for CO₂ transport and injection. Today there is a task of choosing such material design. For pipeline construction the most cost-effective materials are carbon steels, but for their application it is necessary to pay increased attention to the problem of carbon dioxide corrosion, which is intensified in wet, undrained CO₂ flows. At the same time, the choice of material should be made reasonably, taking into account the balance between corrosion resistance, mechanical characteristics and economic aspect of the issue. In this paper, the influence of microstructural state features on the corrosion rate of low-alloy mild steels for CO₂ transport and injection was investigated. The authors studied the features of steels with ferritic-bainitic, bainitic-ferritic-perlitic and ferritic-perlitic microstructures. Tests on corrosion resistance were carried out on the bench autoclave complex, which allows to recreate conditions of high pressure and temperature and to simulate real environments. It was determined that the microstructural state of steel has a significant effect on the corrosion rate, which increases with increasing volume fraction of pearlite. Understanding the relationship between the microstructural characteristics of steels and corrosion rates can simplify material selection for infrastructure facilities and contribute to more efficient and reliable use of low-alloy carbon steels in carbon capture, use, and storage projects. This study will be useful in selecting favorable microstructures for low-alloy mild steels that can be used for CCUS (Carbon Capture, Use and Storage) infrastructure projects.

Keywords: carbon capture, carbon storage, CCUS, decarburization, carbon dioxide corrosion, structure–property relationship, microstructure, chemical composition, corrosion rate

Acknowledgements: The research was supported by the Ministry of Science and Higher Education of the Russian Federation under the World Class Research Centre Programme: Advanced Digital Technologies (agreement No. 075-15-2022-311 dated 20.04.2022).

For citation: Rovbo A.S., Golubev I.A., Shaposhnikov N.O., Penigin A.V., Fedorov A.S. Approaches to the selection of material design of infrastructure facilities for transport and injection of CO₂. *Izvestiya. Ferrous Metallurgy*. 2024;67(2):229–236.

<https://doi.org/10.17073/0368-0797-2024-2-229-236>

ПОДХОДЫ К ВЫБОРУ МАТЕРИАЛЬНОГО ИСПОЛНЕНИЯ ИНФРАСТРУКТУРНЫХ ОБЪЕКТОВ ТРАНСПОРТА И ЗАКАЧКИ CO₂

А. С. Ровбо¹✉, И. А. Голубев¹, Н. О. Шапошников¹,
А. В. Пенигин², А. С. Федоров¹

¹ Санкт-Петербургский политехнический университет Петра Великого (Россия, 195251, Санкт-Петербург, ул. Политехническая, 29)

² Научно-технический центр «Газпром нефти» (Россия, 190000, Санкт-Петербург, наб. реки Мойки, 75–79, литер Д)

✉ harchenko.annna@yandex.ru

Аннотация. Работа посвящена исследованию зависимости скорости углекислотной коррозии от микроструктуры материального исполнения трубопровода для транспорта и закачки CO₂. На сегодняшний день существует задача выбора материального исполнения инфраструктурных объектов транспорта и закачки CO₂. Для строительства трубопроводов наиболее экономически эффективными материалами являются углеродистые стали, однако для их применения необходимо уделять повышенное внимание проблеме углекислотной коррозии, которая интенсифицируется во влажных неосушенных потоках CO₂. При этом выбор материала должен проводиться обоснованно, учитывая баланс между коррозионной стойкостью, механическими характеристиками и экономической стороной вопроса. В данной работе проведено исследование влияния особенностей микроструктурного состояния на скорость коррозии низколегированных малоуглеродистых сталей для транспорта и закачки CO₂. В ходе исследования изучены особенности сталей с ферритно-бейнитной, бейнитно-ферритно-перлитной и ферритно-перлитной микроструктурой. Испытания на стойкость к коррозии проведены на стендовом автоклавном комплексе, позволяющем воссоздавать условия высокого давления и температуры и моделировать реальные среды. Показано, что микроструктурное состояние стали оказывает значительное влияние на скорость коррозии, которая возрастает при увеличении объемной доли перлита. Понимание взаимосвязи микроструктурных особенностей сталей и скорости коррозии может значительно облегчить выбор материала для инфраструктурных объектов и способствовать более эффективному и надежному использованию низколегированных углеродистых сталей в проектах по улавливанию, использованию и хранению углерода. Данное исследование будет полезно при выборе благоприятной микроструктуры для низколегированных малоуглеродистых сталей, которые могут применяться для строительства инфраструктурных объектов CCUS (Carbon Capture, Use and Storage).

Ключевые слова: улавливание углерода, хранение углерода, CCUS, декарбонизация, углекислотная коррозия, взаимосвязь структура – свойства, микроструктура, химический состав, скорость коррозии

Благодарности: Исследование выполнено при финансовой поддержке Министерства науки и высшего образования Российской Федерации в рамках программы Исследовательского центра мирового уровня: Передовые цифровые технологии (соглашение № 075-15-2022-311 от 20.04.2022).

Для цитирования: Ровбо А.С., Голубев И.А., Шапошников Н.О., Пенигин А.В., Федоров А.С. Подходы к выбору материального исполнения инфраструктурных объектов транспорта и закачки CO₂. *Известия вузов. Черная металлургия*. 2024;67(2):229–236.

<https://doi.org/10.17073/0368-0797-2024-2-229-236>

INTRODUCTION

Carbon capture, use, and storage (CCUS) is a research area aimed at reducing CO₂ emissions and combating climate change. In the CCUS process (*Carbon Capture, Use and Storage*) [1; 2], CO₂ emitted into the atmosphere from various sources such as industrial enterprises, power plants, and motor vehicles is captured and subsequently stored in underground formations [3; 4]. This allows for the isolation of carbon dioxide from the atmosphere and prevents its negative impact on the climate.

Currently, there is a challenge in selecting the material design for infrastructure objects used for CO₂ transport and injection under increased environmental and economic risks [5; 6]. The selection of material should strike a balance between effectiveness in preventing intensive carbon dioxide corrosion [7] and the cost of the final solution [8].

A review of open sources on the topic of material selection for CCUS facilities [3; 9] has shown

that carbon steels are the most economically advantageous materials for pipeline construction [10]. However, their application necessitates increased attention to the problem of carbon dioxide corrosion [11], which intensifies in wet CO₂ flows [12]. Additionally, there is no consensus in the literature regarding the influence of steel microstructure and thermomechanical treatment modes on the mechanism and kinetics of corrosion processes [13 – 16]. This is because conditions can vary from one facility to another in terms of mineralization, component composition of environments, partial pressure, and temperature. Consequently, corrosion product deposits of varying morphology form on the steel surface, which can either be protective or accelerate the corrosion process. Therefore, the selection of materials must consider the operational conditions and actual environments at the facility. In this context, the goal of the present work is to investigate the influence of microstructural state features on the corrosion rate of low-alloy mild steels for CO₂ transport and injection, based on the conditions of a specific facility.

MATERIALS AND METHOD

To recreate the conditions of actual facilities, various bench setups are used, such as closed-loop flow stands or autoclave setups that replicate conditions of high pressure and temperature. In this work, an autoclave setup with a 3-liter capacity vessel was used. Currently, there are no standard methodologies for conducting corrosion tests in autoclaves, so the methodology used in this experiment is described below. The test conditions were selected based on the situation at the actual facility.

The essence of the corrosion testing method is to determine the mass loss of samples during their exposure to the corrosive environment. In the gravimetric method, the corrosion rate is determined by the mass parameter ρ , expressed in g/m²·h:

$$\rho = \frac{m_1 - m_2}{S\tau}, \quad (1)$$

where m_1 is the mass of the sample before testing, g; m_2 is the mass of the sample after testing, g; S is the surface area of the sample, m²; τ is the duration of the test, h.

If the change in mass is directly proportional to the depth of corrosion penetration under uniform corrosion conditions, the corrosion rate is recalculated into the depth parameter ν , expressed in mm/year. This parameter characterizes the uniform corrosion loss (thinning) of the sample per unit time:

$$\nu = \frac{8760\rho}{7.85 \cdot 10^3}, \quad (2)$$

where ν is the depth parameter of the corrosion rate, mm/year; 8760 is the number of hours in a year; 7.85 is the density of the investigated steel, g/cm³.

The gravimetric method allows for highly accurate results, as weighing is one of the most precise operations in quantitative analysis. The confidence interval for determining measurement error was 95 %.

Before testing, the samples were degreased using an ultrasonic cleaner in acetone, air-dried, and placed on a suspension in the autoclave, which was then sealed

and deaerated for 60 min with an inert gas flow rate of 100 ml/min per liter of capacity. The deaerated test solution was then saturated with CO₂. The total pressure in the autoclave was 6 MPa, with a partial pressure of CO₂ at 0.3 MPa. The temperature was maintained constant at 25 °C. The test duration was 96 h. For corrosion tests, three samples were selected from each steel.

The test solution consisted of 133 g/l CaCl₂, 31 g/l MgCl₂, 0.5 g/l NaHCO₃, 0.1 g/l Na₂SO₄ in distilled water. The total mineralization was 164.6 g/l. This composition corresponds to the fluid composition in the well being injected with CO₂ into underground formations. After testing, the samples were washed and air-dried, then cleaned of corrosion products using an eraser. The investigated steels correspond to the strength class K52, with their chemical composition presented in Table 1.

The microstructure of the steels was evaluated using a Reichert-Jung MEF3A optical microscope. To perform a quantitative assessment of the phase components, etching was selected to provide a contrasting image of the phases without revealing grain boundaries for subsequent automatic recognition by the Thixomet Pro image analyzer [17]. For this purpose, etching with a 4 % alcoholic solution of picric acid was used to reveal pearlite. For overall microstructure identification, a 3 % nitric acid solution in alcohol was used.

The traditional method for grain size assessment is described in GOST 5639 – 82, which, however, does not allow for the assessment of the heterogeneity of the grain structure. Nowadays, many methods for evaluating the grain structure of a material are known [18; 19]. For instance, in [20], a method for calculating the grain size variation factor F_z is proposed by the formula

$$F_z = \frac{f_{\max} Z_{\max}}{\sum f_i Z_i}, \quad (3)$$

where f_{\max} is the fraction of the grain occupying the maximum area on the cross-section, %; Z_{\max} is the grade of the grain occupying the maximum area on the cross-section; f_i is the fraction of the grain with a specific grade, %; Z_i is the grade of the grain.

Table 1. Chemical compositions of the studied steels

Таблица 1. Химический состав исследуемых сталей

Steel	Quantity, wt. %							
	C	Cr	Cu	Mn	Ni	P	S	Si
1	0.039	0.66	0.50	0.98	0.22	0.0074	0.0011	0.22
2	0.062	0.51	0.10	0.50	0.12	0.0055	0.0015	0.17
3	0.080	0.62	0.34	0.49	0.38	0.0037	0.0014	0.24
4	0.050	0.65	0.14	0.75	0.07	0.0031	0.0018	0.24
5	0.056	0.63	0.16	0.64	0.21	0.0042	0.0019	0.28

RESULTS OF THE QUANTITATIVE ASSESSMENT

OF STRUCTURAL COMPONENTS AND CORROSION TESTING

The materials investigated in this study were obtained from various domestic metallurgical enterprises using a technology that includes converter smelting, ladle treatment, continuous casting, followed by thermomechanical processing. The microstructures of the steels were examined in cross-section (Fig. 1).

The microstructure of steel 1 is characterized as ferritic-bainitic. The pearlite content in this steel is the lowest among all the steels studied, at 2.20 vol. %, and the grain structure (by the grain number occupying more than 10 % of the cross-section area) is evaluated as G_{10} (30 %) and G_{11} (28 %). The microstructure of steel 2 is characterized as ferritic-pearlitic with predominantly non-polygonal ferrite, with the grain structure evaluated as G_9 (13 %) and G_{10} (21 %). The pearlite content in this steel is 3.57 vol. %. The microstructure of steel 3 is also characterized as ferritic-pearlitic. The structure is evaluated as G_{11} (32 %) and G_{12} (32 %), and the pearlite content is 6.72 vol. %. The distribution of pearlite colonies is uneven, appearing as separate clusters with coarse morphology, similar to steel 2 (Fig. 2). The microstructure of steel 4 is characterized as ferritic-pearlitic-bainitic, with a pearlite content of 7.51 vol. %. The distribution of pearlite in this steel is fairly uniform, and the structure is evaluated as G_9 (14 %), G_{10} (28 %), G_{11} (29 %),

and G_{12} (18 %). The microstructure of steel 5 is characterized as ferritic-pearlitic. This steel has the highest pearlite content, 13.80 vol. %, after etching with picric acid. The structure is evaluated as G_{10} (21 %), G_{11} (32 %), and G_{12} (25 %).

RESULTS AND DISCUSSION

In ferritic-pearlitic steels, pearlite consists of a lamellar structure composed of alternating layers of ferrite and iron carbide (cementite). When exposed to aggressive media containing CO₂, the ferrite in the pearlite becomes the anode and dissolves quickly, while the cementite remains intact (Fig. 4). The carbon content is directly proportional to the pearlite content. The results of the corrosion tests shown in Fig. 3, *a* demonstrate that as the pearlite fraction in the microstructure increases, the overall corrosion resistance of the steels decreases.

The study [21] indicates that the most vulnerable areas are the boundaries between ferrite and cementite, where corrosion processes initially begin. It appears that increasing the number of pearlite colony areas leads to an increase in the number of vulnerable ferrite-cementite interphase boundaries and ferrite plates, which subsequently become anodes and dissolve quickly.

It is also worth noting the positive effect of copper on corrosion resistance – increasing the copper content from ~0.12 to 0.50 wt. % led to a reduction in the corrosion rate

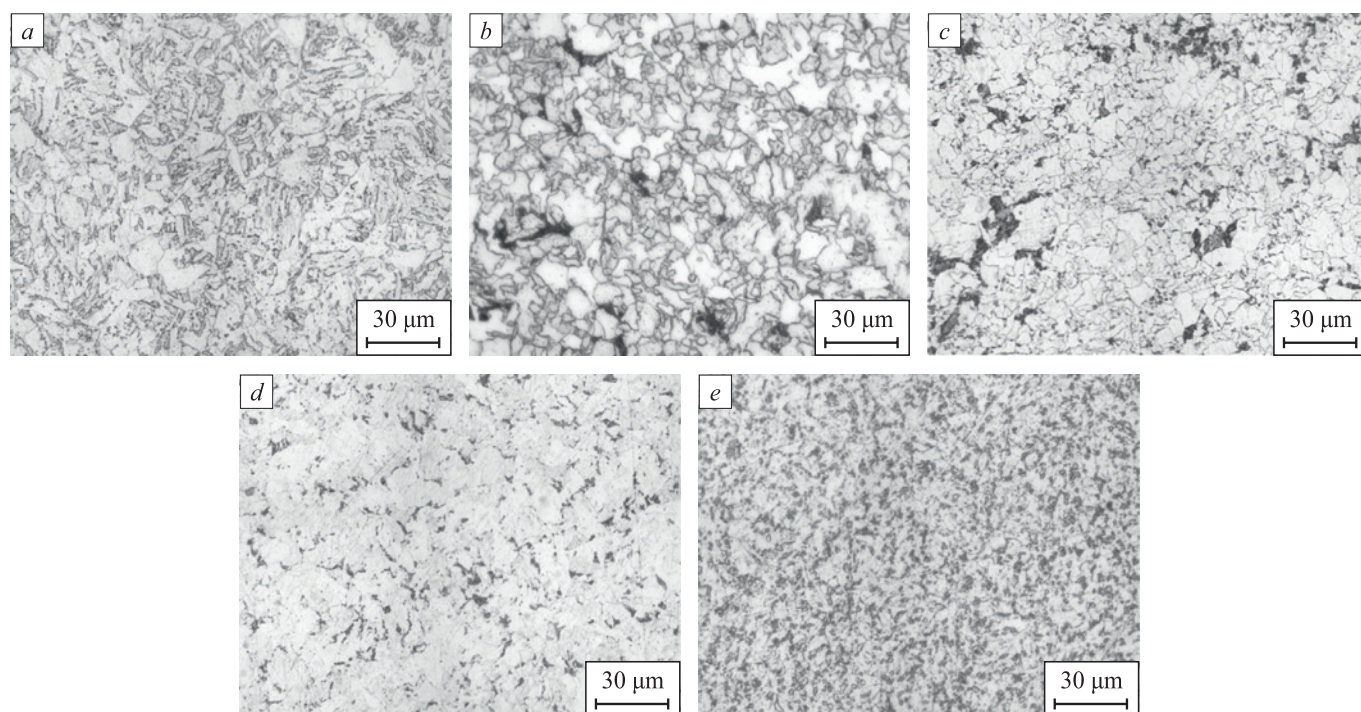


Fig. 1. General view of microstructures of the studied steels: composition 1 (*a*); composition 2 (*b*); composition 3 (*c*); composition 4 (*d*); composition 5 (*e*)

Рис. 1. Общий вид микроструктур исследуемых сталей: состав 1 (*a*); состав 2 (*b*); состав 3 (*c*); состав 4 (*d*); состав 5 (*e*)

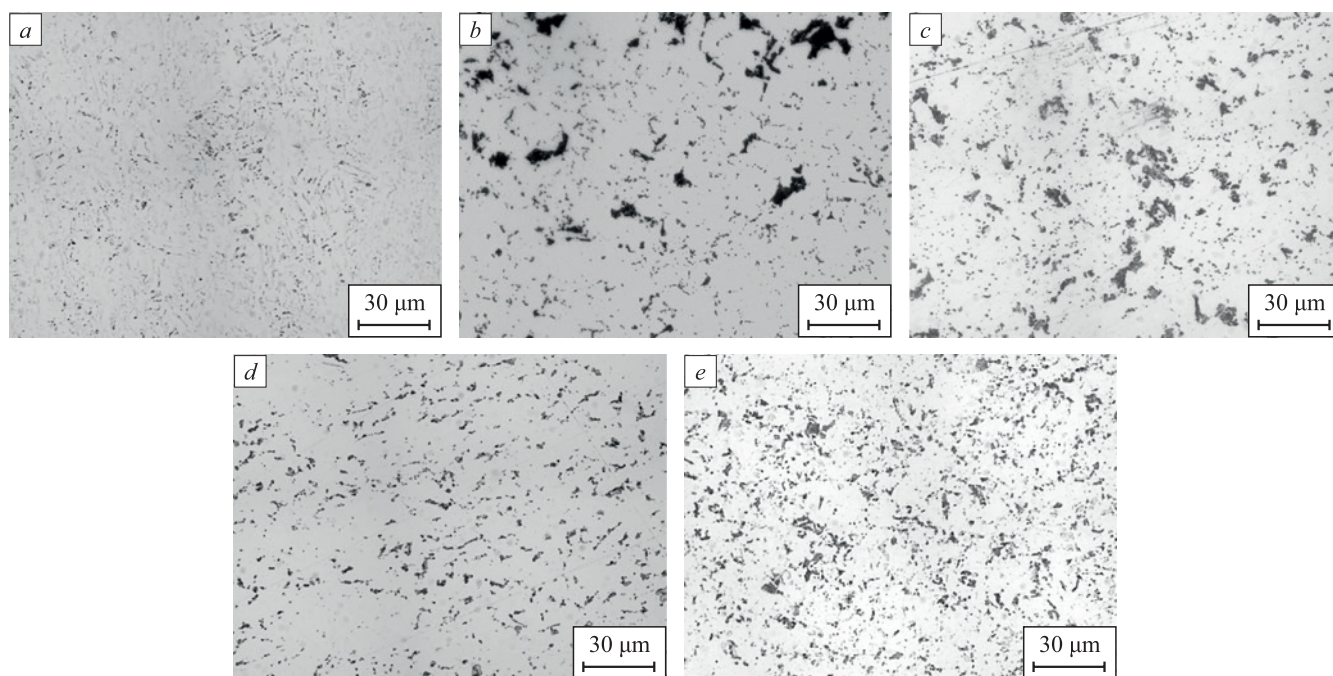


Fig. 2. Detection of perlite in the studied steels:
composition 1 (a); composition 2 (b); composition 3 (c); composition 4 (d); composition 5 (e)

Рис. 2. Выявление перлита в исследуемых сталях:
состав 1 (a); состав 2 (b); состав 3 (c); состав 4 (d); состав 5 (e)

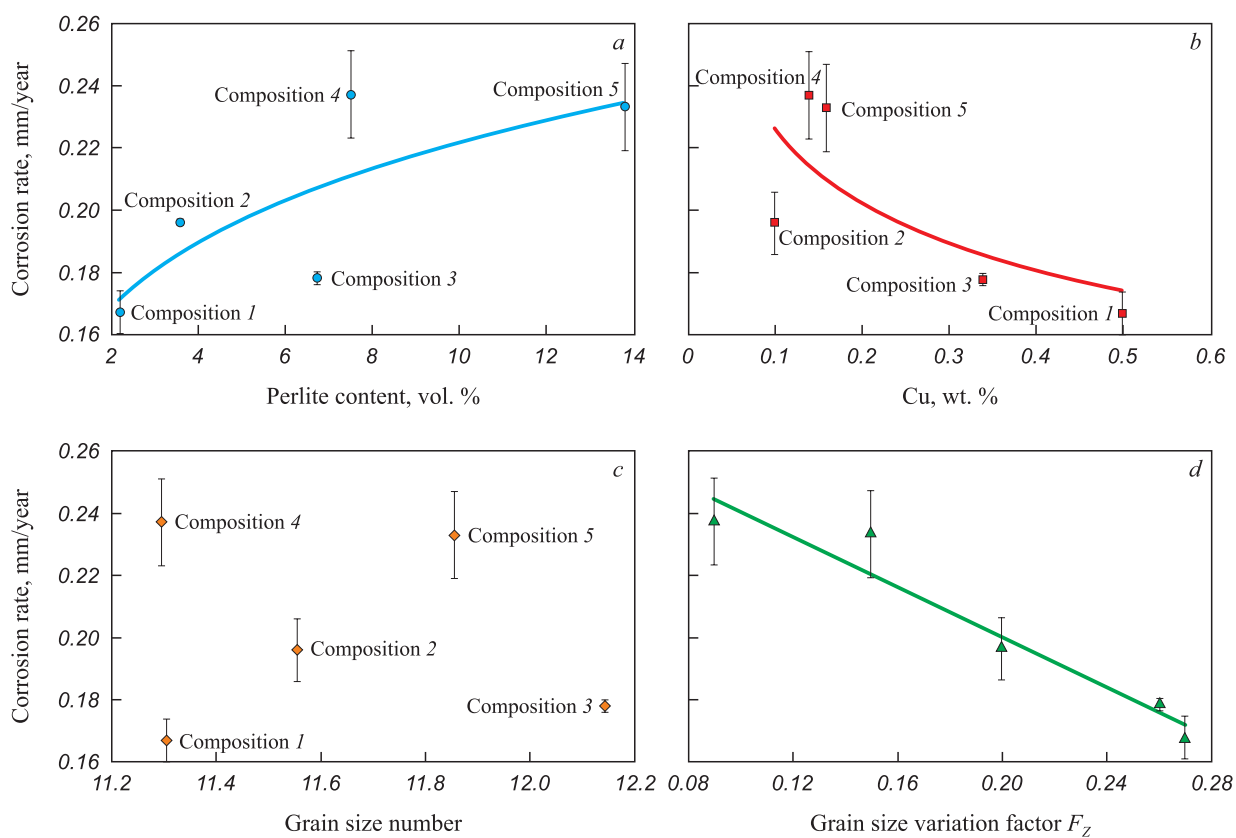


Fig. 3. Dependence of corrosion rate of the studied steels on:
perlite content (a); content of Cu in the steel (b); grain size number G (c); grain size variation factor F_z (d)

Рис. 3. Зависимость скорости коррозии исследуемых сталей от:
содержания перлита (a); содержания Cu в стали (b); номера зерна G (c); фактора разнотерности F_z (d)

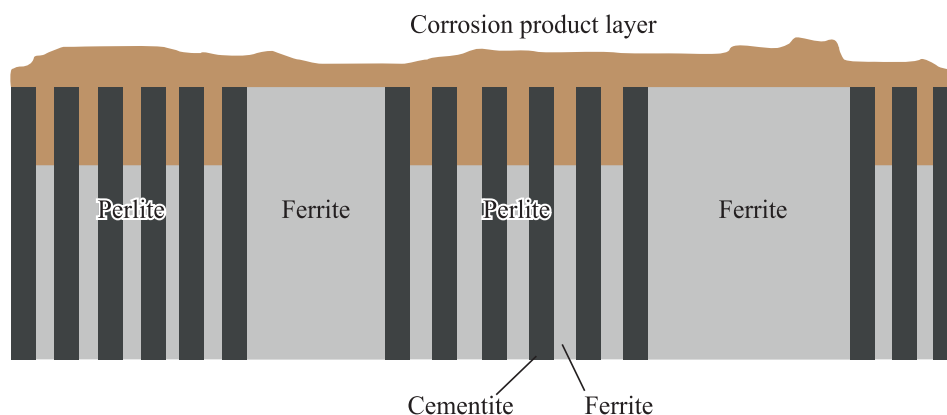


Fig. 4. Mechanism of corrosion of ferritic-pearlitic steels in CO₂-containing environments [22]

Рис. 4. Механизм коррозии ферритно-перлитных сталей в CO₂-содержащих средах [22]

from 0.237 to 0.167 mm/year (Fig. 3, *b*). The beneficial effect of copper on the corrosion properties of steels is noted in many studies. For instance, in [23], it was found that the introduction of a small amount of copper (usually up to 1 %) significantly enhances the corrosion resistance of low-carbon steels. Moreover, in high-strength low-alloy steels, copper is an alloying element that provides high toughness and good weldability. However, despite the advantages of adding copper to steel composition and the corrosion characteristics of ferritic-pearlitic microstructures demonstrated in this work, low-alloy mild steels should be used cautiously for the material design of CO₂ transport and injection infrastructure objects, and only with strict control over the presence of free water in the transported gas – its amount should be minimal. Otherwise, corrosion-resistant materials must be used.

Based on the evaluation of the microstructural parameters of the investigated steels presented in Table 2, it can be concluded that grain size does not have a determining influence on the corrosion resistance of the investigated steels (Fig. 3, *c*). However, the grain size variation, assessed by equation (3), significantly affects corrosion resistance (Fig. 3, *d*). Therefore, it can be concluded that the higher the uniformity of the structure (and, accordingly, the value of the F_z factor), the higher the corrosion resistance of the material.

CONCLUSIONS

A study was conducted on the influence of microstructural state features on the corrosion rate of low-alloy mild steels for CO₂ transport and injection (CCUS). It was shown that in ferritic-pearlitic steels, ferrite is primarily susceptible to corrosion processes, becoming an anode and dissolving quickly within pearlite. As a result, increasing the number of pearlite colony areas in the microstructure leads to a decrease in the overall corrosion resistance of the steel. The positive effect of copper on corrosion resistance was established – increasing the copper content in the investigated compositions from 0.12 to 0.50 wt. % led to a 1.5-fold reduction in the corrosion rate. It was noted that corrosion resistance is significantly influenced not by grain size, but primarily by the heterogeneity of the structure.

REFERENCES / СПИСОК ЛИТЕРАТУРЫ

1. Barker R., Hua Y., Neville A. Internal corrosion of carbon steel pipelines for dense-phase CO₂ transport in carbon capture and storage (CCS) – a review. *International Materials Reviews*. 2017;62(1):1–31.
<https://doi.org/10.1080/09506608.2016.1176306>
2. Zhang Y., Pang X., Qu S., Li X., Gao K. Discussion of the CO₂ corrosion mechanism between low partial pressure

Table 2. Results of assessment of the steels microstructure parameters

Таблица 2. Результаты оценки параметров микроструктуры сталей

Steel	Microstructure	[Cu], wt. %	Pearlite content, vol. %	Corrosion rate, mm/year	Ferrite grain number G	Grain size variation factor F_z
1	Ferritic-bainitic	0.50	2.20	0.167 ± 0.007	11.31	0.27
2	Ferritic-pearlitic	0.10	3.57	0.196 ± 0.010	11.56	0.20
3	Ferritic-pearlitic	0.34	6.72	0.178 ± 0.002	12.15	0.26
4	Ferritic-pearlitic-bainitic	0.14	7.51	0.237 ± 0.014	11.30	0.09
5	Ferritic-pearlitic	0.16	13.80	0.233 ± 0.014	11.86	0.15

- and supercritical condition. *Corrosion Science*. 2012;59:186–197. <https://doi.org/10.1016/j.corsci.2012.03.006>
3. Cecile M., Dwaipayan M., Guillaume N., Leila F. Material integrity aspects of CCS: an overview for CO₂ transport and storage. In: *Trondheim Conference on CO₂ Capture, Transport and Storage Trondheim, Norway – June 21–23, 2021*: 231–236.
 4. IEAGHG. Corrosion and Selection of Materials for Carbon Capture and Storage. 2010;288.
 5. Witkowski A., Majkut M., Rulik S. Analysis of pipeline transportation systems for carbon dioxide sequestration. *Archives of Thermodynamics*. 2014;35(1):117–140. <https://doi.org/10.2478/aoter-2014-0008>
 6. Witkowski A., Rusin M., Majkut S., Rulik K. Advances in Carbon Dioxide Compression and Pipeline Transportation Processes. Springer Cham; 2015:134. <https://doi.org/10.1007/978-3-319-18404-3>
 7. Wang S., Zhao J., Gu Y., Xiong D., Zeng Q., Tian B. Experimental and numerical investigation into the corrosion performance of X100 pipeline steel under a different flow rate in CO₂-saturated produced water. *Journal of Solid State Electrochemistry*. 2021;25(3):993–1006. <https://doi.org/10.1007/s10008-020-04868-9>
 8. Knoope M.M.J., Guijt W., Ramirez A., Faaij A.P.C. Improved cost models for optimizing CO₂ pipeline configuration for point-to-point pipelines and simple networks. *International Journal of Greenhouse Gas Control*. 2014;22:25–46. <https://doi.org/10.1016/j.ijggc.2013.12.016>
 9. Duong C. Quest carbon capture and storage offset project: Findings and learnings from 1st reporting period. *International Journal of Greenhouse Gas Control*. 2019;89:65–75. <https://doi.org/10.1016/j.ijggc.2019.06.001>
 10. Wang Z.M., Liu X.T., Han X., Zhang J. Managing internal corrosion of mild steel pipelines in CO₂ enhanced oil recovery multiphase flow conditions. *Energy Technology*. 2015;3(3): 225–233. <https://doi.org/doi:10.1002/ente.201402159>
 11. McGrail B.P., Schaef H.T., Glezakou V.A., Dang L.X., Owen A.T. Water reactivity in the liquid and supercritical CO₂ phase: Has half the story been neglected? *Energy Procedia*. 2009;1(1):3415–3419. <https://doi.org/10.1016/j.egypro.2009.02.131>
 12. Yoon-Seok C., Srdjan N., Young D. Effect of impurities on the corrosion behavior of CO₂ transmission pipeline steel in supercritical CO₂-water environments. *Environmental Science and Technology*. 2010;44(23):9233–9238. <https://doi.org/10.1021/es102578c>
 13. Lopez D.A., Perez T., Simison S.N. The influence of microstructure and chemical composition of carbon and low alloy steels in CO₂ corrosion. A state-of-the-art appraisal. *Materials & Design*. 2003;24(8):561–575. [https://doi.org/10.1016/S0261-3069\(03\)00158-4](https://doi.org/10.1016/S0261-3069(03)00158-4)
 14. Paolinelli L.D., Perez T., Simison S.N. The influence of steel microstructure, chemical composition and precorrosion on CO₂ corrosion inhibitor efficiency. In: *NACE CORROSION'2007*. Houston, U.S.A., March 2007:07311.
 15. Xu L.N. Influence of microstructure on mechanical properties and corrosion behavior of 3% Cr steel in CO₂ environment. *Materials and Corrosion*. 2012;63(11):997–1003. <https://doi.org/10.1002/maco.201106389>
 16. Ochoa N., Vega C., Pebere N., Lacaze J., Brito J.L. CO₂ corrosion resistance of carbon steel in relation with microstructure changes. *Materials Chemistry and Physics*. 2015;156:198–205. <https://doi.org/10.1016/j.matchemphys.2015.02.047>
 17. Kazakov A., Kiselev D. Industrial application of thixomet image analyzer for quantitative description of steel and alloy's microstructure. *Metallography, Microstructure and Analysis*. 2016;5:294–301. <https://doi.org/10.1007/s13632-016-0289-6>
 18. Grokhovskii V.I. Possibilities of digital microscopy in metallography. In: *Digital microscopy. School-seminar materials*. Yekaterinburg: USTU-UPI; 2001;(1):18–20. (In Russ.).
Гроховский В.И. Возможности цифровой микроскопии в металлографии. *Цифровая микроскопия. Материалы школы-семинара*. Екатеринбург: УГТУ-УПИ; 2001;(1):18–20.
 19. Lezinskaya E.Ya. Evaluation methods for structure non uniformity of metal for cladding tubes and wrapper of corrosion-resistant steels and alloys. *Voprosy atomnoi nauki i tekhniki. Seriya: Fizika radiatsionnykh povrezhdenii i radiatsionnoe materialovedenie = Problems of Atomic Science and Technology. Physics of Radiation Effects and Radiation Materials Science*. 2003;(3):108–112. (In Russ.).
Лезинская Е.Я. Методы оценки структурной неоднородности металла труб оболочек ТВЭЛ и чехлов ТВС из коррозионностойких сталей и сплавов. *Вопросы атомной науки и техники. Серия: Физика радиационных повреждений и радиационное материаловедение*. 2003;(3):108–112.
 20. Lezinskaya E.Ya., Klyuev D.Yu., Nikolaenko Yu.N. New method for assessing the inequigranular structure of pipes of stainless steels and alloys. *Teoriya i praktika metallurgii = Theory and Practice of Metallurgy*. 2012;(1-2):68–73. (In Russ.).
Лезинская Е.Я., Ключев Д.Ю., Николаенко Ю.Н. Новый метод оценки разнотекстурированной структуры труб из нержавеющей сталей и сплавов. *Теория и практика металлургии*. 2012;(1-2):68–73.
 21. Murase Y., Masuda H., Katayama H. Corrosion resistance of finer/coarser pearlitic structures of carbon steel. *Journal of the Electrochemical Society*. 2021;168(4):041501. <https://doi.org/10.1149/1945-7111/abf185>
 22. Akeer E.S. Effect of Carbon Steel Composition and Microstructure on CO₂ Corrosion. Diss. on degree of Dr.(Ph.). Ohio University; 2014:188.
 23. Copper in Ferrous Metals: Coll. of Papers. Mei I. Le, Shetki L.M.-D. eds., Moscow: Metallurgiya; 1988:310. (In Russ.).
Медь в черных металлах: Сб. статей / Под ред. Ле Мэя И., Шётки Л. М.-Д. Москва: Металлургия; 1988:311.

Information about the Authors

Сведения об авторах

Anna S. Rovbo, Engineer, Peter the Great St. Petersburg Polytechnic University
ORCID: 0000-0002-8312-7351
E-mail: harchenko.annna@yandex.ru

Анна Сергеевна Ровбо, инженер, Санкт-Петербургский политехнический университет Петра Великого
ORCID: 0000-0002-8312-7351
E-mail: harchenko.annna@yandex.ru

Ivan A. Golubev, *Cand. Sci. (Eng.), Research Engineer*, Peter the Great St. Petersburg Polytechnic University
ORCID: 0000-0001-7516-3566
E-mail: golubev_ia@spbstu.ru

Nikita O. Shaposhnikov, *Cand. Sci. (Eng.), Director of the Scientific and Educational Center "Gazpromneft-Polytech"*, Peter the Great St. Petersburg Polytechnic University
E-mail: shaposhn_no@spbstu.ru

Artem V. Penigin, *Project Manager*, Gazprom Neft Scientific and Technical Center
E-mail: penigin.av@gazpromneft-ntc.ru

Aleksandr S. Fedorov, *Research Engineer of the Scientific and Technological Complex "New Technologies and Materials"*, Peter the Great St. Petersburg Polytechnic University
ORCID: 0000-0003-2571-060X
E-mail: fedorov_as@spbstu.ru

Иван Андреевич Голубев, *к.т.н., инженер-исследователь*, Санкт-Петербургский политехнический университет Петра Великого
ORCID: 0000-0001-7516-3566
E-mail: golubev_ia@spbstu.ru

Никита Олегович Шапошников, *к.т.н., директор Научно-образовательного центра «Газпромнефть-Политех»*, Санкт-Петербургский политехнический университет Петра Великого
E-mail: shaposhn_no@spbstu.ru

Артём Витальевич Пенигин, *руководитель проекта*, Научно-технический центр «Газпром нефти»
E-mail: penigin.av@gazpromneft-ntc.ru

Александр Сергеевич Федоров, *инженер-исследователь Научно-технологического комплекса Новые технологии и материалы*, Санкт-Петербургский политехнический университет Петра Великого
ORCID: 0000-0003-2571-060X
E-mail: fedorov_as@spbstu.ru

Contribution of the Authors

Вклад авторов

A. S. Rovbo – research, methodology, formal analysis; writing, reviewing and editing the text; visualisation.

I. A. Golubev – conceptualisation, project administration.

N. O. Shaposhnikov – project administration, obtaining funding.

A. V. Penigin – project administration.

A. S. Fedorov – research, methodology, formal analysis, visualisation.

А. С. Ровбо – исследование, методология, формальный анализ; написание, рецензирование и редактирование текста, визуализация.

И. А. Голубев – концептуализация, администрирование проекта.

Н. О. Шапошников – администрирование проекта, получение финансирования.

А. В. Пенигин – администрирование проекта.

А. С. Федоров – исследование, методология, формальный анализ, визуализация.

Received 10.10.2023

Revised 07.03.2024

Accepted 15.03.2024

Поступила в редакцию 10.10.2023

После доработки 07.03.2024

Принята к публикации 15.03.2024



UDC 669.168

DOI 10.17073/0368-0797-2024-2-237-244



Original article
Оригинальная статья

RATIONAL APPLICATION OF HIGH QUALITY MANGANESE CONCENTRATE

I. A. Rybenko, I. D. Rozhikhina, O. I. Nokhrina, M. A. Golodova

■ Siberian State Industrial University (42 Kirova Str., Novokuznetsk, Kemerovo Region – Kuzbass 654007, Russian Federation)

✉ m.irina1976@mail.ru

Abstract. The article presents the results of theoretical and experimental studies of manganese reduction processes from oxides of high-quality manganese concentrate obtained by hydrometallurgical enrichment of ferromanganese ores, as well as, from marokite (product of thermal synthesis of concentrate and dolomite) with carbon and silicon. The method of thermodynamic modeling with TERRA software complex determined the optimal temperatures and consumption of reducing agents that ensure the complete reduction of manganese. It was found that any of the above-mentioned reducing agents, or a combination thereof in certain ratios, can be utilized as a reducing agent when using oxide manganese-containing materials for steel treatment. The results of experimental studies made it possible to develop technology for the production of marokite-manganite concentrate and monophase synthetic material (CaMnO_3). They can be obtained using the technology developed by the authors, which includes mechanical and thermal treatment of a mixture of high-quality manganese concentrate and calcined dolomite or lime. Marokite-manganite concentrate is useful for alloying steel with manganese when it is smelted in an electric furnace or in a ladle furnace unit, and a monophasic synthetic material is efficient for the production of metal manganese. Based on the results of thermodynamic calculations and experimental studies, technological parameters for processing steel with marokite-manganite concentrate in an electric furnace and a ladle furnace unit are proposed. Monophasic synthetic material CaMnO_3 should be used as the charge component for the production of metal manganese by the out-of-furnace aluminum thermal treatment, which will increase the thermality of the process, as well as the extraction of manganese at the level of 90 %. The results of experimental studies were obtained using modern research methods with laboratory and analytical equipment, as well as statistical processing methods.

Keywords: high-quality manganese concentrate, marokite, monophase synthetic material, thermochemical synthesis, thermodynamic reduction, reducing agents, steel treatment, metal manganese

Acknowledgements: The research was supported by the Russian Foundation for Basic Research and the Subject of the Russian Federation (Kemerovo region-Kuzbass) in the framework of the scientific project no. 20-48-420001/22.

For citation: Rybenko I.A., Rozhikhina I.D., Nokhrina O.I., Golodova M.A. Rational application of high quality manganese concentrate. *Izvestiya. Ferrous Metallurgy*. 2024;67(2):237–244. <https://doi.org/10.17073/0368-0797-2024-2-237-244>

РАЦИОНАЛЬНЫЕ ВАРИАНТЫ ПРИМЕНЕНИЯ ВЫСОКОКАЧЕСТВЕННОГО МАРГАНЦЕВОГО КОНЦЕНТРАТА

И. А. Рыбенко, И. Д. Рожихина, О. И. Нохрина, М. А. Голодова

■ Сибирский государственный индустриальный университет (Россия, 654007, Кемеровская обл. – Кузбасс, Новокузнецк, ул. Кирова, 42)

✉ m.irina1976@mail.ru

Аннотация. В работе представлены результаты теоретических и экспериментальных исследований процессов восстановления марганца из оксидов высококачественного марганцевого концентрата, полученного в результате гидрометаллургического обогащения железомарганцевых руд, а также из марокита (продукта термического синтеза концентрата) и доломита углеродом и кремнием. Методом термодинамического моделирования с использованием программного комплекса Терра определены оптимальные температуры и расходы восстановителей, обеспечивающие полное восстановление марганца. В качестве восстановителя при использовании оксидных марганецсодержащих материалов для обработки стали можно использовать любой из рассмотренных восстановителей или их комбинацию в определенных соотношениях. Результаты экспериментальных исследований позволили разработать технологию получения марокит-манганитового концентрата и монофазного синтетического материала (CaMnO_3). Эти материалы можно получать по технологии, которая включает механическую и термическую обработки смеси высококачественного марганцевого концентрата и обожженного доломита или извести. Марокит-манганитовый концентрат применим для легирования стали марганцем при выплавке ее в электропечи и в агрегате ковш-печь, а монофазный синтетический материал – для производства металлического марганца. На основании результатов термоди-

намических расчетов и экспериментальных исследований предложены технологические параметры обработки стали марокит-манганиновым концентратом в электропечи и агрегате ковш-печь. Для получения металлического марганца внепечным алуминотермическим процессом следует использовать в качестве шихтовой составляющей монофазный синтетический материал CaMnO_3 , что позволит повысить термичность процесса, а также извлечение марганца на уровне 90 %. Результаты экспериментальных исследований были получены при использовании современных методов исследования с применением лабораторного и аналитического оборудования, а также методов статистической обработки результатов.

Ключевые слова: высококачественный марганцевый концентрат, марокит, монофазный синтетический материал, термохимический синтез, термодинамическое восстановление, восстановители, обработка стали, металлический марганец

Благодарности: Исследование выполнено при финансовой поддержке РФФИ и Субъекта РФ (Кемеровская обл. – Кузбасс) в рамках научного проекта № 20-48-420001/22.

Для цитирования: Рыбенко И.А., Рожихина И.Д., Нохрина О.И., Голодова М.А. Рациональные варианты применения высококачественного марганцевого концентрата. *Известия вузов. Черная металлургия*. 2024;67(2):237–244. <https://doi.org/10.17073/0368-0797-2024-2-237-244>

RELEVANCE

To supply the metallurgical industry with manganese, a strategically important raw material, state-of-the-art technological developments should be employed for the industrial mining and enrichment of manganese ores from Russian deposits. Russia has significant reserves of manganese ores (more than 290 million tons), but most are of low quality and classified as refractory. These ores have a low manganese content (18 – 24 %), a high specific phosphorus content ($\text{P/Mn ratio} > 0.006$), and increased iron and silicon content [1 – 3].

Significant reserves of ferromanganese ores are concentrated in the Selezenskoye and Kaigadatskoye (32.7 million tons) deposits. Currently, these ores are not utilized in metallurgical production because metallurgical enrichment cannot be applied to them [1; 3; 4].

Over the last two decades, to ensure cost-effective resource use, Russian [5 – 8] and foreign researchers [9 – 12] have been actively exploring new chemical and hydrometallurgical methods for enriching low-grade manganese ores, slags, and sludges [13 – 15]. Nowadays, environmental safety has been added to the existing requirements related to the economic efficiency of the processes [16 – 18].

We conducted thermodynamic calculations and experimental studies on the enrichment of ferromanganese ores in the Kemerovo region (Kuzbass). The findings allowed us to determine the main technological parameters for extracting manganese and iron, and to develop an enrichment process diagram. This enables the production of high-quality concentrates of manganese and iron, with manganese recovery reaching 90 – 92 % and iron recovery amounting to 86 – 90 % [19].

The relevant objectives include studying the processes of manganese reduction from oxides in high-quality manganese concentrate, choosing reducing agents that can significantly enhance manganese extraction, and developing effective technologies for preparing and using high-quality manganese concentrate.

MATERIALS AND METHODS

We determined the phase and chemical compositions of high-quality manganese concentrate using chemical and X-ray phase analysis methods.

The research [1] showed that the metallothermic reduction of manganese from oxides is significantly accelerated with the presence of marokite $(\text{Ca,Mg})\text{Mn}_2\text{O}_4$ and calcium and magnesium manganites $(\text{Ca,Mg})\text{MnO}_3$, which can be obtained from the high-quality manganese concentrate. A constant amount of marokite and calcium and magnesium manganites is required in the initial manganese-containing material for stable reduction of manganese. Marokite-manganite concentrate and monophase synthetic manganese material (CaMnO_3) can be obtained using a technology that includes the mechanical and thermal treatment of a mixture of high-quality manganese concentrate and calcined dolomite or lime.

Marokite-manganite concentrate can be used for alloying steel with manganese when it is smelted in an electric furnace or ladle furnace unit, while monophase synthetic manganese material is efficient for the production of metallic manganese.

For thermodynamic modeling of manganese reduction from oxides of high-quality manganese concentrate and marokite-manganite concentrate, we used the Terra software package. This software, based on the maximum entropy principle, finds the equilibrium composition of a multicomponent, heterogeneous thermodynamic system under high-temperature conditions [20].

To determine the technological parameters of the mixtures for steel treatment in an electrical steel-melting furnace, briquettes were fabricated in the ladle furnace unit from marokite-manganite concentrate and powder of spontaneously scattered alloy FS45Mn25 (25 % Mn and 45 % Si) [1]. The binder consisted of 23.2 % ashes from combined heat and power plants (8.88 % Al_2O_3 ; 23.98 % SiO_2 ; 0.56 % TiO_2 ; 45.85 % CaO ; 4.98 % MgO ; 6.32 % FeO ; 8.18 % Fe_2O_3 ; 1.82 % losses on ignition and water (the rest).

The briquettes were melted in a Tamman furnace at a temperature of 1773 – 1823 K. After holding for 5 min, the metal and slag were drained and analyzed.

Using monophase synthetic material CaMnO_3 to obtain metallic manganese through aluminothermic treatment enhances the process's thermality (since manganese in this compound is in a higher oxidation state), allows smelting to be conducted using an out-of-furnace process, and increases manganese recovery.

A software application was developed to calculate the charge composition, smelting products, and the specific thermal effect of the aluminothermic treatment of metallic manganese, based on the stoichiometric equations of heat balance in the metallothermic process.

For experimental melting, the charge included high-quality concentrate, monophase material (CaMnO_3), and aluminum powder. The melting was carried out in a crucible with an upper opening.

RESULTS AND DISCUSSION

The averaged chemical composition of the high-quality manganese concentrate is as follows: 59.50 % Mn_{tot} ; 0.28 % Fe_{tot} ; 5.35 % CaO ; 4.00 % CaCl_2 ; less than 1.00 % SiO_2 ; and less than 0.01 % P. The results of X-ray phase analysis showed that manganese in the high-quality concentrate mainly exists in the form of Mn_3O_4 , and it also contains small quantities of α -manganese, manganosite MnO , and calcium chloride CaCl_2 .

The study of the carbonothermal reduction of manganese in the Mn_3O_4 –C system, in the absence of iron, showed that the manganese reduction begins at temperatures above 1723 K with carbon consumption exceeding 1.5 moles. At this temperature, manganese starts to evaporate. At 1723 K, with excess carbon, manganese carbide (Mn_7C_3) is present in the system but disappears with increasing temperature. Complete reduction of manganese occurs at a carbon consumption of 2 moles.

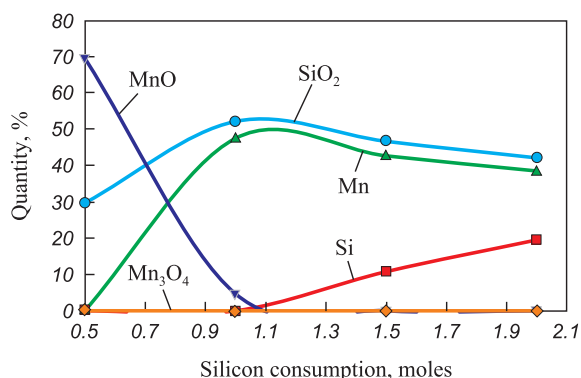


Fig. 1. Dependence of equilibrium compositions in the Mn_3O_4 – Si system on silicon consumption

Рис. 1. Зависимости равновесных составов в системе Mn_3O_4 – Si от расхода кремния

Calculations in the Mn_3O_4 –Si system showed that manganese can be reduced by silicon over the entire specified temperature range. The research results, presented in Fig. 1, indicate that complete reduction of manganese occurs at a silicon molar rate of 1 mole. This value corresponds to the maximum (47 %) manganese content in the system, which decreases with increasing consumption of the reducing agent due to dilution with excess silicon.

During thermodynamic modeling of the manganese reduction from marokite oxides, calculations were performed for 1 kg of CaMn_2O_4 , with the amount of reducing agents (carbon and silicon) ranging from 0 to 0.30 kg/kg marokite at temperatures from 1273 to 2273 K.

The results demonstrated that when carbon is used as a reducing agent, reduction begins at a temperature of 1623 K with carbon consumption exceeding 0.05 kg/kg marokite, and ends at 1723 K. When manganese is reduced from marokite oxides with silicon, the process is independent of temperature within the given range, meaning that at steelmaking temperatures, manganese reduction depends solely on the consumption of the reducing agent.

During the joint reduction of manganese from marokite with carbon and silicon at steelmaking temperatures, manganese is found in the form of metallic manganese in both condensed and gaseous phases, with no manganese carbide present.

Fig. 2 shows the dependence of the manganese recovery coefficient on the consumption of carbon and silicon at $T = 1923$ K, proving that when the consumption of reducing agents exceeds 0.2 kg/kg marokite, manganese is completely reduced.

Thus, any of the considered reducing agents or their combinations in specific proportions can be utilized as a reducing agent when manganese-containing oxide materials are used for steel treatment.

The results of the phase analysis of marokite-manganite concentrate samples obtained by heat treatment

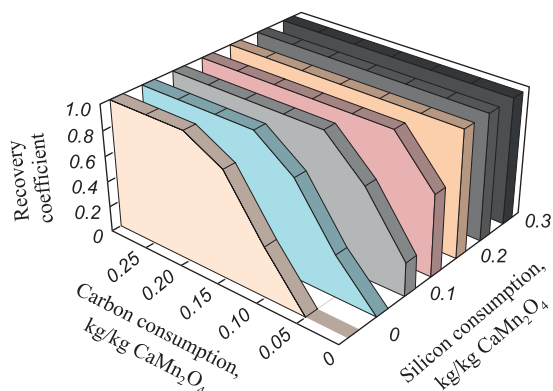


Fig. 2. Manganese recovery coefficient at combined reduction with silicon and carbon at $T = 1923$ K

Рис. 2. Коэффициент извлечения марганца при совместном восстановлении кремнием и углеродом при температуре 1923 K

of mixtures of the high-quality manganese concentrate and calcined flux metal, and their weighing after two weeks of storage in air are presented in Table 1.

The mixture of high-quality manganese concentrate and calcined dolomite, after being held for 2 h at a temperature of 1223 K, transforms into marokite-manganite concentrate, which is practically non-hygroscopic in air as it does not contain free calcium oxides.

Experimental data on the manganese reduction from briquettes with the marokite-manganite concentrate are presented in Table 2. When the marokite-manganite concentrate is obtained from the high-quality manganese concentrate and dolomite, steel treatment with manganese-containing materials becomes practically waste-free.

The ratio $(\text{CaO} + 1.4\text{MgO})/\text{Mn}$ in the marokite-manganite concentrate can range from 0.5 to 1.0. However, during smelting, the best results are obtained with a ratio of $(\text{CaO} + 1.4\text{MgO})/\text{Mn}$ in the marokite-manganite concentrate between 0.50 and 0.72. This is due to the lower consumption of the reducing agent (silicon), which in turn reduces the slag ratio. At $(\text{CaO} + 1.4\text{MgO})/\text{Mn} = 0.51$ to 1.00, all manganese is bound into calcium and magnesium manganites and marokite, ensuring its complete reduction. At $(\text{CaO} + 1.4\text{MgO})/\text{Mn} < 0.50$, free manganese oxides appear, leading to increased manga-

nese loss during reduction. Conversely, when this ratio exceeds 0.72, silicon consumption for reduction and the slag ratio increase, though the reduction value remains high if the ratio is less than 1.0.

Based on the results of thermodynamic calculations and experimental studies, the following technological parameters for steel treatment with marokite-manganite concentrate in an electric furnace and a ladle-furnace unit are proposed: the concentrate should be applied to the surface of the metal, and initially, the metal and slag should be thoroughly deoxidized to reduce the total oxidation of the metal-slag systems. The actual reducing agent that reduces manganese from the melt of the marokite-manganite concentrate is silicon. To conserve silicon, manganese should be initially reduced with carbon introduced with coke onto the surface of the manganese-containing oxide melt.

When using high-quality manganese concentrate to produce metallic manganese through thermochemical synthesis, a monophasic material is obtained, and the results of its X-ray phase analysis are presented in Table 3.

The manganese reduction by aluminum from the synthesized material is accompanied by a significant release of heat and can be represented by the equation

Table 1. Results of phase analysis of the samples

Таблица 1. Результаты фазового анализа образцов

Indicator	Indicator value as an experiment			
	1	2	3	4
Ratio $(\text{CaO} + 1.4\text{Mg})/\text{Mn}$ in the mixture	1.00	0.83	0.72	0.55
Main phase	Manganite	Manganite	Manganite	Marokite
Present in noticeable quantities	–	Marokite	Marokite	–
Traces, a few	Marokite, hausmannite	Gausmanite, manganosite	Gausmannite	Gausmannite
Change in weight after two weeks of holding	Not observed	Not observed	Not observed	Not observed

Table 2. Average results of experiments on reduction of briquettes with marokite-manganite concentrate

Таблица 2. Средние результаты опытов восстановления брикетов с марокит-манганитовым концентратом

Ratio $(\text{CaO} + 1.4\text{MgO})/\text{Mn}$ in the concentrate	Briquette composition, %		Melting indicators		Metal composition, %		Manganese recovery, %		Silicon consumption, kg/kg, manganese reduction	Beneficial use of silicon, %
	Alloy FS45Mn25	Concentrate	Metallic yield, %	Slag ratio, t/t	Mn	Si	from the briquette	from the concentrate		
0.55	52.6	47.4	116.5	0.61	74.14	18.55	95.8	92.80	0.441	90.3
0.72	51.7	48.3	115.7	0.64	75.26	18.90	96.0	94.27	0.422	91.6
0.83	50.5	49.5	115.5	0.71	73.30	18.15	93.1	87.90	0.483	87.0
1.00	50.2	49.8	112.2	0.75	74.50	17.45	92.3	89.48	0.540	82.3

Table 3. Results of X-ray phase analysis of synthesized monophase material

Таблица 3. Результаты рентгенофазового анализа синтезированного монофазного материала

Material	Phase composition
Lime	Large quantity of: lime CaO Present: portland $\text{Ca}(\text{OH})_2$, calcite CaCO_3
High quality manganese concentrate	Large quantity of: hausmannite Mn_3O_4
Synthetic material	Large quantity of: CaMnO_3 Small quantity of: marokite CaMn_2O_4



The resulting Al_2O_3 reacts with CaO to form low-melting aluminates. Therefore, during reduction, manganese losses can theoretically be minimal.

Since a mixture of high-quality manganese concentrate and monophase synthetic material CaMnO_3 was used as the initial manganese-containing material, the optimal ratio of the mixture components had to be determined. Heat balances of the aluminothermic melting of metallic manganese were calculated using the developed method. The calculation results are presented in Fig. 3, *a*.

To achieve a specific thermal effect of 2500 – 2600 kJ/kg of charge required for the spontaneous process and good separation of metal and slag, the charge should contain 25 – 35 % of the synthesized monophase material

CaMnO_3 and 65 – 75 % of the high-quality manganese concentrate, as confirmed by experimental data (Fig. 3, *b*).

As a result of experimental melting, the metal was obtained with the chemical composition presented in Table 4. The results obtained clearly show that the alloy's chemical composition meets the requirements of GOST 6008 – 80.

It should be noted that metallic manganese has a low content of harmful impurities (phosphorus and sulfur), and the iron content does not exceed 1 %. The manganese recovery from the concentrate averaged approximately 90 %, and the slag ratio ranged from 2.30 to 2.65.

During the experiments, the melt temperature was about 2300 – 2373 K, with the optimal ratio of high-quality concentrate to monophase material (CaMnO_3) being 6.5 – 7.5 to 3.5 – 2.5.

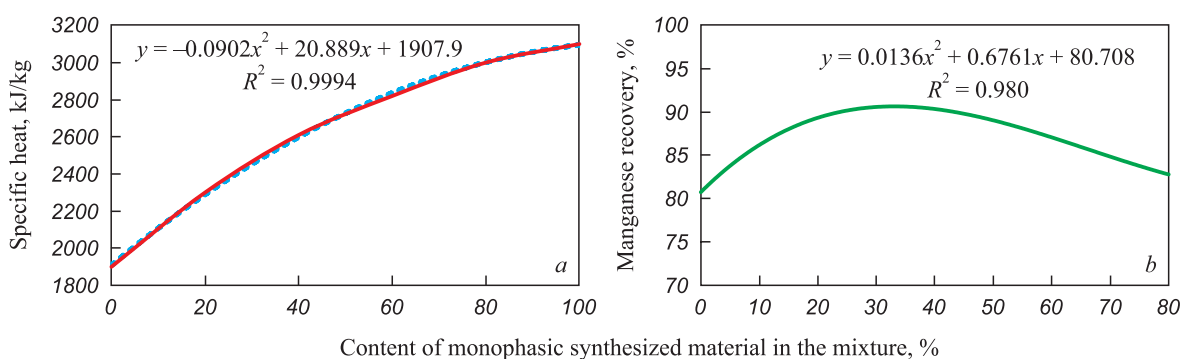
Fig. 3. Dependence of specific heat of the process (*a*) and of manganese yield (*b*) on the content of synthetic monophase materialРис. 3. Зависимость удельной теплоты процесса (*a*) и выхода марганца (*b*) от содержания синтетического монофазного материала

Table 4. Chemical composition of the experimental metal

Таблица 4. Химический состав опытного металла

Melt	Metal composition, %						MnO content in the slag, %	Mn recovery, %
	Mn	Al	Si	Fe	S	P		
1	96.89	0.81	0.45	0.88	0.004	0.006	7.24	90.70
2	97.00	0.75	0.38	0.83	0.002	0.006	6.15	90.11
3	97.12	0.73	0.40	0.74	0.003	0.005	6.01	91.16
4	96.78	0.68	0.58	0.97	0.004	0.004	8.15	87.68
5	96.84	0.83	0.64	0.91	0.004	0.006	7.35	89.89

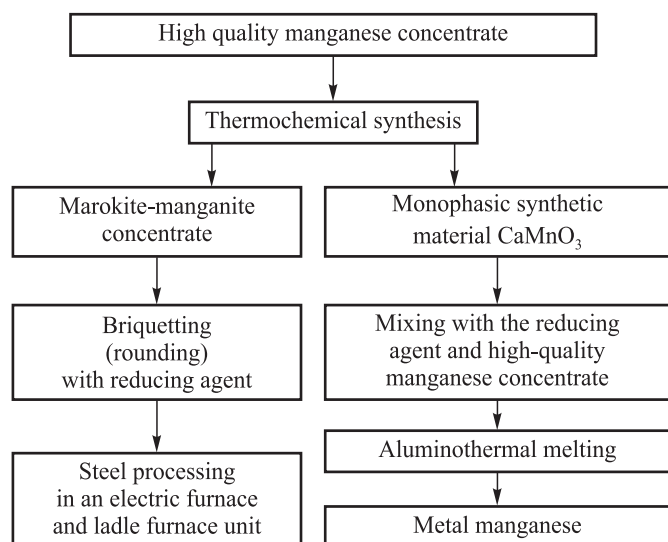


Fig. 4. Process diagram of application of high-quality manganese concentrate

Рис. 4. Технологическая схема применения высококачественного марганцевого концентрата

The recovery of manganese during smelting from the high-quality manganese concentrate reached 85.3 – 89.3 %, which significantly exceeds the manganese recovery when producing metallic manganese from peroxide manganese ores by aluminum thermal out-of-furnace treatment (69 – 72 %). The beneficial use of aluminum was 94 – 96 %.

Based on the thermodynamic and experimental studies, we developed the process diagram (Fig. 4) for using high-quality manganese concentrate obtained through hydrometallurgical enrichment of ferromanganese ores from Kuzbass.

CONCLUSIONS

The results of experimental studies enabled development of a technology for producing marokite-manganite concentrate and single-phase synthetic material (CaMnO_3), the use of which enhances manganese recovery to 90 – 92 %.

Thermodynamic modeling was used to determine the optimal temperatures and consumption of reducing agents (carbon and silicon) to ensure manganese reduction from the oxides of high-quality manganese concentrate obtained from the hydrometallurgical enrichment of ferromanganese ores, as well as from marokite-manganite concentrate. We established that any of the considered reducing agents or their combinations in specific proportions can be used as a reducing agent when oxide manganese-containing materials are used for steel treatment.

Based on the results of thermodynamic calculations and experimental studies, we proposed technological parameters for processing steel with marokite-manganite

concentrate in an electric furnace and a ladle furnace unit. To obtain metallic manganese using the out-of-furnace aluminum thermal treatment, optimal processing methods were developed involving the monophasic synthetic material (CaMnO_3) and high-quality manganese concentrate, which will increase manganese recovery to 90 %.

REFERENCES / СПИСОК ЛИТЕРАТУРЫ

1. Rozhikhina I.D., Nokhrina O.I. Production of Manganese-Containing Materials and Alloys Using Ores from Deposits in Western Siberia. Novokuznetsk: RC SibSIU; 2007:172. (In Russ.).
Рожихина И.Д., Нохрина О.И. Производство марганец-содержащих материалов и сплавов с использованием руд месторождений Западной Сибири. Новокузнецк: ИЦ СибГИУ; 2007:172.
2. Nokhrina O.I., Rozhikhina I.D., Edil'baev A.I., Edil'baev B.A. Manganese ores of the Kemerovo region – Kuzbass and methods of their enrichment. *Izvestiya. Ferrous Metallurgy*. 2020;63(5):344–350. (In Russ.).
<https://doi.org/10.17073/0368-0797-2020-5-344-350>
Нохрина О.И., Рожихина И.Д., Едильбаев А.И., Едильбаев Б.А. Марганцевые руды Кемеровской области – Кузбасса и методы их обогащения. *Известия вузов. Черная металлургия*. 2020;63(5):344–350.
<https://doi.org/10.17073/0368-0797-2020-5-344-350>
3. Tiginov L.P., Smirnov L.A., Menadisieva R.A. Manganese: Geology, Production, Application. Ekaterinburg: NSA; 2006:183. (In Russ.).
Тигунов Л.П., Смирнов Л.А., Менадисиева Р.А. Марганец: геология, производство, использование. Екатеринбург: АНБ; 2006:183.
4. Nokhrina O.I., Rozhikhina I.D., Golodova M.A., Izrail'skii A.O. Study of Kuzbass iron-manganese ores enrichment possibilities. *Ferrous Metallurgy. Bulletin of Scientific, Technical and Economic Information*. 2020;76(9):904–909. (In Russ.).
Нохрина О.И., Рожихина И.Д., Голодова М.А., Израильский А.О. Изучение возможности обогащения железомарганцевых руд Кузбасса. *Черная металлургия. Бюллетень научно-технической и экономической информации*. 2020;76(9):904–909.
5. Sutyurin Yu.E. Analysis of the state of hydrometallurgical processing of manganese raw materials. *Natsional'naya metallurgiya*. 2003;(2):99–104. (In Russ.).
Сутырин Ю.Е. Анализ состояния гидрометаллургической переработки марганцевого сырья. *Национальная металлургия*. 2003;(2):99–104.
6. Chernobrovin V.P., Mizin V.G., Sirina T.P., Dashevskii V.Ya. Complex Processing of Carbonate Manganese Raw Materials: Chemistry and Technology. Chelyabinsk: SUSU; 2009:294. (In Russ.).
Чернобровин В.П., Мизин В.Г., Сирина Т.П., Дашевский В.Я. Комплексная переработка карбонатного марганцевого сырья: химия и технология. Челябинск: ЮУрГУ; 2009:294.
7. Tiginov L.P., Ozhogina E.G., Litvintsev E.G., Bronitskaya E.S., Anufrieva S.I., Kalish E.A. Up-to-date technologies for concentration and hydrometallurgical process-

- ing of manganese ores. *Gornyi zhurnal*. 2007;(2):78–84. (In Russ.).
- Тигунов Л.П., Ожогина Е.Г., Литвинцев Э.Г., Броницкая Е.С., Ануфриева С.И., Калиш Е.А. Современные технологии обогащения и гидрометаллургического передела марганцевых руд. *Горный журнал*. 2007;(2):78–84.
8. Kurkov A.V., Mamoshin M.Yu., Rogozhin A.A. Break-through Hydrometallurgical Processes for the Sustainable Development of Mineral Processing Technologies. Moscow: VIMS; 2019:106. (In Russ.).

Курков А.В., Мамошин М.Ю., Рогожин А.А. Прорывные гидрометаллургические процессы для устойчивого развития технологий переработки минерального сырья. Москва: Научное издание ФГБУ «ВИМС»; 2019:106.

 9. Dreisinger D. Keynote address: Hydrometallurgical process development for complex ores and concentrates. *Journal of the Southern African Institute of Mining and Metallurgy*. 2009;109(5):253–271.
 10. Hatk P.K., Sukla L.B., Das S.C. Aqueous SO₂ leaching studies on Nishikhal manganese ore through factorial experiment. *Hydrometallurgy*. 2000;54(2–3):217–228.
 11. Trifoni M., Toso L., Vegliu F. Reductive leaching of maniferous ores by glucose and H₂SO₄: effect of alcohols. *Hydrometallurgy*. 2001;59(1):1–14.
[https://doi.org/10.1016/S0304-386X\(00\)00138-9](https://doi.org/10.1016/S0304-386X(00)00138-9)
 12. Ding P., Liu Q., Pang W. A review of manganese ore beneficiation: Situation and development. *Applied Mechanics and Materials*. 2013;380–384:4431–4433.
<http://dx.doi.org/10.4028/www.scientific.net/AMM.380-384.4431>
 13. Yang Z.Z., Li G.Q., Huang C.G., Ding J. Mn ore smelting reduction based on double slag operation in BOF. *Applied Mechanics and Materials*. 2013;753–755:76–80.
<http://dx.doi.org/10.4028/www.scientific.net/AMR.753-755.76>
 14. Pan M.C., Liu X.L., Zou R., Huang J., Han J.C. Study of heat treatment technology on medium-carbon-low-alloy-steel large hammer formation of gradient performance. *Advanced Materials Research*. 2014;881–883:1288–1292.
<http://dx.doi.org/10.4028/www.scientific.net/AMR.881-883.1288>
 15. Ayala J., Fernandez B. Recovery of manganese from silico-manganese slag by means of a hydrometallurgical process. *Hydrometallurgy*. 2015;158:68–73.
<https://doi.org/10.1016/j.hydromet.2015.10.007>
 16. Veglio F., Trifoni M., Abbruzzese C., Toro L. Column leaching of a manganese dioxide ore: a study by using fractional factorial design. *Hydrometallurgy*. 2001;59(1):31–44.
[http://dx.doi.org/10.1016/S0304-386X\(00\)00139-0](http://dx.doi.org/10.1016/S0304-386X(00)00139-0)
 17. Kang T.T., Liu Y., Huang Y.B., Dong J., Huang Q., Li Y. Synthesis and dephosphorization of iron manganese composite oxide by acid leaching on iron manganese ore. *Advanced Materials Research*. 2012;554–556:489–493.
<http://dx.doi.org/10.4028/www.scientific.net/AMR.554-556.489>
 18. Sun D., Li M.L., Li C.H., Cul R., Zheng X.Y. A green enriching process of Mn from low grade ore of manganese carbonate. *Applied Mechanics and Materials*. 2014;644–650:5427–5430.
<http://dx.doi.org/10.4028/www.scientific.net/AMM.644-650.5427>
 19. Nokhrina O.I., Rozhikhina I.D., Golodova M.A. Production of high-quality concentrates by method of hydrometallurgical concentration of manganese ores. *Russian Internet Journal of Industrial Engineering*. 2023;10(1):47–51. (In Russ.).

Нохрина О.И., Рожихина И.Д., Голодова М.А. Получение высококачественных концентратов методом гидрометаллургического обогащения марганцевых руд. *Машиностроение: сетевой электронный научный журнал*. 2023;10(1):47–51.

 20. Trusov B.G. TERRA software system for modeling phase and chemical equilibria at high temperatures. In: *III Int. Symp. "Combustion and Plasma Chemistry". August 24-26, 2005, Almaty, Kazakhstan*. Almaty: Kazak universiteti; 2005:52–57. (In Russ.).

Трусов Б.Г. Программная система ТЕРРА для моделирования фазовых и химических равновесий при высоких температурах. В кн.: *III между. симпозиум «Горение и плазмохимия». 24-26 августа 2005. Алматы, Казахстан*. Алматы: Казак университеті; 2005:52–57.

Information about the Authors

Сведения об авторах

Inna A. Rybenko, Dr. Sci. (Eng.), Prof., Head of the Chair of Applied Information Technologies and Programming, Siberian State Industrial University

ORCID: 0000-0003-1679-0839

E-mail: rybenkoi@mail.ru

Irina D. Rozhikhina, Dr. Sci. (Eng.), Prof. of the Chair of Ferrous Metallurgy, Siberian State Industrial University

ORCID: 0000-0002-3034-4539

E-mail: roghina_id@mail.ru

Ol'ga I. Nokhrina, Dr. Sci. (Eng.), Prof. of the Chair of Ferrous Metallurgy, Siberian State Industrial University

ORCID: 0000-0001-9448-8948

E-mail: nvi52@mail.ru

Marina A. Golodova, Cand. Sci. (Eng.), Assist. Prof. of the Chair of Architecture, Siberian State Industrial University

ORCID: 0000-0003-0105-9285

E-mail: m.irina1976@mail.ru

Инна Анатольевна Рыбенко, д.т.н., профессор, заведующий кафедрой прикладных информационных технологий и программирования, Сибирский государственный индустриальный университет

ORCID: 0000-0003-1679-0839

E-mail: rybenkoi@mail.ru

Ирина Дмитриевна Рожихина, д.т.н., профессор-консультант кафедры металлургии черных металлов, Сибирский государственный индустриальный университет

ORCID: 0000-0002-3034-4539

E-mail: roghina_id@mail.ru

Ольга Ивановна Нохрина, д.т.н., профессор-консультант кафедры металлургии черных металлов, Сибирский государственный индустриальный университет

ORCID: 0000-0001-9448-8948

E-mail: nvi52@mail.ru

Марина Анатольевна Голодова, к.т.н., доцент кафедры архитектуры, Сибирский государственный индустриальный университет

ORCID: 0000-0003-0105-9285

E-mail: m.irina1976@mail.ru

Contribution of the Authors

Вклад авторов

I. A. Rybenko – conducting thermodynamic calculations, processing calculation results.

I. D. Rozhikhina – problem statement, analysis of literary sources, writing the main text of the article, conducting experiments and processing their results.

O. I. Nokhrina – conducting experiments and processing their results, editing the article.

M. A. Golodova – processing thermodynamic calculations, plotting and describing them, design of drawings.

И. А. Рыбенко – проведение термодинамических расчетов, обработка результатов расчетов.

И. Д. Рожихина – постановка задачи, анализ литературных источников, написание основного текста статьи, проведение экспериментов и обработка их результатов.

О. И. Нохрина – проведение экспериментов и обработка их результатов, редактирование статьи.

М. А. Голодова – обработка термодинамических расчетов, построение графиков и их описание, выполнение рисунков.

Received 04.04.2022

Revised 25.04.2022

Accepted 11.05.2022

Поступила в редакцию 04.04.2022

После доработки 25.04.2022

Принята к публикации 11.05.2022

ИНФОРМАЦИОННЫЕ ТЕХНОЛОГИИ
И АВТОМАТИЗАЦИЯ В ЧЕРНОЙ МЕТАЛЛУРГИИИНФОРМАЦИОННЫЕ ТЕХНОЛОГИИ
И АВТОМАТИЗАЦИЯ В ЧЕРНОЙ МЕТАЛЛУРГИИ

UDC 669.162.263

DOI 10.17073/0368-0797-2024-2-245-253



Original article

Оригинальная статья

INFORMATION MODELING SYSTEM FOR MOVEMENT OF CHARGE LAYERS AND MELT ACCUMULATION IN A BLAST FURNACE WELL

N. A. Spirin[✉], I. A. Gurin, V. V. Lavrov, L. A. Zainullin

Ural Federal University named after the first President of Russia B. N. Yeltsin (28 Mira Str., Yekaterinburg 620002, Russian Federation)

✉ n.a.spirin@urfu.ru

Abstract. The article presents the results of development of an information modeling system for movement of charge layers and melt accumulation in a blast furnace well. The work is based on mathematical models reflecting modern ideas on the course of physico-chemical phenomena of blast furnace melting and technological features of the blast furnace process. The use of such system makes it possible to determine and visualize the configuration of layers of iron ore materials and coke according to the working space height, taking into account a given ore load in equal-sized annular zones of the blast furnace. In constructing the configuration of the charge layers, when materials are approaching the furnace belly, the peculiarities of their movement are taken into account. This is due to the influence of tuyere zone, primary slag formation processes, and changes in thickness of the coke layer caused by development of the direct reduction process. Calculation of the melt accumulation process in the blast furnace well provides determining the volume of slag remaining there after the notch closure of previous tapping, calculating the dynamics of filling the furnace well with melts of cast iron and slag, determining the volume output of melts of cast iron and slag for the inter-tapping period and calculating the duration of tapping. The developed information modeling system makes it possible to evaluate the dynamics of changes in configuration of layers in the working space height, as well as the process of melt accumulation in the blast furnace well, using really accessible information about a working furnace. The software architecture is described, the characteristics of the modules are presented and its operation is illustrated. The developed system can be used by technological staff of a blast furnace shop to study the processes occurring in blast furnaces, improve the technological modes of operation, predict the melting progress in real time in conditions of operation instability.

Keywords: blast furnace, modeling of blast furnace process, movement of charge materials in a furnace, accumulation of molten iron and slag in a furnace, software, software architecture, functional modeling

For citation: Spirin N.A., Gurin I.A., Lavrov V.V., Zainullin L.A. Information modeling system for movement of charge layers and melt accumulation in a blast furnace well. *Izvestiya. Ferrous Metallurgy*. 2024;67(2):245–253. <https://doi.org/10.17073/0368-0797-2024-2-245-253>

ИНФОРМАЦИОННО-МОДЕЛИРУЮЩАЯ СИСТЕМА ДВИЖЕНИЯ СЛОЕВ ШИХТЫ И НАКОПЛЕНИЯ РАСПЛАВА В ГОРНЕ ДОМЕННОЙ ПЕЧИ

Н. А. Спирин[✉], И. А. Гурин, В. В. Лавров, Л. А. Зайнуллин

Уральский федеральный университет имени первого Президента России Б. Н. Ельцина (Россия, 620002, Екатеринбург, ул. Мира, 28)

✉ n.a.spirin@urfu.ru

Аннотация. В статье представлены результаты разработки информационно-моделирующей системы движения слоев шихты и накопления расплава в горне доменной печи. В основу работы положены математические модели, отражающие современные представления о протекании физико-химических явлений доменной плавки и технологические особенности ведения доменного процесса. Применение системы позволяет определить и визуализировать конфигурацию слоев железорудных материалов и кокса по высоте рабочего пространства с учетом заданной рудной нагрузки в равновеликих кольцевых зонах доменной печи. В построении конфигурации слоев шихты при подходе материалов в распар печи учтены особенности их движения. Это обусловлено влиянием фурменных очагов, процессов первичного шлакообразования, изменения толщины слоя кокса, вызванного развитием процесса прямого восстановления. Расчет процесса накопления расплава в горне доменной печи предусматривает определение объема шлака, оставшегося в горне печи после закрытия летки предыду-

щего выпуска, расчет динамики заполнения горна печи расплавами чугуна и шлака, определение объемного выхода расплавов чугуна и шлака за межвыпускной период и расчет продолжительности выпуска из печи. Разработанная информационно-моделирующая система позволяет по реально доступной информации о работающей печи оценивать динамику изменения конфигурации слоев по высоте рабочего пространства, а также процесс накопления расплава в горне доменной печи. Описана архитектура программного обеспечения, представлена характеристика модулей и проиллюстрирована его работа. Разработанная система может быть использована технологическим персоналом доменного производства для изучения процессов, протекающих в доменных печах, совершенствования технологических режимов функционирования, прогнозирования хода плавки в режиме реального времени в условиях нестабильности их работы.

Ключевые слова: доменная печь, моделирование доменного процесса, движение шихтовых материалов в печи, накопление расплава чугуна и шлака в горне, программное обеспечение, архитектура программного обеспечения, функциональное моделирование

Для цитирования: Спирин Н.А., Гурин И.А., Лавров В.В., Зайнуллин Л.А. Информационно-моделирующая система движения слоев шихты и накопления расплава в горне доменной печи. *Известия вузов. Черная металлургия*. 2024;67(2):245–253.

<https://doi.org/10.17073/0368-0797-2024-2-245-253>

INTRODUCTION

The rational distribution of charge materials in a blast furnace [1 – 3], which fully aligns with the thermal, blast, and slag parameters as well as current blast furnace practices overall [4 – 6], remains an urgent challenge for both industrial engineers and researchers studying the blast furnace process [7 – 9].

The processes within the blast furnace well significantly affect its performance [10 – 12], thus drawing increased attention from engineering and technological personnel [13; 14]. The most challenging task is to arrange effective well performance, specifically the dynamics of filling the furnace hearth with cast iron and slag [15 – 19]. An information modeling system was developed to study the movement of charge layers throughout the furnace working space height and the accumulation of melt in the furnace well. This system is based on the mathematical models that reflect modern concepts of physical and chemical processes during blast furnace melting, as well as the technological features of the blast furnace process [19; 20].

FUNCTIONAL MODELING OF AN INFORMATION MODELING SYSTEM

The information system was designed using the concepts of functional modeling and the graphical notation of the IDEF0 method of structural analysis and design [21; 22]. The Federal Agency on Technical Regulation and Metrology recommends the IDEF0 methodology for constructing functional models of business and industrial engineering systems and applying them in practice. The advantage of the IDEF0 method is that IT specialists can easily exchange information with engineering personnel regarding the functioning of the software under development.

This methodology was employed to develop the functional model of the information modeling system for the movement of charge layers and melt accumulation in a blast furnace well. The model, created using Ramus software [22], contains more than 30 blocks at three levels of decomposition. It defines the main functions and relationships between individual functional blocks of the system, control activities, and mechanisms for performing each function.

Fig. 1 shows the decomposition of the first level of the functional model. The first level of decomposition of the context diagram includes four blocks: selecting the required task, calculating the dynamics of changes in the charge layers configuration, calculating the melt level in the blast furnace well, and analyzing and saving the results.

ARCHITECTURE OF THE INFORMATION MODELING SYSTEM

Fig. 2 shows the architecture of the developed information modeling system for the movement of charge layers and melt accumulation in the blast furnace well. The information modeling system is divided into small independent blocks – modules that functionally implement complete program segments. The idea behind this approach is that the functionality of software modules can be updated without the need to change the entire system, making it more reliable and scalable. The mathematical libraries and classes function as modules [23].

The information modeling system includes the following modules:

- the module for calculating the dynamics of changes in the configuration of the blast furnace charge layers (used to calculate the configuration of the charge layers throughout the height of the blast furnace profile based on a mathematical model);
- the module for calculating the melt accumulation in the blast furnace well (used to calculate the height of slag and cast iron before the next tapping based on a given mathematical model);
- the module for analyzing and presenting the results (analyzes the results obtained from the calculation modules; displays the results in numerical and graphical forms, and can generate and export a report to a Microsoft Excel file format).

SOFTWARE IMPLEMENTATION OF THE INFORMATION MODELING SYSTEM

The software implementation of the information system is based on a client-server approach, considering integration possibilities with existing company software products and data exchange via API (*Application Programming*

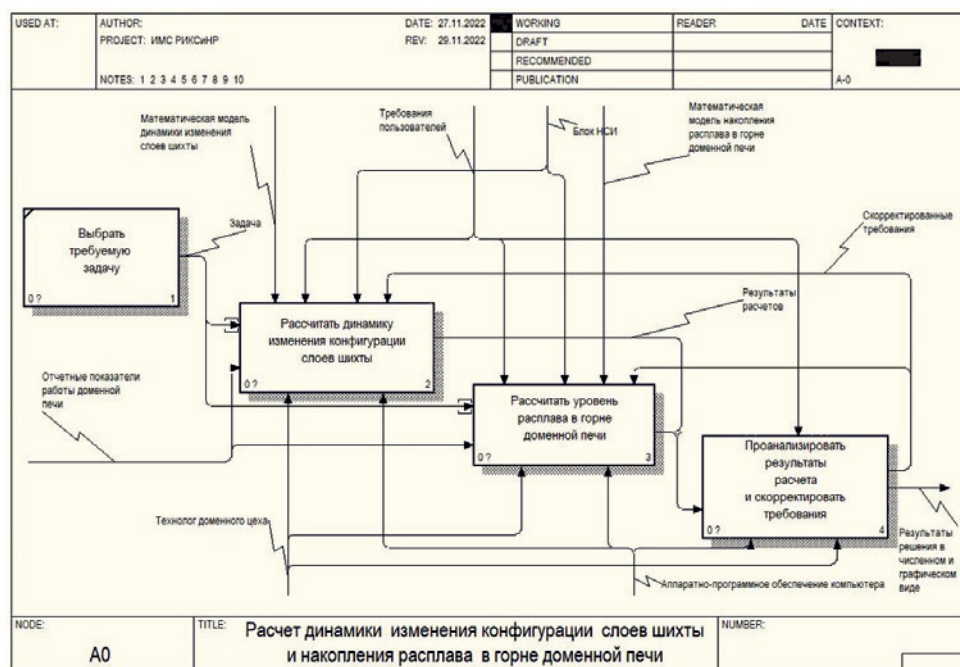


Fig. 1. Decomposition of the first level of the functional model

Рис. 1. Декомпозиция первого уровня функциональной модели

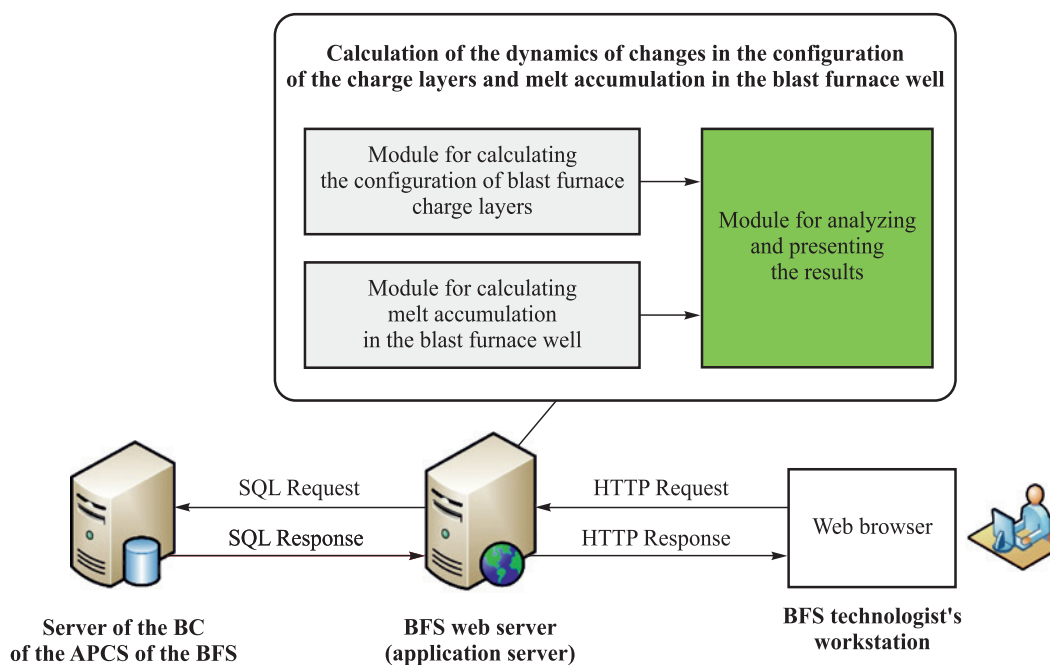


Fig. 2. Architecture of the information modeling system for movement of charge layers and melt accumulation in the blast furnace well

Рис. 2. Архитектура информационно-моделирующей системы движения слоев шихты и накопления расплава в горне доменной печи

Interface). The client-server architecture follows a classic three-tier structure, including presentation, application, and data levels.

The presentation level is implemented using high-level programming languages such as C#, JavaScript, HTML5, and CSS (*Cascading Style Sheets*). The visual design is based on Bootstrap framework. DOM (*Document Object*

Model) objects are manipulated by the jQuery library, and plotting is handled by the Chart.js library. This level is supported by the users' computing resources (web browsers).

The application level is implemented in C# using the ASP.NET Core MVC framework on the .NET 6 software platform [24]. ASP.NET Core framework manages pipelining of user requests, and middleware. The informa-

tion system includes *error handling middleware*, *authentication middleware*, *MVC middleware* and *session middleware*.

Error handling middleware enables the system to flag issues in case of error conditions and ensures the system continues to operate and correctly display web pages, even when encountering database communication errors or executing calculation algorithms.

Authentication middleware introduces the standard ASP.NET Identity authentication and authorization mechanism and account management into the information system.

MVC middleware integrates routing systems, dependency injections, as well as model binding and data validation.

Session middleware processes temporary data of users as they interact with the system.

The data level includes a database and a software for controlling read and write access. The Microsoft SQL Server DBMS is used as the database for the system. The system communicates with the database through Entity Framework Core, which is based on Object-Relational Mapping (ORM) programming, used in object-oriented programming languages to create virtual circuits for databases, allowing data manipulation at the object or class level.

STRUCTURE OF THE INFORMATION MODELING

SYSTEM

The structure of the information modeling system for the movement of charge layers and melt accumulation in the blast furnace well includes the following major blocks:

1. Setting operating conditions for blast furnaces:

- setting the production rate of the blast furnace, the dimensions of its profile, and the number of tappings per day;
- setting the characteristics of the fuel-enriched blast (blast consumption, oxygen content in the blast, humidity, and natural gas consumption);
- setting the physical properties of individual charge components, specific consumption of iron ore material, and coke;
- setting the ore load in annular zones of the blast furnace;
- setting the required indicators for iron smelting (iron, manganese, silicon, and carbon content) and coke (ash, sulfur, and volatile content).

2. Calculating changes in the configuration of charge layers and melt accumulation in the blast furnace well based on mathematical models. Modeling is performed as follows [19; 20]:

2.1 – calculating the parameters of equal-sized annular zones (diameter and radius) on the furnace mouth and the distance from the furnace mouth walls to the middle of each annular section;

2.2 – determining the distribution of ore load in the annular zones of the furnace mouth based on the results

of loading models or using indirect indicators such as the distribution of CO₂ or temperature in the furnace mouth cross-section. The calculations assume that the distribution of ore load is proportional to the CO₂ content and inversely proportional to the temperature distribution;

2.3 – determining the configuration of layers of iron ore materials and coke in the annular sections of the blast furnace mouth, calculated for a given ore load. This involves calculating the masses and volumes of iron ore materials (IOM) and coke for each annular section, and determining the height of the layers of charge materials in the annular zones of the furnace mouth based on the volume of coke and iron ore materials and the area of the annular section;

2.4 – determining the configuration of IOM and coke layers at all levels of the horizon of the furnace shaft and furnace belly.

When modeling the movement of materials in a blast furnace, it is important to consider that the stock line is shaped like a funnel towards the center of the furnace.

In this regard, the type of the formed iron ore materials (IOM) and coke layers will depend on the angle of inclination of the stock line surface, which is a variable value and included in the block of normative reference data (NRD) for the model.

Constructing the configuration of the charge layers when materials approach the furnace belly, we took into account the peculiarities of their movement caused by the impact of the tuyere zone, as well as the processes of primary slag formation that begin in the region of the belly bottom and bosh.

Reproducing the type and size of the charge layers in the region of the belly, we considered changes in the thickness of the coke layer caused by direct reduction of iron, cast iron impurities (silicon, manganese, etc.), and carbon required to carburize cast iron. Calculating the rate of charge lowering due to IOM softening in the belly, we took into account that in the zone of primary slag formation, material shrinks by approximately 20 %, which numerically equals the volume of fractional voids of the IOM layer (bed void fractions).

Above the tuyere zone, there is a rubblized region shaped as an ellipsoid of revolution [20]. The top of this zone is located in the lower part of the shaft and in the upper part of the belly. At the top of this zone, the accelerated movement of charge particles begins.

2.5 – calculating the blast consumption corresponding to the furnace production rate and specific blast consumption. It should be noted that there is a difference between the estimated and actual blast consumption, which is attributed to various factors such as inevitable losses of blast moving along the air supply path and inaccuracies in recording the blast consumption.

2.6 – calculating the volume of slag remaining in the furnace well after the notch closure of previous tapping;

2.7 – calculating the dynamics of filling the furnace well with melts of cast iron and slag. Calculations are

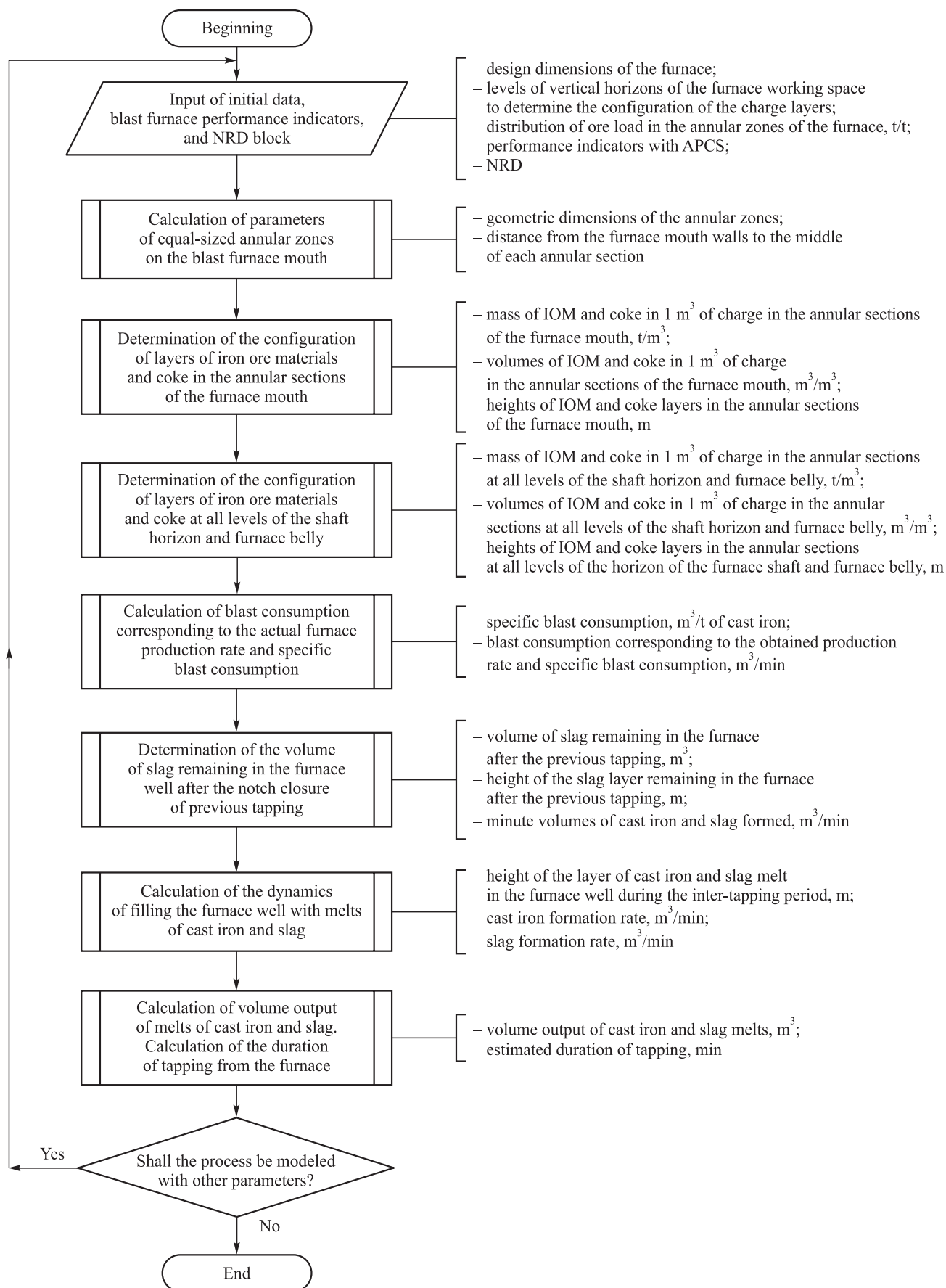


Fig. 3. Block diagram of the algorithm for calculating the configuration of layers of iron ore and coke, melt accumulation in the blast furnace well

Рис. 3. Блок-схема алгоритма расчета конфигурации слоев ЖРМ и кокса, накопления расплава в горне доменной печи

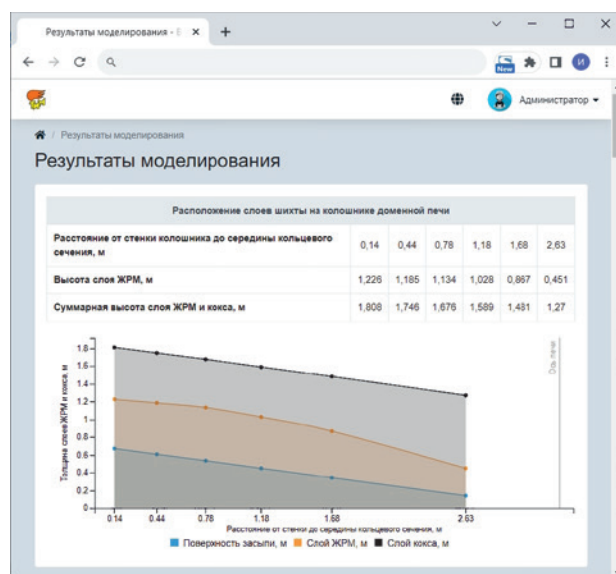
performed at 10 min intervals. During each 10 min interval, adjustments are made to reflect changes in the actual parameters of blast furnace melting, causing changes in the production of cast iron per unit time (blast and natural gas consumption, oxygen concentration in the blast). The thickness of the layers of cast iron and slag is then determined step by step every 10 min cumulatively, with the total height of the melts being adjusted for the volume of slag remaining in the furnace well from the previous tapping.

3. The findings are analyzed as follows:

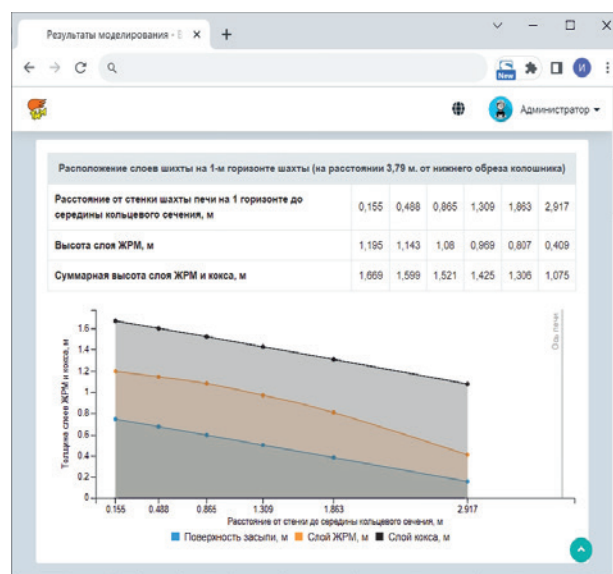
– the dynamics of changes in IOM and coke layers are shown as these layers move towards the tuyere zones of the blast furnace;

– the dynamics of filling the furnace hearth with cast iron and slag is displayed.

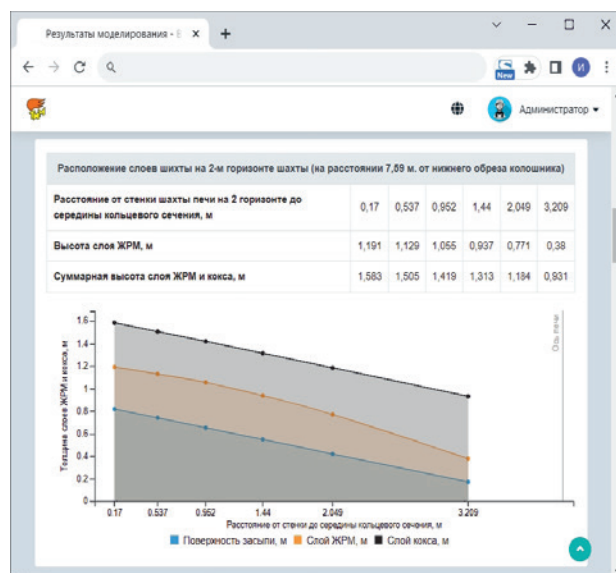
The initial data is entered by an authorized user on the corresponding web pages. Then, the data from the forms is sent to the web server for validation, where the entered values are checked for correctness. If the validation is successful, the calculation is performed according to the specified calculation algorithms.



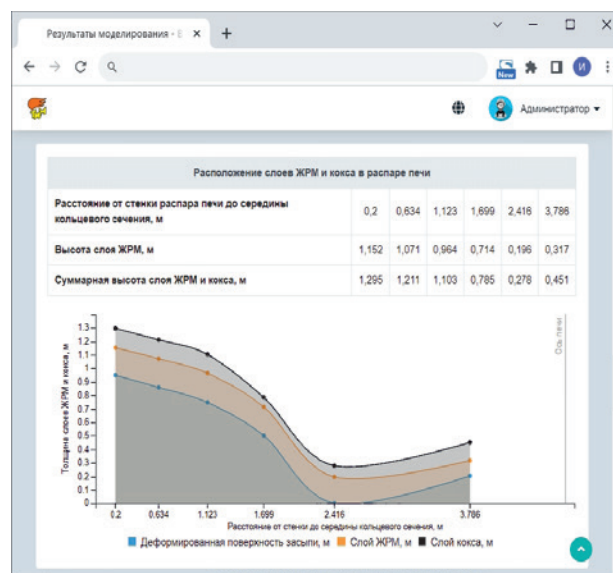
a



b



c



d

Fig. 4. Fragment of a web page with the results of modeling the configuration of charge layers on blast furnace mouth (a), on the first horizon of the furnace shaft (at a distance of 3.79 m from the level of furnace mouth lower edge) (b), on the second horizon of the furnace shaft (at a distance of 7.59 m from the level of the lower edge) (c), at the level of the blast furnace belly (d)

Рис. 4. Фрагмент веб-страницы с результатами моделирования конфигурации слоев шихты на колошнике доменной печи (a), на первом горизонте шахты (на расстоянии 3,79 м от уровня нижнего обреза колошника) (b), на втором горизонте шахты (на расстоянии 7,59 м от уровня нижнего обреза колошника) (c), на уровне распара доменной печи (d)

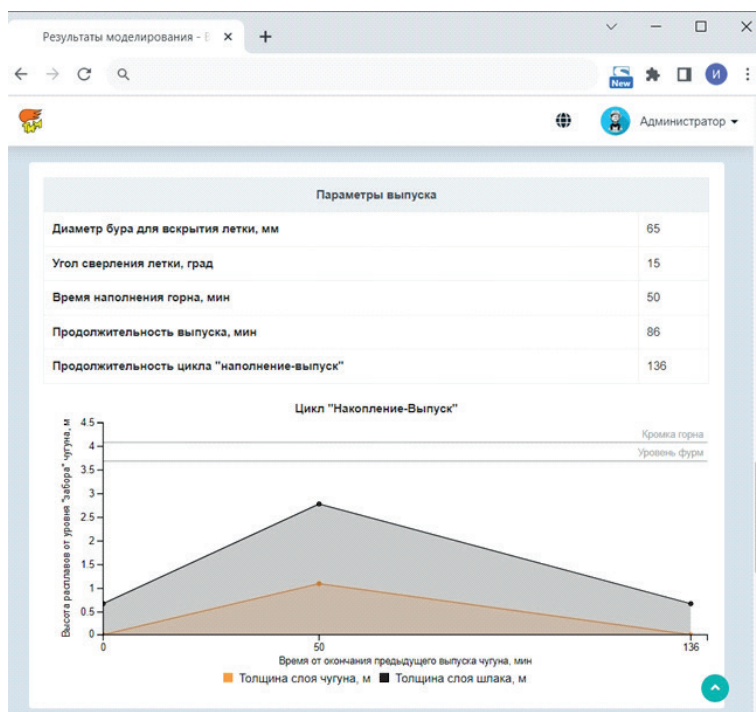


Fig. 5. Fragment of a web page with the results of modeling the cycle “filling – tapping” of liquid melting products in the blast furnace

Рис. 5. Фрагмент веб-страницы с результатами моделирования цикла «наполнение – выпуск» жидких продуктов плавки в доменной печи

ALGORITHM FOR USER INTERACTION WITH THE SYSTEM

The algorithm for modeling the dynamics of changes in the configuration of the charge layers and filling of the blast furnace well as the charge moves to the tuyere zones of the blast furnace is presented in Fig. 3 and includes the following main blocks:

1. Input of parameters and NRD block (ore load in annular zones, blast consumption, oxygen content in blast, humidity, natural gas flow, etc.).

2. Calculation of the parameters of equal-sized annular zones (diameter and radius of the annular zones, mass and volume of coke and iron ore material in the annular zones).

3. Calculation of the configuration of IOM and coke layers, taking into account the slope of the charge level on the furnace mouth, changes in the diameter throughout the furnace height, direct reduction processes, primary slag formation, and rubblized region above the tuyere zones.

4. Calculation of the volume minute output of slag and cast iron.

5. Calculation of the slag and cast iron layer height.

Fig. 4 presents fragments of the results of modeling changes in the configuration of IOM and coke layers on individual horizons of a blast furnace.

Fig. 5 shows a fragment of a web page with the results of modeling melt accumulation in a blast furnace well. The results of modeling the cycle “filling – tapping” of liquid melting products in the blast furnace are presented. The tapping begins 50 min after the previous one finishes.

CONCLUSIONS

We utilized modern information technologies to develop an information modeling system for the movement of charge layers and the accumulation of the melt in the blast furnace well. The system enables calculations of the dynamics of changes in the configuration of the IOM and coke layers throughout the height of the blast furnace working space, as well as the dynamics of filling the blast furnace hearth with liquid melting products.

The developed information modeling system can be used by technological staff to study the processes occurring in blast furnaces, improve the technological modes of operation, and predict the melting progress in real-time.

REFERENCES / СПИСОК ЛИТЕРАТУРЫ

1. Sibagatullin S.K., Makhmutov R.F., Sibagatullina M.I., Starodubov V.A., Buranova E.F. On the optimal distribution of materials in the blast furnace space of the blast furnace. *Teoriya i tekhnologiya metallurgicheskogo proizvodstva*. 2014;(2(15)):31–34. (In Russ.).
Сибигатуллин С.К., Махмудов Р.Ф., Сибигатуллина М.И., Стародубов В.А., Буранова Э.Ф. Об оптимальности распределения материалов в колошниковом пространстве доменной печи. *Теория и технология металлургического производства*. 2014;(2(15)):31–34.
2. Sibagatullin S.K. Formation of Charge Layer in Furnace Mouth Space. Magnitogorsk: MSTU; 2014:188. (In Russ.).
Сибигатуллин С.К. Формирование слоя шихты в колошниковом пространстве печи. Магнитогорск: МГТУ; 2014:188.

3. Tovarovskii I.G. Predictive assessment of the influence of charge materials distribution along the radius of furnace mouth on processes and indicators of blast furnace smelting. *Metallurg.* 2014;(8):46–52. (In Russ.).
Товаровский И.Г. Прогнозная оценка влияния распределения шихтовых материалов по радиусу колошника на процессы и показатели доменной плавки. *Металлург.* 2014;(8):46–52.
4. Bolshakov V.I., Semenov Yu.S., Ivancha N.G., Vishnyakov V.I., Shumelchik E.I., Podkorytov A.L., Semion I.Yu., Kuznetsov A.M., Zubenko A.V. Study of the flow of burden materials and their distribution on the furnace top of a modern blast furnace. *Metallurgical and Mining Industry.* 2012;4(3):158–165.
5. Bol'shakov V.I., Tovarovskii I.G., Gladkov N.A., Shutylev F.M. Distribution of materials along the radius of furnace mouth and development of heat and mass transfer processes and phase transformations in the volume of a blast furnace. *Ferrous Metallurgy. Bulletin of Scientific, Technical and Economic Information.* 2008;(3):22–34. (In Russ.).
Большаков В.И., Товаровский И.Г., Гладков Н.А., Шутылев Ф.М. Распределение материалов по радиусу колошника и развитие процессов тепломассообмена и фазовых превращений в объеме доменной печи. *Черная металлургия. Бюллетень научно-технической и экономической информации.* 2008;(3):22–34.
6. Tarasov P.V. Distribution of materials and gases around the circumference of a blast furnace. *Izvestiya. Ferrous Metallurgy.* 2007;50(5):17–22. (In Russ.).
Тарасов П.В. Распределение материалов и газов по окружности доменной печи. *Известия вузов. Черная металлургия.* 2007;50(5):17–22.
7. Fojtik D., Tuma J., Faruzel P. Computer modelling of burden distribution in the blast furnace equipped by a bell-less top charging system. *Ironmaking & Steelmaking.* 2021;48(10):1226–1238.
<https://doi.org/10.1080/03019233.2021.1952829>
8. Teng Z.-J., Cheng S.-S., Du P.-Y., Guo X.-B. Mathematical model of burden distribution for the bell-less top of a blast furnace. *International Journal of Minerals, Metallurgy, and Materials.* 2013;20(7):620–626.
<https://doi.org/10.1007/s12613-013-0775-7>
9. Di Z., Huang M., Zhou X., Liu J., Sun J., Wang P., Wang H. The influence of central coke charging mode on the burden surface shape and distribution of a blast furnace. *International Journal of Chemical Reactor Engineering.* 2022;21(2): 169–179. <https://doi.org/10.1515/ijcre-2022-0066>
10. Bol'shakov V.I. Technology of High-Efficiency Energy-Saving Blast Furnace Smelting. Kiev: Naukova dumka; 2007:411. (In Russ.).
Большаков В.И. Технология высокоэффективной энергосберегающей доменной плавки. Киев: Наукова думка; 2007:411.
11. Tovarovskii I.G. Blast Furnace Smelting. Dnepropetrovsk: Porogi; 2009:768. (In Russ.).
Товаровский И.Г. Доменная плавка. Днепропетровск: Пороги; 2009:768.
12. Babarykin N.N. Theory and Technology of Blast Furnace Process. Magnitogorsk: MSTU; 2009:257. (In Russ.).
Бабарыкин Н.Н. Теория и технология доменного процесса. Магнитогорск: МГТУ; 2009:257.
13. Cameron I., Sukhram M., Lefebvre K., Davenport W. Blast Furnace Ironmaking: Analysis, Control and Optimization. 1st ed. Elsevier Science; 2019:828.
<https://doi.org/10.1016/C2017-0-00007-1>
14. Bol'shakov V.I., Murav'eva I.G., Semenov Yu.S. Forecasting the thermal condition of a blast furnace well. *Stal'.* 2009;(5):7–9. (In Russ.).
Большаков В.И., Муравьева И.Г., Семенов Ю.С. Прогнозирование теплового состояния горна доменной печи. *Сталь.* 2009;(5):7–9.
15. Spirin N.A., Lavrov V.V., Rybolovlev V.Yu., Gileva L.Yu., Krasnobaev A.V., Shvydkii V.S., Onorin O.P., Shchipanov K.A., Burykin A.A. Mathematical Modeling of Metallurgical Processes in Automated Process Control Systems. Yekaterinburg: UrFU; 2014:558. (In Russ.).
Спирин Н.А., Лавров В.В., Рыболовлев В.Ю., Гилева Л.Ю., Краснобаев А.В., Швыдкий В.С., Онорин О.П., Щипанов К.А., Бuryкин А.А. Математическое моделирование металлургических процессов в АСУ ТП. Екатеринбург: УрФУ; 2014:558.
16. Spirin N.A., Lavrov V.V., Burykin A.A., Rybolovlev V.Yu., Krasnobaev A.V., Kosachenko I.E. Spirin N.A., Lavrov V.V., Burykin A.A., Rybolovlev V.Yu., Krasnobaev A.V., Kosachenko I.E. Model Decision Support Systems in Automated Process Control System of Blast Furnace Smelting. Yekaterinburg: UrFU; 2011:462. (In Russ.).
Спирин Н.А., Лавров В.В., Бuryкин А.А., Рыболовлев В.Ю., Краснобаев А.В., Косаченко И.Е. Модельные системы поддержки принятия решений в АСУ ТП доменной плавки. Екатеринбург: УрФУ; 2011:462.
17. Onorin O.P., Spirin N.A., Terent'ev V.L., Gileva L.Yu., Rybolovlev V.Yu., Kosachenko I.E., Lavrov V.V., Terent'ev A.V. Computer Methods for Modeling of Blast Furnace Process. Yekaterinburg: USTU–UPI; 2005:301. (In Russ.).
Онорин О.П., Спирин Н.А., Терентьев В.Л., Гилева Л.Ю., Рыболовлев В.Ю., Косаченко И.Е., Лавров В.В., Терентьев А.В. Компьютерные методы моделирования доменного процесса. Екатеринбург: УГТУ–УПИ; 2005:301.
18. Gordon Y., Izumskiy N., Matveienko G., Chaika O., Lebid V., Vyshinskaya O. Diagnostics, optimization and mathematical models of coke-sinter-hot metal production process. *AISTech 2019 – Proceedings of the Iron & Steel Technology Conf. 2019;2019-May:479–484.*
<https://doi.org/10.33313/377/050>
19. Pavlov A.V., Onorin O.P., Spirin N.A., Lavrov V.V., Gurin I.A. Some Issues of Technology, Management and Diagnostics of Blast Furnace Smelting. Yekaterinburg: Den' RA; 2023:282. (In Russ.).
Павлов А.В., Онорин О.П., Спирин Н.А., Лавров В.В., Гурин И.А. Некоторые вопросы технологии, управления и диагностики доменной плавки. Екатеринбург: АМК «День РА»; 2023:282.
20. Onorin O.P., Spirin N.A., Lavrov V.V., Gurin I.A., Fedotov G.A. Mathematical model of the burden layers' movement and melt accumulation in the blast furnace hearth. *Stal'.* 2023;(4):2–6. (In Russ.).
Онорин О.П., Спирин Н.А., Лавров В.В., Гурин И.А., Федотов Г.А. Математическая модель движения слоев

- шихты и накопления расплава в горне доменной печи. *Сталь*. 2023;(4):2–6.
21. Saliy V.V., Frolov R.N., Tsebrenko K.N. Construction of economic information-analytical system for optimization of management organization. *Informatsionnye resursy Rossii*. 2021;(3(181)):37–40. (In Russ.).
https://doi.org/10.46920/0204-3653_2021_03181_37
Салий В.В., Фролов Р.Н., Цебренько К.Н. Построение экономической информационно-аналитической системы для оптимизации управления деятельностью организации. *Информационные ресурсы России*. 2021;(3(181)):37–40.
https://doi.org/10.46920/0204-3653_2021_03181_37
 22. Popov A.I. Free Tools for Designing Information Systems. Moscow: Izdatel'stvo standartov; 2014;78. (In Russ.).
Попов А.И. Свободные инструменты проектирования информационных систем. Москва: ИПК «Издательство стандартов»; 2014;78.
 23. Gurin I.A., Lavrov V.V., Spirin N.A., Nikitin A.G. Web-technologies for construction of automated information-modeling systems of technological processes in metallurgy. *Izvestiya. Ferrous Metallurgy*. 2017;60(7):573–579. (In Russ.).
<https://doi.org/10.17073/0368-0797-2017-7-573-579>
Гурин И.А., Лавров В.В., Спиринов Н.А., Никитин А.Г. Веб-технологии построения автоматизированных информационно-моделирующих систем технологических процессов в металлургии. *Известия вузов. Черная Металлургия*. 2017;60(7):573–579.
<https://doi.org/10.17073/0368-0797-2017-7-573-579>
 24. Frimen A. ASP.NET Core MVC 2 with C# Examples for Professionals. 7th ed. St. Petersburg: Dialectics LLC; 2019:1008. (In Russ.).
Фримен А. ASP.NET Core MVC 2 с примерами на C# для профессионалов. 7-е изд. Санкт-Петербург: ООО «Диалектика»; 2019:1008.

Information about the Authors

Сведения об авторах

Nikolai A. Spirin, Dr. Sci. (Eng.), Prof., Head of the Chair “Thermal Physics and Informatics in Metallurgy”, Ural Federal University named after the First President of Russia B.N. Yeltsin

ORCID: 0000-0001-6582-3428

E-mail: n.a.spirin@urfu.ru

Ivan A. Gurin, Cand. Sci. (Eng.), Assist. Prof. of the Chair “Thermal Physics and Informatics in Metallurgy”, Ural Federal University named after the First President of Russia B.N. Yeltsin

ORCID: 0000-0002-4989-7029

E-mail: ivan.gurin@urfu.ru

Vladislav V. Lavrov, Dr. Sci. (Eng.), Prof. of the Chair “Thermal Physics and Informatics in Metallurgy”, Ural Federal University named after the First President of Russia B.N. Yeltsin

ORCID: 0000-0002-6953-5519

E-mail: v.v.lavrov@urfu.ru

Lik A. Zainullin, Dr. Sci. (Eng.), Prof. of the Chair “Thermal Physics and Informatics in Metallurgy”, Ural Federal University named after the First President of Russia B.N. Yeltsin

ORCID: 0009-0000-9439-5792

E-mail: aup@vniimt.ru

Николай Александрович Спиринов, д.т.н., профессор, заведующий кафедрой теплофизики и информатики в металлургии, Уральский федеральный университет имени первого Президента России Б.Н. Ельцина

ORCID: 0000-0001-6582-3428

E-mail: n.a.spirin@urfu.ru

Иван Александрович Гурин, к.т.н., доцент кафедры теплофизики и информатики в металлургии, Уральский федеральный университет имени первого Президента России Б.Н. Ельцина

ORCID: 0000-0002-4989-7029

E-mail: ivan.gurin@urfu.ru

Владислав Васильевич Лавров, д.т.н., профессор кафедры теплофизики и информатики в металлургии, Уральский федеральный университет имени первого Президента России Б.Н. Ельцина

ORCID: 0000-0002-6953-5519

E-mail: v.v.lavrov@urfu.ru

Лик Анварович Зайнуллин, д.т.н., профессор кафедры теплофизики и информатики в металлургии, Уральский федеральный университет имени первого Президента России Б.Н. Ельцина

ORCID: 0009-0000-9439-5792

E-mail: aup@vniimt.ru

Contribution of the Authors

Вклад авторов

N. A. Spirin – formation of the article idea, substantiation of the topic relevance, formation of the concept, writing detailed plan and draft version of the article, selection of bibliographic references, final editing, preparation of the conclusions.

I. A. Gurin – elaboration of content of sections related to the development and software implementation of modern information systems in metallurgy, writing the abstract and keywords, translation into English.

V. V. Lavrov – elaboration of content of the main sections, selection of bibliographic references, design of the article.

L. A. Zainullin – elaboration of the content of the main sections, preparation of examples of practical implementation of modern information systems in industry.

Н. А. Спиринов – создание идеи статьи, обоснование актуальности темы, подготовка концепции, развернутого плана и чернового варианта статьи; подбор библиографических ссылок, окончательная правка, подготовка заключения.

И. А. Гурин – проработка содержания разделов, связанных с разработкой и программной реализацией современных информационных систем в металлургии; подготовка аннотации и ключевых слов, перевод на английский язык материалов статьи.

В. В. Лавров – проработка содержания основных разделов, подбор библиографических ссылок, оформление статьи.

Л. А. Зайнуллин – проработка содержания основных разделов, подготовка примеров практической реализации современных информационных систем в промышленности.

Received 20.12.2023

Revised 09.01.2024

Accepted 16.01.2024

Поступила в редакцию 20.12.2023

После доработки 09.01.2024

Принята к публикации 16.01.2024

Над номером работали:

Л.И. Леонтьев, главный редактор

Е.В. Протопопов, заместитель главного редактора

Е.А. Ивани, заместитель главного редактора

Л.П. Бащенко, заместитель ответственного секретаря

Е.Ю. Потапова, заместитель главного редактора по развитию

О.А. Долицкая, научный редактор

Е.М. Запольская, ведущий редактор

А.О. Гашникова, ведущий редактор

В.В. Расенец, верстка, иллюстрации

Г.Ю. Острогорская, менеджер по работе с клиентами

Подписано в печать 25.04.2024. Формат 60×90 ¹/₈. Бум. офсетная № 1.
Печать цифровая. Усл. печ. л. 15,0. Заказ 19636. Цена свободная.

Отпечатано в типографии Издательского Дома МИСИС.
119049, Москва, Ленинский пр-кт, д. 4, стр. 1.
Тел./факс: +7 (499) 236-76-17



Assessment of homogeneity of ladle-furnace refining slag by calculation and experimental methods

Estimation of accident rate of blast furnace tuyeres

Investigation of changes in temperature of pressing tool during laser processing

Influence of additives on properties of high-carbon ferrochrome slag

Internal stresses and their sources in steels with BCC lattice

Evolution of dislocation structure and phase composition of deformed $Al_{0.3}CoCrFeNi$ high-entropy alloy during heating

Formation of the gradient of structural-phase states of high-speed steel during surfacing.

Part 2. The role of the Mullins-Sekerka instability in formation of crystallization structures

Effect of heat treatment modes on structure and properties of 08Kh18N6AG10S steel

Effect of basicity on physical properties of ladle slags of $CaO - SiO_2 - Ce_2O_3 - Al_2O_3 - MgO$ system


Stress-strain state of ceramic shell mold during formation of spherical steel casting in it. Part 1

Increasing the corrosion properties of duplex steel with REM modification

Approaches to the selection of material design of infrastructure facilities for transport and injection of CO_2

Rational application of high quality manganese concentrate

Information modeling system for movement of charge layers and melt accumulation in a blast furnace well



**Зарегистрирован Федеральной службой
по надзору в сфере связи, информационных
технологий и массовых коммуникаций.
Свидетельство о регистрации
ПИ № ФС77-35456.**

Подписной индекс 70383.

